HELLENIC REPUBLIC
National and Kapodistrian University of Athens
EST. 1837

SCHOOL OF SCIENCE
DEPARTMENT OF PHYSICS
DIVISION OF ENVIRONMENTAL PHYSICS AND METEOROLOGY

MASTER'S THESIS

Study of cases of intense snowfall over Greece employing satellite data combined with thermodynamic/dynamic parameters


Onassis Foundation

STEFANOS KRYONAS

Student ID Number: **7110122300402**

Supervision: **Professors Flocas H. and Cartalis C.**

Athens, 2025

HELLENIC REPUBLIC
National and Kapodistrian University of Athens
EST. 1837

SCHOOL OF SCIENCE
DEPARTMENT OF PHYSICS
DIVISION OF ENVIRONMENTAL PHYSICS AND METEOROLOGY

MASTER'S THESIS

Study of cases of intense snowfall over Greece employing satellite data combined with thermodynamic/dynamic parameters



STEFANOS KRYONAS

Student ID Number: **7110122300402**

Three-member committee:

Professor Flocas H. **Professor Cartalis C.**

Associate Professor Tzanis C.

Athens, 2025

ACKNOWLEDGEMENTS

This thesis was conducted as part of the postgraduate program in “Applied Physics”, with specialization in Environmental Physics and Meteorology, at the department of Physics, National and Kapodistrian University of Athens.

I would like to express my deepest gratitude to my supervisor, Professor Helena Flocas, for her invaluable guidance, support, and encouragement throughout the course of this research. Her expertise and constructive feedback have been instrumental in shaping both the content and direction of this study. I am also sincerely thankful to the members of my thesis committee, Professor Constantinos Cartalis and Associate Professor Chris Tzanis, for their insightful comments and suggestions, which greatly enriched this work.

A special acknowledgment is extended to Dr. Platon Patlakas, postdoctoral researcher, whose guidance and assistance in creating maps using WRF data were critical to the successful completion of this thesis. His support in applying advanced meteorological tools and models provided a deeper layer of analysis and understanding. I would also like to thank Dr. Ilias Agathagelidis, a postdoctoral researcher, for his prompt support and valuable advice regarding satellite products.

I am also grateful to all faculty members of the postgraduate program for their valuable instruction and mentorship. Their lectures and academic guidance have played a crucial role in equipping me with the necessary knowledge and skills, both for this research and for my future professional development.

Lastly, I wish to thank my family and friends, whose unwavering encouragement and understanding have been a source of strength during this challenging yet fulfilling journey. Their support has been a cornerstone of my academic and personal growth throughout this process.

Table of Contents

1. INTRODUCTION 1

2. THEORETICAL FOUNDATIONS WITH REGIONAL PERSPECTIVES OF SNOWFALL AND METEOROLOGICAL APPLICATIONS 3

2.1. Snow dynamics: From formation to environmental impact 3

2.1.1. From formation to environmental impact 3

2.1.2. Dry vs. Wet snow 4

2.2. Fronts 6

2.2.1. Cold front 6

2.2.2. Warm front 7

2.2.3. Occluded front 7

2.3. Orographic precipitation 8

2.4. "Lake-effect" snow 9

2.5. Updraft Strength and Severe Convection Dynamics 10

2.6. Omega Block 11

2.7. Satellite Data and its application in Meteorology 12

2.7.1. Visible and Infrared Satellite Imagery 13

2.7.2. Airmass RGB 15

2.7.3. Cloud Top Height 16

2.7.4. Cloud Microphysics and Severe Convection RGB 16

2.8. Regional snowfall events in Greece 19

2.9. Favorable conditions for snowfall in Athens 19

2.9.1. Type A 20

2.9.2. Type B 20

2.10. The most significant snowfall events in Athens since 1911 21

3. METHODOLOGY AND DATA 22

3.1. Selection of the cases 'Elpida' and 'Medea': Importance and Context 22

3.1.1. Overview of 'Elpida' 22

3.1.2. Overview of 'Medea' 24

3.2. Methodology 25

3.3. Data Sources Overview 26

4. ELPIDA SNOWSTORM 28

4.1. Analysis of Atmospheric Dynamics 28

4.1.1. Synoptic Setup Leading to the Elpida Snowstorm 28

4.1.2. Convective Dynamics and Snowfall Patterns on January 24, 2022 31

4.2. Satellite-Based Analysis of Atmospheric Dynamics and Cloud Microphysics 40

4.2.1. Analysis of Cloud Coverage using Visible and Infrared Satellite Imagery 40
4.2.2. Air Mass analysis using Airmass RGB 44
4.2.3. Cloud Top Height analysis 47
4.2.4. Cloud Microphysics and Severe Convection RGB Analysis 53
5. MEDEA SNOWSTORM 63
5.1. Analysis of Atmospheric Dynamics 63
5.1.1. Synoptic Setup Leading to the Medea Snowstorm 63
5.1.2. Convective Dynamics and Snowfall Patterns on February 16, 2021 65
5.2. Satellite Data Analysis 74
5.2.1. Onset of Snowfall – February 13, 2021 74
5.2.2. Continued Snowfall Expansion – February 14, 2021 77
5.2.3. Lake-Effect Snow Intensification – February 15, 2021 80
5.2.4. Peak Snowfall Impact in Eastern Regions – February 16, 2021 83
6. COMPARISON BETWEEN THE TWO CASES AND DISCUSSION 87
6.1. Structure Scientific Comparison: 'Medea' vs. 'Elpida' Snowstorms 87
6.1.1. Genesis and Synoptic Setup 88
6.1.2. Duration and Affected Regions 88
6.1.3. Both snowstorms' impact in Athens 89
6.1.4. Thermodynamic and Dynamic Characteristics 90
6.1.5. Snow Type and Density analysis 93
6.1.6. Convective Dynamics and Cloud Development 95
6.2. Snowfall Forecast Indices for Nowcasting Applications 97
6.2.1. General Snowfall Index 98
6.2.2. Severe Snowfall/Thundersnow Index 99
6.2.3. Validation of Snowfall Indices 100
6.3. Critical Analysis and Comparison of Snowfall Indices: Forecasting vs. Nowcasting 103
6.3.1. Forecasting Applications 104
6.3.2. Nowcasting Applications 104
7. EMERGING SATELLITE-DERIVED PRODUCTS FOR ENHANCING SNOWFALL INDICES 106
7.1. Cloud Phase RGB 106
7.2. Cloud Type RGB 108
7.3. Combining Blended SEVIRI/LEO MW Precipitation and Rapidly Developing Thunderstorms Products 109
8. CONCLUSIONS 112
9. REFERENCES 114

ABSTRACT

This thesis explores the dynamics and microphysics of two significant high impact snowstorm events, ‘Elpida’ (January 2022) and ‘Medea' (February 2021) in Greece, with the aid of combined synoptic-scale atmospheric analysis, high-resolution satellite imagery, and advanced numerical analysis. The objective is to get a better insight in the mechanisms of severe snowfall events in Greece and the Mediterranean region and to contribute to the nowcasting of these events.

Special emphasis is placed on leveraging modern tools such as RGB satellite products (Airmass, Day/Night Microphysics, Severe Convection) and Cloud Top Height, which enhance the capacity to identify and nowcast extreme weather events. By integrating satellite-derived insights with thermodynamic/dynamic atmospheric parameters, this research aims to contribute to the advancement of snowfall nowcasting techniques, particularly in regions where such events, though rare, have substantial societal and economic impacts.

It was found that ‘Elpida’ exhibited a more intense but shorter-lived snowstorm, driven by a closed cyclonic structure, resulting in stronger atmospheric instability and exceptionally high cloud tops, leading to heavier snowfall, mainly in the eastern and southern suburbs of Athens, further enhanced by the Snow Aegean Effect. In contrast, ‘Medea’ had a broader reach and longer duration sufficient snowfall, with moderate convection and uniform snow coverage across Attica. Both storms produced wet, dense snow due to similar near-surface thermal and humidity conditions, significantly affecting infrastructure. Most importantly, the study developed General and Severe Snowfall Indices, integrating satellite RGB composites and thermodynamic parameters, improving nowcasting accuracy for such rare Mediterranean events.

1. INTRODUCTION

Severe snowfall events have significant impacts on society, infrastructure, and the environment, highlighting the need for advanced predictive capabilities to mitigate their effects. In regions like Greece, where such events are relatively rare, their impact is often amplified, leading to profound economic and societal consequences.

The Mediterranean region's unique geographical and climatic conditions make it particularly vulnerable to extreme weather phenomena, including rare but impactful heavy snowfalls. Previous research on snowfall events in Greece is rather limited (Houssos et al., 2007; Louka et al., 2010; Prezerakos & Angouridakis, 1984; Sahsamanoglou, 1989) and only recently some modelling research was published on snowfall dynamics (e.g., Hobbs, 2010; Voudouri et al., 2023; Patlakas et al., 2024). However, further work is needed to enhance forecasting capabilities. This study aims to address this gap by improving the understanding and forecasting of such events through an analysis of atmospheric dynamics and satellite data. Emphasis is placed on exploring correlations between large-scale and mesoscale circulation patterns and satellite-derived indices, such as temperature, humidity, cloud properties, and snow cover, to enhance predictive accuracy for severe snowstorms.

This research investigates two major snowstorms –'Medea' and 'Elpida', in February 2021 and January 2022, respectively– to identify the synoptic scale and mesoscale atmospheric mechanisms that contributed to their development and clarify the dynamics behind extreme snowfall episodes. These storms were selected due to their significant societal and economic impacts, with Elpida disrupting transportation and daily life in Attica and Euboea (Patlakas et al., 2024), and Medea bringing severe frost and power outages across central and northern regions (Lagouvardos et al., 2021). By focusing on their development and dynamics, this study highlights the need for advanced forecasting tools and provides insights into improving nowcasting techniques in the Mediterranean.

Satellite data provides indispensable tools for monitoring and predicting rapidly developing weather events in real-time, providing timely updates and offering detailed insights into storm characteristics. This is particularly essential during snowstorms associated with cyclonic activity over oceans where traditional observational data is limited. Such storm characteristics include structure and intensity of storm systems,

vertical extent of clouds (indicative of convective strength), and cloud-top temperatures, along with cloud phase composition (whether consisting of ice or water droplets). These parameters, accompanied by temperature profiles, indicate conditions conducive to snowfall. Despite advancements in satellite technology, limited research exists in Greece on utilizing such data for snowfall forecasting, particularly for nowcasting applications. Relevant studies (Ziakopoulos, 2008; Cartalis & Feidas, 2013) provide a foundation for understanding the integration of satellite data in weather prediction.

Key satellite products, including Cloud Top Height, Day Microphysics RGB, Night Microphysics RGB, Airmass RGB, and Severe Convection RGB, play a crucial role in identifying clouds likely to produce heavy snowfall. Such products become particularly valuable in regions with insufficient radar coverage, as they allow meteorologists to monitor storm evolution and cloud characteristics with high temporal and spatial resolution. When combined with numerical weather prediction models, these tools enhance nowcasting precision, which in turn can improve the accuracy of short-term forecasts, particularly during rapidly developing snowstorms in regions with limited observational data.

This thesis integrates satellite products with thermodynamic and dynamic atmospheric analyses to investigate the drivers of intense snowfall in Greece. By analyzing recent snowstorm events and leveraging EUMETSAT data alongside numerical models, it highlights the value of combining observational tools and modeling approaches. In doing so, it demonstrates how satellite data can bridge the gaps left by radar limitations, enhancing the accuracy and timeliness of snowfall forecasts. The findings aim to address critical gaps in snowfall prediction by demonstrating how satellite data enhances nowcasting precision, contributing to more effective practices on operational meteorology, especially in the Mediterranean region.

2. THEORETICAL FOUNDATIONS WITH REGIONAL PERSPECTIVES OF SNOWFALL AND METEOROLOGICAL APPLICATIONS

2.1. Snow dynamics: From formation to environmental impact

2.1.1. From formation to environmental impact

Snow plays a pivotal role in the hydrological cycle, serving as a crucial source of precipitation, significantly contributing to groundwater recharge and river runoff, particularly during the spring thaw. Key metrics for understanding snow include snowfall, snow depth, snow water equivalent (SWE), accumulation and melt rates. Snowfall measures the amount of snow or ice pellets since the last recorded event, while snow depth represents the total snow present on the ground. SWE indicates the amount of water contained within the snowpack if it were melted, providing a crucial parameter for hydrological studies. Snow accumulation refers to the total snowfall within a specific period, and snowmelt describes the process and rate at which snow melts into water (Voudouri et al., 2023).

Formed from individual ice crystals that develop in the atmosphere, snow begins its lifecycle when conditions allow these crystals to nucleate around microscopic particles. As these crystals grow, they fall to the ground, accumulating and undergoing various changes depending on the environmental conditions (Hobbs, 2010). Snowstorms, which provide the atmospheric moisture and cold air necessary for snow formation, play a crucial role in this process. The shapes of snowflakes vary, with common forms including platelets, needles, columns and rime. Over time, accumulated snow undergoes metamorphosis through processes such as sintering, sublimation and free-thaw cycles. In regions where the climate supports persistent accumulation, glaciers may form, while in other areas, seasonal melting leads to significant runoff, impacting both natural and human-modified landscapes. Snow's impact extends beyond natural ecosystems, influencing human activities such as transportation, agriculture and recreation. It necessitates the maintenance of clear roads and paths and impacts agricultural timing and techniques.

The formation of snow is intricately linked to cloud formation within larger atmospheric systems, particularly low-pressure areas which can range from producing light snowfalls to severe blizzards. The development of snow involves complex

interactions of moisture content and atmospheric temperature, with snow clouds often forming within frontal systems associated with these low-pressure systems. Such systems can generate diverse snow events from widespread, light snow to intense snowsqualls and thundersnow events, which are marked by brief, intense periods of snowfall accompanied by wind and sometimes even lightning and thunder.

2.1.2. Dry vs. Wet snow

Snowfall can exhibit significant variability in both form and texture with notable differences between wet snow and dry snow. These distinctions are influenced primarily by air temperature near the surface, which determines the snow's water content and, consequently, its weight and impact (Fig. 2.1).

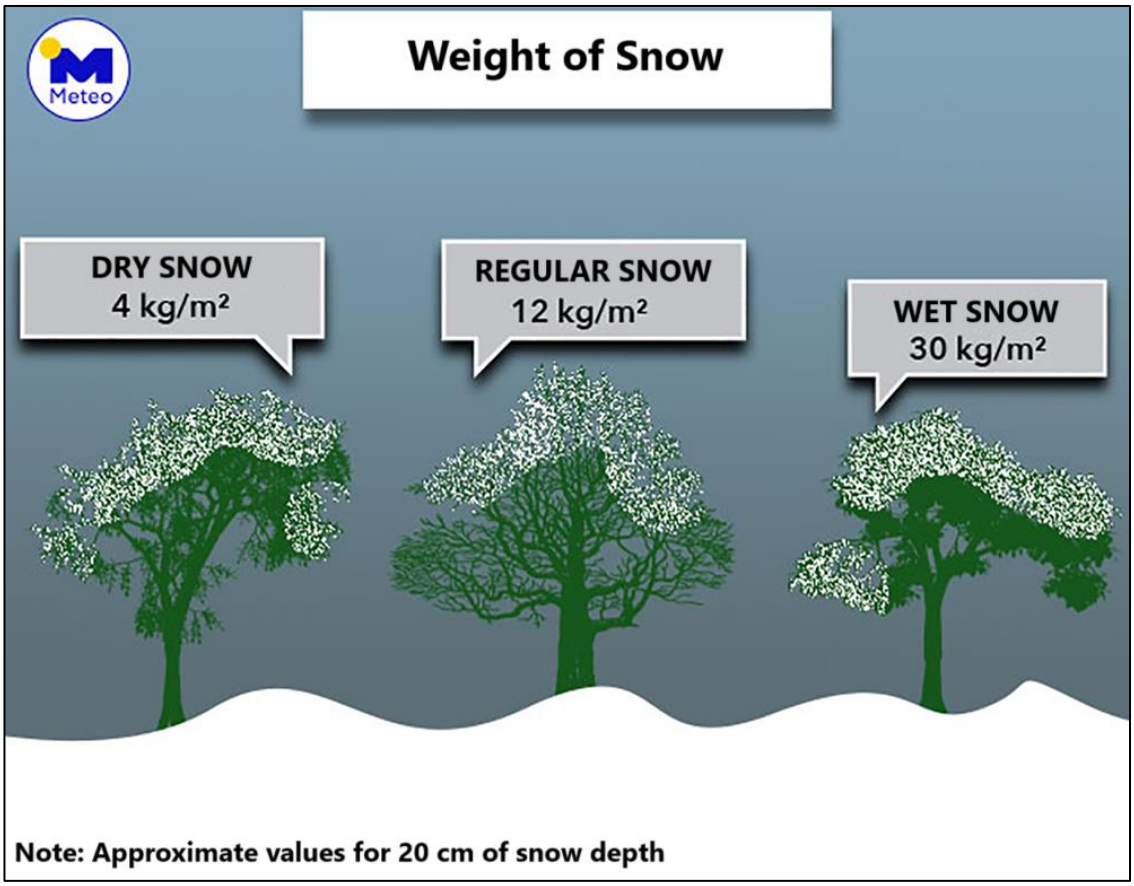


Fig. 2.1: Schematic representation of the weight difference among the three main categories of snow: dry, regular and wet snow. The weight is calculated based on the volume and density of the snow (~150 kg/m³ for wet snow). (*https://www.meteo.gr/article_view.cfm?entryID=1647*)

Dry snow typically forms under very cold conditions, when surface air temperatures are below freezing. In such an environment, water vapor in the atmosphere freezes directly into ice crystals, creating light, powdery snow with minimal water content. Dry snow accumulates primarily on flat surfaces and does not adhere to trees,



Fig. 2.2: Dry snow being blown by the wind, highlighting its low density and light, powdery texture. (*https://compuweather.com/the-important-difference-between-wet-snow-and-dry-snow/*)

power lines, or vertical structures (Fig. 2.2). It is easy to shovel and cannot be compacted easily to form snowballs. However, due to its low density, dry snow is highly susceptible to blowing and drifting when accompanied by strong winds, which can complicate efforts to clear roads and pathways.

Conversely, wet snow occurs when surface temperatures hover close to freezing, allowing snowflakes to partially melt before reaching the ground. This partial melting increases the snow's water content, making it denser, heavier and stickier. Wet snow easily adheres to tree branches, power lines, and other surfaces, creating picturesque winter landscapes but also introducing significant hazards (Fig. 2.3). Even a few inches of accumulation can cause structural strain, breaking tree limbs and power lines, which may lead to power outages. Additionally, the increased weight of snow –estimated to contain 2 to 3 times more water per inch compared to dry snow– makes it particularly difficult to shovel and poses risks of roof collapses under heavy accumulation.



Fig. 2.3: Wet snow clinging to tree branches and creating a heavy, dense appearance. (*https://compuweather.com/the-important-difference-between-wet-snow-and-dry-snow/*)

The weight of snow per square meter can vary dramatically depending on its type. For example, dry, fluffy snow is the lightest, while wet snow can be approximately seven times heavier due to its higher water content. This variability underscores the differing impacts of snow on infrastructure, vegetation, and daily life. In regions

experiencing heavy snowfall, the type of snow becomes a critical factor in assessing potential hazards and implementing appropriate mitigation strategies.

2.2. Fronts

Fronts play a critical role in weather dynamics, particularly in determining the type, intensity, and duration of snowfall events. Understanding the differences between cold and warm fronts provides valuable insight into forecasting snowstorm characteristics.

2.2.1. Cold front

A cold front is defined by the leading edge of a cooler air mass displacing warmer air (Fig. 2.4). As this cooler air forces the warm, moist air upward, it creates intense convective snowfall known as snowsqualls. These are brief, heavy bursts of snow that can lead to whiteout conditions. The dynamics of a cold front are marked by the rapid movement of the front, which can lead to sudden and severe changes in weather within short periods. Snowfall associated with cold fronts is typically heavier but shorter in duration compared to warm fronts. The vertical mixing of the atmosphere during such events can also lead to phenomena such as thundersnow, where the intense convection associated with the cold front leads to thunder and lightning within the snowstorm.

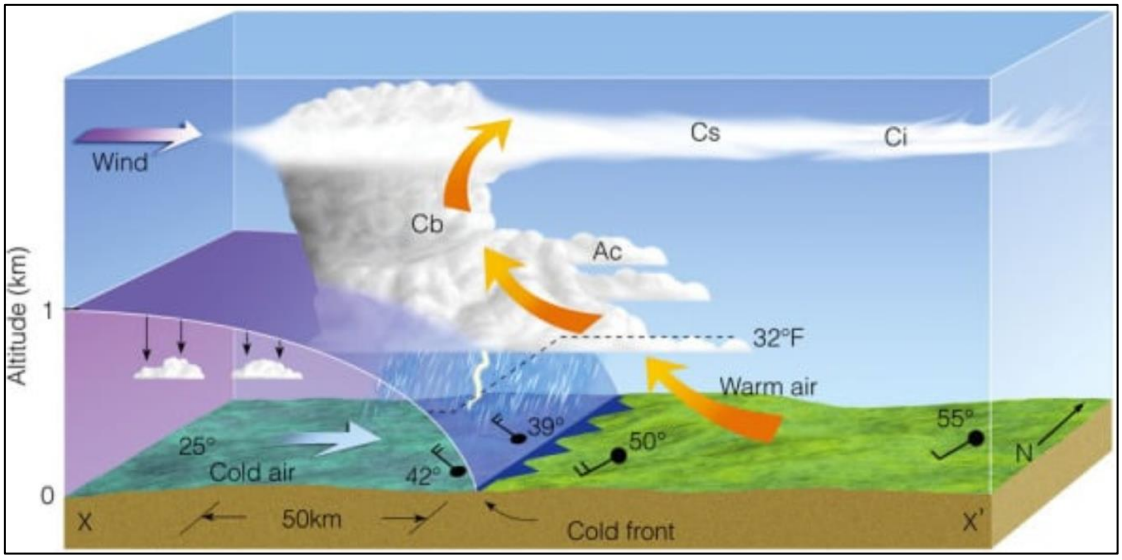


Fig. 2.4: Cross-section of a cold front interaction with warm air. (*https://www.stratusdeck.co.uk/fronts*)

2.2.2. Warm front

Conversely, a warm front occurs when a warmer air mass overtakes a colder air mass, sliding over the cooler air due to its lighter density (Fig. 2.5). The snowfall associated with warm fronts is generally steadier and more prolonged than that produced by cold fronts. As the warm, moist air rises gradually over the cold air, it cools slowly, leading to sustained snowfall that can last several hours or even days. While less intense per hour, the snow accumulates over a longer duration, potentially resulting in significant snowfall. This type of snowfall typically covers larger areas with a more uniform snow depth.

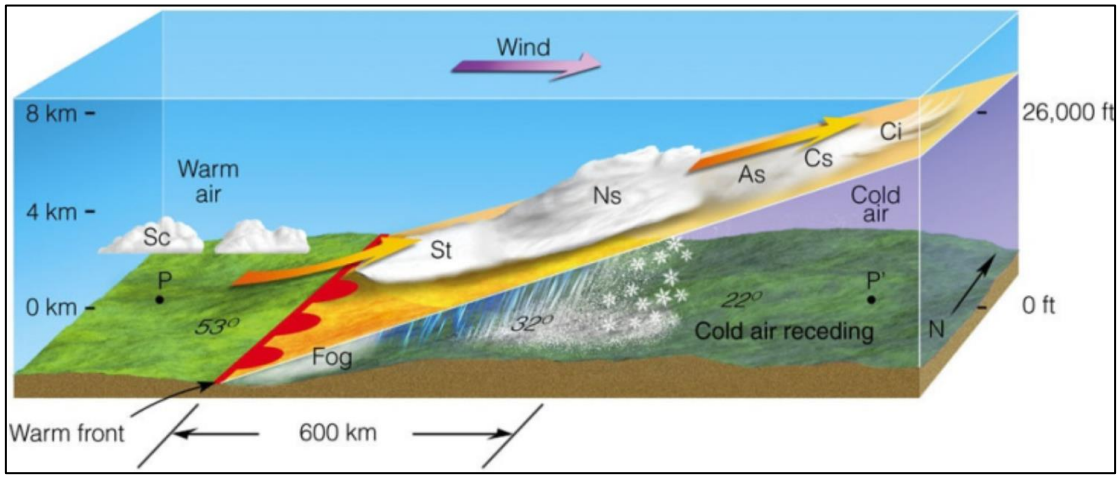


Fig. 2.5: Cross-section of a warm front interaction with cold air. (*https://www.stratusdeck.co.uk/fronts*)

2.2.3. Occluded front

An occluded front occurs when a cold front overtakes a warm front, forcing the warm air aloft and creating a complex weather pattern associated with a closed surface low (Fig. 2.6). These fronts often produce prolonged and widespread precipitation, which can include a mix of rain, sleet, or snow depending on the vertical temperature profile of the atmosphere.

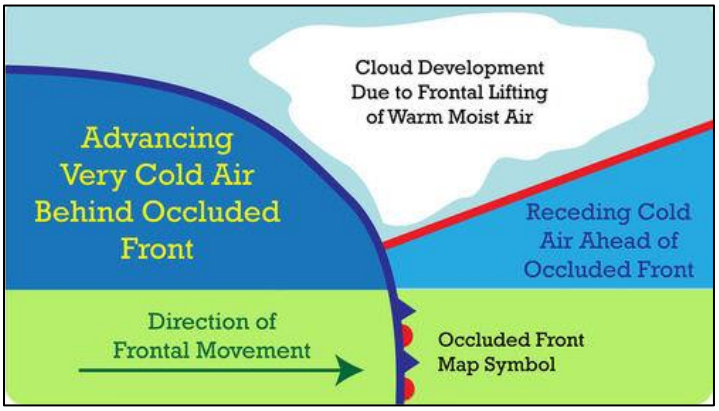


Fig. 2.6: Cross-section of an occluded front interaction with cold air. (*https://flexbooks.ck12.org/*)

In winter, occluded fronts are frequently associated with heavy sustained snowfall, particularly in the regions where the lifted warm air enhances moisture availability. This

setup can lead to significant accumulations, especially in regions influenced by orographic lift or lake-effect processes, where local geography intensifies the precipitation.

2.3. Orographic precipitation

Orographic precipitation occurs when moist air is driven up the windward slopes of mountain ranges by prevailing winds. As the air ascends, it expands and cools adiabatically, leading to the condensation of water vapor and subsequent precipitation. This process removes moisture from the air, increasing its potential temperature (Fig. 2.7). The result is significantly drier air and warmer temperatures on the leeward side of the mountains, a phenomenon known as the rain shadow effect (Roe, 2005).

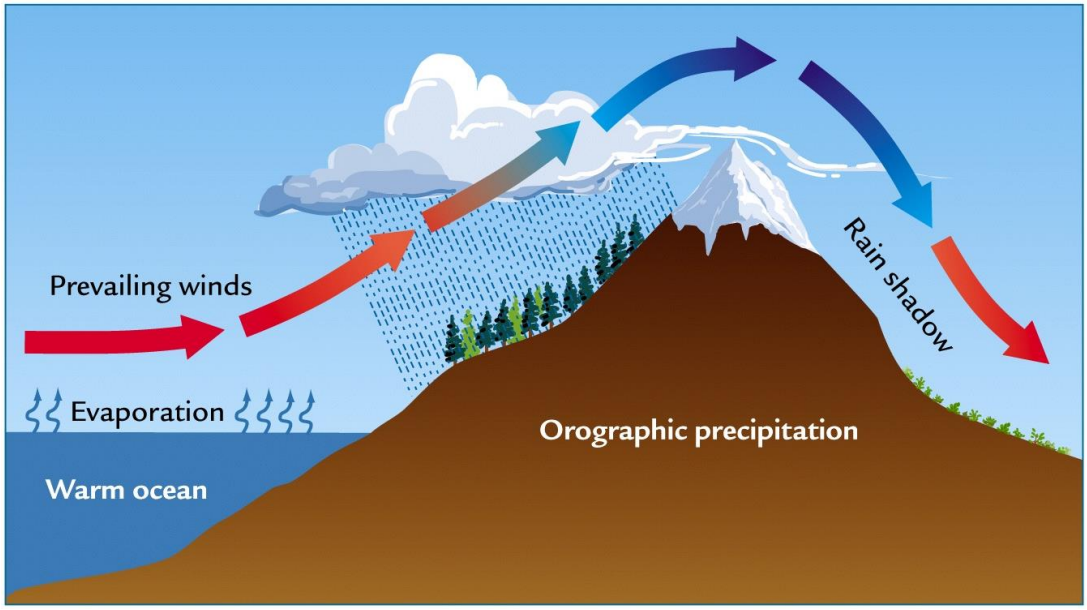


Fig. 2.7: Classic orographic precipitation model. (*https://kbkb-wx.blogspot.com/2014/04/orographic-precipitation.html*)

At higher elevations, the cooler temperatures further enhance snowfall formation, resulting in greater snow depths and prolong snowpack duration in regions favorably aligned with prevailing winds. Additionally, mountain waves –atmospheric patterns induced by mountainous terrain– can amplify upward air motion on the windward side, further enhancing snowfall efficiency.

The dynamics of orographic snowfall are critical in areas with significant elevation changes, as they contribute to localized weather patterns and influence the hydrological cycle. These regions often experience enhanced snowfall, which serves as a crucial water

resource for ecosystems and human activities that rely on sustained water supply from mountain snowpacks.

Forecasting becomes particularly complex when combining orographic and lake-enhanced precipitation. Studies indicate that these interactions can strengthen precipitation significantly, influenced by factors such as the influence of upstream mountain ranges and orographically forced convergence by concave terrain (Alcott & Steenburgh, 2013).

2.4. "Lake-effect" snow

Lake-effect snow occurs when a cold air mass travels over warmer lake waters, causing the air near the surface to warm, absorb moisture, and become unstable. This leads to rapid cloud formation as the moist air rises, cools, and releases snow on the leeward shores, creating conditions favorable for heavy and localized snowfall (Fig. 2.8).

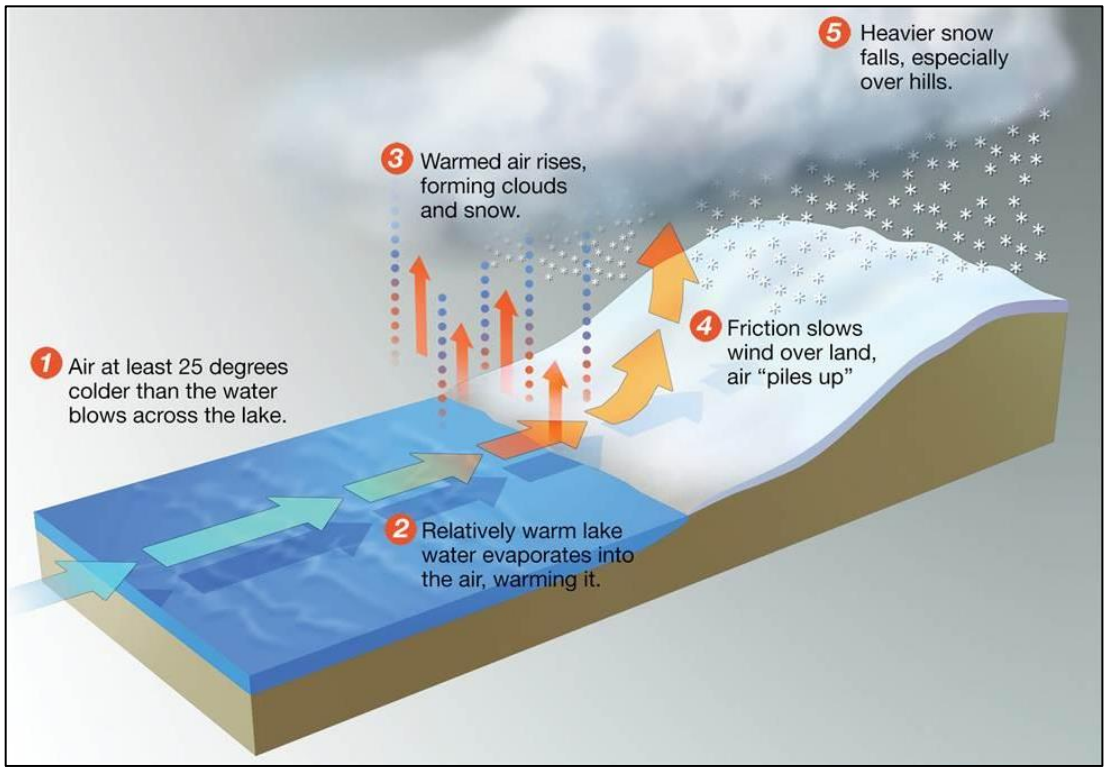


Fig. 2.8: Illustration depicting the process of lake-effect snow, showing how cold air moving over warmer lake waters leads to cloud and snow formation. (*https://www.aopa.org/news-and-media/all-news/2018/february/flight-training-magazine/weather-lake-effect-snow*)

A similar process occurs over saltwater bodies, known as ocean-effect or bay-effect snow. The effect becomes more intense when the air mass encounters elevated terrain, which forces the air to ascend further, amplifying precipitation. This can produce heavy

bands of snow that accumulate rapidly, sometimes exceeding several centimeters per hour, resulting significant total accumulation (Mass, 2021).

Regions prone to this kind of snowfall, such as areas adjacent to the Great Lakes or specific coastal regions in Japan and Russia, are often referred to as snowbelts. In Greece, a similar phenomenon, referred to as the "Snow Aegean effect", occurs when cold air masses from the north pass over the warmer waters of the Aegean Sea. The combination of moist air and the orographic lift provided by the terrain in regions like Attica, Euboea, and other nearby areas enhances the snow-producing mechanism, frequently leading to heavy snowfall.

2.5. Updraft Strength and Severe Convection Dynamics

The following figure (Fig. 2.9) demonstrates how updraft strength within cumulonimbus clouds influences droplet size and ice crystal formation – a critical aspect in the development of severe convection (Heymsfield et al., 2005; Williams et al., 2005). In regions where updrafts are particularly strong, water droplets are quickly lifted upward through the cloud, reducing the time available for them to coalesce and grow. This rapid ascent leads to smaller droplets, which freeze into small ice crystals in the upper cloud layers. These smaller ice crystals are a distinctive marker of intense convection and are often associated with severe weather conditions.

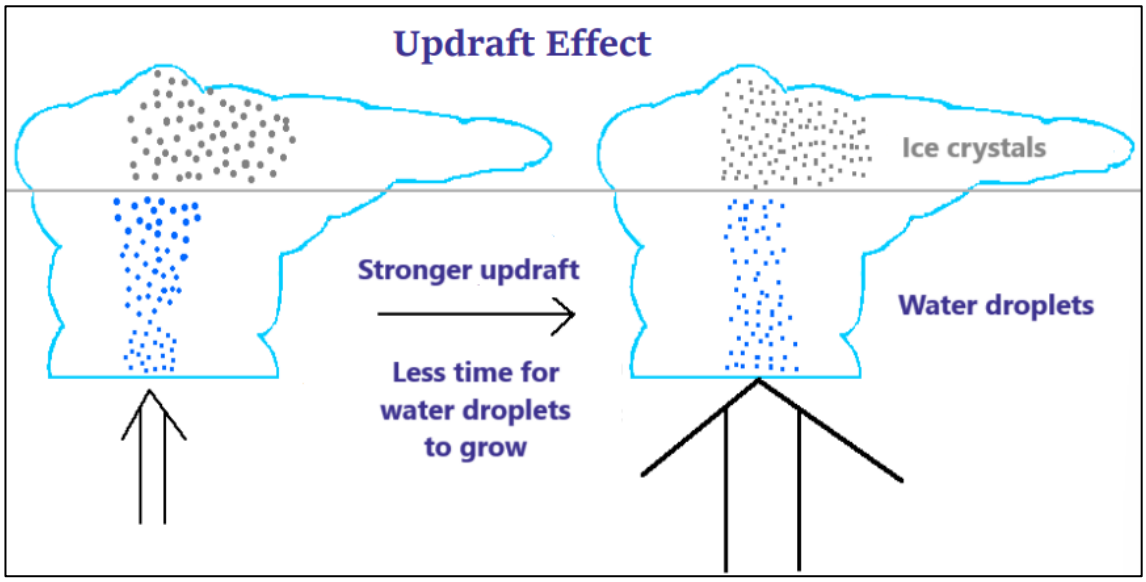


Fig. 2.9: Updraft effect (Heymsfield et al., 2005; Williams et al., 2005)

Conversely, in areas with weaker updrafts (as depicted on the left side of the diagram), droplets spend more time in the lower cloud layers, enabling them to grow larger through coalescence before ascending. As a result, the ice crystals formed in these

regions tend to be larger. This differentiation in droplet and crystal size provides key insights into the intensity of convection within clouds, offering valuable indicators of potential severe weather. Understanding these dynamics is essential for improving the identification and forecasting of severe convective events, particularly through nowcasting techniques.

2.6. Omega Block

An Omega Block is a large-scale atmospheric pattern characterized by a high-pressure system flanked by two low-pressure systems to the southeast and southwest in the Northern Hemisphere (Bott, 2012; Woollings et al., 2018). This configuration disrupts the usual westerly flow, forcing the jet stream to divert around the high-pressure center (Fig. 2.10), creating a flow pattern that resembles the Greek letter "Ω" (Omega). This atmospheric configuration has significant implications for regional weather patterns, as it creates prolonged periods of stable or extreme weather conditions (Fig, 2.11).

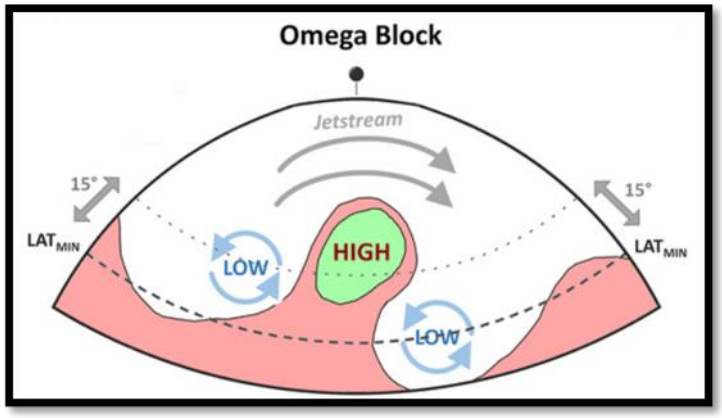


Fig. 2.10: Conceptual diagram of an omega block showing the high-pressure system flanked by two low-pressure systems, altering the jet stream flow. (*https://journals.ametsoc.org/*)

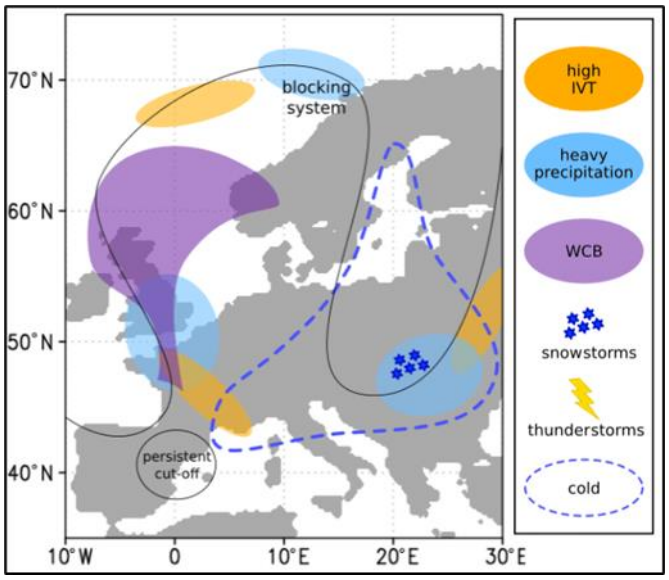


Fig. 2.11: Example schematic illustration of a blocking system (black line, indicating a geopotential height or PV contour) and associated surface extremes during the cold season (October–March). (*https://wcd.copernicus.org/articles/3/305/2022/*)

Omega Blocks are more commonly observed over the North Pacific, North America and Eurasia regions (Bott, 2012). Due to the stationery and persistent nature of these blocks, they can last several days to weeks, with a minimum duration generally defined as 4 to 10 days (Barriopedro et al., 2006, 2010;

Pelly & Hoskins, 2003; Rex, 1950). Their longevity significantly impacts weather patterns within their influence area by "trapping" weather systems, leading to extended periods of consistent weather.

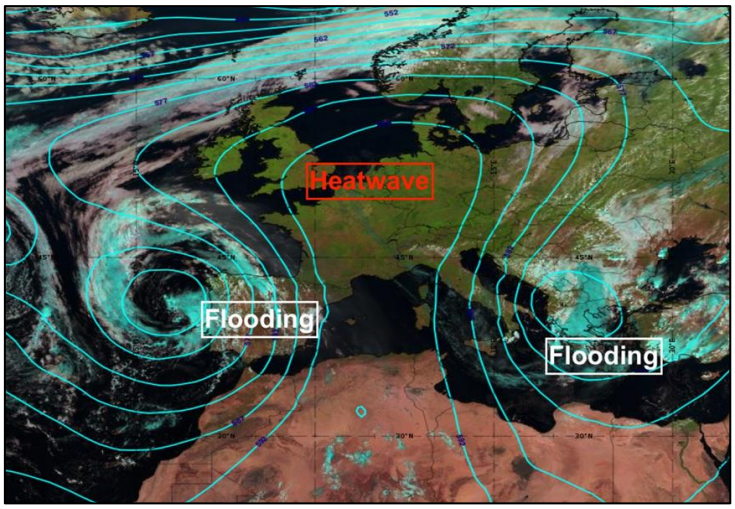


Fig. 2.12: Example of summer-season (April–September) atmospheric patterns associated with extreme weather events, including heatwave and flooding areas, highlighted in Europe and the Mediterranean region. (*https://weather2go.gr/systimata-empodismoy-omega-block/*)

Areas beneath the high-pressure center often experience stable and dry conditions, increasing the risk of heatwaves or droughts. Conversely, regions under the influence of lows may see cooler, wetter weather, potentially leading to flooding or extreme snow accumulation, depending on the season (Fig. 2.11 & Fig. 2.12). These sustained weather extremes highlight the Omega Block's potential for severe regional impacts.

Understanding the blocking effect of the Omega pattern is crucial for predicting long-lasting weather extremes, as it disrupts atmospheric circulation and locks regions into persistent conditions (Barriopedro et al., 2010; Pelly & Hoskins, 2003).

2.7. Satellite Data and its application in Meteorology

Over the last decades, both satellite remote sensing has drastically transformed meteorology, providing critical insights into atmospheric conditions on a global scale. Unlike traditional ground-based observations, which are limited in coverage, satellite observations capture continuous, high temporal and spectral-resolution data across vast areas of the Earth's atmosphere, oceans and land. This capability offers unique advantages in monitoring and forecasting extreme weather phenomena, including hurricanes and thunderstorms during summer, and violent snowstorms during winter.

Satellites equipped with advanced remote-sensing instruments monitor various meteorological parameters such as temperature, humidity, cloud structure, and precipitation intensity. These instruments measure reflected sunlight, emitted thermal infrared radiation and microwave energy, enabling a detailed analysis of atmospheric

properties and processes at different altitudes. Satellites in geostationary orbit, such as those from the GOES and METEOSAT series of satellites, provide near real-time data over a specific region. Satellites in polar orbits include Sentinel 2, Sentinel-3, Aqua and Terra (carrying the MODIS instrument), and VIIRS, that provide global coverage albeit at higher spatial resolution and less frequent updates.

By integrating multiple satellite products at high temporal resolution, meteorologists can track the development and movement of weather systems, analyze cloud formation and behavior and identify the dynamics of cyclonic storms. This real-time observation allows for nowcasting, which refers to the short-term forecasting of weather phenomena as they evolve (on scale of minutes to hours), crucial for responding to fast-developing and potentially hazardous conditions.

2.7.1. Visible and Infrared Satellite Imagery

Visible and infrared satellite imagery are crucial tools in the field of meteorology, as they complement our understanding and prediction of weather phenomena. These spectral ranges reveal distinct atmospheric details, including cloud appearance, thickness, and height, which are critical for accurate weather analysis. Clouds are identified based on their geometric characteristics, appearance, and spectral values in both the IR and VIS channels, providing insights into their types and associated weather impacts.

The primary sources of visible and infrared satellite imagery in modern meteorology are the MSG (Meteosat Second Generation) geostationary satellites and the MetOp (Meteorological Operational Satellite) polar-orbiting satellites. The MSG satellites, located in geostationary orbit 36,000 km above Earth, continuously monitor atmospheric conditions over Europe, Africa, the Atlantic Ocean, the Middle East, and parts of Latin America. They provide full-disk scans every 15 minutes and rapid-scan updates every 5 minutes for Europe, enabling near-real-time weather monitoring. Conversely, MetOp satellites, equipped with the Advanced Very High-Resolution Radiometer (AVHRR), deliver high spatial resolution imagery but with limited temporal coverage, as their polar orbit restricts them to a few passes over a specific region per day.

In late 2023, the MTG (Meteosat Third Generation) satellites became operational, representing a significant advancement over MSG. With a temporal resolution of 10 minutes for full-disk imagery and 2.5 minutes for rapid scans, alongside visible bands of 0.5 km and infrared bands of 1 km spatial resolution, MTG marks a leap forward.

Additionally, new instruments, such as the Lighting Imager (LI) and the Infrared Sounder (IRS), further enhance capabilities, offering real-time lightning detection and atmospheric profiling. However, as MTG data was not available during the snowstorms analyzed in this study, the focus remains on the complementary roles of MSG and MetOp.

Visible imagery (0.4-0.7 μm) displays images resembling what would be visible by the naked eye from space, capturing the reflectivity of the Earth's surface and cloud cover. Brighter, whiter clouds indicate thicker and denser formations, reflecting more sunlight. This makes visible imagery particularly useful for analyzing cloud density and structure during the daytime (Cartalis & Feidas, 2013). However, its reliance on solar radiation limits its application to daylight hours. MSG and MTG satellites excel in delivering continuous visible imagery throughout the day, supporting real-time cloud monitoring. For continuous monitoring, MSG and MTG satellites provide frequent daytime imagery, while MetOp's AVHRR offers high-spatial resolution observations during its overpasses.

Cloud recognition relies on geometric characteristics (size, shape) and appearance (texture), according to Cartalis & Feidas, 2013. For instance, towering cumulonimbus clouds indicate deep convection and severe weather potential, while stratiform clouds suggest stable conditions. Cumulus clouds with a "cauliflower" texture signify active updrafts and potential instability, whereas smooth, layered clouds suggest atmospheric stability. Recognizing these patterns is essential for distinguishing convective systems from stratiform ones, crucial for assessing precipitation and storm potential.

Infrared imagery (10.8 to 12.0 μm) captures thermal radiation emitted by the Earth and atmosphere, making it invaluable for both day and night observations. For conventional reasons, higher, colder clouds appear whiter, while lower, warmer clouds appear darker, enabling meteorologists to estimate cloud altitude and atmospheric structure (Cartalis & Feidas, 2013). This spectral data provides insights into cloud top height and temperature, with cold, high-altitude clouds often linked to severe weather.

Combining data from visible and infrared channels enhances cloud classification and impact assessment (Cartalis & Feidas, 2013). For example, cumulonimbus clouds appear bright white in both VIS and IR imagery due to their thickness and high altitude, while lower stratiform clouds appear grayer in VIS and darker in IR imagery. This differentiation is crucial for identifying areas of strong convection and assessing severe weather risks.

In conclusion, visible imagery offers essential daytime information on cloud density and structure, while infrared imagery provides critical round-the-clock information on cloud height and temperature. By integrating these data streams with geometric and spectral characteristics, meteorologists gain a comprehensive understanding of atmospheric conditions, supporting improved weather forecasting and nowcasting. While MSG satellites excel in frequent updates for continuous weather monitoring, especially for rapidly evolving events, MetOp satellites deliver detailed imagery ideal for targeted analysis or validation purposes, and MTG satellites represent the future of geostationary monitoring with their advanced capabilities. Together, these systems enhance the ability to track cloud patterns, identify convective systems, and predict severe weather phenomena.

2.7.2. Airmass RGB

Airmass RGB imagery is one of the most critical tools in meteorological analysis, allowing forecasters to differentiate between air masses and monitor atmospheric dynamics. This RGB product, derived from MSG satellites, combines several satellite channels to highlight gradients in temperature, humidity, and ozone concentration in the upper atmosphere. It provides detailed insights into frontal systems, jet streams, cyclogenesis, and areas of subsidence, aiding in accurate severe weather forecasting.

By combining data from infrared (IR) and water vapor (WV) channels, the Airmass RGB enhances contrasts between air masses with differing thermal and chemical properties, revealing the atmospheric structure and ongoing processes (Table 2.1). This tool is particularly effective in identifying synoptic-scale weather patterns and potential convective activity. The Airmass RGB can be used both day and night throughout the year, ensuring consistent and reliable monitoring of atmospheric changes across seasons.

Table 2.1: *Key spectral channels in Airmass RGB imagery and their contributions to atmospheric feature detection based on water vapor, ozone content, and cloud levels. (https://www.eumetsat.int/)*

Color-Channel [µm]	Physically relates to	Smaller contribution to the signal of	Larger contribution to the signal of
Red (WV6.2–WV7.3)	Vertical water vapor distribution, Mid- and high-level clouds	Mid-level humidity, Mid-level clouds	Dry upper levels, High-level clouds
Green (IR9.7–IR10.8)	Height of tropopause, Cloud at all levels	Polar air mass (Ozone rich)	Tropical air mass (Ozone poor)
Blue (WV6.2)	Water vapor content in upper layer – High clouds	Dry upper levels	Moist upper levels

2.7.3. Cloud Top Height

The Cloud Top Height (CTH) product offers precise cloud height measurements using a color-coded scale. Unlike standard infrared imagery, which only indicates relative cloud temperature and height, CTH data delivers specific altitude values. When combined with synoptic model outputs defining the heights for low-, mid-, and high-level clouds, it enhances our ability to distinguish between cloud types and their associated weather phenomena. This approach is important for identifying vertically developed clouds, such as cumulonimbus, which are often linked to active weather systems and increased precipitation potential (including snowfall), and distinguish them from thin high-level clouds like cirrus.

While CTH provides critical insights into cloud vertical development, forecasting winter precipitation –distinguishing between rain, sleet, freezing rain, and snow– requires a more comprehensive analysis of the atmospheric column. Moreover, meteorologists examine temperature and humidity data across key atmospheric layers, particularly at the 500 hPa and 850 hPa levels, as well as near the surface, to complement CTH data. This integrated approach helps evaluate precipitation potential more effectively, especially in complex winter weather scenarios.

CTH data is especially valuable in nowcasting severe weather, as it offers a rapid visual assessment of areas with intense convective activity. By understanding vertical cloud extents, meteorologists can better anticipate storm development, enabling timely weather warnings and accurate forecasts for intense snowfall events. Additionally, CTH improves the identification of cloud layers and enhances the assessment of atmospheric dynamics, particularly in regions with complex topography where local factors can amplify precipitation intensity.

In subsequent sections, CTH data will be applied to analyze atmospheric conditions and cloud structures over Greece. By integrating CTH with synoptic models, recurring patterns can be identified, and precipitation potential validated with greater precision.

2.7.4. Cloud Microphysics and Severe Convection RGB

The study of cloud microphysics involves the properties and behaviors of particles within clouds, including droplets and ice crystals, which play a fundamental role in cloud formation, development, and precipitation processes. These microphysical properties

provide critical insights into severe convection, closely associated with intense weather phenomena such as thunderstorms, heavy rainfall, hail, and snowfall. Satellite products like the Severe Convection RGB and Day Microphysics RGB, derived from MSG satellites, facilitate the identification of severe convection by analyzing the size and distribution of cloud particles, particularly in upper cloud layers where ice crystals predominate.

As outlined in the introductory section of this study, the key indicator of severe convection is updraft strength. Strong updrafts produce smaller particle sizes at higher altitudes due to rapid ascent, leaving minimal time for coalescence and growth. Newer Meteosat Third Generation (MTG) satellites complement the Day Microphysics RGB with advanced products like the Cloud Phase RGB, offering improved spatial and spectral resolution. These tools enable precise identification of microphysical cloud properties, although MTG data was unavailable during the events analyzed in this study.

2.7.4.1. Day Microphysics RGB

Derived from MSG satellites, Day Microphysics RGB, is a vital tool for analyzing cloud analysis during daylight hours. It combines visible and infrared channels to differentiate cloud phase (ice vs. water), particle size, temperature, and optical thickness (Table 2.2). This gives meteorologists the opportunity to monitor convective development by tracking microphysical changes, such as the initiation of glaciation at cloud tops and variations in particle size, which signal cloud growth stages or dissipation. Moreover, the Day Microphysics RGB is valuable in detecting fog and low clouds, especially in the morning hours when visibility issues are a concern. The product is also effective in detecting fog and low clouds, particularly during the morning when visibility is limited. However, its use in high-latitude winter scenarios is restricted due to reduced sunlight.

Table 2.2: *Key spectral channels in Day Microphysics RGB and their role in detecting cloud optical thickness, microphysical properties, and temperature variations across atmospheric conditions during daytime. (https://www.eumetsat.int/)*

Color-Channel [µm]	Physically relates to	Smaller contribution to the signal of	Larger contribution to the signal of
Red (VIS0.8)	Cloud optical thickness	Thin clouds	Thick clouds
Green (IR3.9) (reflected)	Cloud phase and microphysical properties	Ice clouds, Large particles	Water clouds, Small particles
Blue (IR10.8)	Temperature (land/cloud top)	Cold thick clouds	Warm land/sea, Warm clouds

2.7.4.2. Night Microphysics RGB

Optimized for nighttime application, Night Microphysics RGB uses thermal infrared channels to detect fog and low clouds when visible channels are ineffective. This product provides strong color contrast between fog, low clouds, and cloud-free areas, making it ideal for monitoring nighttime phenomena (Table 2.3). Additionally, it can indirectly indicate severe convection or precipitation by highlighting thick, high-reaching clouds often associated with intense weather systems. However, this inference is less direct compared to products specifically tuned for severe convection.

The MSG satellite provides continuous coverage with frequent updates, making it suitable for monitoring evolving nighttime weather. Polar-orbiting MetOp satellites, despite limited passes per day, offer higher spatial resolution, making them useful for validating MSG observations.

Table 2.3: *Key spectral channels in Night Microphysics RGB, illustrating how cloud phase, temperature, and moisture boundaries vary with cloud and surface properties during nighttime conditions. (https://www.eumetsat.int/)*

Color-Channel [µm]	Physically relates too	Smaller contribution to the signal of	Larger contribution to the signal of
Red (IR12.0-IR10.8)	Cloud optical thickness	Thin clouds	Thick clouds
Green (IR10.8-IR3.9)	Cloud phase	Thin ice clouds	Thick fog/water clouds
Blue (IR10.8)	Cloud top temperature, Land Sea temperature	Cold clouds	Warm surface, Warm clouds

2.7.4.3. Severe Convection RGB

Designed to track daytime convective storms, Severe Convection RGB is particularly effective in low to mid-latitudes during peak convective seasons. By combining channels that highlight cloud top microphysics, including phase and particle size, it identifies storm severity (Table 2.4).

Table 2.4: *Key spectral channels in Severe Convection RGB, highlighting their sensitivity to cloud height, particle size, and cloud top phase. (https://www.eumetsat.int/)*

Color-Channel [µm]	Physically relates to	Smaller contribution to the signal of	Larger contribution to the signal of
Red (WV6.2–WV7.3)	Cloud top height	Cloud free, or low-mid level clouds	High-level clouds
Green (IR3.9–IR10.8)	Cloud top particle size and temperature	Opaque ice cloud with large cloud top particles and/or not very cold cloud top temperature	Opaque ice cloud with small crystals and/or very cold cloud top temperature
Blue (NIR1.6–VIS0.6)	Cloud top phase	Thick ice clouds	Water clouds and Land, sea surface

High, cold clouds with small ice particles are associated with intense updrafts and severe weather phenomena, such as thunderstorms and hail. However, interpretation requires caution, as non-convective high-altitude clouds with small particles may appear similar in hue.

2.8. Regional snowfall events in Greece

Heavy snowfall in Greece occurs primarily in central and northern areas under specific synoptic condition. These conditions are marked by a combination of high-pressure systems to the north and low-pressure systems over the central Mediterranean, creating a convergence zone across the country, due to the extension of this setup from west-southwest (W-SW) to east-northeast (E-NE). This zone forms as cold air masses from northern or eastern Europe meet warmer, moisture-laden air masses from the Mediterranean, resulting in southerly winds that precede the advancing low-pressure system.

This convergence zone creates a dynamic interplay between atmospheric and topographical factors, significantly influencing snowfall distribution. Meteorologists must consider that this synoptic pattern typically shifts gradually, often moving north to south depending on the trajectory of the low-pressure system. For instance, when the system moves southward, regions such as Thessaly, Macedonia, and Epirus are most affected, experiencing significant snowfall (Ziakopoulos, 2008). These conditions may persist for four to seven days, though precise timing remains challenging due to natural uncertainties in extended forecasts.

The influence of terrain is critical in assessing snowfall distribution and intensity. Orographic lift, particularly along the Pindus Mountain range, amplifies precipitation on the windward side, while rain shadow effects reduce snowfall on the leeward side. Additionally, terrain features in regions like the Peloponnese further delineate climatic contrasts between western and eastern Greece, where local topography often dictates snow accumulation patterns.

2.9. Favorable conditions for snowfall in Athens

The atmospheric structure conducive to snowfall in Athens includes a stable stratification, a difference of 3°C between Temperature and Dew Point Temperature within the layer from 950 to 800 hPa, along with northerly winds from 950 to 750 hPa,

transitioning to northwesterly winds in the higher atmospheric layers (Prezerakos, 1984). Generally, synoptic conditions in Athens can be categorized into two types, A and B, based on the synoptic characteristics (Prezerakos & Angouridakis, 1984).

2.9.1. Type A

Type A conditions are predominantly linked to the presence of a strong surface anticyclone in the northwestern Europe, specifically over France, Switzerland and Germany, along with an extending ridge at the 500 hPa level generating northwest winds. Concurrently, a field of low pressure emerges in the southeastern Mediterranean area, primarily due to a recession approaching from the west or because of a maximum vorticity originating from the north or northwest. In such scenarios, the air masses transported to our region from Scandinavia or further north are of polar or even arctic origin.

Characteristics of type A include its prominence as the most frequent type of snowfall occurrence, accounting for approximately 65% of instances, with the highest frequency in January. Snowfall can persist for up to three days in the Attica region. Snow forecast criteria include a thickness of 1000-500 hPa measured at 5280 gpm above Athens, temperatures at the 850 hPa level ranging from -11°C to -5.5°C, and temperatures at the 500 hPa level from -35°C to -29.5°C. Geopotential heights are between 1330-1585 gpm at the 850 hPa level and 5270-5385 gpm at the 500 hPa level. Surface winds from the northwest also play a crucial role in shaping these conditions.

2.9.2. Type B

Type B conditions typically occur with a frequency of 35%, peaking during January and February. This synoptic setup allows for up to two days of snowfall in the Attica region. Furthermore, it is characterized by the presence of a strong, mixed-type anticyclone in Eastern Europe, north of Greece, and low-pressure areas in the Eastern Mediterranean, affecting Eastern Greece. This combination of barometric pressures generates strong northeast winds and typically leads to heavy snowfall on the eastern parts of Greece (Attica, Euboea etc.), while weather in Western Greece tends to be predominantly clear. With this synoptic situation, Athens may experience two or more days of snow. A significant factor in these conditions is the moisture supply to the air masses from the Aegean Sea (known as “Snow Aegean effect”), which influences the precipitation patterns. Moreover, the key system in this case is a warm-type anticyclone

over Scandinavian Peninsula, at the 500 hPa level, which is a crucial element of the so-called omega-type circulation. Air masses on the eastern flanks of the anticyclone are transported to our area from Ukraine or even further north.

As for the criteria for forecasting snow under Type B, a thickness of 1000-500 hPa measured at 5280 gpm above Athens is crucial, similar to Type A. Temperatures at the 850 hPa level range from -13°C to -7°C, while at the 500 hPa level, they range from -31.5°C to -23.5°C. Geopotential heights are observed between 1390-1505 gpm at 850 hPa and 5400-5460 gpm at 500 hPa. Surface winds generally blow from the northeast, in contrast to Type A.

2.10. The most significant snowfall events in Athens since 1911

According to the National Observatory of Athens, the most significant weather event occurred in February 1911. Since 2000, the heaviest snowfall recorded in Athens was in 2008, when 25 cm of snow fell. This was closely followed by Elpida snowfall in 2022, which brought approximately 20 cm of snow, alongside Medea, which occurred 11 months earlier (February 2021). Slightly less important are the snowfall of 2002 and 2004 when snow depths of about 15 cm were registered.

It is also worth noting that the snowstorm of Elpida is unprecedented in the scale and extent of electrical activity, while lesser-intensity snowstorms were recorded during the initial phase of the 2004 snowfall and Medea snowfall in 2021 (Table 2.5).

Table 2.5: *The most significant snowfall events in Athens over the past 114 years, as well as the absolute minimum temperatures recorded by the meteorological station of the National Observatory of Athens in Thissio. (https://www.meteo.gr/article_view.cfm?entryID=2113)*

Date	Lowest Temperature (°C)	Snow Amount (cm)	Duration of Snowfall (hours)
08-11/02/1911	-5.2	150	-
02-6/02/1929	-5.0	50	-
14-15/02/1934	-5.7	30	48
01-04/01/1942	-4.4	30	-
17-18/01/1964	-2.3	20	48
18-19/02/1983	-4.0	10	36
09/03/1987	-2.0	15	12
4-6/01/2002	-3.0	15	48
12-13/02/2004	-4.8	15	20
17-18/02/2008	-5.0	25	30
16-17/02/2021	-0.9	15	22
24/01/2022	-0.2	20	18

3. METHODOLOGY AND DATA

3.1. Selection of the cases ‘Elpida’ and ‘Medea’: Importance and Context

In the present study, the snowstorms ‘Elpida’ (January 2022) and ‘Medea’ (February 2021) were chosen as the primary case studies for detailed analysis due to their significant societal and economic impacts on Greece, particularly in the regions of Attica and Euboea. Their selection offers a unique opportunity to examine severe snowfall events that caused widespread disruptions and highlights the necessity of enhancing forecasting and nowcasting techniques. Their recent occurrence ensures access to comprehensive and high-resolution data, offering significant advantages over older events and aligning perfectly with the research objectives.

The availability of advanced satellite products by EUMETSAT further justifies their selection. Tools such as RGB composites (Day Microphysics RGB, Severe Convection RGB) and Cloud Top Height (CTH) became widely operational only after 2020, coinciding with the timeframe of these storms. These products provide enhanced insights into cloud dynamics and microphysical properties. However, while newer satellite products (e.g., Blended SEVIRI/LEO MW precipitation, Rapidly Developing Thunderstorms) became operational after 2022 offering additional analytical capabilities for studying snowfall mechanisms, they could not be applied to these cases, underscoring the potential for future research.

3.1.1. Overview of ‘Elpida’

Elpida snowstorm was an extreme meteorological event that lasted from January 23 to January 26, 2022, including a significant cold wave in Greece and Turkey. In Greece, the storm primarily impacted Attica, Euboea, the islands of Cyclades and Crete. It brought snowstorms and drastically low temperatures (-18.1^{o}C in Lefkochori, Pthiotida), along with snow accumulation reaching up to 70 cm at its peak.

During the days leading up to the Elpida snowstorm, atmospheric conditions were characterized by a shift of large-scale weather patterns. Moreover, a persistent ridge over Western Europe, and a series of troughs in the jet stream to its east facilitated multiple outbreaks of polar air into the Balkans and Eastern Mediterranean.

On January 21, a weak low-pressure area formed near the Aegean Sea due to a stronger low moving southeast from Western Russia, which was part of the synoptic setup pushing polar air towards Southeast Europe. This scenario was conducive to frontal snowfall, with "lake-effect" snow squalls expected to be a significant contributor of the snow totals because of temperature contrasts between the warm sea surfaces and the incoming cold air (Patlakas et al., 2024). The HNMS reported that this weather phenomenon exhibited unusual meteorological events such as a landspout on Andros (Fig. 3.1) and thundersnows in Euboea and Attica (Fig. 3.2 & Fig. 3.3), driven by the instability of this cold air passing over the relatively warmer waters of the Aegean Sea, which activated the "lake-effect" snow.

This storm brought significant weather disturbances in Greece. In Athens, citizens were stranded for up to 24 hours on Attiki Odos, which is the primary ring road encircling the capital. The situation escalated to the point where the Greek army was deployed to distribute essential supplies. Approximately 3500 citizens were rescued from the ring road, although 1200 vehicles remained immobilized due to the freezing conditions. Similar issues were reported also in Turkey. Notably, the effects of Elpida extended as far as Israel.



Fig. 3.1: Landspout in Stenies (Andros) on January 24, 2022. (*https://x.com/meteogr/status/1485553738530148357*)




Fig. 3.2 & 3.3: Pictures taken on January 24, 2022, in Agia Paraskevi, Attica.

3.1.2. Overview of 'Medea'

Medea was a significant and intense cold invasion that lasted four days, from February 13 to February 16, 2021, impacting the entire country. Cold air masses originating from Northern Europe merged with the considerably warmer and more humid air masses from the Mediterranean. This convergence led to the formation of strong barometric systems in the region. Although the extreme weather phenomena persisted for four days, it is noted that severe frost during the morning hours was observed at least until February 19 (Lagouvardos et al., 2021).

The cold wave impacted numerous areas bringing snow even to coastal regions of mainland of Greece, along with numerous Aegean islands. Some places in Crete were also affected by this cold wave. Furthermore, according to the Hellenic National Meteorological Service (HNMS), the snowfall was particularly intense in the aforementioned areas, with Attica, Boeotia and Euboea being the most hard-hit (Papapetrou & Karatarakis, 2021).

In addition to the amount of snow in Attica (Fig. 3.4 & Fig. 3.5), the weather system brought unusually low temperatures, with the coldest day recorded on February 16. The region of Western Macedonia experienced notably severe frost (Lagouvardos et al., 2021). Specifically, an extremely low temperature of -25.1°C was recorded in Neos Kafkasos, a small village located in Florina, on the morning of that day, according to the

National Observatory of Athens (NOA). On the same day, temperatures between -0.8°C and -0.6°C were recorded around the suburbs of Athens. It is worth mentioning that gale-force winds, reaching speeds of up to 97 km/h, were also recorded.





Fig. 3.4 & 3.5: Pictures taken on February 16, 2021, in Keratsini, Attica.

This extreme weather system caused major disruptions in the sea and road transport, rendering some roads impassable. Additionally, the storm caused power outages in Athens and some suburbs. This snowstorm tragically resulted in the loss of three lives.

3.2. Methodology

The methodological framework adopted in this study is centered on two primary objectives: analyzing the atmospheric dynamics and synoptic scale and mesoscale patterns leading to each snowstorm and leveraging satellite imagery to characterize cloud dynamics, particle properties, and snowfall patterns. This structured approach ensures a multi-dimensional understanding of the meteorological processes and enhances the effectiveness of forecasting methods.

The first component involves a detailed examination of the atmospheric dynamics and synoptic-scale conditions that precipitated the snowstorms. By analyzing the synoptic scale atmospheric circulation, the storms can be classified as Type A or Type B, based on the criteria discussed earlier in the theoretical framework. This comparative

analysis identifies both shared and distinct meteorological drivers, providing insights into the similarities and differences between Elpida and Medea.

Building upon this synoptic-scale analysis, the second component focuses on leveraging satellite products to assess cloud and snowfall characteristics. Visible and infrared imagery provides an initial assessment of cloud cover and thermal properties, while Airmass RGB is employed to differentiate between air masses and track atmospheric dynamics. Subsequently, Cloud Top Height (CTH) data offers valuable information about the vertical structure of clouds and their connection to snowfall and intensity. Day and Night Microphysics RGB products further enhance this analysis by identifying cloud particle size, phase transitions, and other microphysical properties relevant to heavy snowfall. Severe Convection RGB is then used to pinpoint regions of strong convection, identifying areas with large and small ice particles to assess the severity of convection within the snowstorm systems.

This combined analysis of atmospheric and satellite imagery ensures a comprehensive examination of each snowstorm, integrating synoptic-scale observations with mesoscale and microphysical insights. By synthesizing these tools, the methodology not only aims to deepen the understanding of ‘Elpida’ and ‘Medea’, but also contributes to advancing snowfall prediction and nowcasting techniques, with broader implications for severe weather forecasting.

3.3. Data Sources Overview

This study integrates a variety of data sources to analyze the ‘Elpida’ and ‘Medea’ snowstorms, combining atmospheric model outputs, satellite products, and observational data. Atmospheric dynamics and synoptic-scale patterns were examined using GFS analysis data, which provided key variables such as geopotential heights, temperature fields, and wind vectors.

For a higher-resolution analysis, dynamical downscaling was performed using the Advanced Weather Research and Forecasting Model (WRF-ARW) version 4.1.3 (Skamarock et al., 2008; Powers et al., 2017; Skamarock et al., 2019), a limited-area atmospheric model, based on a fully-compressible, non-hydrostatic dynamic core and driven by ERA5 reanalysis data. The model was set up to run with three two-way nested domains (9-3-1 km). Key physics options and parametrizations included the Thompson microphysics scheme (Thompson et al., 2004), Kain-Fritsch cumulus parameterization

(Kain, 2004), RRTMG radiation schemes (Iacono et al., 2008), and the Yonsei University (YSU) planetary boundary layer scheme (Hong et al., 2006). The coarser domain (9 km) provides an overview of large-scale atmospheric structures, focusing on mid-tropospheric dynamics (500-850 hPa). This output was particularly useful for assessing synoptic-scale features, such as troughs, ridges, and large-scale atmospheric forcing affecting the development of the snowstorms.

The fine-resolution domain was employed to capture mesoscale and localized weather phenomena. This output included both pressure levels (500-850 hPa) and surface-level data (2m, 10m), as well as accumulated snow and total precipitation, allowing for an in-depth examination of near-surface thermodynamics. All visualizations of WRF output, including maps of temperature, geopotential height, accumulated snow, 10m wind speed and direction, and total precipitation, were generated by the author using Python with specialized meteorological libraries.

Satellite data from the Meteosat Second Generation (MSG) satellites formed a cornerstone of the analysis, offering high-resolution visible, infrared, and RGB composite imagery. Products such as Airmass RGB, Cloud Top Height (CTH), Day and Night Microphysics RGB, and Severe Convection RGB were crucial for understanding cloud structures, microphysical properties, and the convective processes associated with snowfall. Observational records from the National Observatory of Athens (NOA) added critical information on surface-level conditions, including snow accumulation and temperature extremes.

Additionally, this research draws on relevant scientific literature and metadata from EUMETSAT to contextualize the satellite products and enhance the accuracy of the analysis. This comprehensive integration of data sources enables a detailed examination of the atmospheric processes and cloud dynamics underlying the selected snowstorms, advancing forecasting and nowcasting approaches for severe snowfall events.

4. ELPIDA SNOWSTORM

4.1. Analysis of Atmospheric Dynamics

4.1.1. Synoptic Setup Leading to the Elpida Snowstorm

Three days before the onset of severe snowstorms and blizzards in eastern Greece, on January 21, a large-scale omega block dominated the upper levels over the North Atlantic (Patlakas et al., 2024). This ridge began developing dynamically unstable features (Prezerakos et al., 1999), with the upper-level trough moving southward over the Balkans, which led to the formation of a closed cyclonic circulation at high altitudes, accompanied by a polar front jet streak along its western side. A zone of upper-level frontogenesis associated with strong northerly winds at 300 hPa became apparent over eastern Europe, where an extended closed diffluent system formed, trending south-southeastward and deepening (Fig. 4.1). At higher altitudes, a tropopause fold developed, linked to a stratospheric intrusion of cold air with high potential vorticity (Fig. 4.2), which has the potential to initiate surface cyclogenesis (Hoskins & Berrisford, 1988).

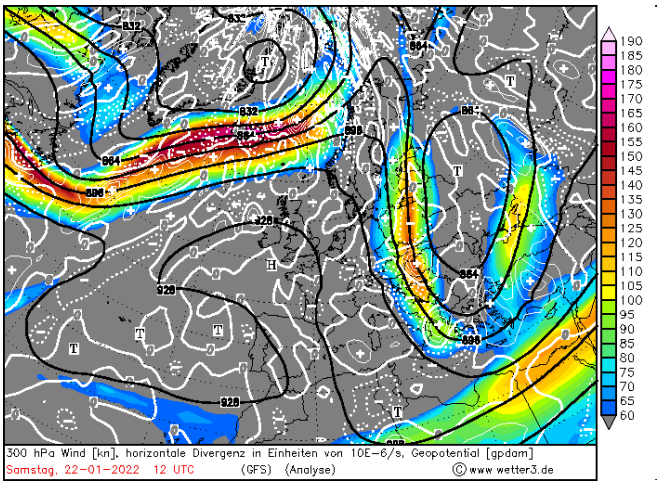


Fig. 4.1: 300 hPa geopotential (gpdam) & isotachs (ms^{-1}). (*https://www.wetter3.de/*)

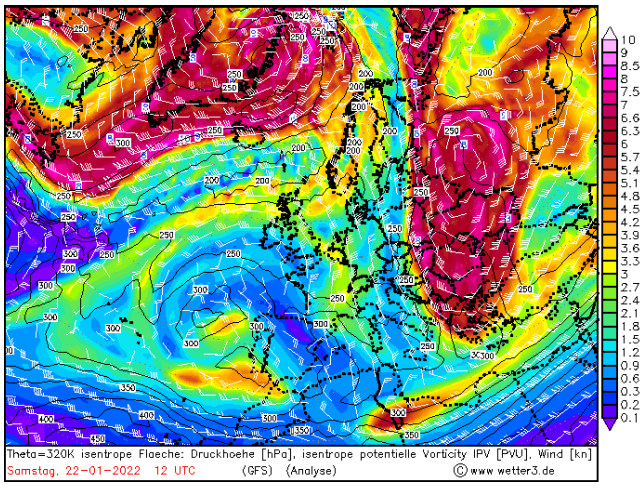


Fig. 4.2: 320 K isentropic potential vorticity (PVU) and wind field (knots). (*https://www.wetter3.de/*)

This atmospheric setup supported downstream development on the eastern edges of the block from north to south, further deepening the trough (Fig. 4.1). Consequently, from January 22nd at 12:00 to January 24th at 00:00, the 500 hPa trough, accompanied by cold air masses (around -35°C at 500 hPa), shifted from northern eastern Europe towards the Balkans and the Black Sea, showing rapid deepening. On January 25th at

00:00, a closed, nearly stationary low-pressure system established itself over Greece (Fig. 4.3). Winds over the Balkans shifted to a northerly/northeasterly direction, supporting the formation of a dynamically unstable ridge and secondary troughs (Prezerakos & Flocas, 1996). Additionally, strong cold air advection led to the establishment of extremely cold conditions, reaching temperatures as low as -42°C at 500 hPa over Greece (Fig. 4.4). The asymmetric wind structure of the deep trough implied an anticyclonic disruption, leading to the division of the circulation into two branches, with the southern branch facilitating the formation of a new surface cyclone (Fig. 4.3).

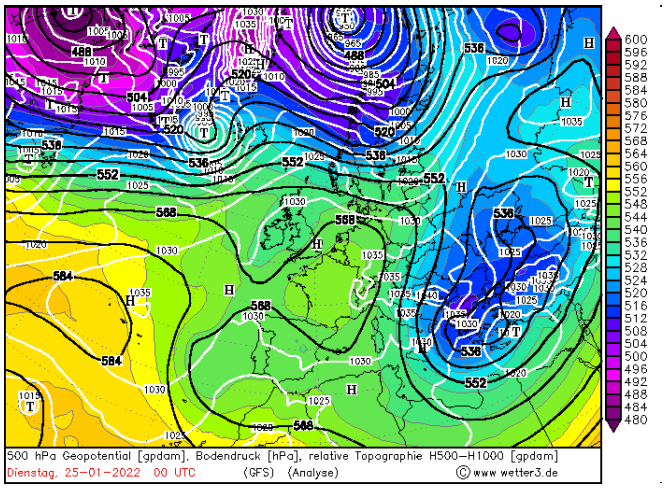


Fig. 4.3: Geopotential (gpdam) at 500 hPa, MSLP (hPa) & 1000-500 hPa Thickness. (*https://www.wetter3.de/*)

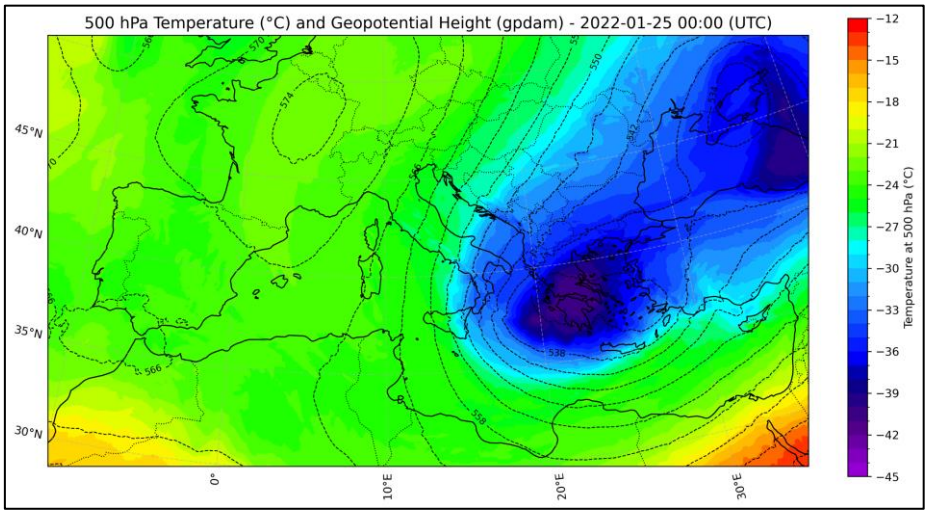


Fig. 4.4: Geopotential (gpdam) & Temperature (°C) at 500 hPa. (WRF 9 km)

At lower atmospheric levels, the cold front associated with a strong frontal depression over northeastern Europe advanced southward towards Greece. Due to cold air advection and a rise in pressure behind the cold front, a surface anticyclone moved from central Europe toward Greece between January 22 at 18:00 and January 23 at 18:00 UTC (Fig. 4.5), followed by a strong

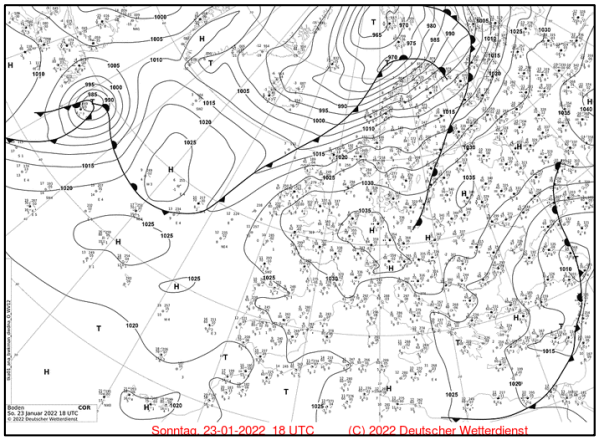


Fig. 4.5: DWD Surface Analysis. (*https://www.wetter3.de/*)

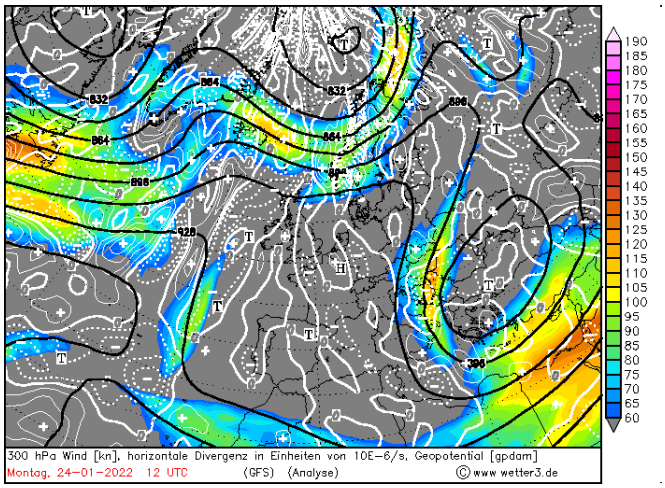


Fig. 4.6: 300 hPa geopotential (gpdam) & isotachs (ms^{-1}). (*https://www.wetter3.de/*)

northerly/northeasterly airflow over the Aegean Sea. This synoptic setup is typical during cold outbreaks in Greece (Houssos et al., 2007). However, in this instance, successive cyclonic disturbances caused by the upper-level downstream development hindered the usual prolonged influence of the cold anticyclone over Greece (Fig. 4.5).

Between January 24th at 00:00 and January 24th at 18:00, as the upper-level closed low moved from the eastern Balkans and the Black Sea towards Greece, it was accompanied by a polar front jet streak on its western edge (Fig. 4.6), triggering the development of a new shortwave upper-level trough. This trough initiated the formation of a surface cyclone with a central pressure around 1015 hPa (Fig. 4.7) over the southern Ionian Sea and southwestern Aegean Sea (Patlakas et al., 2024). Concurrently, the 850 hPa temperature dropped due to the gradual southward progression of the upper-level trough (Fig. 4.8).

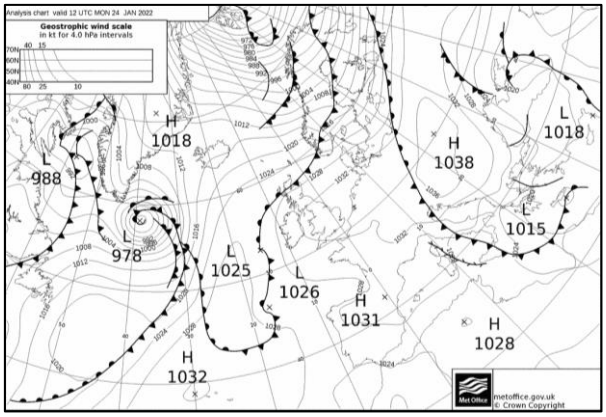


Fig. 4.7: Met Office mean sea-level pressure, based on GFS analysis data. (*https://www.wetter3.de/*)

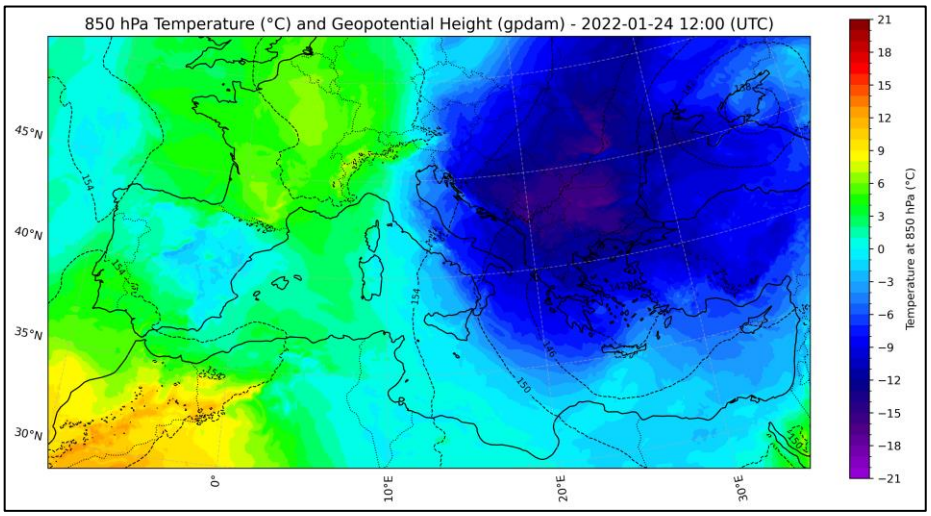


Fig. 4.8: Geopotential (gpdam) & Temperature (°C) at 850 hPa. (WRF 9 km)

The emergence of a closed and vertically organized cyclonic circulation over southern Greece, combined with the presence of the cold anticyclone over central Europe, caused the airflow to intensify from northern to southern Greece due to negative vorticity advection. These atmospheric conditions, together with the topography of eastern continental areas, created an environment favorable for heavy snowfall in Attica. Building upon the synoptic setup outlined above, the following section delves into the specific convective dynamics that influenced the snowfall patterns observed on January 24, 2022.

4.1.2. Convective Dynamics and Snowfall Patterns on January 24, 2022

On January 24, notable convective snowfall occurred across eastern Greece, including regions such as Euboea and Attica. Throughout the day, the Q-vector analysis at 500 hPa level highlighted strong convergence over the Aegean Sea, indicating substantial upward motion and convective activity (Fig. 4.10). Persistent northeasterly winds transported moist air from the sea towards Euboea and Attica, amplifying snowfall through the lake-effect mechanism.

GFS analysis data indicated the absence of high clouds above Greece, predicting only low to mid-level cloud cover (Fig. 4.9). However, satellite data captured cloud tops reaching 8-10 km, particularly over the Aegean Sea and locally over Euboea and northern Attica during peak periods. The interaction between cold air and warmer waters led to the formation of convective clouds at multiple altitudes. This caused widespread heavy snowfalls, significant snow accumulation, and lightning associated with snowstorms, which were observed in some suburbs of Athens after 20:00 (local time).

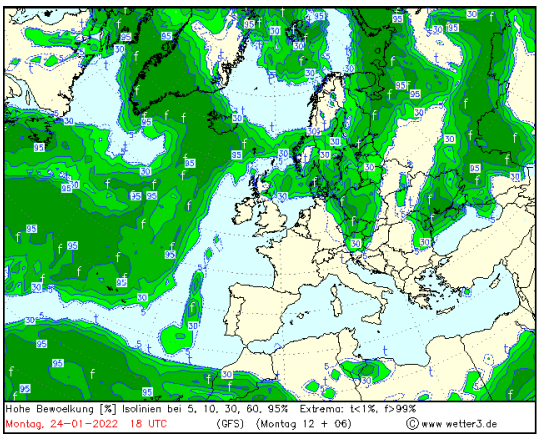


Fig. 4.9: High-level cloud cover on January 24. (*https://www.wetter3.de/*)

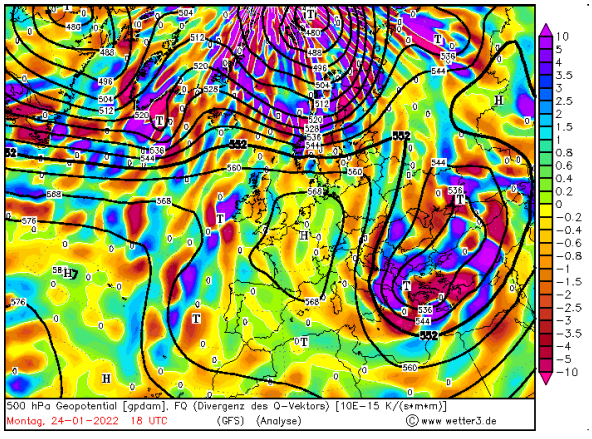


Fig. 4.10: Geopotential (gpdam) at 500 hPa & Q-Vector Divergence on January 24. (*https://www.wetter3.de/*)

In the following analysis, key atmospheric patterns based on both GFS analysis and WRF reanalysis data are presented, including geopotential heights, temperature distributions (Fig. 4.13 & Fig. 4.14), and surface winds (Fig. 4.12). These model charts will be examined alongside EUMETSAT'S various satellite products to provide a comprehensive view of the cloud development and convective processes that contributed to this intense snowfall in eastern Greece.

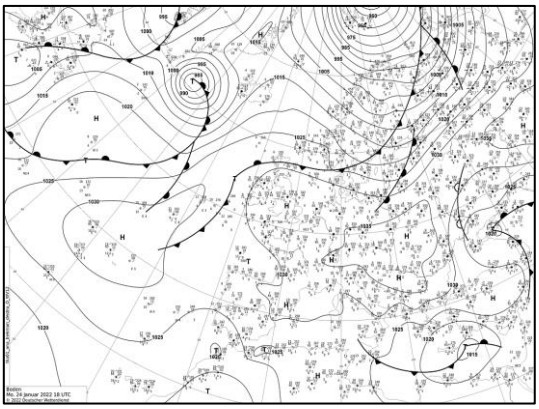


Fig. 4.11: DWD Surface Analysis on January 24. (*https://www.wetter3.de/*)

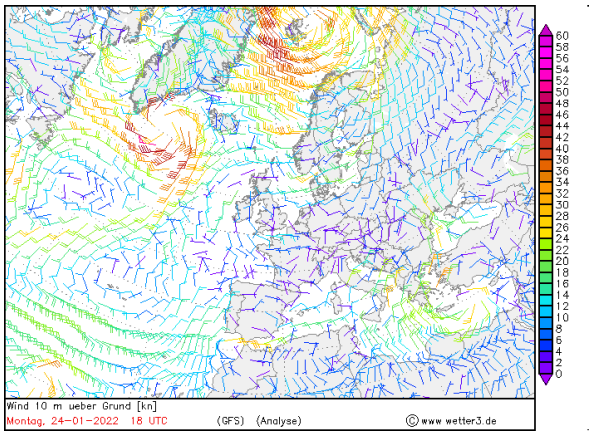


Fig. 4.12: 10m wind on January 24. (*https://www.wetter3.de/*)

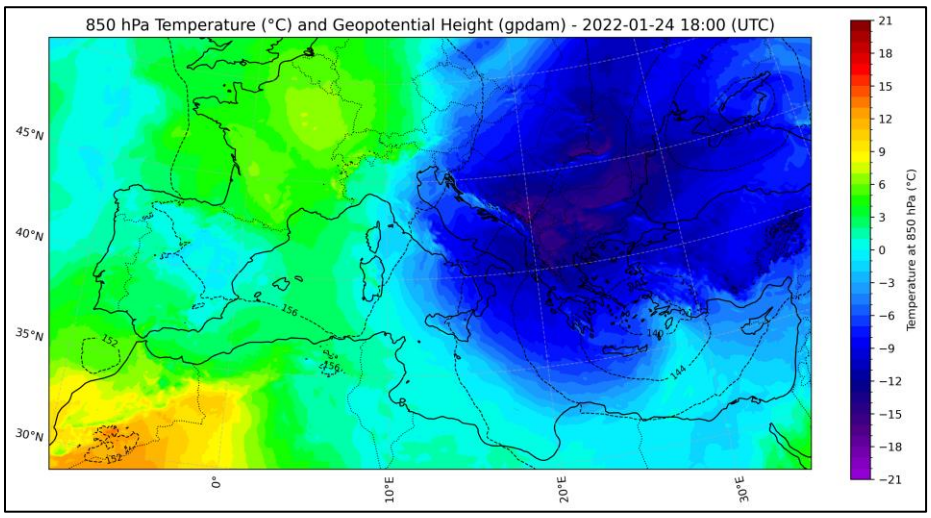


Fig. 4.13: Geopotential (gpdam) & Temperature (°C) at 850 hPa on January 24. (WRF 9 km)

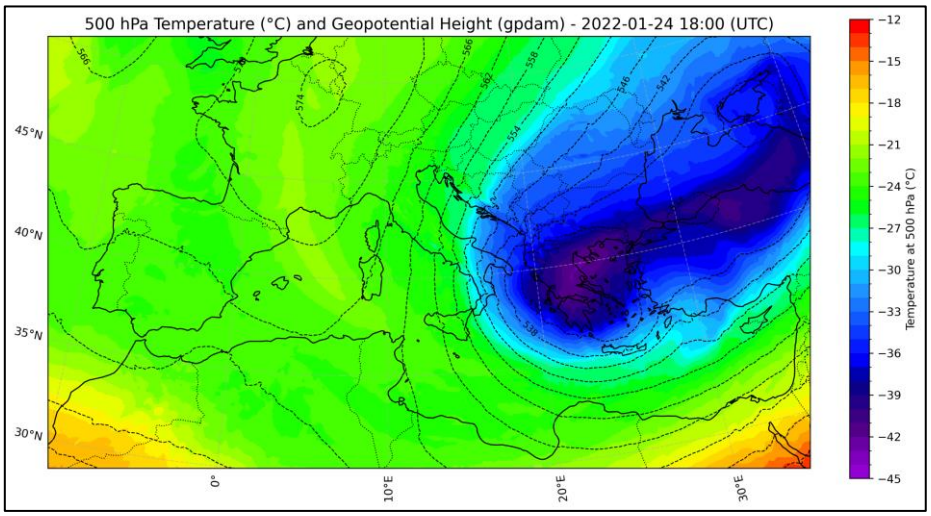


Fig. 4.14: Geopotential (gpdam) & Temperature (°C) at 500 hPa on January 24. (WRF 9 km)

Furthermore, the observed temperature values at the 850 hPa pressure level during the Elpida snowstorm were recorded as -7.5°C in the morning and -8.7°C in the afternoon of January 24, according to that day's radiosonde measurements (Table 4.1, Table 4.2, Fig. 4.27 & Fig. 4.28). These values closely align with the reanalysis data (Fig. 4.17 & Fig. 4.18). Concurrently, at the 500 hPa level, temperatures measured -35.9°C in the morning and decreased to -38.7°C by the afternoon, which similarly align with the reanalysis data (Fig. 4.19 & Fig. 4.20). Geopotential heights for these respective levels were approximately 1440-1480 gpdam at 850 hPa and between 5280-5360 gpdam at 500 hPa above Athens (Fig 4.25 & Fig. 4.26). The thickness between the 1000 hPa and 500 hPa levels was approximately 5160 gpdam, as indicated by radiosonde data and atmospheric model outputs on that day. Wind profiles revealed that between the 950 hPa and 750 hPa levels, the prevailing wind direction was from the N, shifting to NW above 550 hPa (Fig. 4.27 & Fig. 4.28). At the surface (10 meters height) winds were predominantly from N-NW, gradually shifting from midday onward to N-NE (Fig. 4.15 & Fig. 4.16).

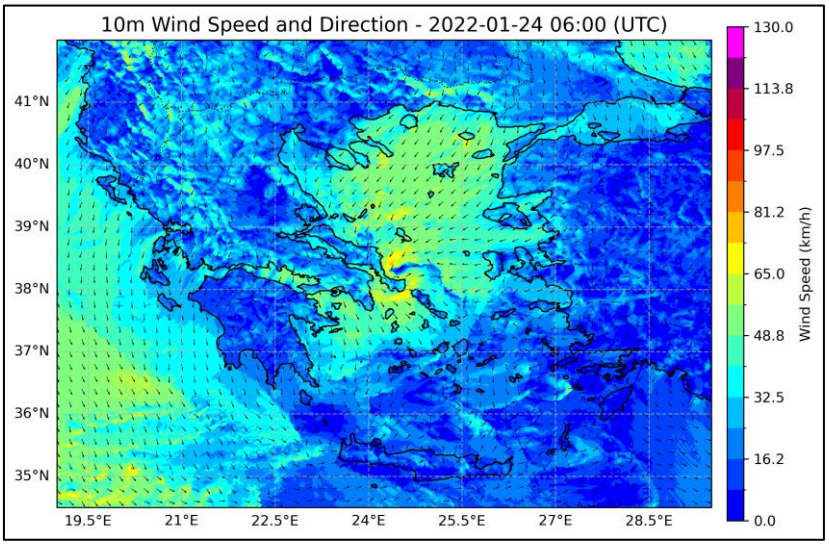


Fig. 4.15: 10m wind speed and direction on January 24, at 08:00 local time. (WRF 1 km)

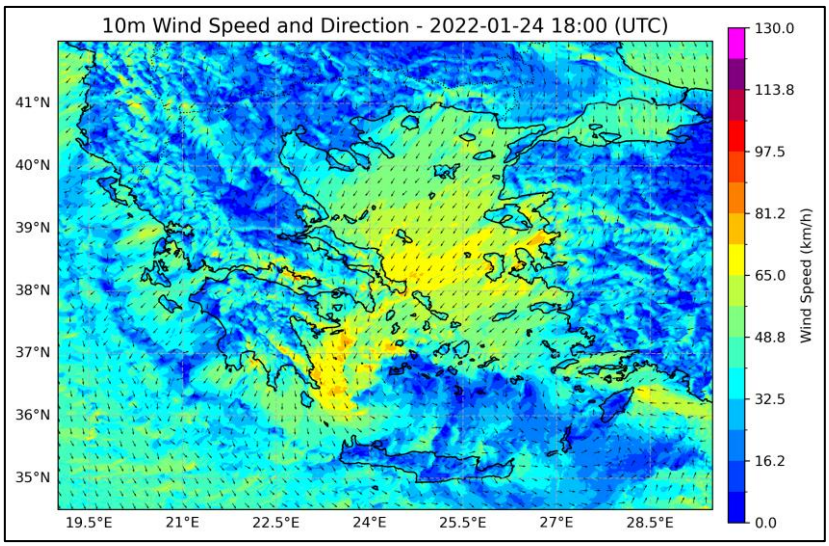


Fig. 4.16: 10m wind speed and direction on January 24, at 20:00 local time. (WRF 1 km)

Based on extensive meteorological analysis, it is evident that the Elpida snowstorm exhibited characteristics of both Type A and Type B snowstorm criteria, aligning more closely with Type A. This classification is

substantiated by the presence of a significant surface anticyclone in Northwest Europe, coupled with the development of a ridge at the 500 hPa level extending over France and Germany. Concurrently, a distinct cyclonic system was observed in the Southeastern Mediterranean region.

In conclusion, although Elpida exhibited some characteristics consistent with the colder and more severe criteria of Type B snowstorm, including both the “lake-effect” snow, the overall meteorological evidence and synoptic analysis more firmly categorize it as Type A event. This classification is primarily due to the specific temperature profiles, geopotential heights and the synoptic dynamics involving a ridge in northweastern Europe and a Mediterranean Low.

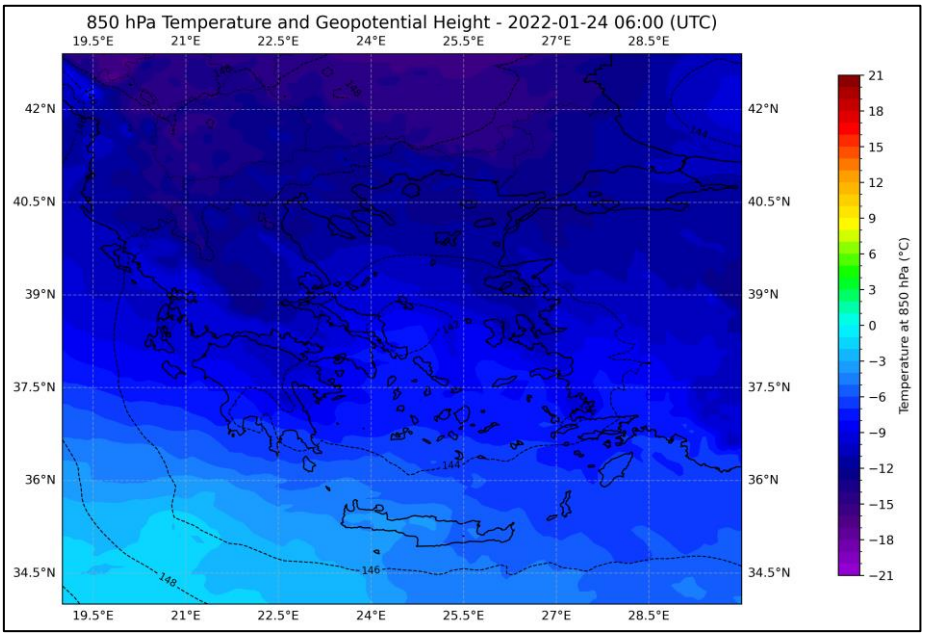


Fig. 4.17: Geopotential (gpdam) & Temperature (°C) at 850 hPa on January 24, at 08:00 local time. (WRF 9 km)

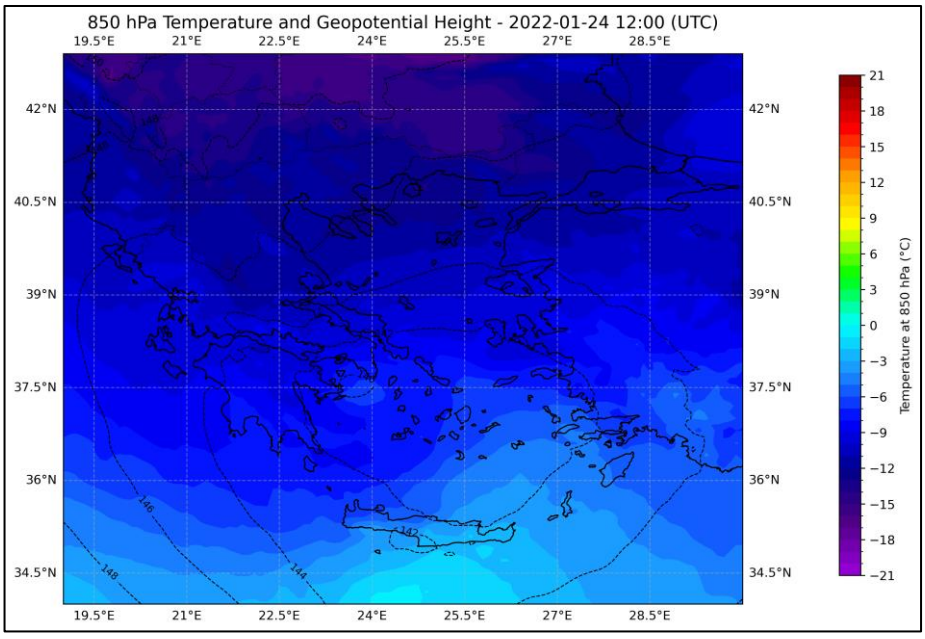


Fig. 4.18: Geopotential (gpdam) & Temperature (°C) at 850 hPa on January 24, at 14:00 local time. (WRF 9 km)

Table 4.1: *Radiosonde data from station 16716 LGAT Athinai (Airport) on January 24, 2022, at 08:00 local time. (https://weather.uwyo.edu/upperair/sounding.html)*

16716 LGAT Athinai (Airport) Observations at 06Z 24 Jan 2022

PRES	HGHT	TEMP	DWPT	RELH	MIXR	DRCT	SKNT	THTA	THTE	THTV
hPa	m	C	C	%	g/kg	deg	knot	K	K	K
1014	15	1.6	-7.4	51	2.17	340	7	273.7	279.8	274
1000	158	1	-7	55	2.27	350	16	274.1	280.6	274.5
931	728	-4.2	-7.4	79	2.37	355	24	274.5	281.2	274.9
925	779	-4.7	-7.4	81	2.38	355	26	274.5	281.2	274.9
909	916	-5.7	-8.6	80	2.21	349	28	274.8	281.1	275.2
898	1012	-4.7	-12.8	53	1.6	345	29	276.9	281.6	277.1
894	1048	-4.3	-14.3	46	1.42	345	28	277.6	281.8	277.8
867	1289	-6	-16.8	42	1.19	345	20	278.2	281.8	278.4
857	1380	-6.7	-17.7	41	1.12	339	19	278.5	281.8	278.6
850	1444	-7.5	-17.5	45	1.14	335	19	278.3	281.7	278.5
816	1757	-10	-19.7	45	0.99	320	19	278.9	281.9	279
774	2162	-13.3	-22.5	46	0.82	315	19	279.6	282.1	279.7
767	2232	-13.8	-23	46	0.79	330	14	279.7	282.2	279.9
755	2353	-14.8	-23.8	46	0.74	20	10	279.9	282.2	280.1
754	2363	-14.9	-23.9	46	0.74	20	10	279.9	282.2	280.1
700	2919	-20.1	-25.1	64	0.72	25	10	280.2	282.4	280.3
687	3057	-21.4	-25.5	70	0.71	40	9	280.2	282.4	280.3
662	3329	-24.1	-26.2	83	0.68	35	11	280.2	282.3	280.3
641	3563	-25.3	-32.3	52	0.4	31	12	281.4	282.7	281.5
615	3860	-28.1	-33.2	61	0.38	25	14	281.6	282.8	281.7
586	4206	-31.3	-34.3	75	0.36	16	16	281.8	282.9	281.8
584	4230	-31.5	-34.9	72	0.34	15	16	281.8	283	281.9
581	4267	-31.7	-35.7	68	0.32	10	16	282	283	282
568	4427	-31.7	-44.7	26	0.13	345	17	283.8	284.2	283.8
552	4628	-33.2	-45.3	29	0.12	315	19	284.3	284.8	284.4
551	4641	-33.3	-45.3	29	0.12	314	20	284.4	284.8	284.4
537	4821	-32.9	-54.9	9	0.04	299	27	286.9	287.1	287
534	4861	-33.1	-58.1	6	0.03	295	29	287.2	287.3	287.2
525	4979	-33.8	-57	8	0.03	285	34	287.7	287.8	287.7
500	5320	-35.9	-53.9	14	0.05	280	35	289.2	289.4	289.2
424	6452	-40.6	-64.5	6	0.02	280	67	297.1	297.2	297.1
411	6666	-41.5	-66.5	5	0.01	280	67	298.6	298.7	298.6
400	6850	-41.7	-68.7	4	0.01	280	67	300.7	300.8	300.7
366	7449	-43.3	-71	3	0.01	275	74	306.4	306.4	306.4
357	7617	-43.7	-71.7	3	0.01	276	72	308	308	308
347	7809	-43.3	-74.3	2	0	276	70	311	311	311
300	8780	-47.1	-75.1	3	0	280	59	318.9	318.9	318.9

Table 4.2: *Radiosonde data from station 16716 LGAT Athinai (Airport) on January 24, 2022, at 14:00 local time. (https://weather.uwyo.edu/upperair/sounding.html)*

16716 LGAT Athinai (Airport) Observations at 12Z 24 Jan 2022

PRES	HGHT	TEMP	DWPT	RELH	MIXR	DRCT	SKNT	THTA	THTE	THTV
hPa	m	C	C	%	g/kg	deg	knot	K	K	K
1015	15	0.2	-0.4	96	3.68	340	5	272.2	282.2	272.8
1005	115	-0.8	-1.2	97	3.5	330	10	272	281.6	272.5
1000	165	-1.3	-1.6	98	3.42	330	14	271.9	281.2	272.4
942	639	-3.8	-4.4	96	2.95	20	35	274	282.3	274.5
925	784	-4.5	-5.2	95	2.82	20	34	274.7	282.6	275.2
890	1087	-5.9	-8.3	83	2.31	27	34	276.3	282.9	276.7
850	1445	-8.7	-9.7	92	2.16	35	35	277	283.3	277.4
846	1481	-8.9	-9.8	93	2.15	35	36	277.1	283.4	277.5
816	1760	-10.7	-10.9	98	2.05	36	35	278.1	284.1	278.5
738	2524	-15.6	-19.1	75	1.15	40	31	280.9	284.4	281.1
728	2628	-16.3	-20.2	72	1.06	45	29	281.2	284.5	281.4
700	2921	-19.1	-21	85	1.03	60	22	281.3	284.5	281.5
667	3275	-22	-23.7	86	0.85	65	20	281.9	284.6	282.1
650	3464	-23.6	-25.2	87	0.76	45	15	282.2	284.6	282.4
622	3786	-26.3	-27.7	88	0.64	31	14	282.7	284.7	282.8
610	3926	-27.4	-29.7	81	0.54	25	14	283	284.7	283.1
587	4201	-29.6	-33.6	68	0.38	40	10	283.6	284.8	283.6
580	4287	-30.3	-34.8	65	0.35	38	9	283.8	284.9	283.8
544	4737	-34.5	-36.2	85	0.32	30	1	284	285	284
536	4841	-35.5	-36.5	90	0.32	2	3	284	285.1	284.1
509	5198	-38.5	-41.1	76	0.21	265	9	284.6	285.3	284.6
506	5238	-38.7	-43	64	0.17	254	10	284.8	285.4	284.9
505	5252	-38.7	-43.6	60	0.16	250	10	285	285.5	285
500	5320	-38.7	-46.7	43	0.12	260	13	285.8	286.2	285.8
488	5487	-38.7	-52.7	21	0.06	275	22	287.8	288	287.8

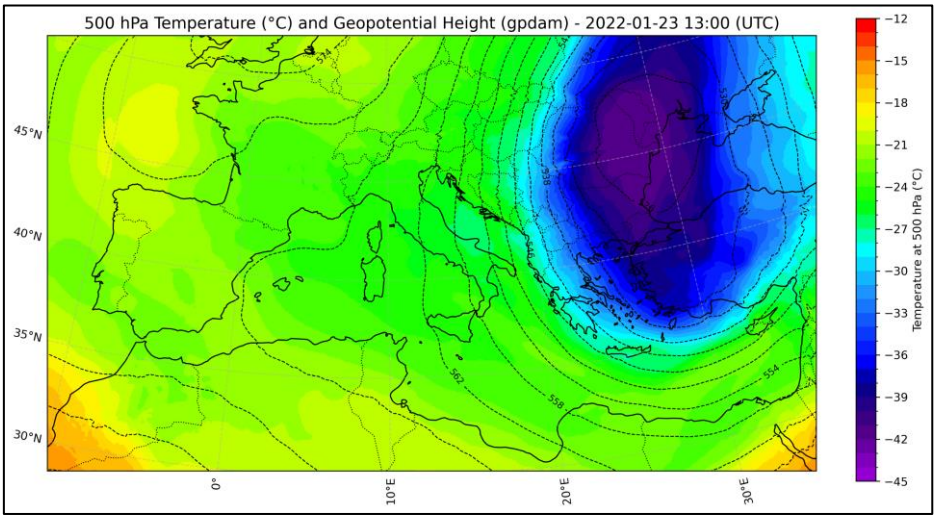


Fig. 4.19: Geopotential (gpdam) & Temperature (°C) at 500 hPa on January 23. (WRF 9 km)

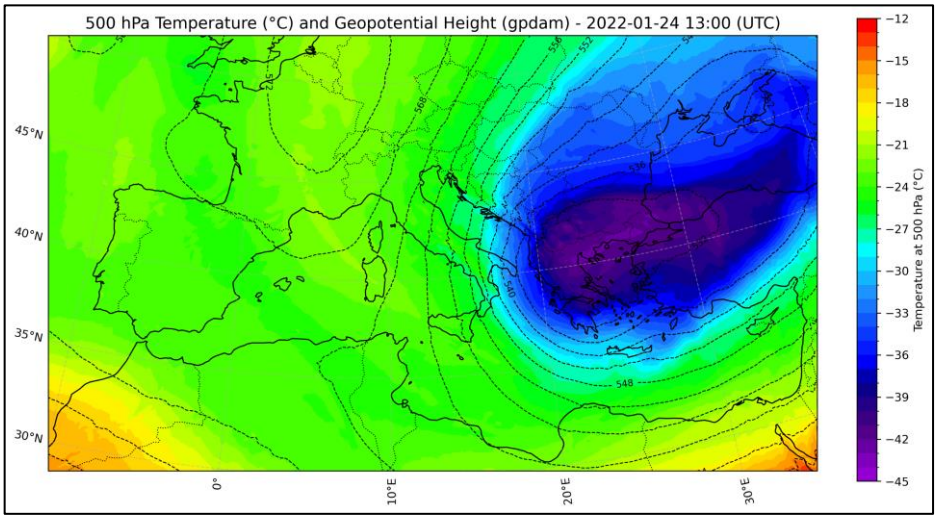


Fig. 4.20: Geopotential (gpdam) & Temperature (°C) at 500 hPa on January 24. (WRF 9 km)

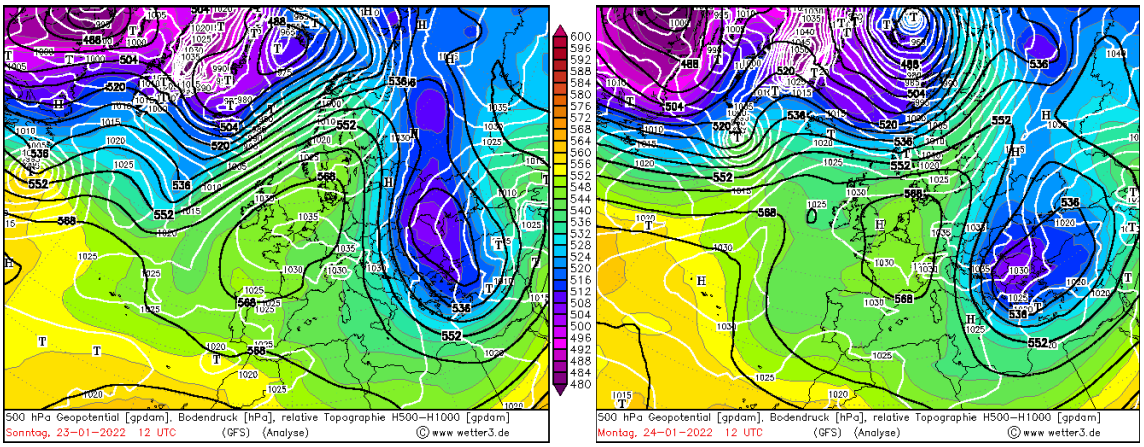


Fig. 4.21 & 4.22: Geopotential (gpdam) at 500 hPa, MSLP (hPa) & 1000-500 hPa Thickness on January 23 (left) and January 24 (right). (*https://www.wetter3.de/*)

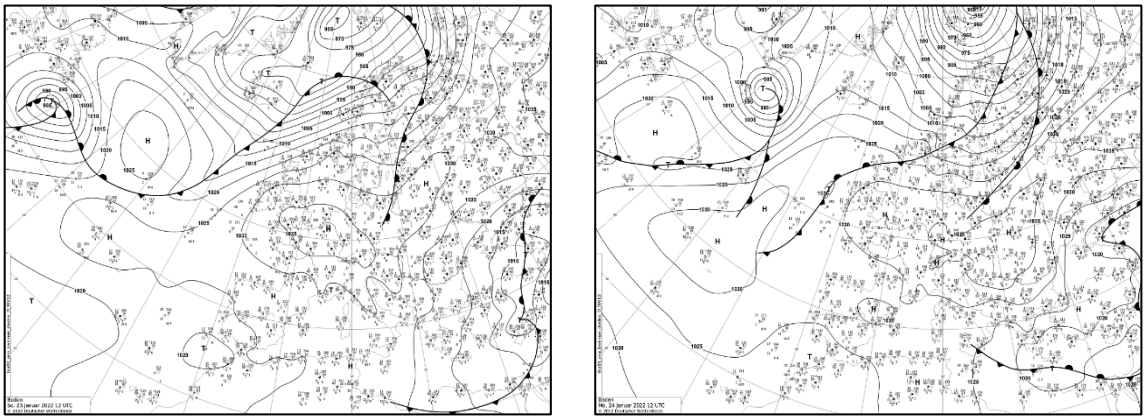


Fig. 4.23 & 4.24: DWD Surface Analysis on January 23 (left) and January 24 (right). (*https://www.wetter3.de/*)

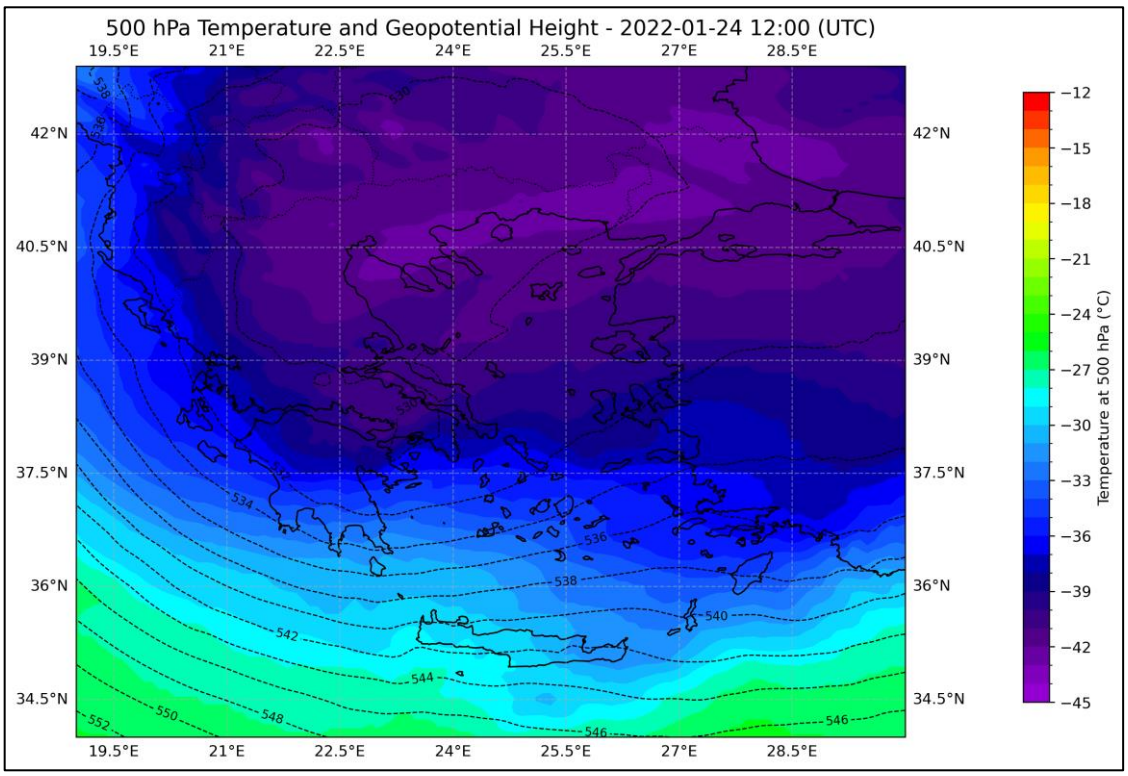


Fig. 4.25: Geopotential (gpdam) & Temperature (°C) at 500 hPa on January 24, at 14:00 local time. (WRF 9 km)

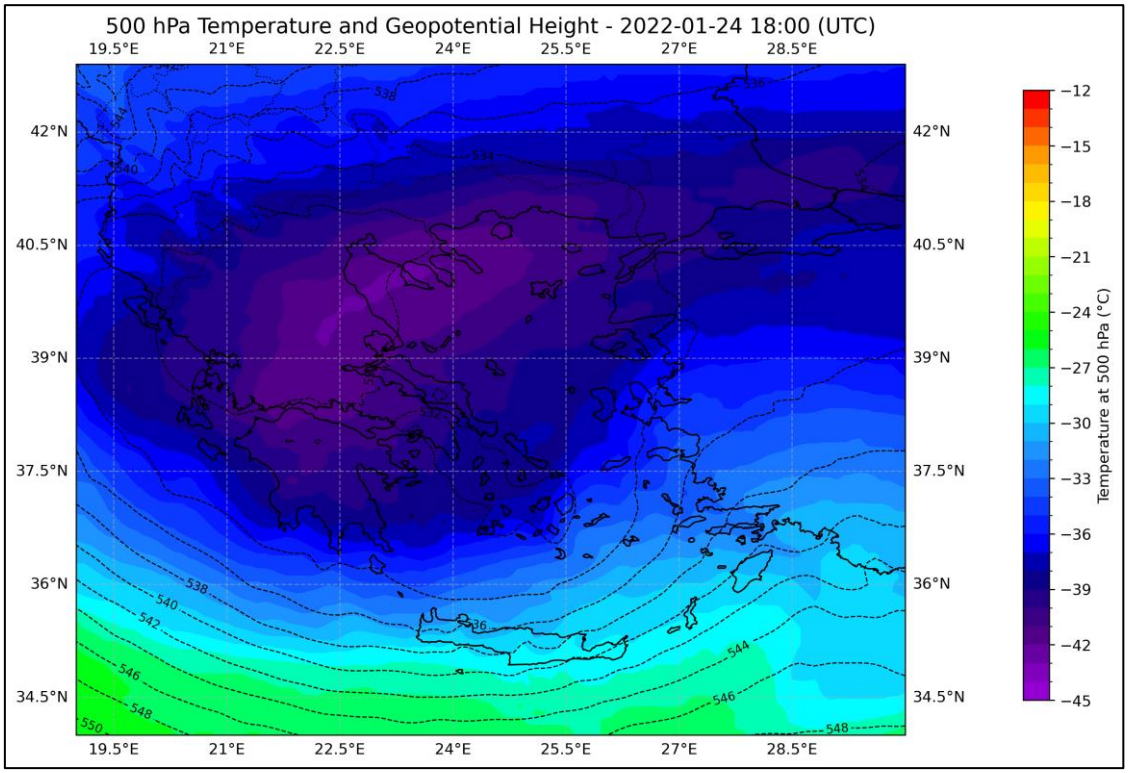


Fig. 4.26: Geopotential (gpdam) & Temperature (°C) at 500 hPa on January 24, at 20:00 local time. (WRF 9 km)

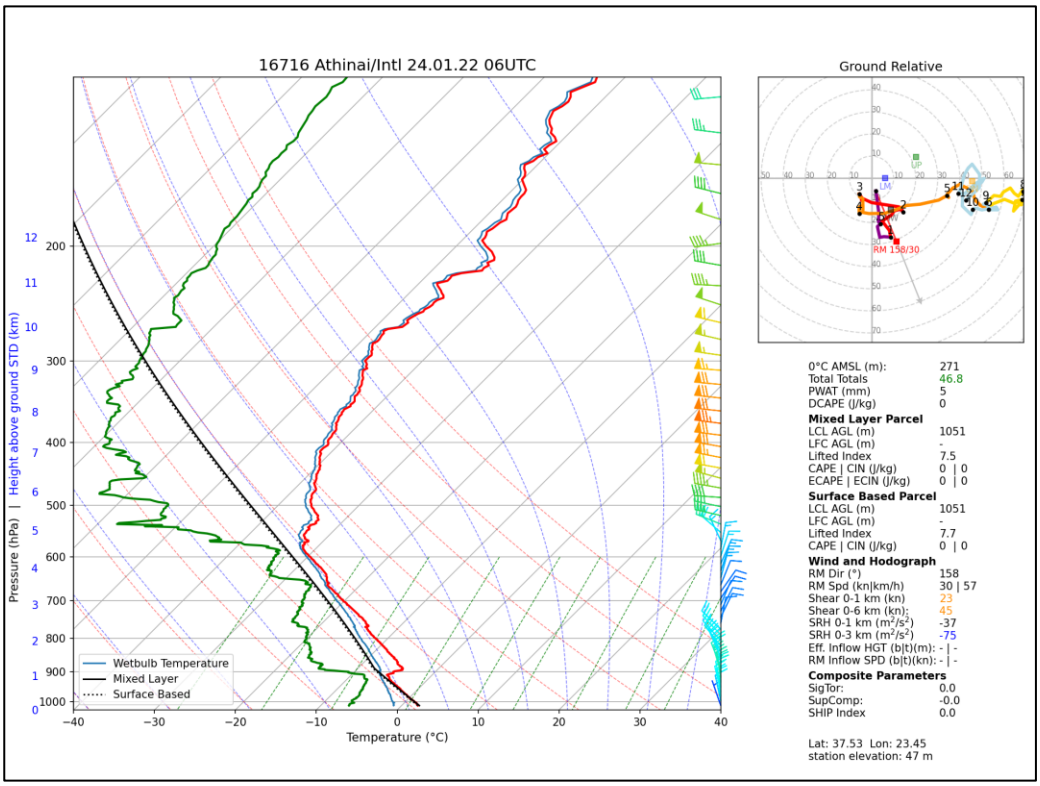


Fig. 4.27: Skew-T diagram from radiosonde data at station 16716 LGAT Athinai (Airport) on January 24, 2022, at 08:00 local time. (*https://meteologix.com/gr/*)

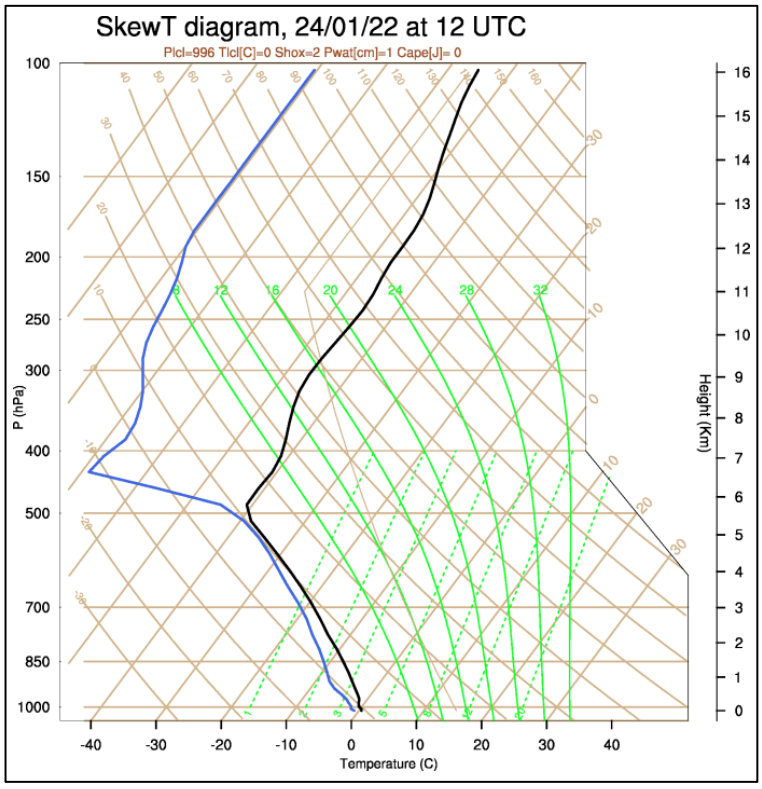


Fig. 4.28: Skew-T diagram at Elliniko, on January 24, 2022, at 14:00 local time, based on WRF reanalysis data.

4.2. Satellite-Based Analysis of Atmospheric Dynamics and Cloud Microphysics

4.2.1. Analysis of Cloud Coverage using Visible and Infrared Satellite Imagery

In the visible spectrum, we can see clear, bright white cloud bands over the Aegean Sea, moving into the area of Attica. The bright white coloration suggests high reflectivity, which could be interpreted as corresponding to a higher thickness of clouds. These cloud bands are associated with convective cloud structures, often featuring linear elements ranging from 30 km to hundreds of km in length.

During the day imagery, between 09:00 and 12:00 UTC, these clouds show high reflectivity in the visible channel (Fig. 4.29 & Fig. 4.30), which supports the hypothesis of thick cloud cover over the Aegean. In corresponding infrared channel imagery (Fig. 4.31 & Fig. 4.32), we can note very bright white or highly illuminated cloud tops, further indicating vertically extensive clouds with cold tops, characteristic of deep convection.

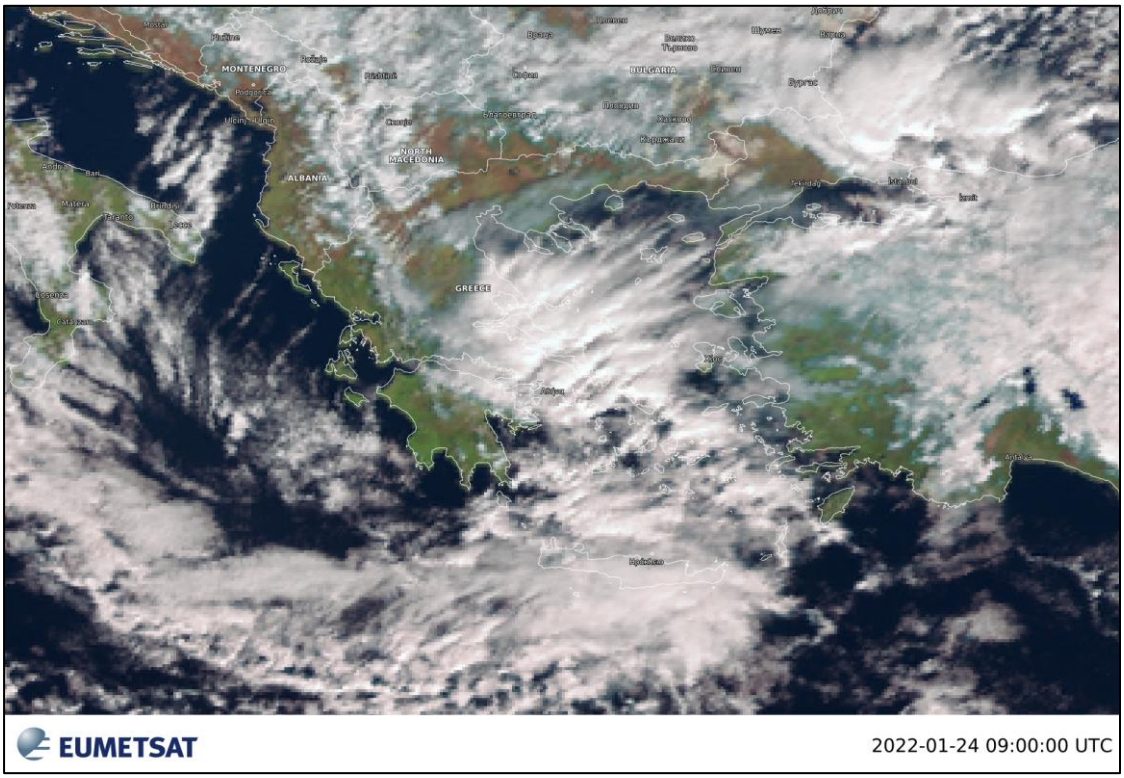


Fig. 4.29: Visible image at 09:00 UTC, on January 24. (*https://www.eumetsat.int/*)

Focusing specifically on the Attica region and the Athens basin, there is an apparent discrepancy in the intensity of cloud cover between the eastern and the western part. In the visible imagery, one notices that the eastern suburbs, particularly the area around the Hymettus Mountain and the surrounding areas, are more intensely white,

indicating thicker clouds. In contrast, the western suburbs and Piraeus show comparatively grayer tones, which we interpret as thinner clouds based on reflectivity observed in the visible spectrum.

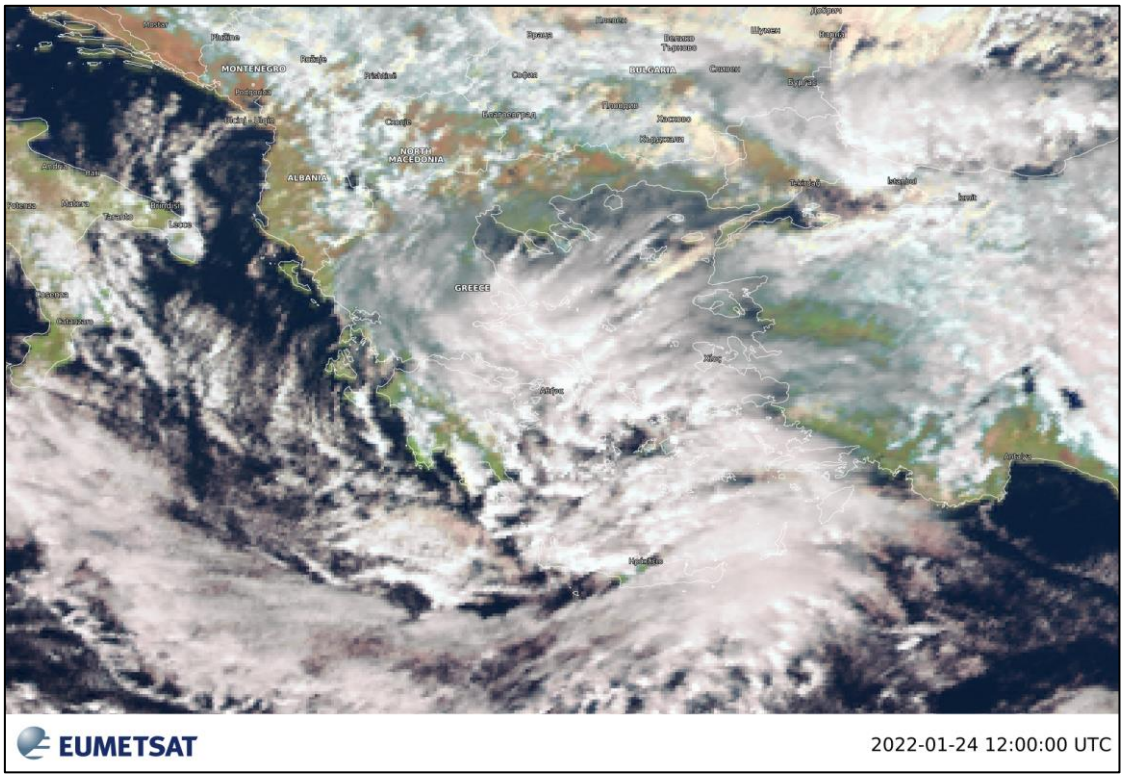


Fig. 4.30: Visible image at 12:00 UTC, on January 24. (*https://www.eumetsat.int/*)

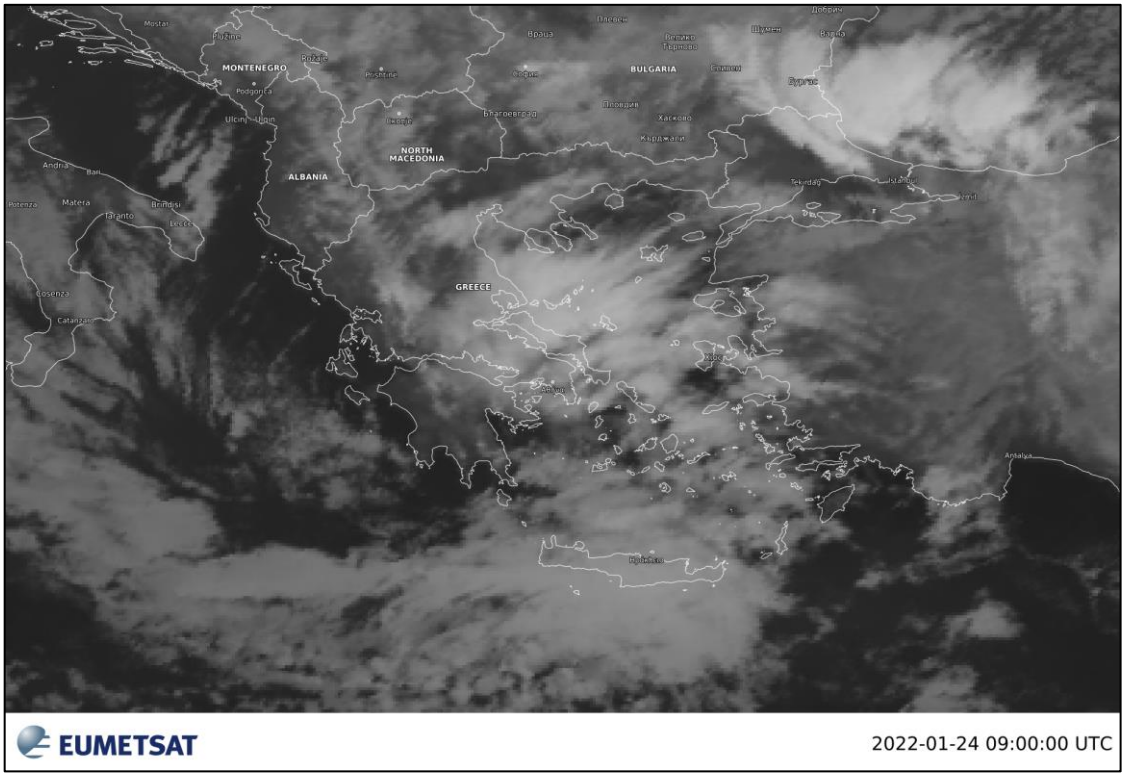


Fig. 4.31: Infrared image at 09:00 UTC, on January 24. (*https://www.eumetsat.int/*)

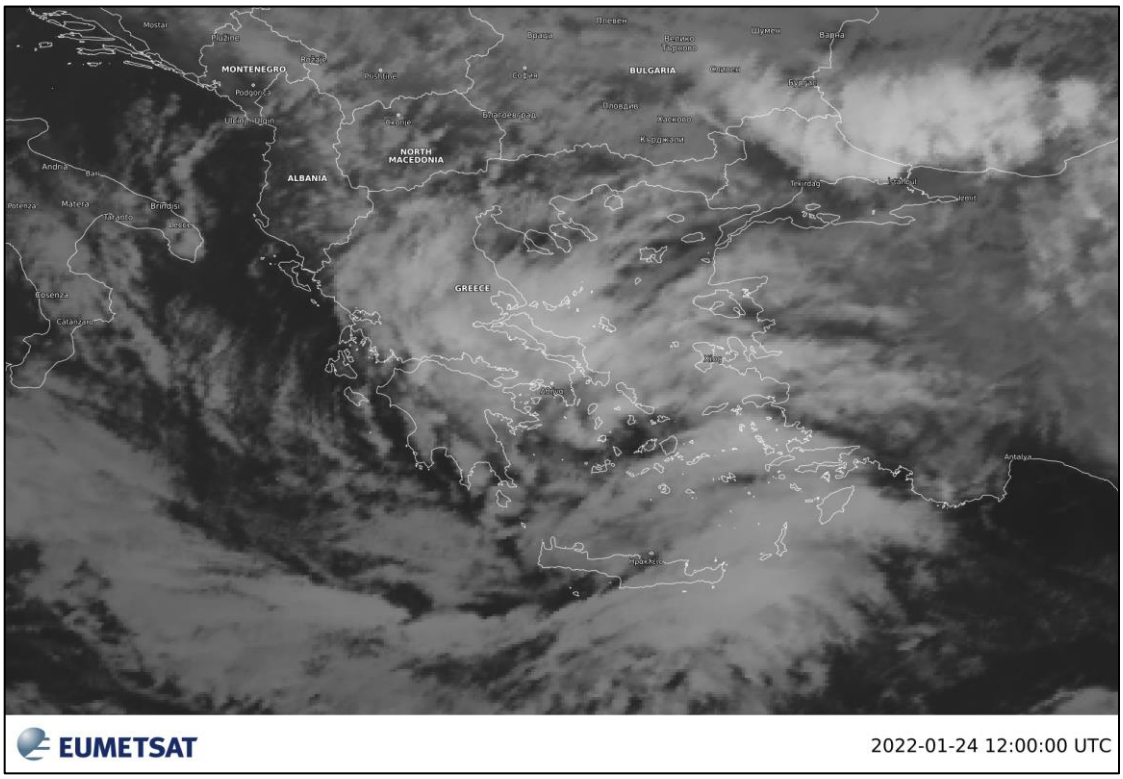


Fig. 4.32: Infrared image at 12:00 UTC, on January 24. (*https://www.eumetsat.int/*)

Furthermore, the infrared imagery supports this analysis by showing less intense white shades over the western areas, indicating not only thinner clouds but also lower cloud tops. The reduced brightness in the infrared implies that cloud tops are lower in altitude compared to those over the eastern suburbs. This combination of both thinner and lower clouds over the western parts explains the variation in snowfall, where heavier snowfall and accumulation were concentrated in the eastern areas affected by the thicker and higher-altitude clouds. Fig. 4.33 has been selected for its superior resolution, which is due to its acquisition from a polar-orbiting satellite, specifically MetOp. The higher resolution of AVHRR imagery allows more precise cloud structure analysis, essential for observing detailed cloud formations and assessing meteorological phenomena with greater accuracy.

Significant snowfall accumulation was restricted to the eastern and southern suburbs of Athens, the eastern Attica region and generally the region around Hymettus, while western suburbs and the area of Piraeus received less intense snowfall with little or no snow cover at all (Fig. 4.34). The latter probably was created by local wind circulation influencing cloud convergence zones and thus increasing the intensity of snowfall in specific areas. This role of winds in creating localized areas of convergence is consistent with the observation, as they contributed to the channeling of moisture and

cold air that drove convective cloud development and resulted in higher snowfall in specific zones across eastern Attica.

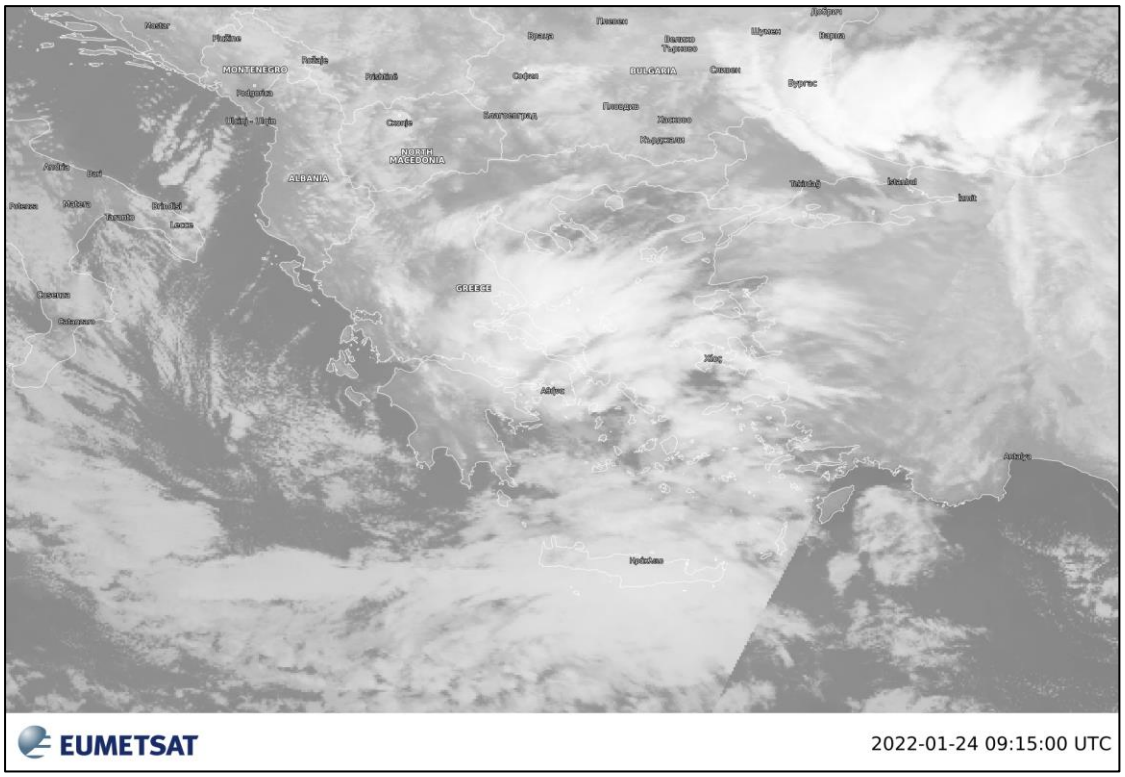


Fig. 4.33: Infrared high-resolution image at 09:15 UTC, on January 24. (*https://www.eumetsat.int/*)

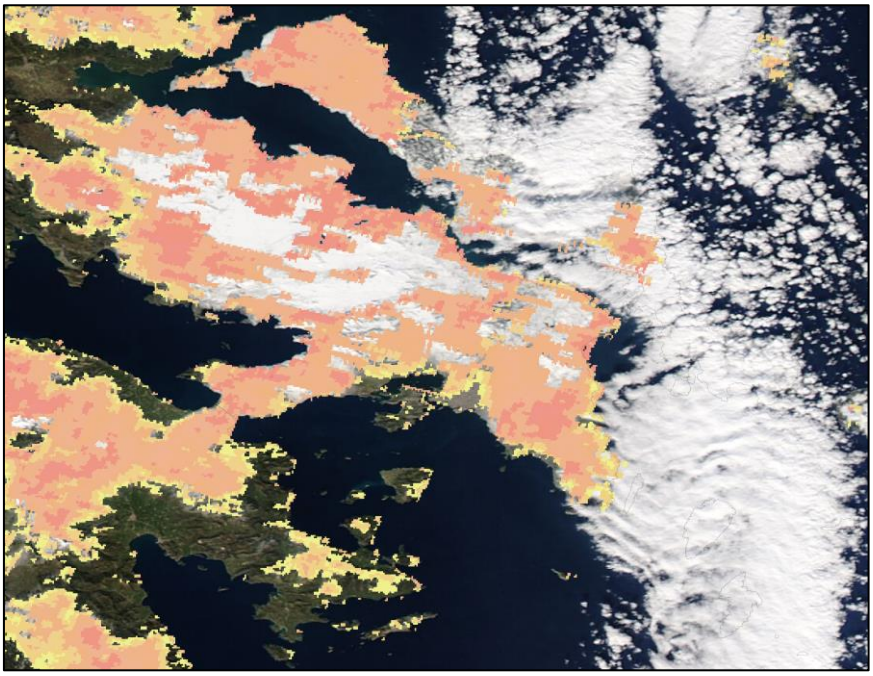


Fig. 4.34: Snow cover on January 26, 2022. Clouds depicted in white, while the intensity of snow cover is presented by color shades – the deeper orange-red hues indicate higher snow depths, whereas lighter yellow tones signify areas with less snow accumulation. (*https://worldview.earthdata.nasa.gov*)

4.2.2. Air Mass analysis using Airmass RGB

According to the color interpretation (Fig. 4.35), which provides visual guidance for distinguishing between various air masses and cloud types, we can observe a complex interplay of air masses and cloud structures above Greece. Northeastern Aegean and Black Sea display blue-purple hues (label 1), indicative of cold, ozone-rich polar air masses, descending from higher latitudes. This cold air is usually very stable but can bring strong surface-level cooling, enhancing the potential of snow when interacting with moist air near the surface. Moving southwestward, over the Ionian Sea and extending toward southern Italy, dark green shades (label 2) indicate warm, ozone-poor tropical air masses being advected northward from subtropical regions. Such warm air masses are typically moisture-laden in the upper troposphere, creating instability when they interact with colder air.

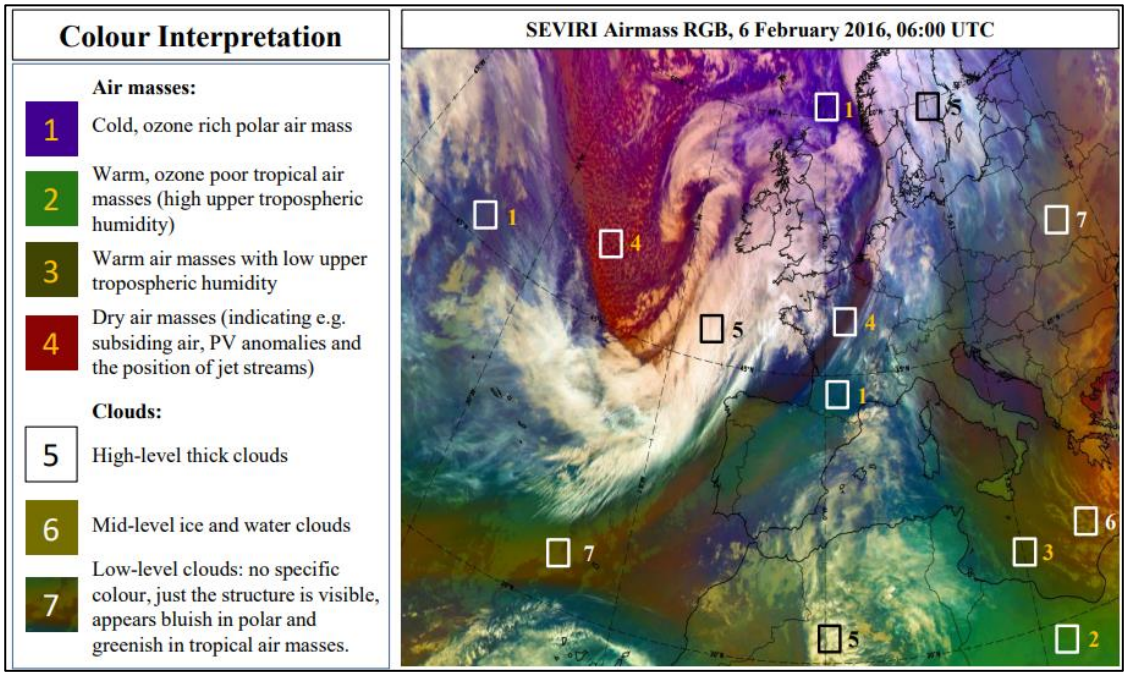


Fig. 4.35: This color interpretation provides visual guidance for distinguishing between various air masses and cloud types. (*https://www.eumetsat.int/*)

Over the Adriatic and western Greece, reddish-brown colors signal the presence of dry, subsiding air associated with PV anomalies and jet streams, further intensifying regional atmospheric instability. Light green hues (label 6) over southern Italy and parts of the central Mediterranean reveal mid-level clouds with a mix of ice and water particles, likely resulting in moderate precipitation. Additionally, high-level thick clouds (label 5) appear above the Aegean Sea and the eastern parts of continental Greece, linked to active frontal systems with significant moisture.

The sharp contrast between polar air masses in the north and tropical air masses to the south delineates a clear boundary over Greece, especially over the Aegean and eastern continental areas, forming a zone of cyclogenesis. Consequently, much of Attica and Euboea are covered by thick cloud structures typical of mid- to upper-level moisture convergence and convective activity. The interaction of cold polar air with warm, moist tropical air induces atmospheric lift, leading to cloud formation capable of producing precipitation. This setup suggests likely snowfall or mixed precipitation, depending on the surface and vertical temperature profiles. In Fig. 4.36 to Fig. 4.40, the different air mass types (1-4) and cloud types (5-7) are labeled with numbers based on it, allowing for easier identification.

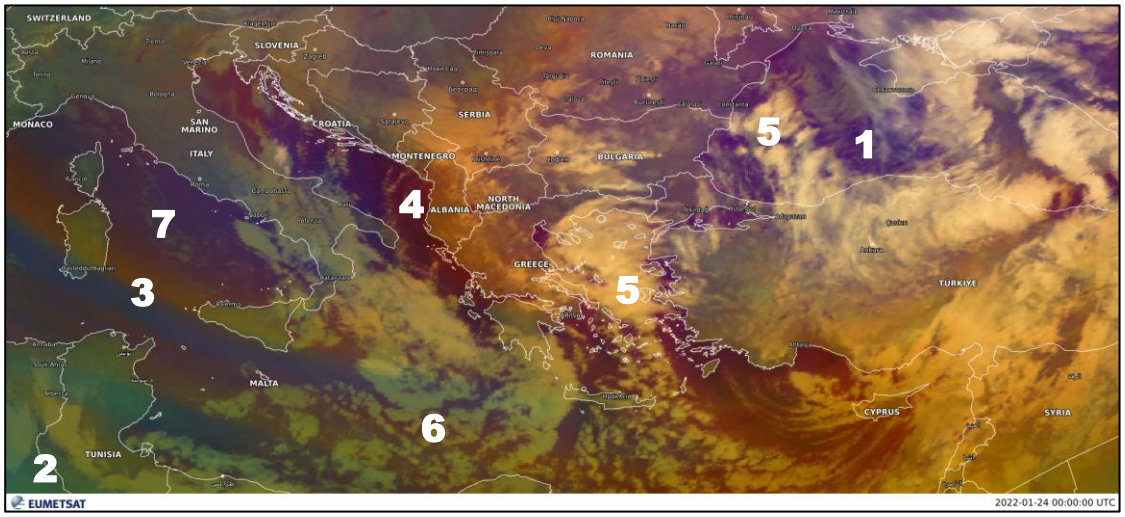


Fig. 4.36: Airmass RGB image at 00:00 UTC, on January 24. (*https://www.eumetsat.int/*)

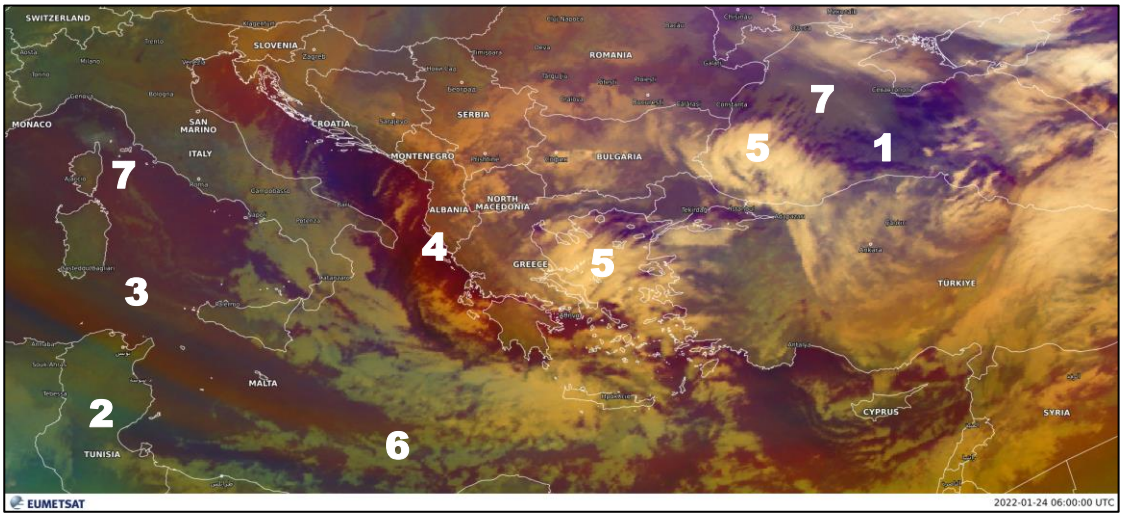


Fig. 4.37: Airmass RGB image at 06:00 UTC, on January 24. (*https://www.eumetsat.int/*)

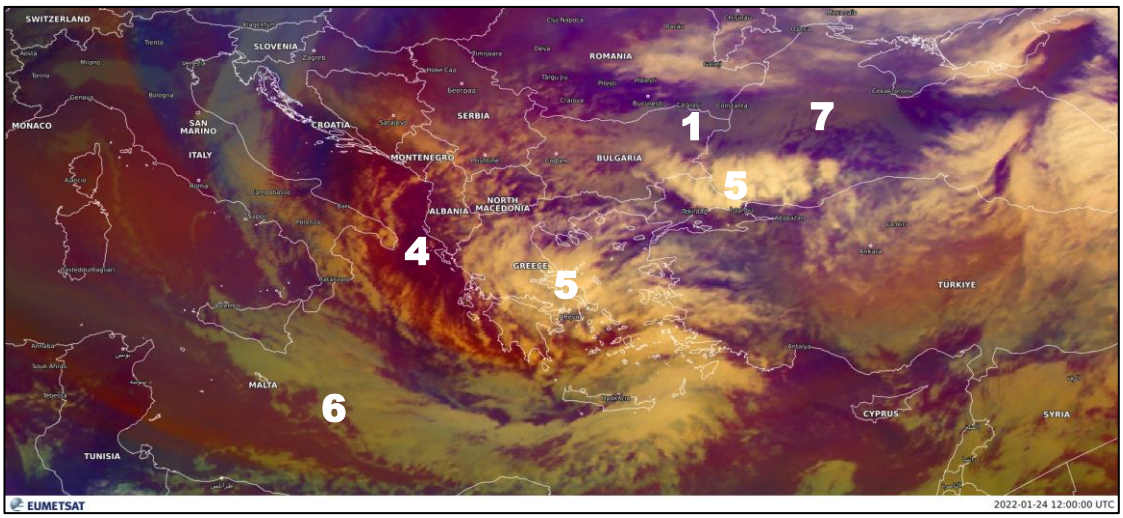


Fig. 4.38: Airmass RGB image at 12:00 UTC, on January 24. (*https://www.eumetsat.int/*)

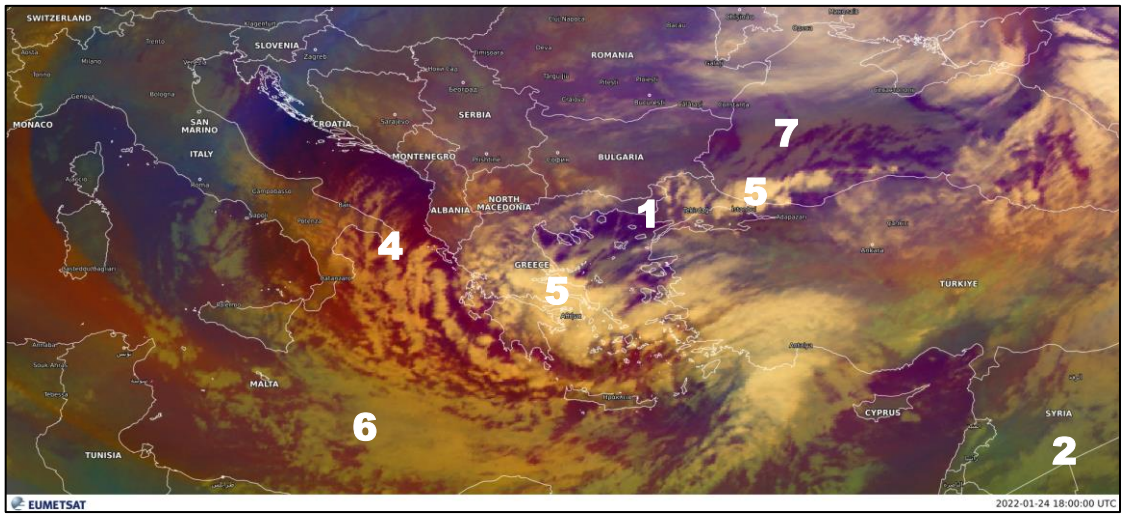


Fig. 4.39: Airmass RGB image at 18:00 UTC, on January 24. (*https://www.eumetsat.int/*)

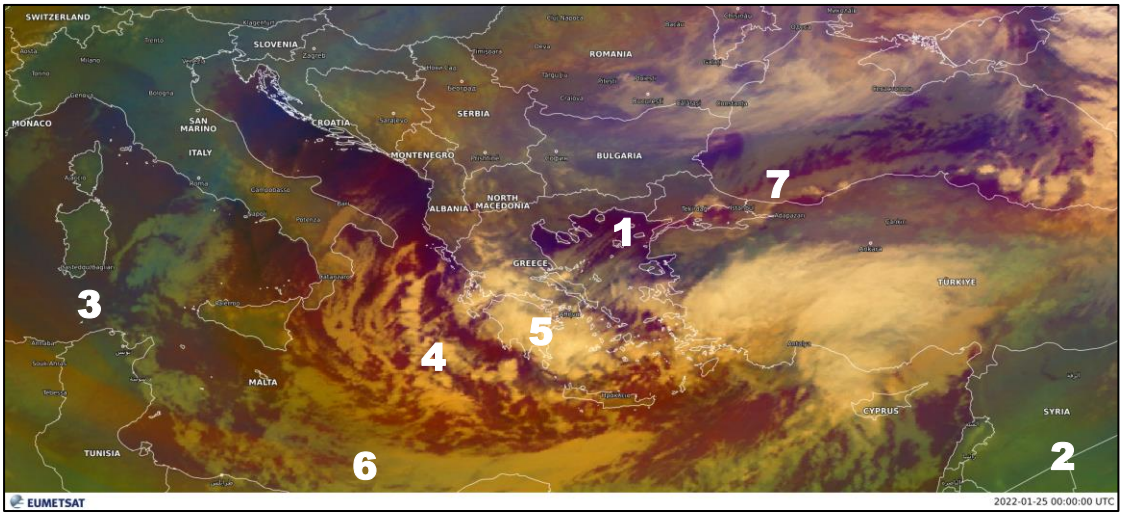


Fig. 4.40: Airmass RGB image at 00:00 UTC, on January 25. (*https://www.eumetsat.int/*)

4.2.3. Cloud Top Height analysis

Based on the CTH analysis at 02:00 local time (Fig. 4.45) and considering GFS analysis data indicating no high cloud presence over Greece, with only mid to low-level clouds forecasted (Fig. 4.41, Fig 4.42 & Fig. 4.43), the satellite image reveals the development of vertically extensive clouds reaching altitudes of approximately 6-7 km above the Aegean, giving extensive snowfall over the area (Fig. 4.44).

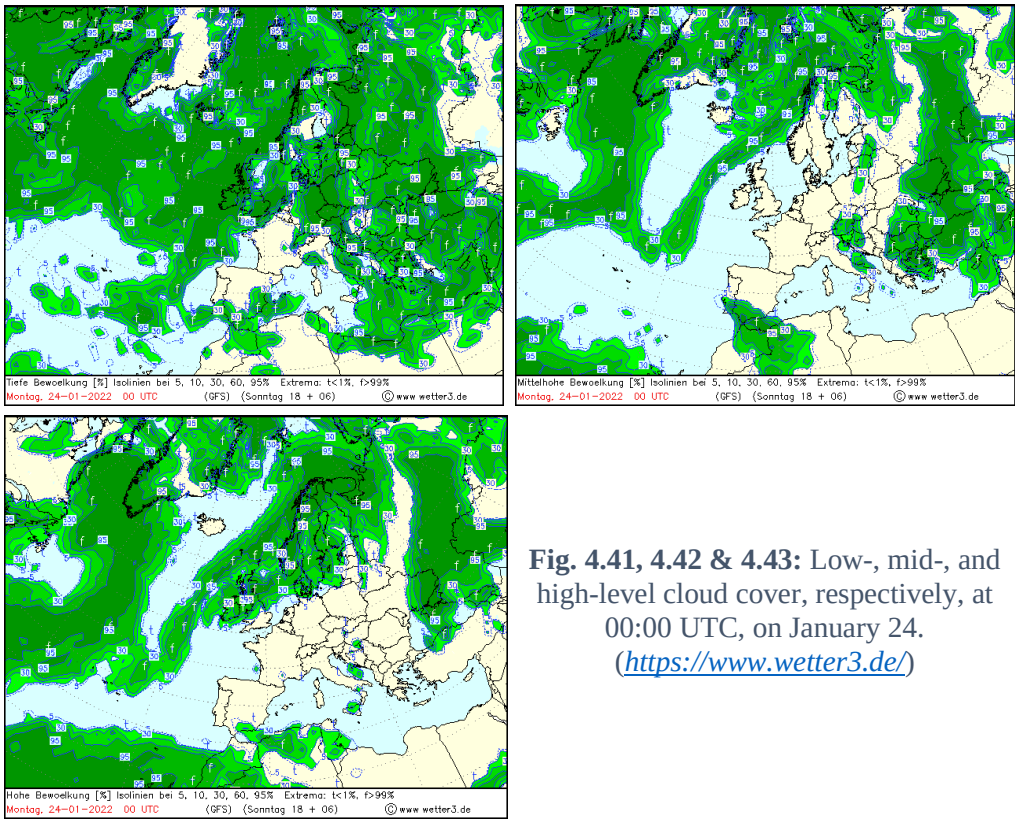


Fig. 4.41, 4.42 & 4.43: Low-, mid-, and high-level cloud cover, respectively, at 00:00 UTC, on January 24. (*https://www.wetter3.de/*)

Over the Attica region, cloud formations of around 4 km are observed, predominantly over the northern parts of the region, with similar heights noted over Euboea. In contrast, within the Athens basin itself, cloud tops are limited to lower altitudes, estimated around 300-500 meters, giving no phenomenon.

This analysis occurs just a few hours before the onset of significant weather phenomena in Attica, which

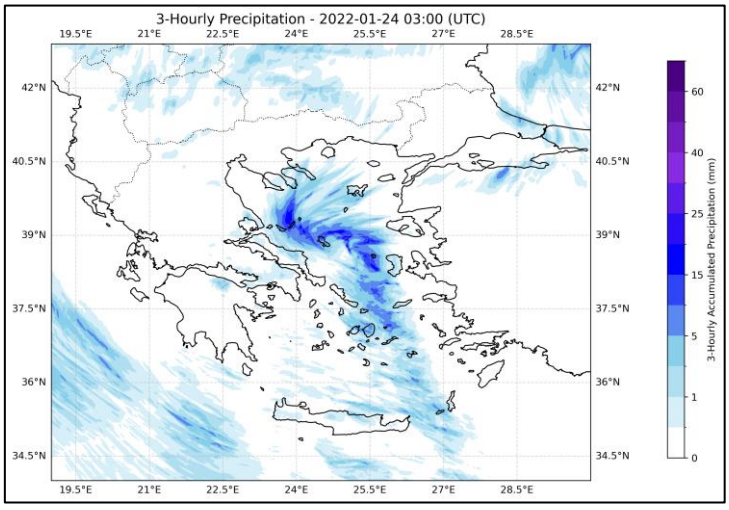


Fig. 4.44: Total precipitation (00:00-03:00 UTC), on January 24. (WRF 1 km)

began after 08:00 local time, and gradually intensified across the region. The observed cloud heights and their vertical extent suggest an atmosphere primed for further development, aligning with the expected increase in precipitation.

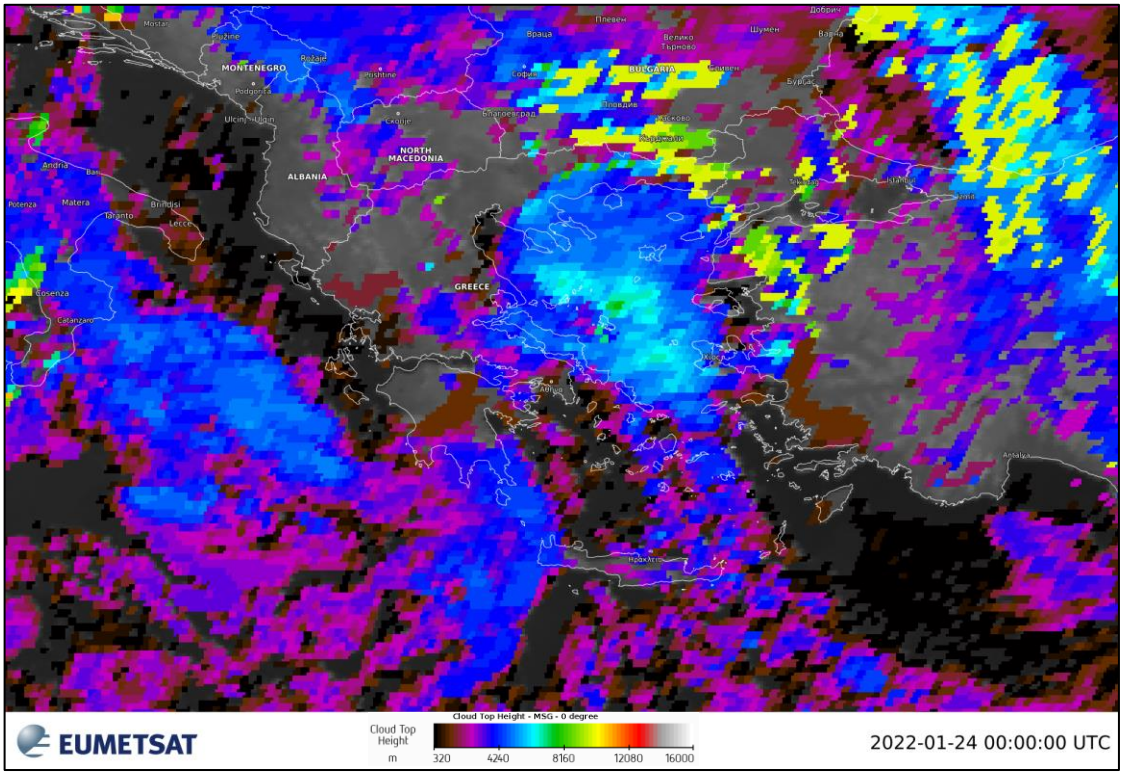


Fig. 4.45: CTH at 00:00 UTC, on January 24. (*https://www.eumetsat.int/*)

At 08:00 local time (Fig. 4.47), even greater cloud heights over the Aegean Sea are observed, indicated by the increased presence of green and yellow hues. This suggests extensive convection over a broader area of the Aegean, with cloud tops reaching altitudes of 8-10 km. Over Euboea and northeastern Attica, cloud heights ranging from 6 to 8 km are detected.

Meanwhile, within the Athens basin, cloud heights are observed between 3 and 5 km, indicating that the weather system is gradually approaching with initial phenomena appearing locally.

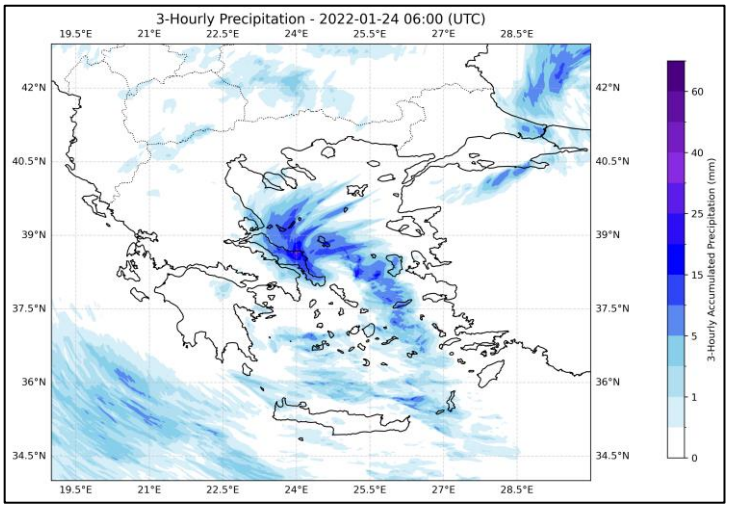


Fig. 4.46: Total precipitation (03:00-06:00 UTC), on January 24. (WRF 1 km)

The WRF reanalysis data (Fig. 4.46) confirms the expansion of precipitation over northeastern Attica and Euboea, with localized intensification of phenomena.

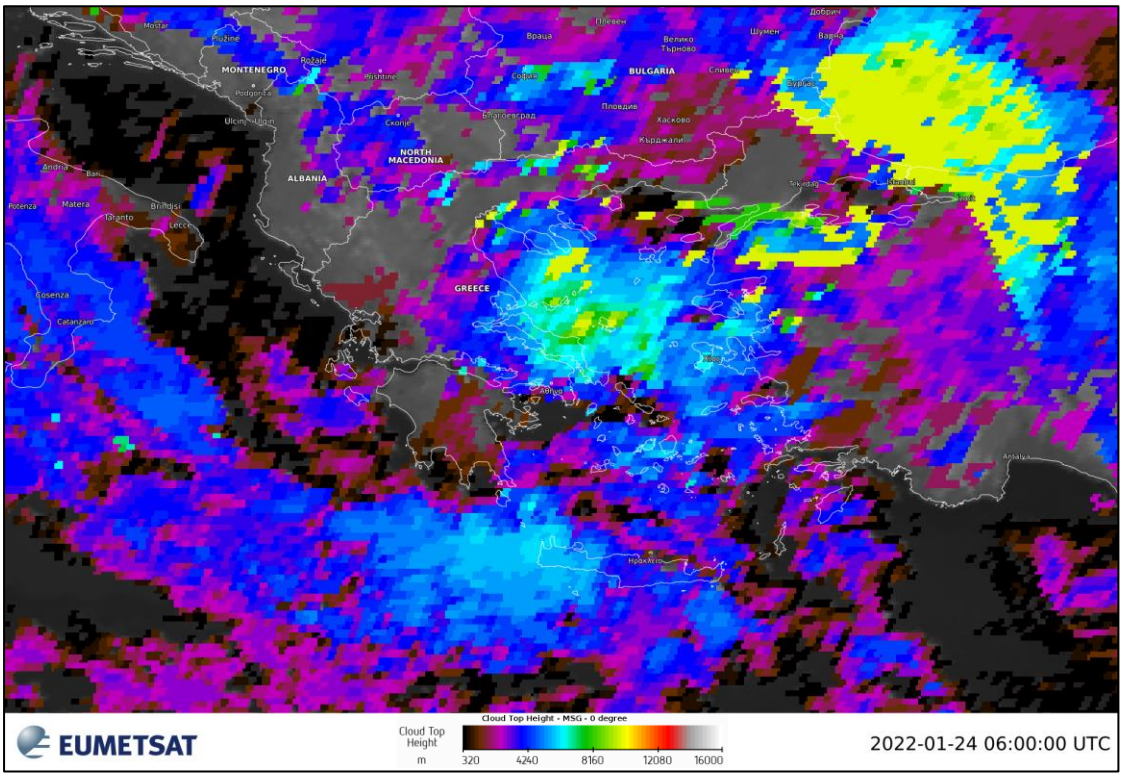


Fig. 4.47: CTH at 06:00 UTC, on January 24. (*https://www.eumetsat.int/*)

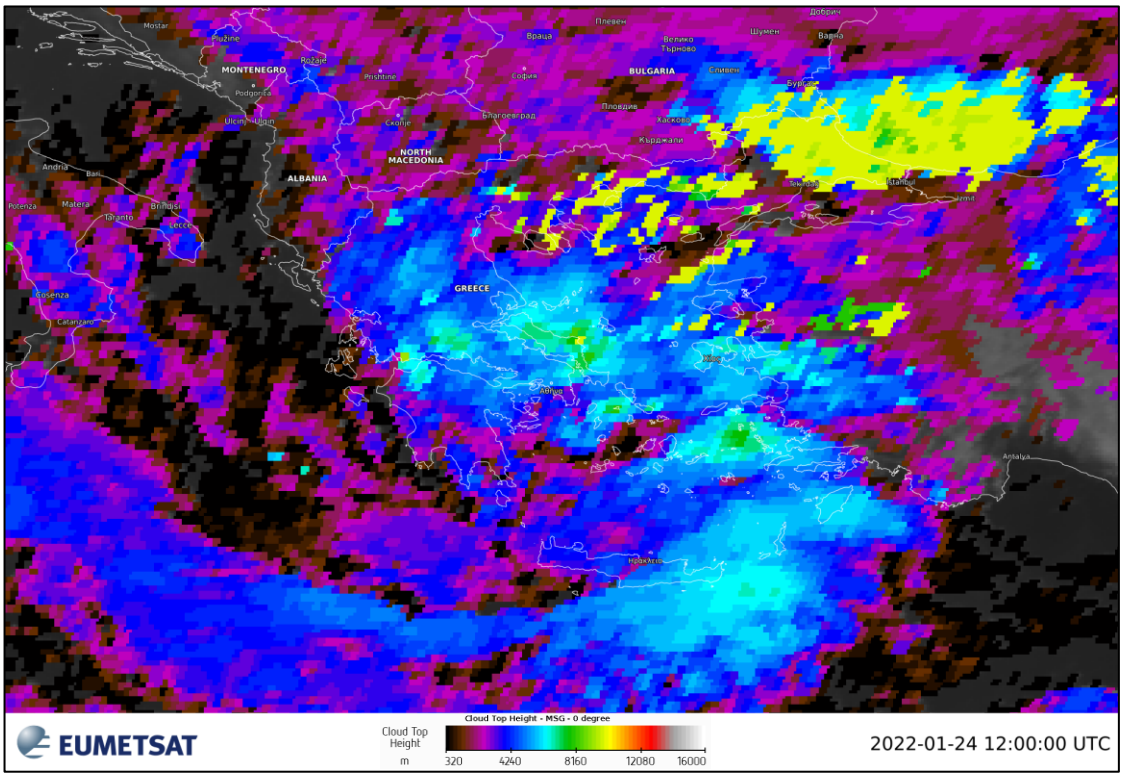


Fig. 4.48: CTH at 12:00 UTC, on January 24. (*https://www.eumetsat.int/*)

At 14:00 local time (Fig. 4.48), the satellite imagery reveals a similar atmospheric setup to previous observation, with a further southward and westward expansion of the cloud cover –as well as precipitation according to Fig. 4.49– suggesting an

intensification of the weather system's influence over the country. Compared to earlier hours, cloud cover appears more widespread, indicating a progressively overcast sky across the region. WRF reanalysis data supports these observations, confirming the ongoing extension of the weather phenomena (Fig. 4.49).

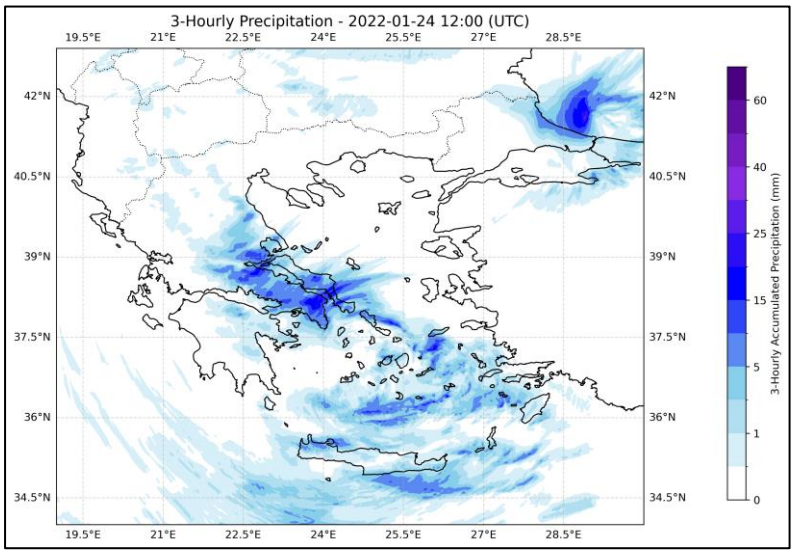


Fig. 4.49: Total precipitation (09:00-12:00 UTC), on January 24. (WRF 1 km)

During the late evening hours, specifically at 20:00 local time (Fig. 4.53), a significant increase in cloud top heights is observed over the eastern mainland of Greece and Euboea. Notably, the Athens basin shows cloud tops reaching up to 10 km, indicating intense convective activity which corresponds to the peak of the weather phenomena observed during this event. The heightened cloud structure is more widespread compared to previous hours, as shown by the expanded areas of high cloud tops on the satellite imagery. This increased cloud height aligns with intense convective processes, which led to localized lightning and thunderstorm activity, even within the Athens basin (Fig. 4.52).

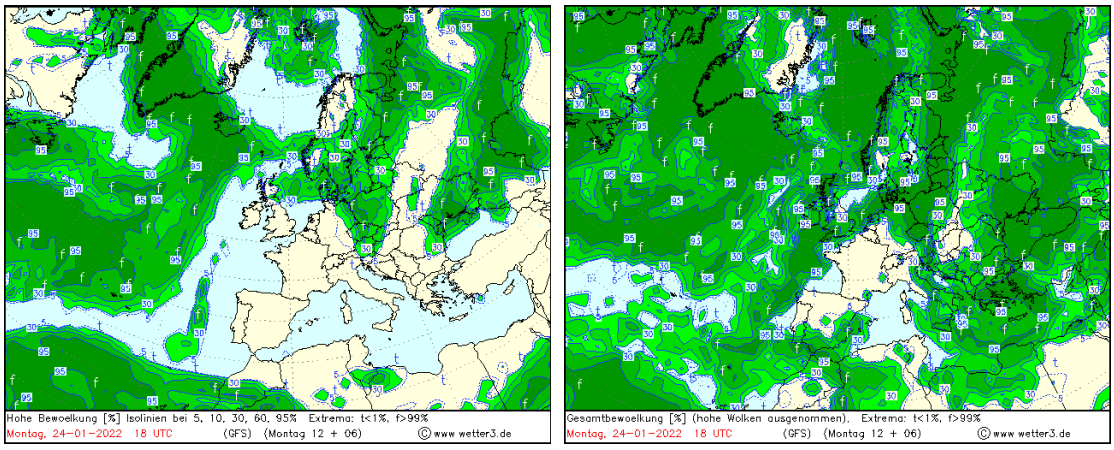


Fig. 4.50 & 4.51: High-level cloud cover & total cloud cover, respectively, at 18:00 UTC, on January 24. (*https://www.wetter3.de/*)

Additionally, a gradual decrease in cloud heights over the Northern Aegean is observed, with values dropping to approximately 2-4 km. This reduction in cloud height

over the Aegean Sea suggests a weakening of moisture support, along with a subsequent reduction in the atmospheric instability responsible for deep convective cloud formation. Moreover, it indicates a progressive decline in moisture supply, essential for the development of vertically extensive clouds, and thus, may signal an eventual reduction in the intensity and coverage of precipitation in the affected areas.

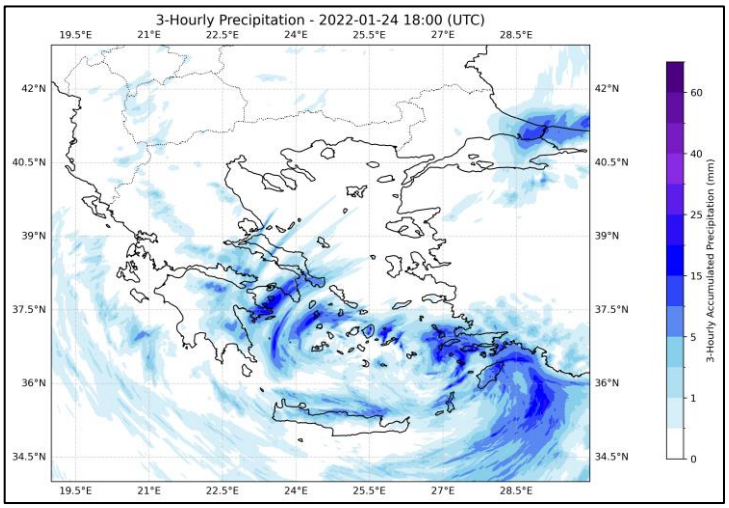


Fig. 4.52: Total precipitation (15:00-18:00 UTC), on January 24. (WRF 1 km)

This transition, marked by the gradual reduction of cloud heights over the Aegean, hints at an upcoming deactivation of the "lake-effect" phenomenon, and thus the stabilization of the atmosphere, ultimately leading to a weakening of the storm systems impacting Attica and Euboea.

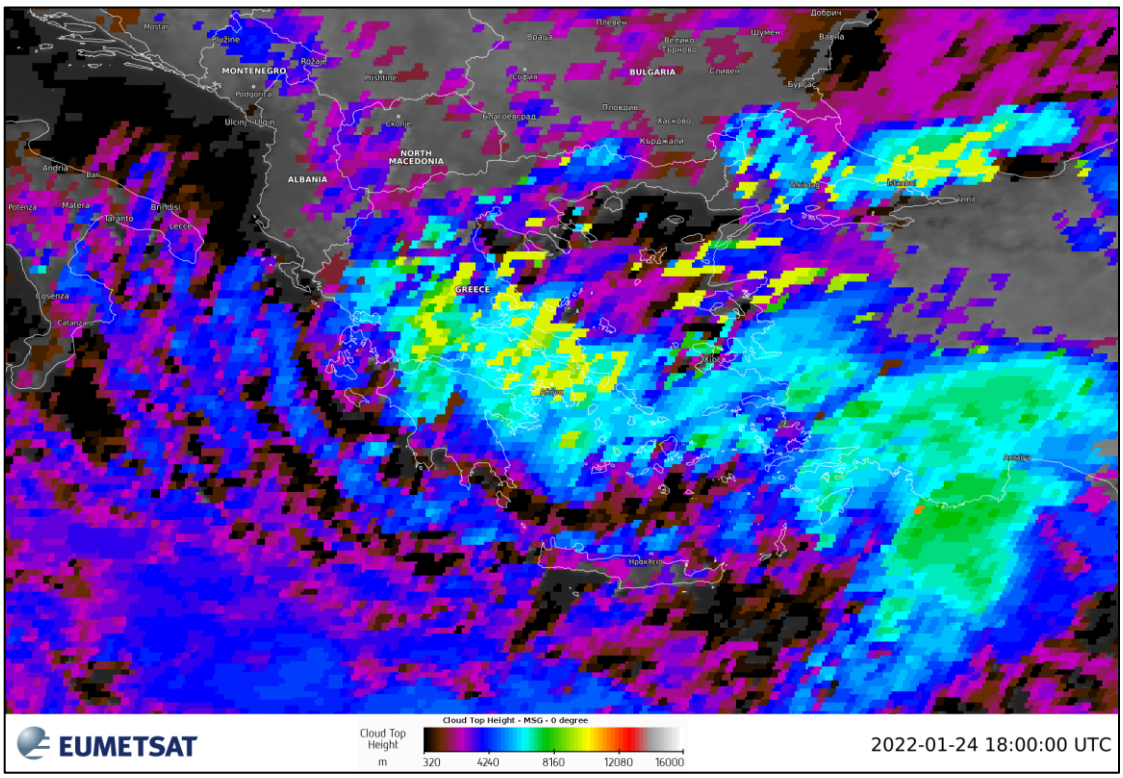


Fig. 4.53: CTH at 18:00 UTC, on January 24. (*https://www.eumetsat.int/*)

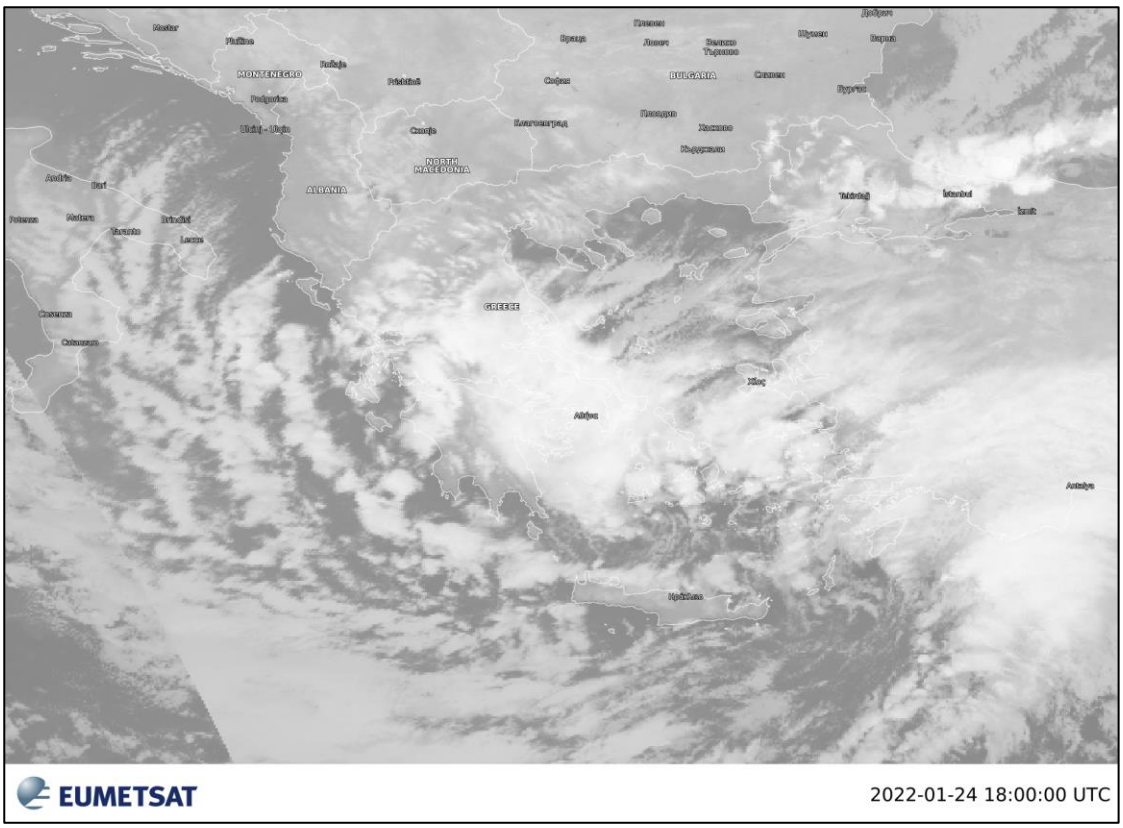


Fig. 4.54: Infrared high-resolution image at 18:00 UTC, on January 24. (*https://www.eumetsat.int/*)

In the early hours of the following day (January 25, 02:00 local time), a further reduction in cloud top heights across the Aegean Sea, Eastern Central Greece, and Euboea is detected (Fig. 4.56), as well as a weakening of weather phenomena in these regions (Fig. 4.55). Specifically, over the northern Aegean, cloud top heights range between 0.3-1 km, with localized areas reaching up to 4 km. In Attica and Euboea, heights have now diminished to approximately 2-5 km, indicating a weakening atmospheric structure and decreasing convective activity in these areas. This progressive reduction in cloud heights, particularly over the northern Aegean, suggests a further decline in moisture supply and vertical development of clouds, marking the importance of the "lake-effect" phenomenon that had previously contributed to sustained cloud formation and

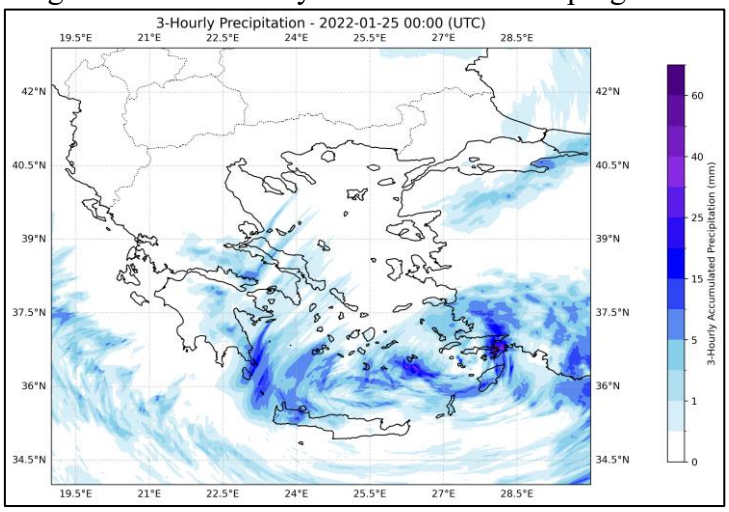


Fig. 4.55: Total precipitation (21:00-00:00 UTC), on January 25. (WRF 1 km)

precipitation in these regions. Meanwhile, the highest cloud tops, measuring 8-10 km, are now predominantly observed over southwestern Aegean, along with some isolated

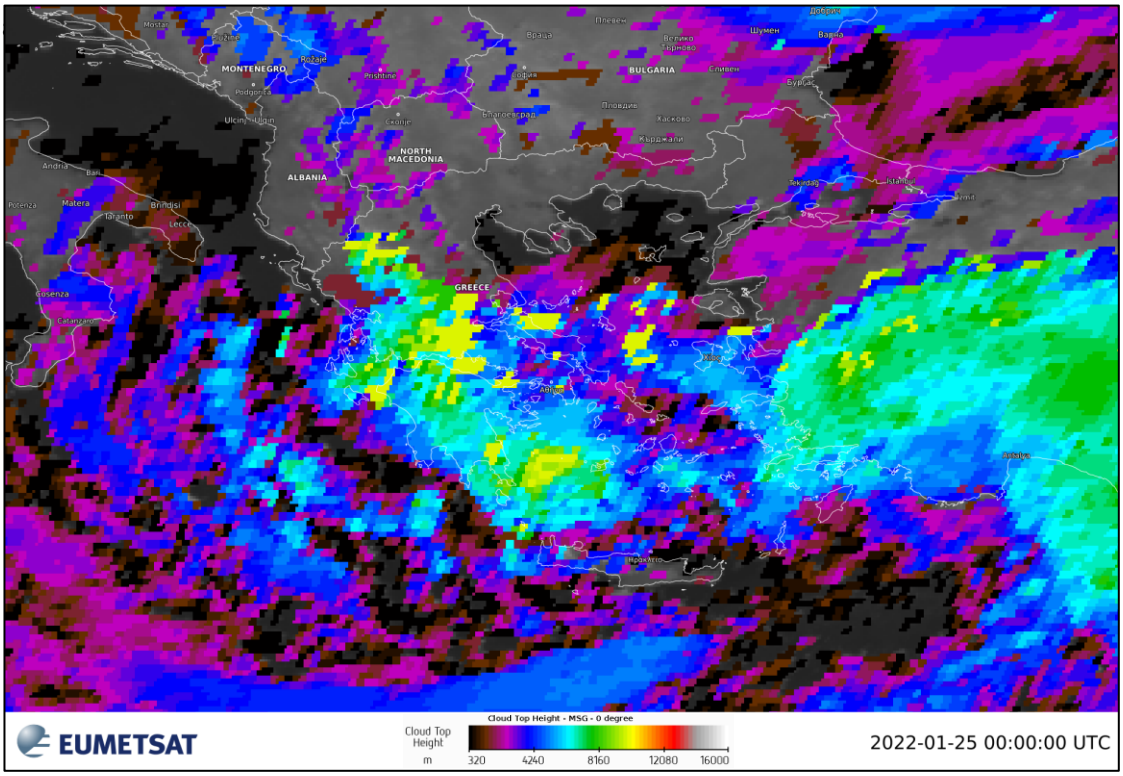


Fig. 4.56: CTH at 00:00 UTC, on January 25. (*https://www.eumetsat.int/*)

4.2.4. Cloud Microphysics and Severe Convection RGB Analysis

4.2.4.1. Day Microphysics RGB

The following color interpretation (Fig. 4.57) provides visual guidance for distinguishing between various cloud types, ice particles, surface snow, and land-water features. In Fig. 4.58 to Fig. 4.60, the different cloud and surface types are labeled with numbers (1-8) based on this interpretation, allowing for easier identification and analysis of atmospheric and surface conditions.

According to the SEVIRI Day Microphysics RGB imagery, areas over the Aegean, Euboea, and Attica predominantly exhibit the orange color (label 2), which is indicative of thick ice clouds with small ice crystals at the top. Over Attica, orange and red colors alternate throughout the day, reflecting dynamic cloud properties. Intense orange tones are also observed around Istanbul, particularly over the Black Sea region.

Combining this information with data from the CTH product, it becomes evident that these regions are characterized by cloud tops reaching altitudes of up to 10 km, indicative of vertically extensive clouds. The prevalence of thick ice clouds with small ice crystals on top over these areas suggests strong updrafts, a typical feature of vigorous

convective activity. In contrast, areas exhibiting a red hue correspond to thick ice clouds with large ice crystals at the top, where cloud heights are lower, around 5-6 km, signifying weaker convective activity compared to regions with orange tones.

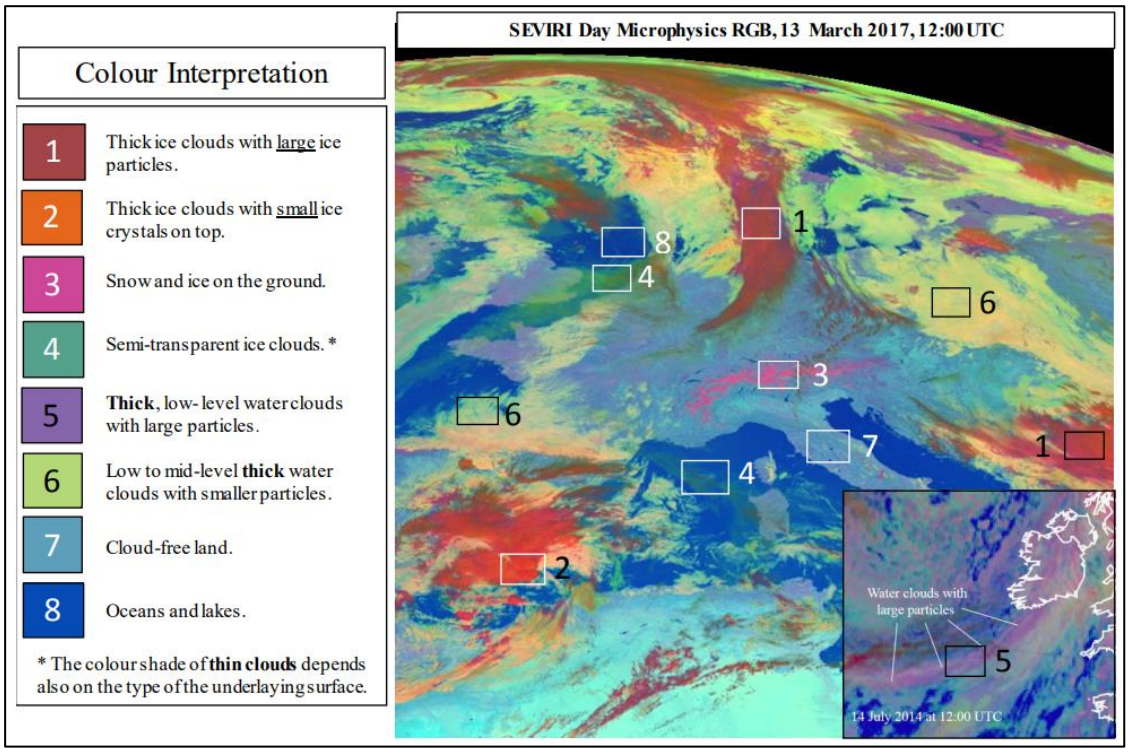


Fig. 4.57: This color interpretation provides visual guidance for distinguishing between various cloud types, ground conditions, and water bodies, enhancing the identification of cloud particle size, cloud opacity, and surface features. (*https://www.eumetsat.int/*)

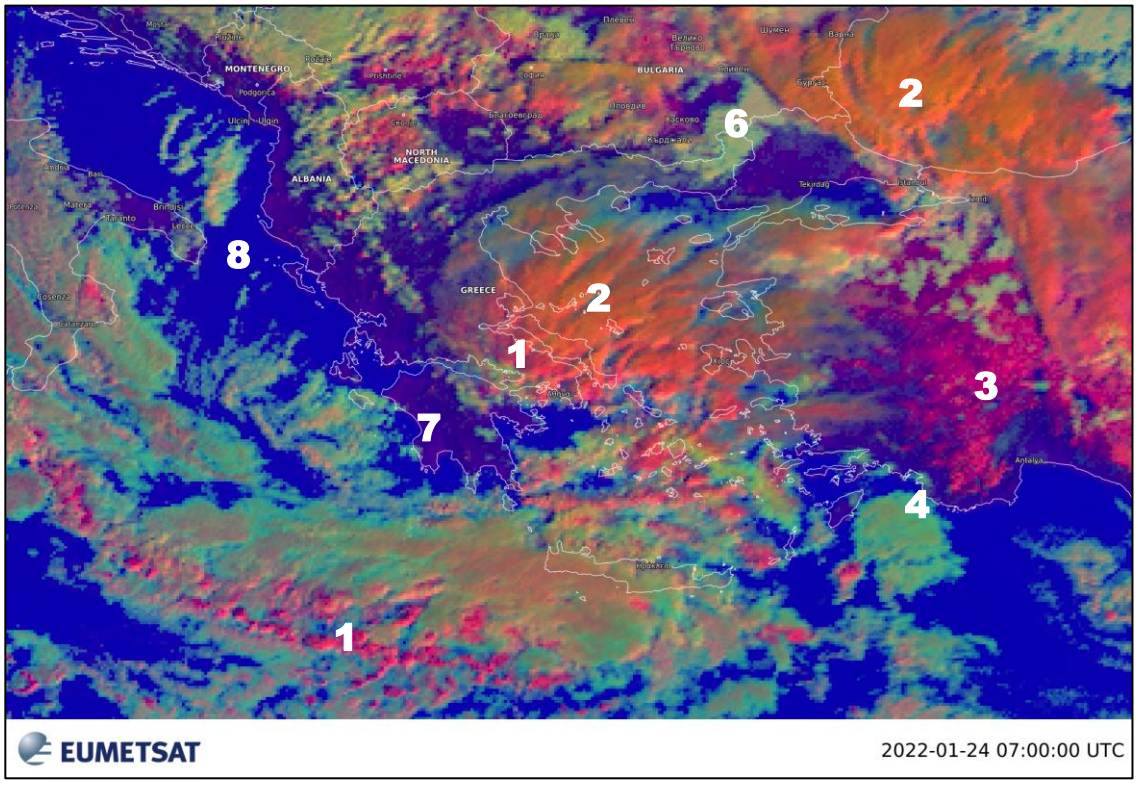


Fig. 4.58: Day Microphysics RGB at 07:00 UTC, on January 24. (*https://www.eumetsat.int/*)

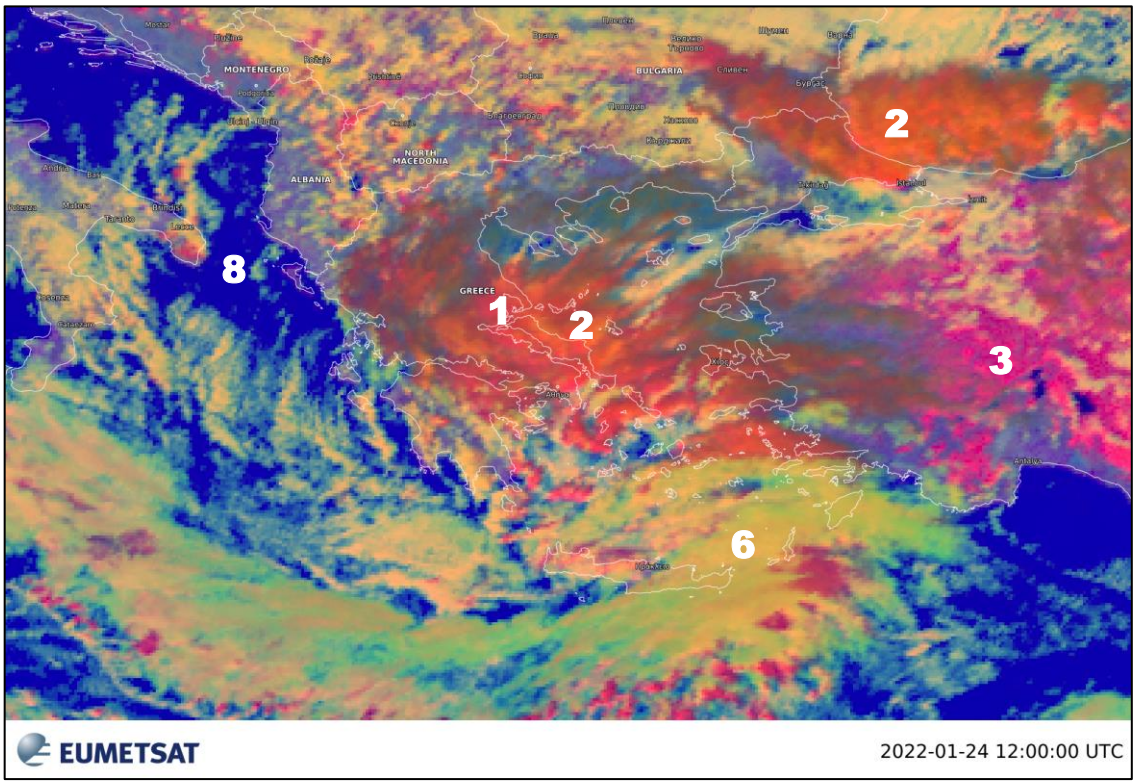


Fig. 4.59: Day Microphysics RGB at 12:00 UTC, on January 24. (*https://www.eumetsat.int/*)

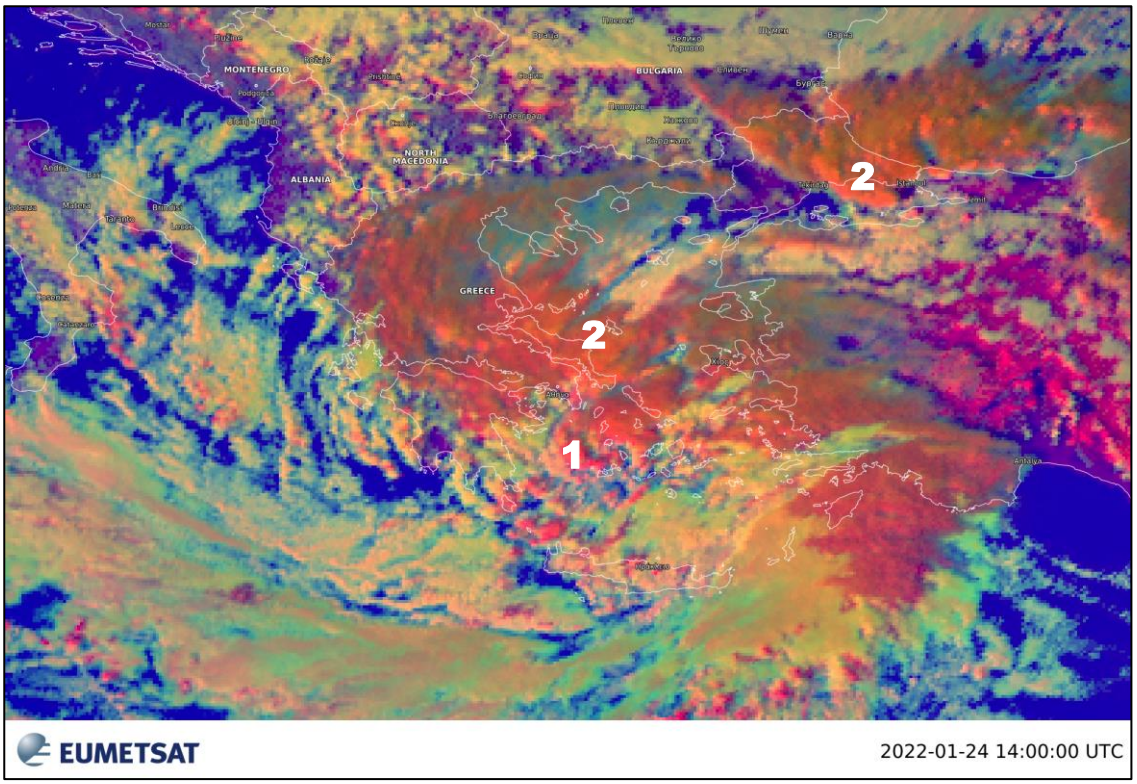


Fig. 4.60: Day Microphysics RGB at 14:00 UTC, on January 24. (*https://www.eumetsat.int/*)

4.2.4.2. Night Microphysics RGB

At 03:00 UTC (Fig. 4.62), convective activity was prominent over the Aegean Sea, especially around the Sporades islands. The MSG imagery highlights reddish-brown

areas (label 6), locally interspersed with green-speckled patterns (label 7), indicating thick ice clouds with localized regions being very cold (according to Fig. 4.61). These features signify strong upward motions and the presence of vertically extensive clouds. Cross-referencing with CTH data confirms cloud tops reaching 6-8 km, consistent with active convection and enhanced precipitation, suggesting dynamic snowfall in the Sporades during this time.

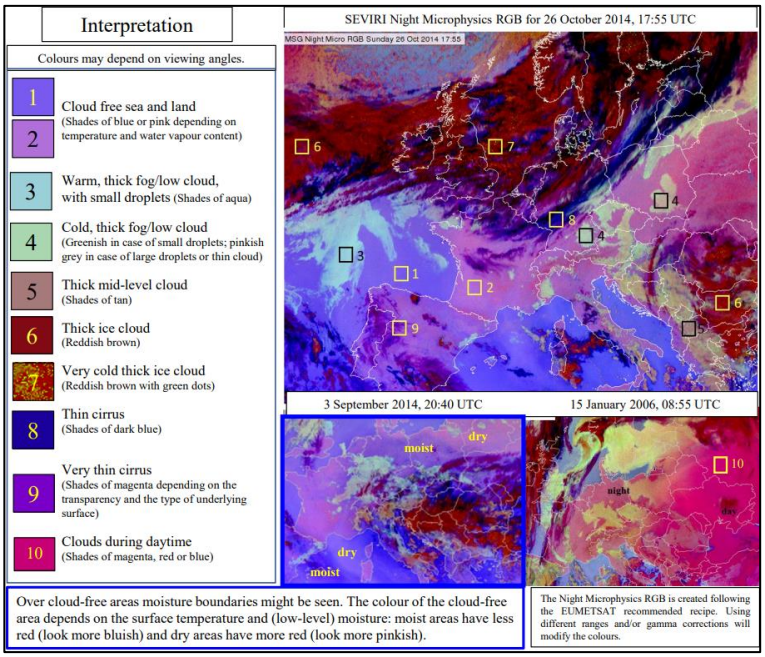


Fig. 4.61: This color interpretation provides visual guidance for distinguishing between different cloud types and moisture levels at night. (*https://www.eumetsat.int/*)

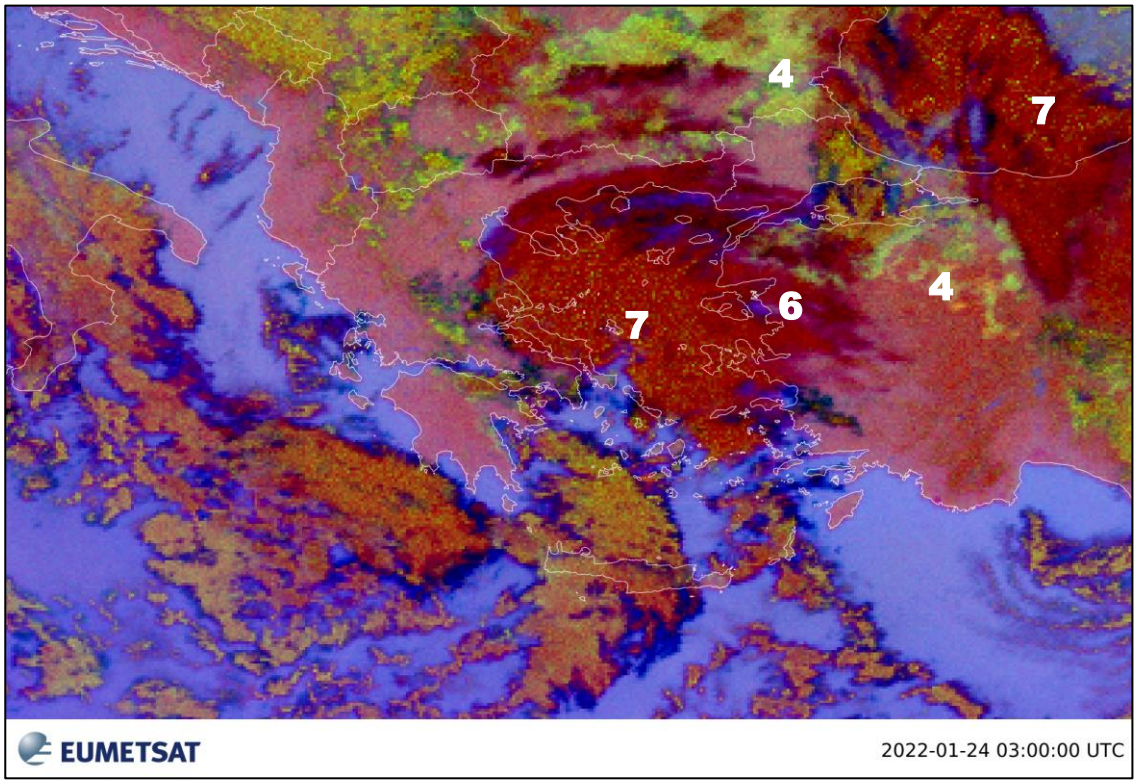


Fig. 4.62: Night Microphysics RGB at 03:00 UTC, on January 24. (*https://www.eumetsat.int/*)

At 18:30 UTC (Fig. 4.63), during the peak of the snowstorm, intense convective activity was observed over the Aegean Sea, Euboea, and Attica. The MSG imagery identified reddish-brown areas with green speckles (label 7), signifying very cold thick

ice clouds, associated with severe convection and heavy snowfall. In this seasonal and regional context, such cloud formations generally represent intense weather phenomena due to their vertical extent and thickness. MetOp imagery, known for its higher spatial resolution, was used to complement and validate these observations (Fig. 4.64). It confirmed the MSG findings, revealing well-defined, vertically developed cloud structures consistent with severe convection.

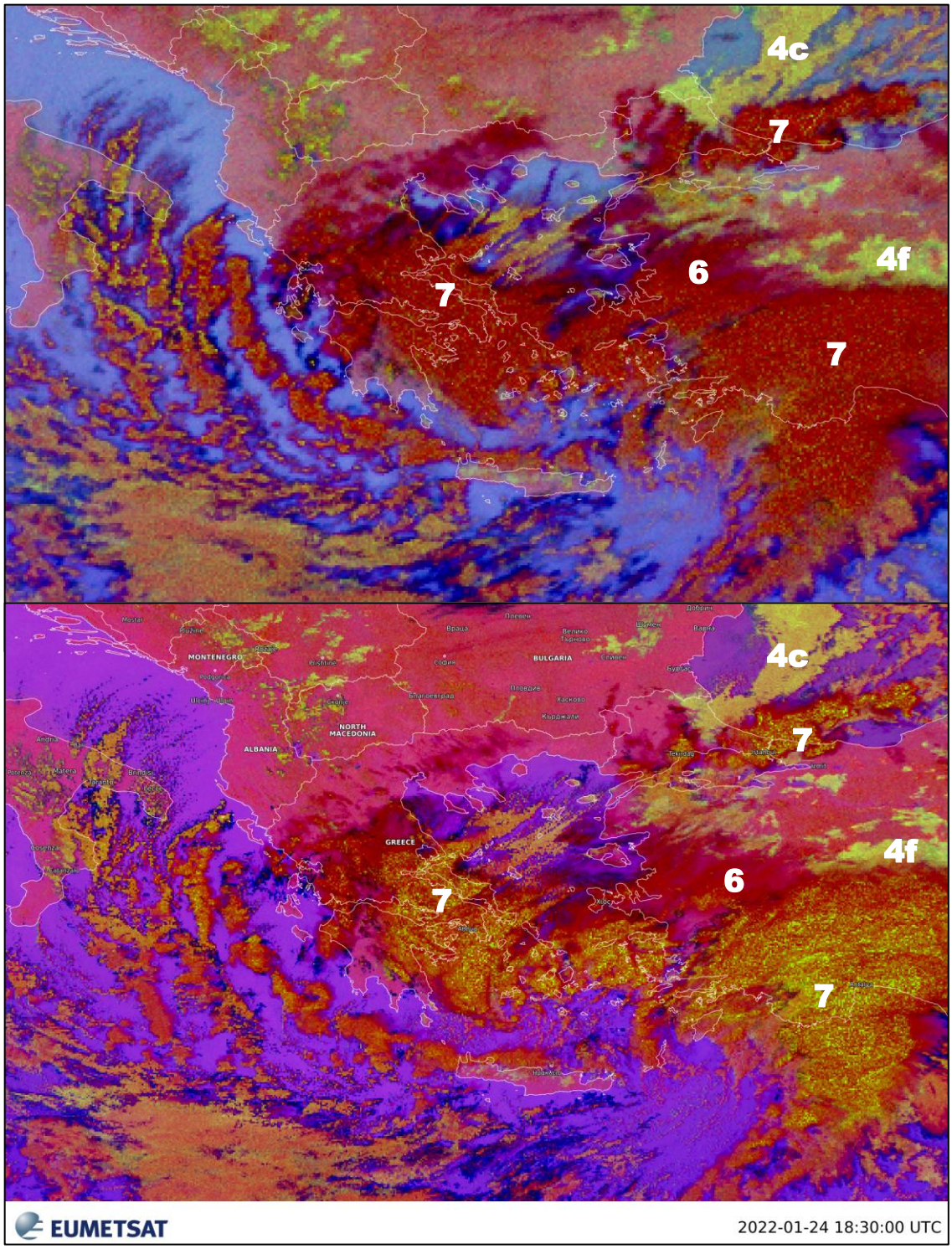


Fig. 4.63 & 4.64: Night Microphysics RGB at 18:30 UTC, from MSG and MetOP, respectively, on January 24. (*https://www.eumetsat.int/*)

By combining the CTH data with Night Microphysics RGB imagery and WRF reanalysis data, the yellow/green speckled patterns are identified as markers of intense weather activity, with the intensity of the phenomena correlating with the brightness of these speckled patterns. Additionally, A distinction is evident between cold thick fog/low clouds and higher cloud tops. For instance, in the "4f" area, CTH data shows no-to-minimal cloud presence, which supports the interpretation of fog (with "f" denoting fog). In contrast, in the "4c" area, CTH data indicates clouds around 2 km in height, suggesting the presence of low-level clouds.

At 21:00 UTC (Fig. 4.65), the storm's progression shifted, with convective activity observed over the northeastern Peloponnese, Attica, and localized parts of the Cyclades. The MSG imagery shows thick ice clouds, with localized very cold regions. Cross-referencing with CTH data further verifies the presence of vertically extensive clouds, consistent with sustained snowfall and convective activity. This pattern highlights the storm's evolution, as the most intense phenomena moved southeastward while maintaining high cloud tops in the convective zones.

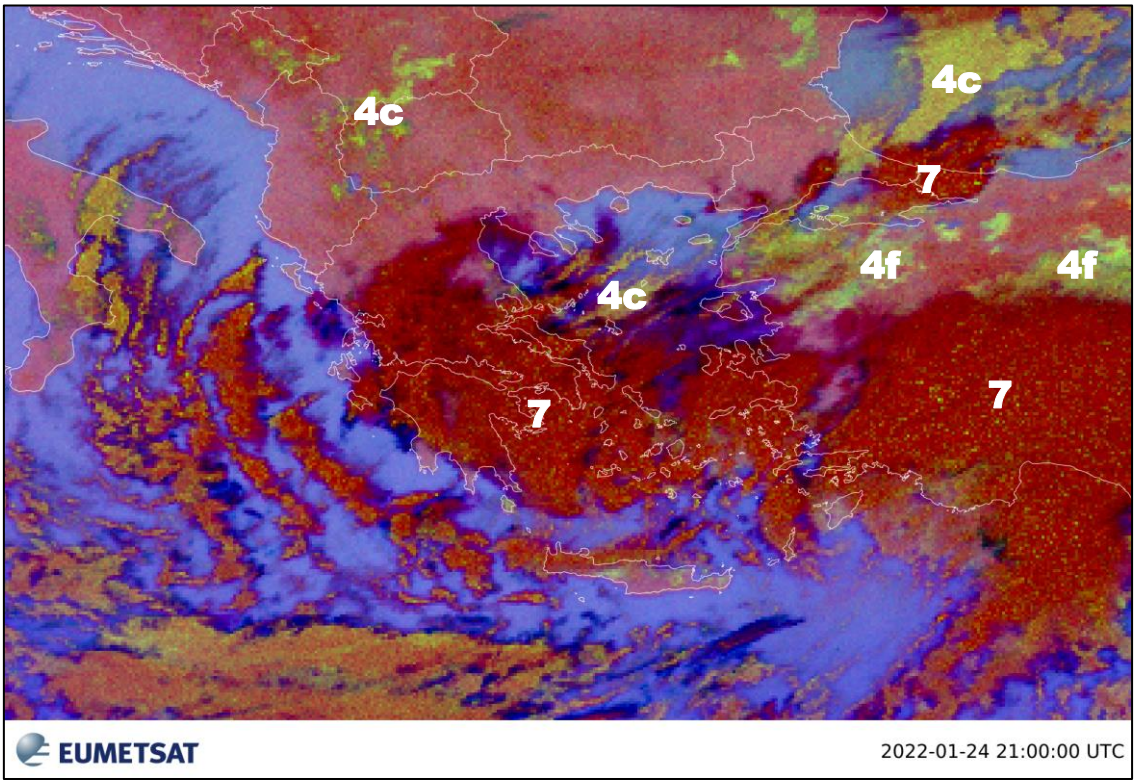


Fig. 4.65: Night Microphysics RGB at 21:00 UTC, on January 24. (*https://www.eumetsat.int/*)

4.2.4.3. Severe Convection RGB

Over the Aegean Sea, as well as parts of Attica and Euboea (Fig. 4.67 & Fig. 4.68), light yellow shades are evident, corresponding to thick ice clouds with small ice crystals

at top (label 1), according to Fig. 4.66. This coloration suggests the presence of intense cloud tops, which are associated with vertically developed, convective clouds. In comparison, a similar but more extensive yellow pattern is observed over the Black Sea and the areas surrounding Istanbul, indicating stronger convective activity. Although tropical storms exhibit more vibrant yellow hues due to their intense updrafts, the yellow tones observed in the Aegean region and Black Sea highlight noteworthy convection, especially in the context of winter storms.

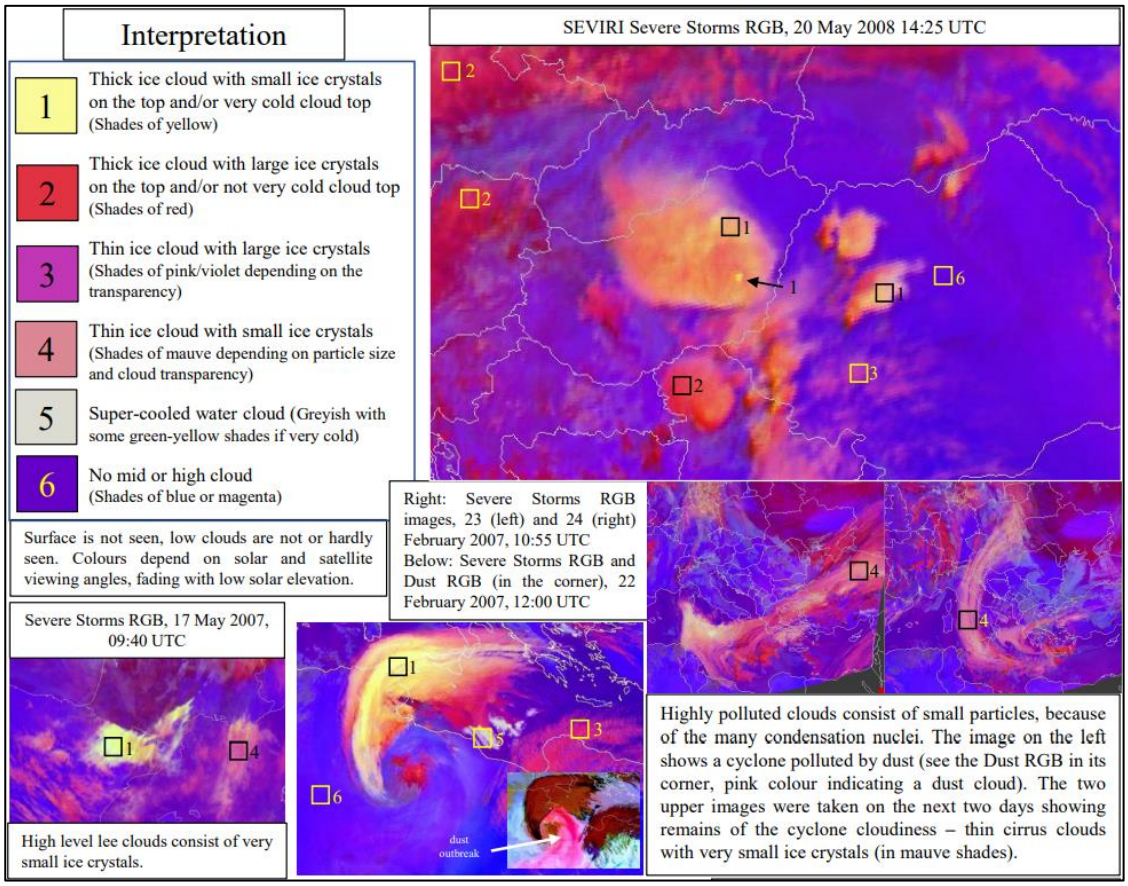


Fig. 4.66: This color interpretation provides visual guidance for distinguishing between various cloud types, including high-level ice clouds with different crystal sizes, water clouds, and low clouds, aiding in the identification of severe storm structures and cyclone remnants. (*https://www.eumetsat.int/*)

Over southeastern Greece, particularly in areas like the Dodecanese islands and eastern Crete, the images indicate super-cooled water clouds (label 5), represented by grayish shades with subtle green-yellow hues, suggesting colder, stable cloud formations typically found at lower altitudes. This cloud type is generally associated with less convective activity and provides insight into the stable atmospheric conditions in these regions, contrasting with high-altitude convection observed further north.

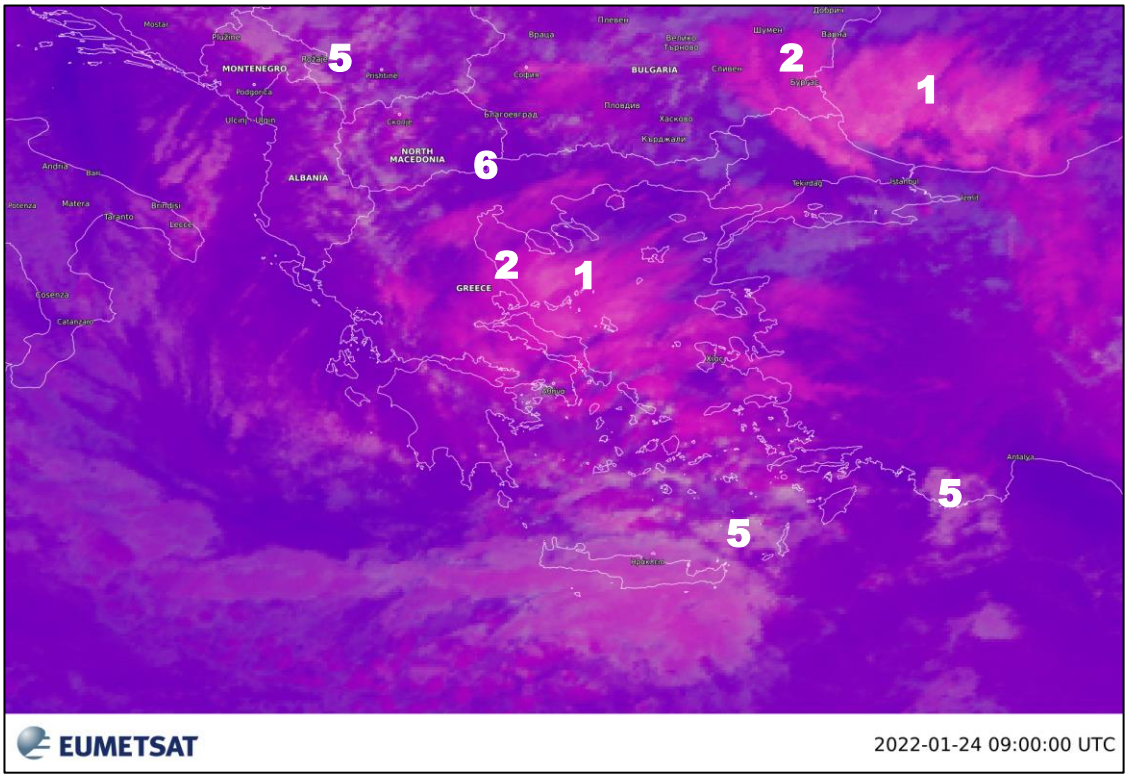


Fig. 4.67: Severe Convection RGB at 09:00 UTC, on January 24. (*https://www.eumetsat.int/*)

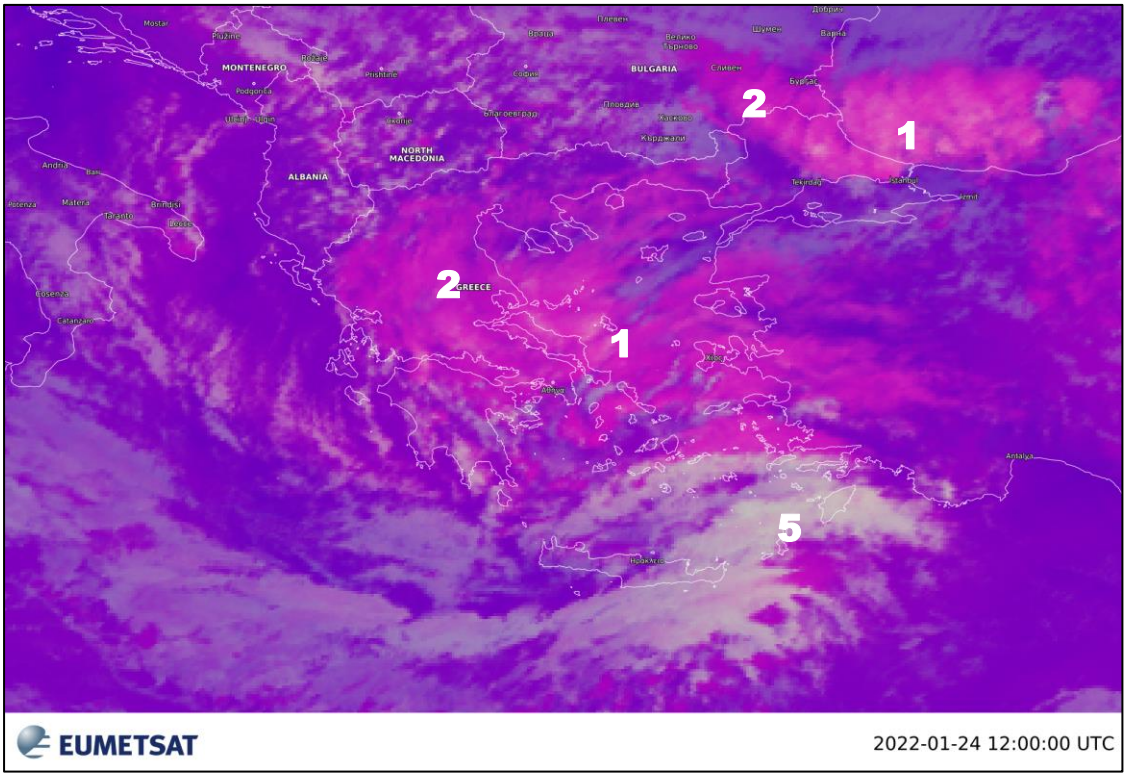


Fig. 4.68: Severe Convection RGB at 12:00 UTC, on January 24. (*https://www.eumetsat.int/*)

Additionally, a technical discrepancy in color representation is noticeable within the Severe Convection RGB product. From September 1, 2020, to 13:15 UTC on May

12, 2022, the typical red shades associated with thick ice clouds with large ice crystals (label 2) were not present, with these cloud types instead depicted in purple hues (Fig. 4.69, Fig. 4.70, Fig. 4.71 & Fig. 4.72). This color shift might suggest an update or adjustment in the visualization algorithms or data processing methods by EUMETSAT, potentially implemented to enhance cloud-phase differentiation and improve the accuracy of visual data interpretation. Such changes in color coding underscore the importance of data calibration in satellite imaging, as they can significantly affect weather analysis, especially in contexts where subtle distinctions are critical. This calibration inconsistency is the reason for marking purple areas with '2' in this analysis, as these areas would typically be represented in red shades to denote thick ice clouds with large ice crystals under standard color interpretation.

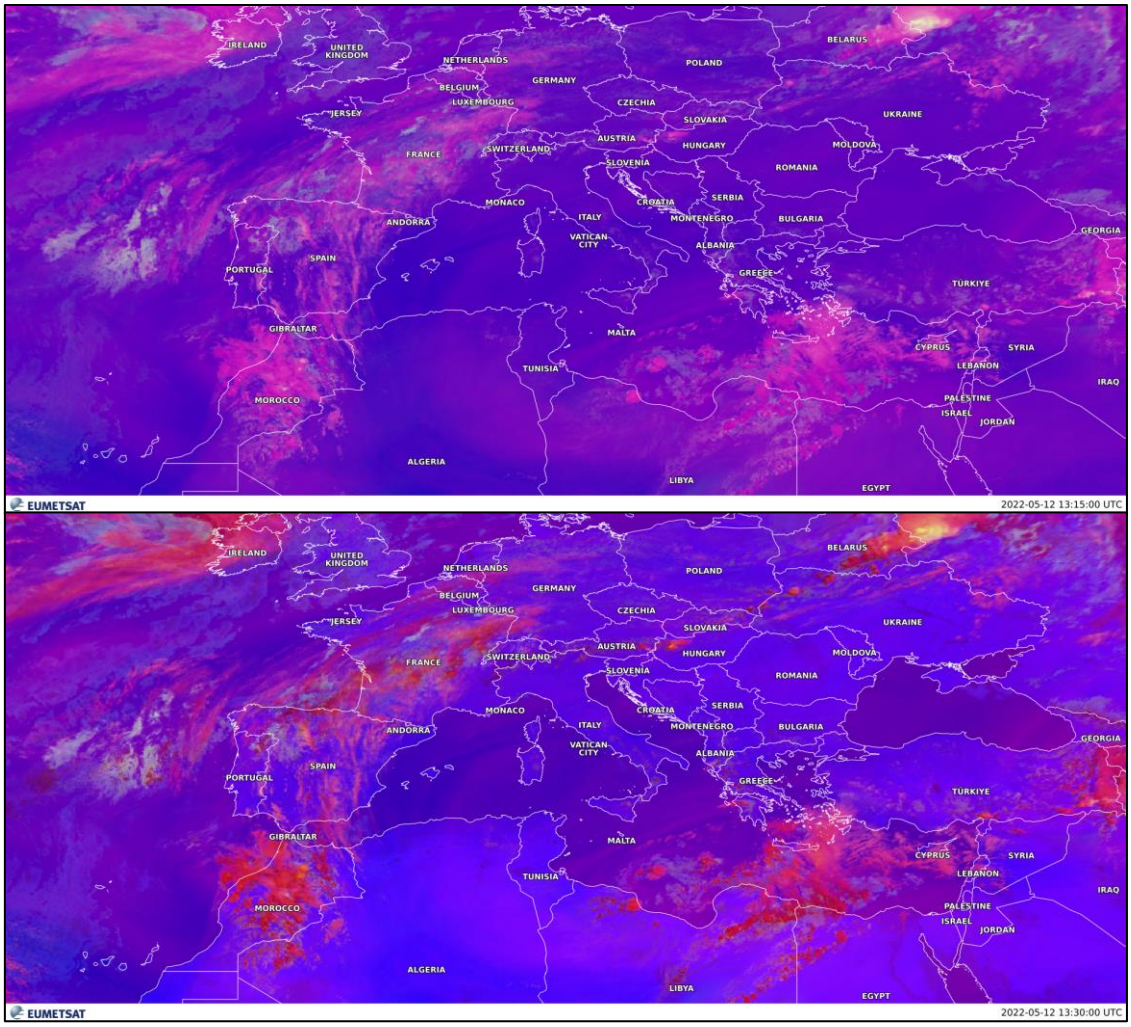


Fig. 4.69 & Fig. 4.70: Severe Convection RGB at 13:15 & 13:30 UTC, respectively, on May 12, 2022, showing the difference between the color hues. (*https://www.eumetsat.int/*)

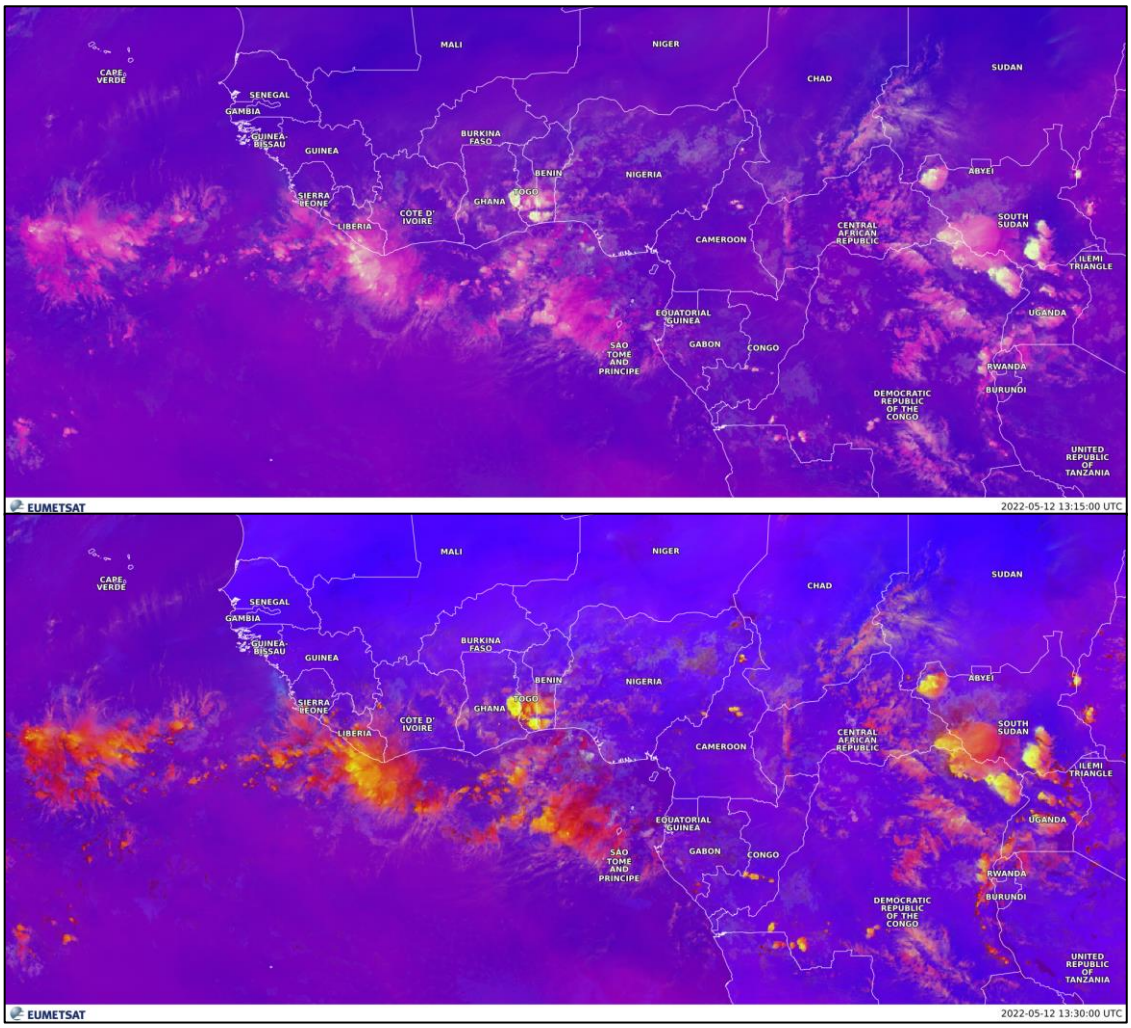


Fig. 4.71 & Fig. 4.72: Severe Convection RGB at 13:15 & 13:30 UTC, respectively, on May 12, 2022, showing the difference between the color hues. (*https://www.eumetsat.int/*)

5. MEDEA SNOWSTORM

5.1. Analysis of Atmospheric Dynamics

5.1.1. Synoptic Setup Leading to the Medea Snowstorm

On February 13, three days prior to the arrival of severe snowstorms and blizzards in the eastern parts of continental Greece, an omega block began to dominate the upper levels over the North Atlantic. This ridge gradually took on dynamically unstable characteristics, prompting an upper-level trough to advance southward over the Balkans. This progression triggered the development of cyclonic circulation at high altitudes, accompanied by a polar front jet streak along its western side (Fig. 5.1). The presence of this jet streak on the western edge of the trough contributed to enhanced cyclonic development and further supported the intensification and southward propagation of the trough. This long-wave trough in eastern Europe between February 12 and February 17 was associated with the advection of cold air masses from northern Europe (Fig. 5.3 & Fig. 5.4), resulting in extremely low temperatures and intense phenomena,

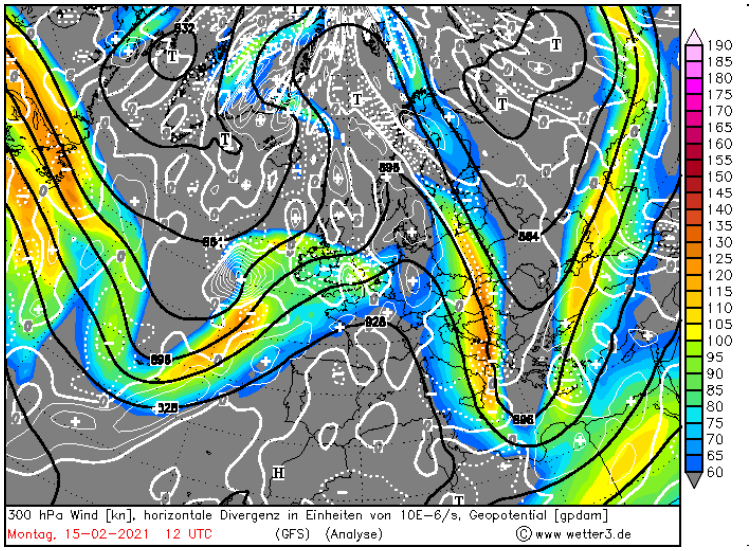


Fig. 5.1: 300 hPa geopotential (gpdam) & isotachs (ms^{-1}). (*https://www.wetter3.de/*)

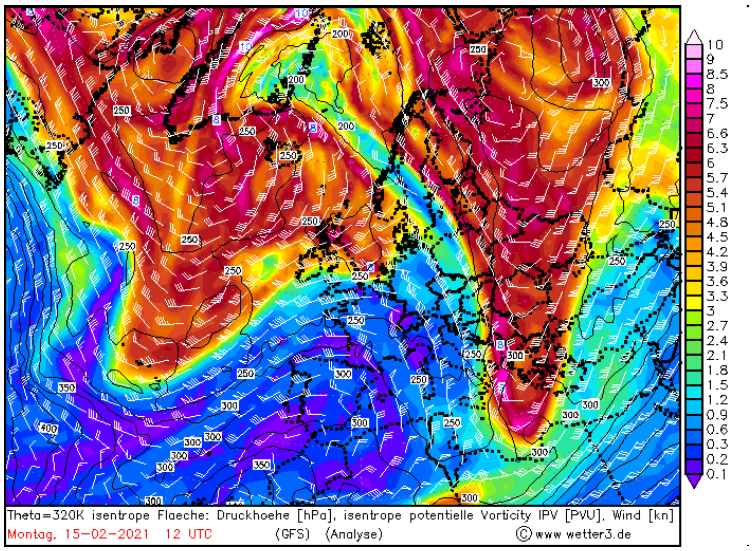


Fig. 5.2: 320K isentropic potential vorticity (PVU) and wind field (knots). (*https://www.wetter3.de/*)

which were well-forecasted several days in advance by global and regional models (Kotroni et al., 2021).

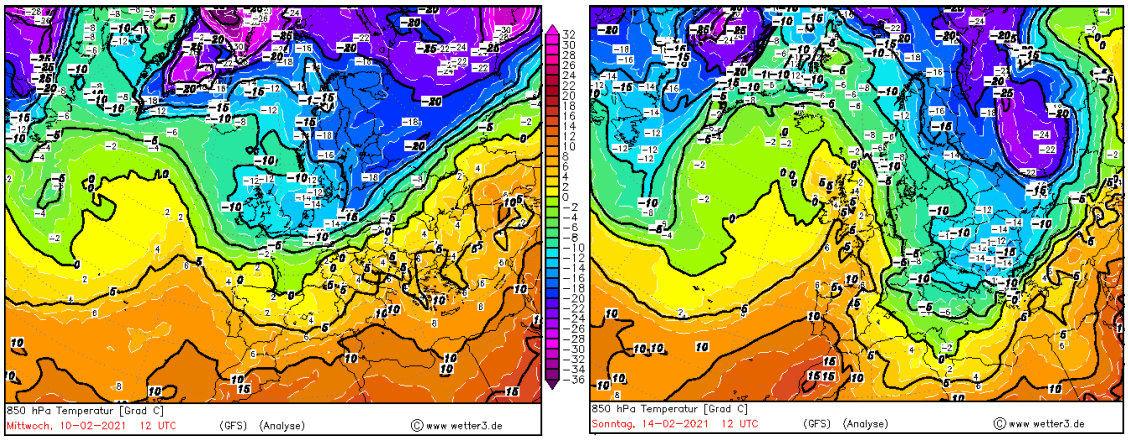


Fig. 5.3 & 5.4: Temperature (°C) at 850 hPa on February 10 (left) and February 14 (right), showing the advection of cold air masses from northern Europe. (*https://www.wetter3.de/*)

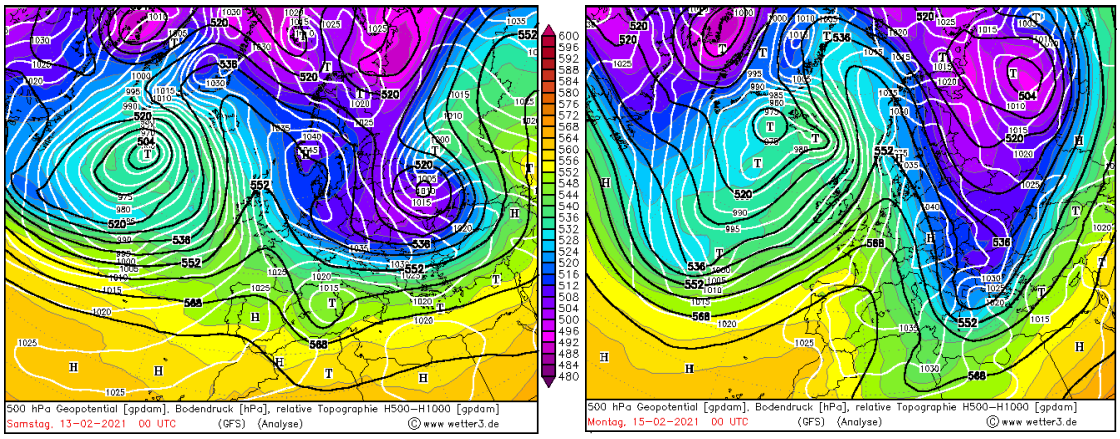


Fig. 5.5 & 5.6: Geopotential (gpdam) at 500 hPa, MSLP (hPa) & 1000-500 hPa Thickness on February 13 (left) and February 15 (right). (*https://www.wetter3.de/*)

A zone of upper-level frontogenesis, driven by strong northerly winds at 300 hPa, became evident over eastern Europe, which led to the formation of an extended diffluent system that trended south-southeastward and continued to intensify. Concurrently, a tropopause fold emerged at higher altitudes, associated with a stratospheric intrusion of cold air with high potential vorticity (Fig. 5.2). This intrusion had the potential to trigger surface cyclogenesis, creating favorable conditions for dynamic intensification of the surface cyclone.

Furthermore, Greece was impacted by a surface low-pressure system that advanced rapidly eastward from southern Italy towards southern Greece on February 14, as shown in Fig. 5.7 & Fig 5.8. This system resulted in widespread heavy rainfall and snowfall across a large part of the country, with gale-force winds recorded over maritime and island regions. By February 15, this system had shifted over southwestern Turkey, establishing a strong northeasterly flow over the Aegean Sea. Simultaneously, a

positively tilted mid-tropospheric trough from Eastern Europe extended into Greece, further destabilizing the already unstable air masses over the sea. This lead in significant snowfall with substantial ground accumulation in the southern and eastern regions of Greece, along with intense rainfall and powerful winds reaching over 100 km/h.

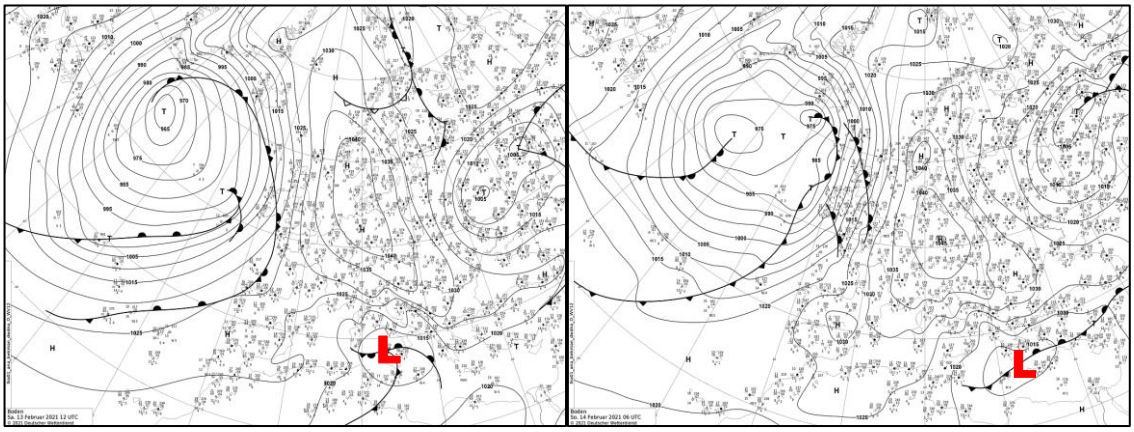


Fig. 5.7 & 5.8: DWD Surface Analysis on February 13 (12:00 UTC) and February 14 (06:00 UTC), respectively, showing the movement of the low-pressure system (L). (*https://www.wetter3.de/*)

5.1.2. Convective Dynamics and Snowfall Patterns on February 16, 2021

On February 16, dynamic atmospheric conditions gave rise to significant convective snowfall with substantial snow accumulation across eastern and southern Greece, notably affecting regions such as Euboea, Attica, and the mountainous areas of Crete. During the peak of the snowfall event, occurring from the night of February 15 through the morning of February 16, Q-vector analysis at the 500 hPa level indicated convergence over the Aegean Sea (Fig. 5.11), signaling upward motion and convective activity. Strong northeasterly winds transported moisture-laden air from the Aegean towards Euboea and Attica, enhancing snowfall through the lake-effect mechanism. Notably, these persistent winds extended their influence as far south as Crete, where they contributed to snowfall in the island's higher elevations.

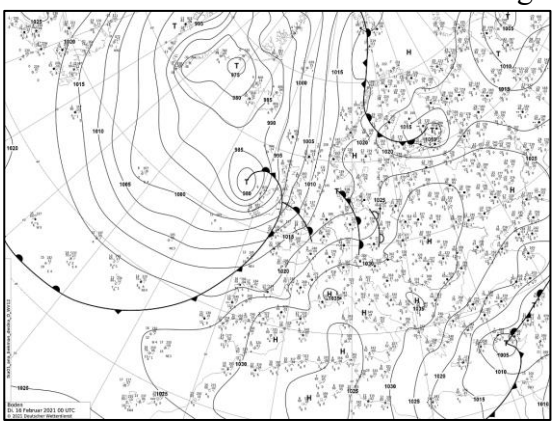


Fig. 5.9: DWD Surface Analysis on February 16. (*https://www.wetter3.de/*)

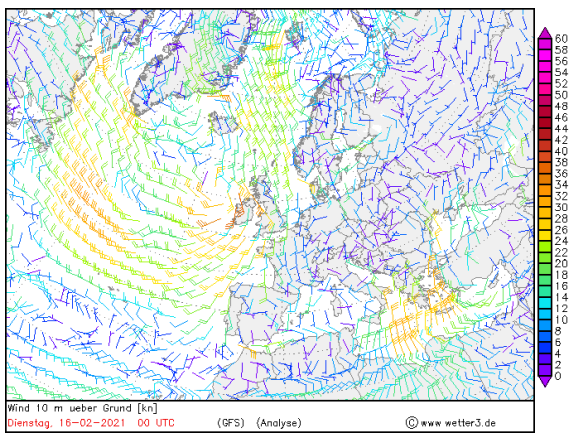


Fig. 5.10: 10m wind on February 16. (*https://www.wetter3.de/*)

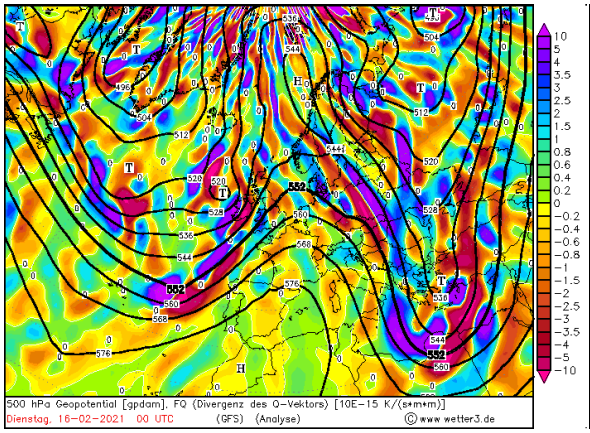


Fig. 5.11: Geopotential (gpdam) at 500 hPa & Q-Vector Divergence on February 16. (*https://www.wetter3.de/*)

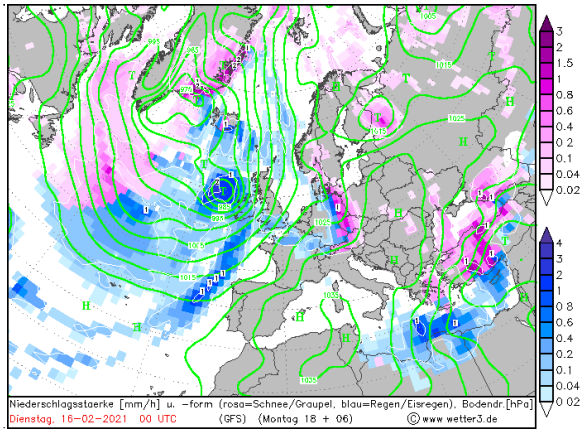


Fig. 5.12: Precipitation (phase/intensity), on February 16. (*https://www.wetter3.de/*)

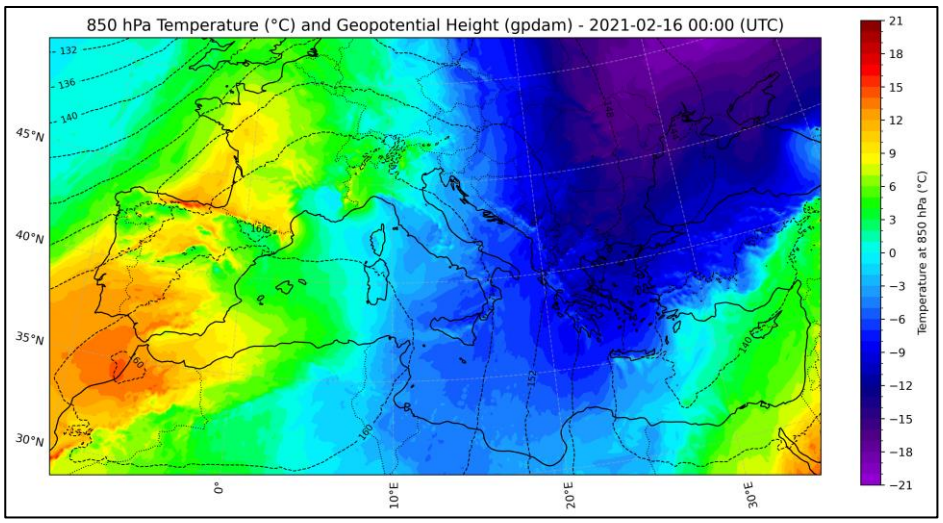


Fig. 5.13: Geopotential (gpdam) & Temperature (°C) at 850 hPa on February 16. (WRF 9 km)

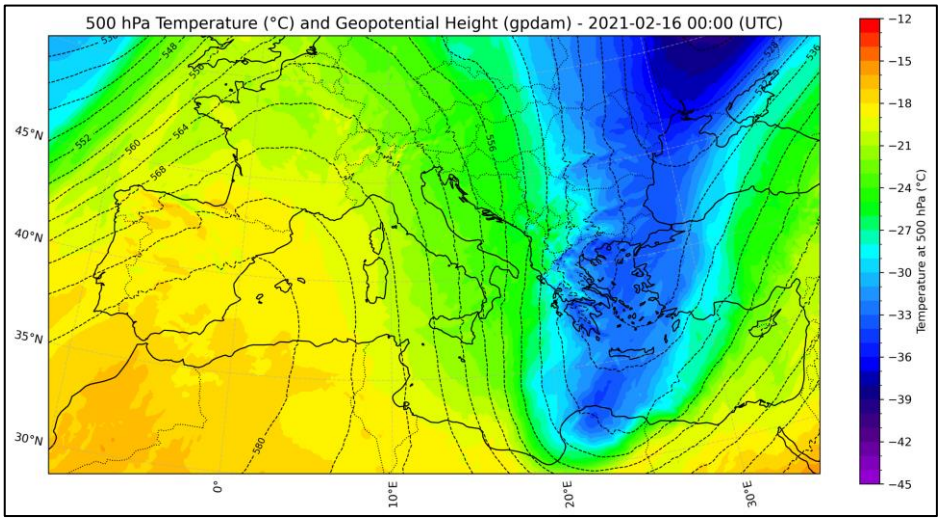


Fig. 5.14: Geopotential (gpdam) & Temperature (°C) at 500 hPa on February 16. (WRF 9 km)

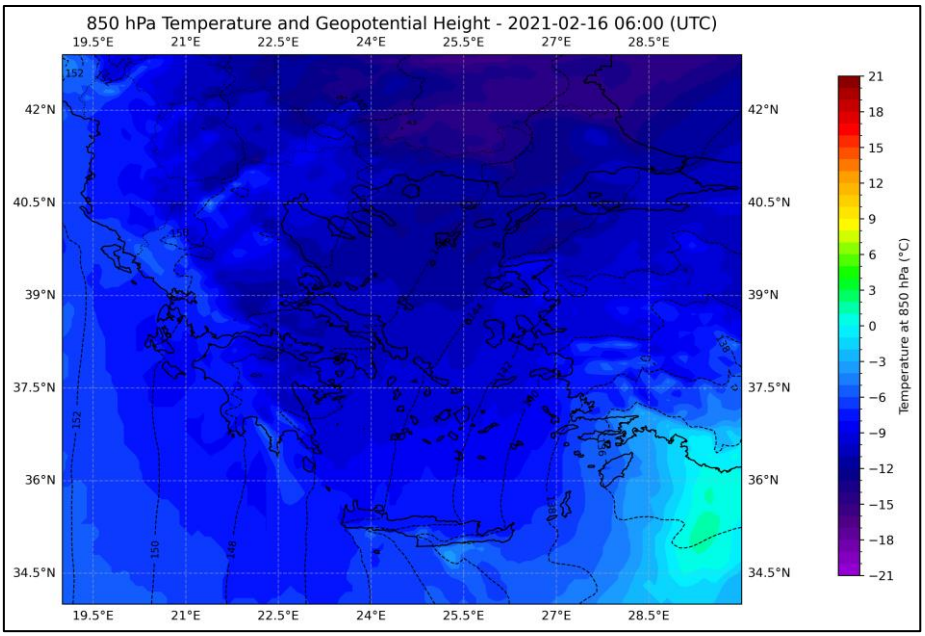


Fig. 5.15: Geopotential (gpdam) & Temperature (°C) at 850 hPa on February 16, at 08:00 local time. (WRF 9 km)

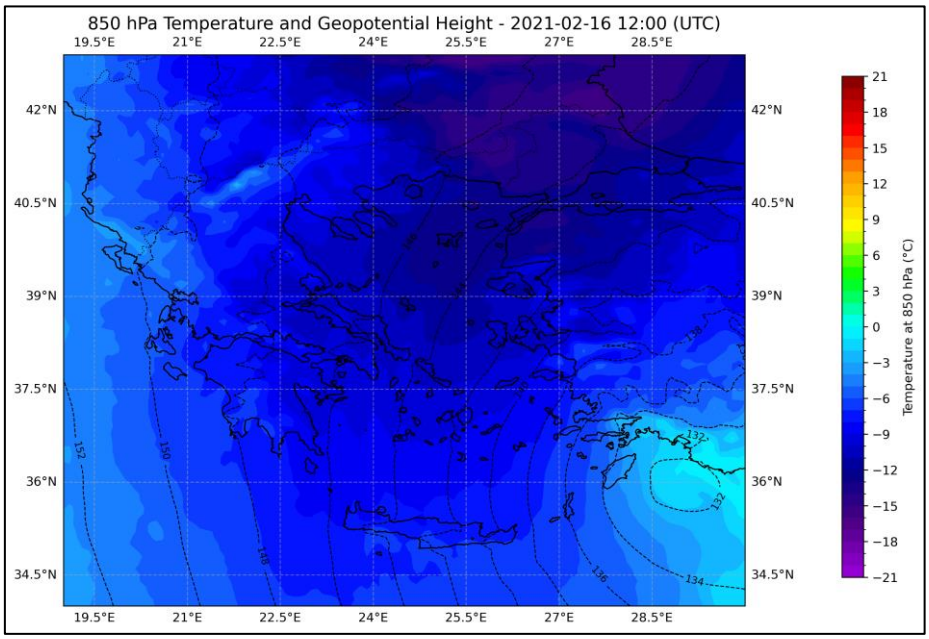


Fig. 5.16: Geopotential (gpdam) & Temperature (°C) at 850 hPa on February 16, at 14:00 local time. (WRF 9 km)

During the Medea snowstorm on February 16, the observed temperatures at the 850 hPa pressure level remained constant at -9.5°C both in the morning and in the afternoon. At the 500 hPa level, temperatures were recorded at -29.9°C in the morning, rising slightly to -27.7°C in the afternoon. The geopotential height was approximately 1460 gpdam at 850 hPa (Fig. 5.15 & Fig. 5.16) and around 5380 gpdam at 500 hPa above Athens (Fig. 5.18). The atmospheric thickness between the 1000 hPa and 500 hPa levels ranged from 5190 to 5230 gpdam, according to the radiosonde data from that day. Wind profiles indicated predominantly N between the 950 and 750 hPa levels, shifting to NW above approximately 300 hPa (Table 5.1, Table 5.2, Fig. 5.28 & Fig. 5.29). At the surface (10 meters height) the wind was strong, blowing from the N-NW (Fig. 5.25 - Fig. 5.27).

A detailed assessment of the synoptic scale configurations and the meteorological conditions reveals that the event exhibited distinct characteristics that align more closely with Type B criteria, though elements of Type A are also observed. This nuanced classification is grounded in a deeper analysis of the atmospheric patterns and their dynamic interactions. Initially, the presence of a surface anticyclone over Central-Eastern Europe above Greece played a pivotal role in defining the weather patterns during the Medea snowstorm. Simultaneously, the formation of a pronounced low-pressure system in the Southeastern Mediterranean introduced a substantial influx of moist air.

Table 5.1: *Radiosonde data from station 16716 LGAT Athinai (Airport) on February 16, 2021, at 08:00 local time. (https://weather.uwyo.edu/upperair/sounding.html)*

16716 LGAT Athinai (Airport) Observations at 06Z 16 Feb 2021										
PRES	HGHT	TEMP	DWPT	RELH	MIXR	DRCT	SKNT	THTA	THTE	THTV
hPa	m	C	C	%	g/kg	deg	knot	K	K	K
1018	15	-0.5	-1.1	96	3.48	0	0	271.3	280.8	271.8
1012	71	-0.8	-1.3	96	3.44	325	10	271.4	280.8	272
1000	184	-1.5	-1.8	98	3.37	330	16	271.6	280.9	272.2
944	639	-3.9	-4.5	96	2.92	345	30	273.8	281.9	274.2
925	800	-4.7	-5.4	95	2.78	350	28	274.5	282.3	275
890	1102	-6.7	-7.7	92	2.41	355	27	275.5	282.3	275.9
850	1461	-9.1	-10.5	90	2.03	0	35	276.6	282.5	276.9
794	1978	-12.8	-14	91	1.64	10	42	278.1	282.9	278.3
700	2933	-19.7	-20.5	93	1.08	20	34	280.6	283.9	280.8
699	2944	-19.9	-20.6	94	1.07	20	34	280.5	283.8	280.7
655	3421	-23	-27.8	65	0.6	30	33	282.3	284.2	282.4
653	3444	-23.1	-28.1	64	0.58	29	33	282.4	284.3	282.5
645	3534	-21.7	-38.7	20	0.21	26	35	285	285.7	285.1
639	3603	-21.5	-46.5	9	0.09	24	36	286	286.3	286
602	4041	-22.1	-53.1	4	0.05	10	45	290.2	290.4	290.2
589	4198	-23	-53.9	4	0.04	5	48	291	291.1	291
500	5380	-29.9	-59.9	4	0.02	10	72	296.5	296.6	296.5
463	5926	-33.9	-58.9	6	0.03	6	75	298.1	298.2	298.1
450	6125	-34.4	-61	5	0.02	5	76	299.9	300	299.9
436	6347	-35	-63.4	4	0.02	5	75	301.8	301.9	301.9
408	6812	-36.3	-68.3	2	0.01	9	97	306	306	306
404	6881	-36.3	-58.3	8	0.04	9	101	306.9	307	306.9
400	6950	-36.7	-54.7	14	0.06	10	104	307.2	307.4	307.2
388	7158	-38.7	-53.5	20	0.07	10	106	307.2	307.5	307.3
371	7463	-41.7	-51.7	33	0.09	9	102	307.2	307.6	307.3
349	7874	-43.3	-61.3	12	0.03	8	96	310.5	310.6	310.5
306	8740	-49.7	-68.6	9	0.01	5	84	313.4	313.4	313.4
300	8870	-50.7	-69.7	9	0.01	5	80	313.8	313.8	313.8

Table 5.2: *Radiosonde data from station 16716 LGAT Athinai (Airport) on February 16, 2021, at 14:00 local time. (https://weather.uwyo.edu/upperair/sounding.html)*

16716 LGAT Athinai (Airport) Observations at 12Z 16 Feb 2021										
PRES	HGHT	TEMP	DWPT	RELH	MIXR	DRCT	SKNT	THTA	THTE	THTV
hPa	m	C	C	%	g/kg	deg	knot	K	K	K
1018	15	1.2	0.3	94	3.86	340	4	273	283.5	273.6
1010	89	-0.3	-0.6	98	3.64	338	9	272.1	282	272.7
1002	164	-0.6	-1.1	97	3.54	335	14	272.4	282.1	273
1000	183	-0.7	-1.2	96	3.52	340	14	272.4	282.1	273
977	367	-1.8	-2.5	95	3.27	5	18	273.2	282.2	273.7
937	699	-3.7	-4.9	92	2.85	0	27	274.5	282.5	275
925	801	-4.3	-5.6	91	2.73	0	28	274.9	282.6	275.4
850	1462	-9.1	-10	93	2.11	355	32	276.6	282.7	276.9
844	1517	-9.6	-10.2	95	2.09	355	31	276.7	282.7	277
835	1600	-10.3	-10.6	98	2.05	356	32	276.8	282.7	277.1
790	2020	-13.2	-13.8	96	1.68	0	37	278	282.9	278.3
726	2662	-17.8	-18.6	93	1.22	10	20	279.9	283.5	280.1
724	2683	-17.9	-18.8	93	1.2	10	21	279.9	283.6	280.1
700	2934	-19.5	-21.9	81	0.95	15	28	280.9	283.8	281
699	2945	-19.6	-22.1	80	0.94	15	28	280.9	283.8	281.1
682	3127	-20.5	-25.1	67	0.73	358	32	281.8	284.1	282
669	3271	-17.3	-42.3	9	0.14	345	35	287	287.5	287
661	3361	-16.3	-53.3	3	0.04	347	37	289.1	289.3	289.1
643	3569	-17.5	-46.5	6	0.09	351	40	290	290.4	290.1
573	4416	-23.1	-49.2	7	0.08	10	55	293.1	293.4	293.2
526	5045	-27.3	-51.3	8	0.06	4	66	295.4	295.6	295.4
504	5353	-27.9	-55.9	5	0.04	1	72	298.3	298.4	298.3
500	5410	-27.7	-57.7	4	0.03	0	73	299.2	299.3	299.2
471	5837	-29.3	-61.3	3	0.02	357	78	302.4	302.5	302.4
447	6204	-32.1	-55.1	8	0.05	355	83	303.4	303.6	303.4
412	6776	-36.5	-45.5	39	0.16	359	82	304.9	305.5	304.9
400	6980	-37.9	-49.9	27	0.1	0	81	305.6	306	305.7
389	7171	-39.4	-51.4	27	0.09	5	77	306.1	306.4	306.1
369	7531	-42.3	-54.3	26	0.06	1	75	306.9	307.2	306.9
312	8650	-48.3	-67.1	10	0.01	350	67	313.7	313.8	313.7
303	8845	-49.3	-69.3	8	0.01	343	64	314.9	314.9	314.9
300	8910	-48.7	-68.7	8	0.01	340	63	316.6	316.7	316.6

Critical to the classification of this event was the emergence of an “Omega block” over Scandinavia at the 500 hPa level (Fig. 5.17 & Fig. 5.18). This blocking pattern typically leads to prolonged weather conditions, as it prevents the movement of weather systems across the block. Moreover, it is characterized by a persistent large-scale loop of the jet stream, which effectively locks in cold air masses over the region. In the case of Medea, this resulted in an extended period of cold and snowy conditions, a strong

characteristic of Type B snowstorms that are characterized by their duration and intensity due to such upper-level blockades (Prezerakos & Angouridakis, 1984).

In summary, while Medea shares some wind direction and temperature profile similarities with Type A snowstorms, the overall synoptic situation –marked by the anticyclone in Central-Eastern Europe, the Low in the Southeastern Mediterranean and particularly the Omega block at 500 hPa– strongly tilts its classification towards Type B.

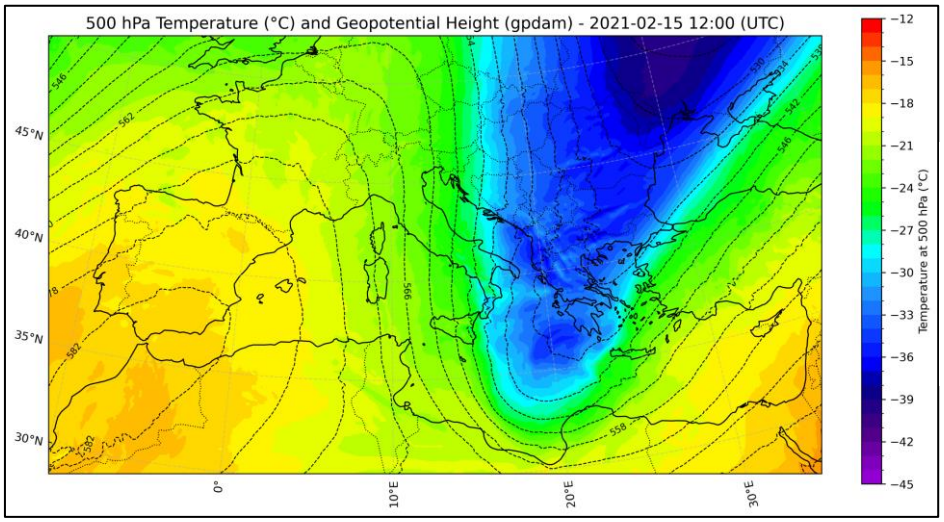


Fig. 5.17: Geopotential (gpdam) & Temperature (°C) at 500 hPa on February 15. (WRF 9 km)

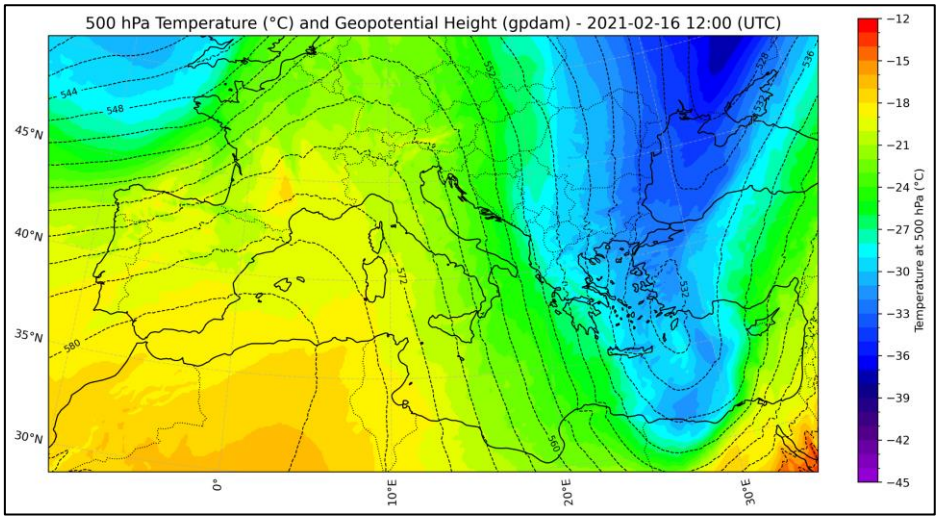


Fig. 5.18: Geopotential (gpdam) & Temperature (°C) at 500 hPa on February 16. (WRF 9 km)

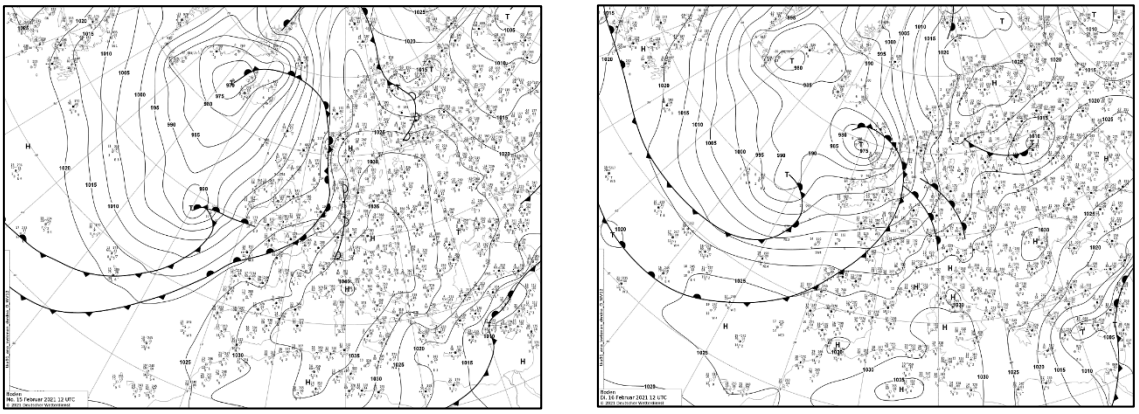


Fig. 5.19 & 5.20: DWD Surface Analysis on February 15 (left) and February 16 (right). (*https://www.wetter3.de/*)

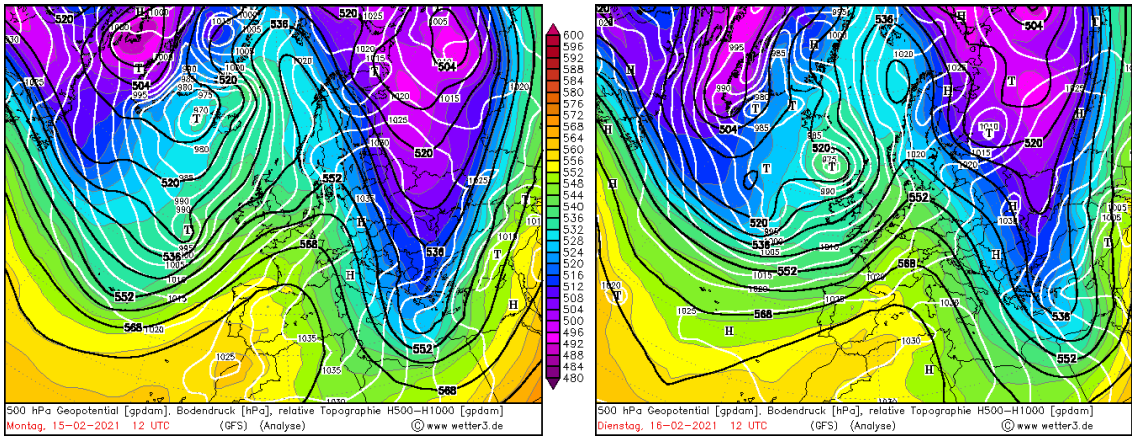


Fig. 5.21 & 5.22: Geopotential (gpdam) at 500 hPa, MSLP (hPa) & 1000-500 hPa Thickness on February 15 (left) and February 16 (right). (*https://www.wetter3.de/*)

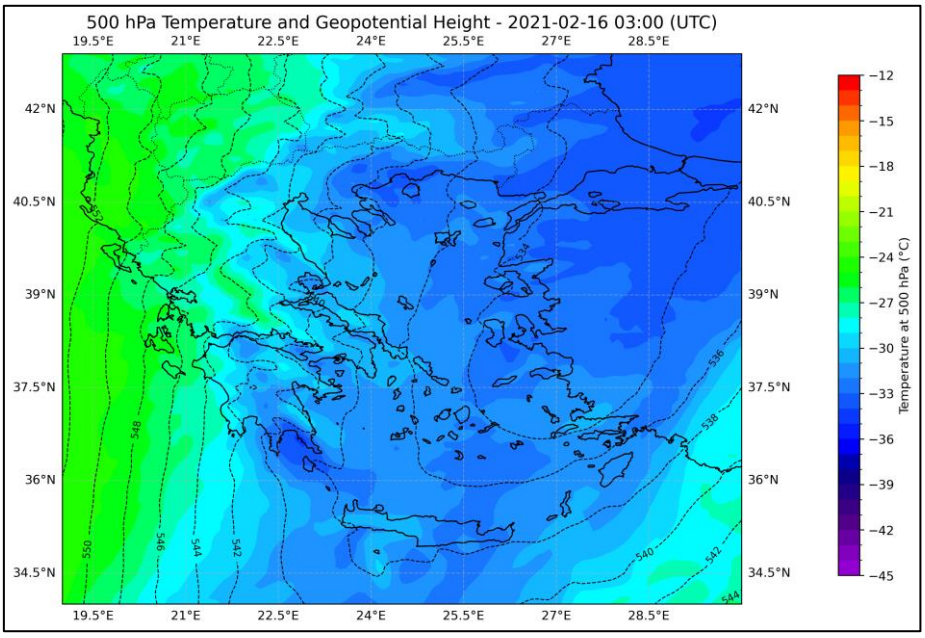


Fig. 5.23: Geopotential (gpdam) & Temperature (°C) at 500 hPa on February 16, at 05:00 local time. (WRF 9 km)

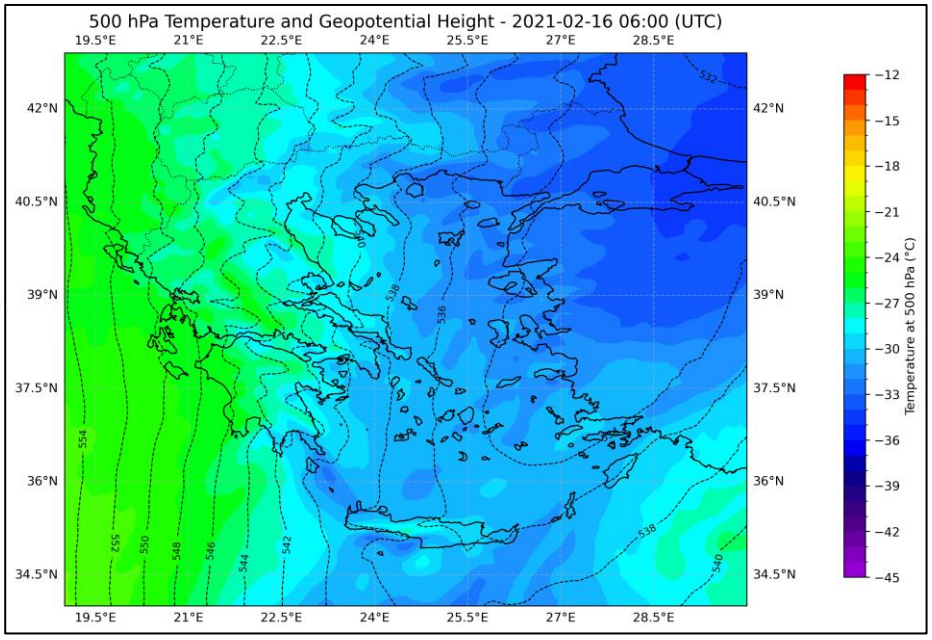


Fig. 5.24: Geopotential (gpdam) & Temperature (°C) at 500 hPa on February 16, at 08:00 local time. (WRF 9 km)

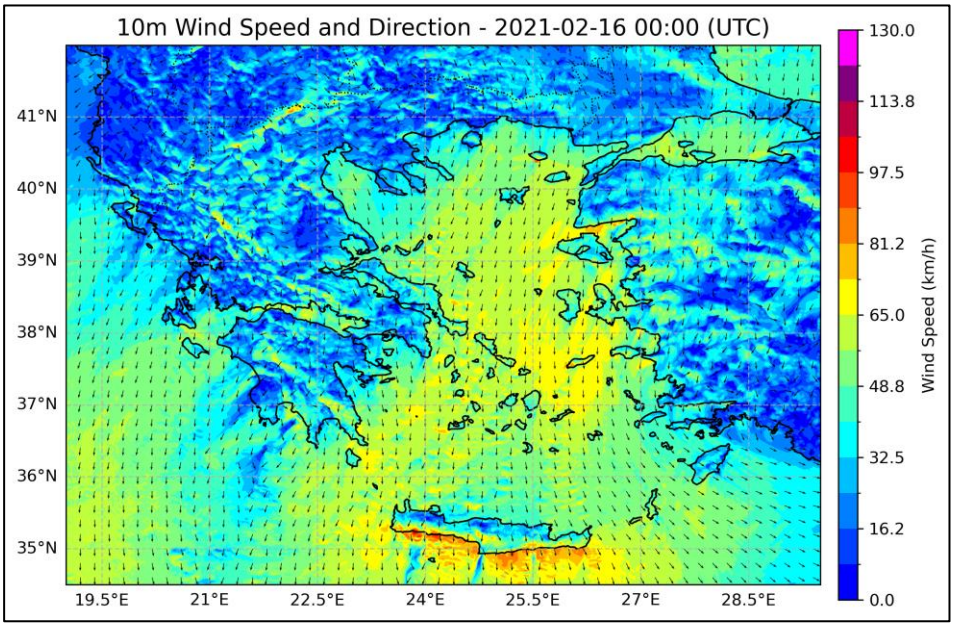


Fig. 5.25: 10m wind speed and direction on February 16, at 02:00 local time. (WRF 1 km)

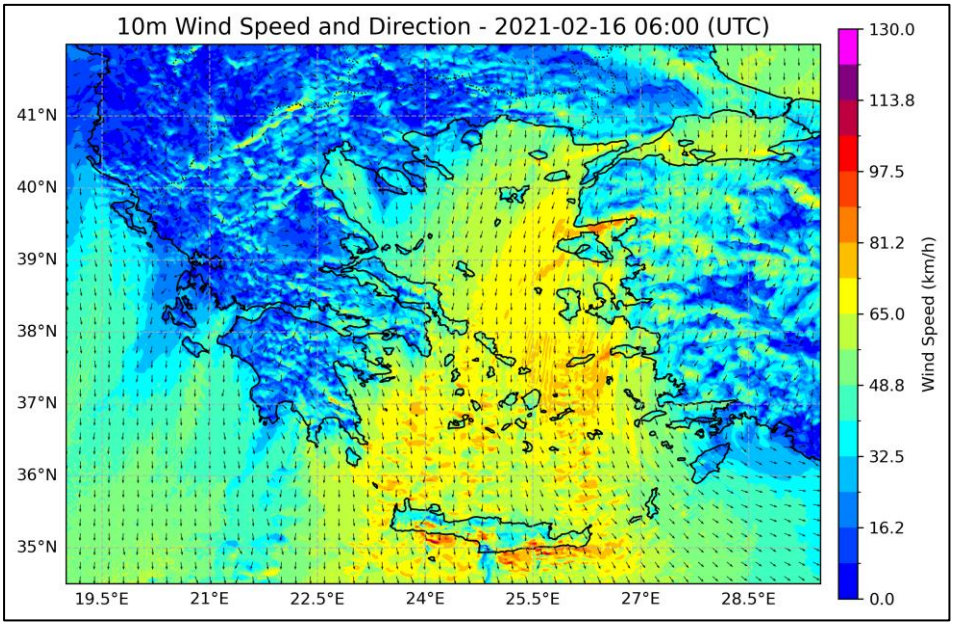


Fig. 5.26: 10m wind speed and direction on February 16, at 08:00 local time. (WRF 1 km)

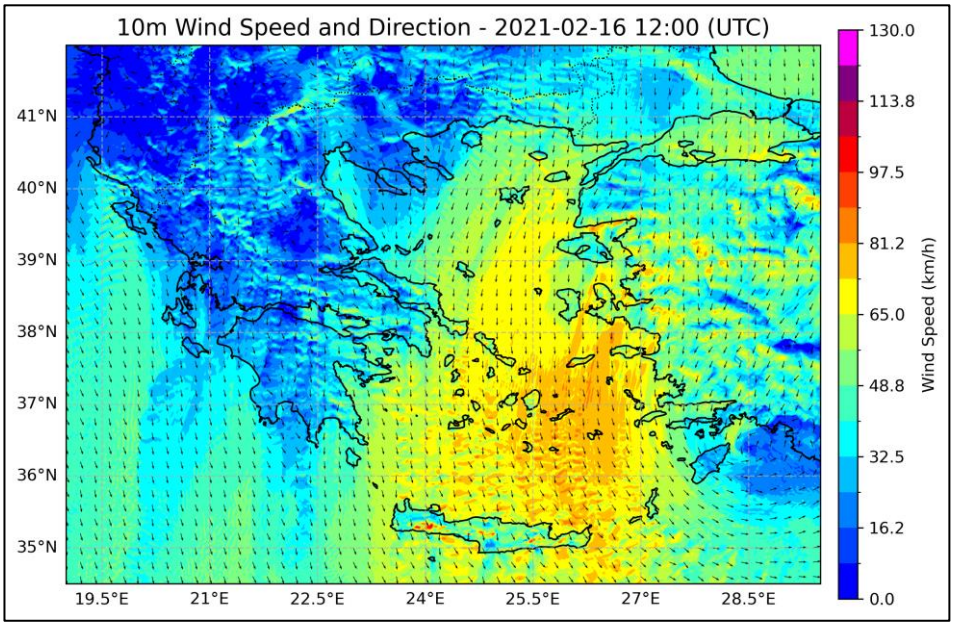


Fig. 5.27: 10m wind speed and direction on February 16, at 14:00 local time. (WRF 1 km)

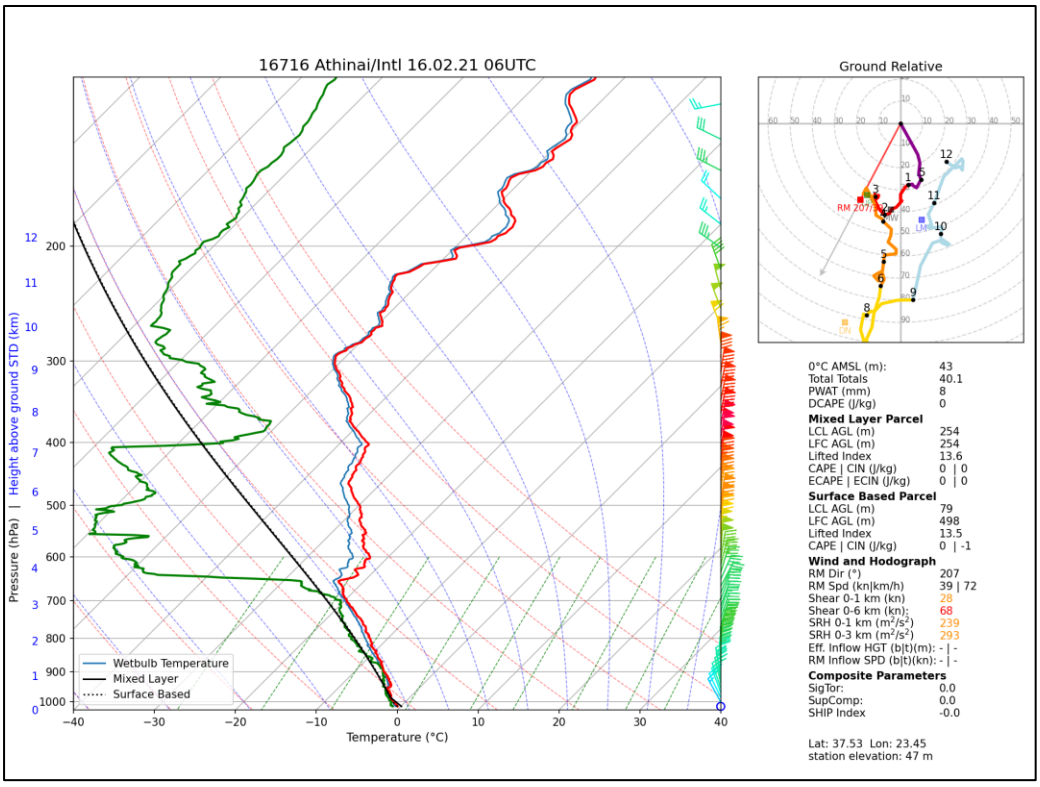


Fig. 5.28: Skew-T diagram from radiosonde data at station 16716 LGAT Athinai (Airport) on February 16, 2021, at 08:00 local time. (*https://meteologix.com/gr*)

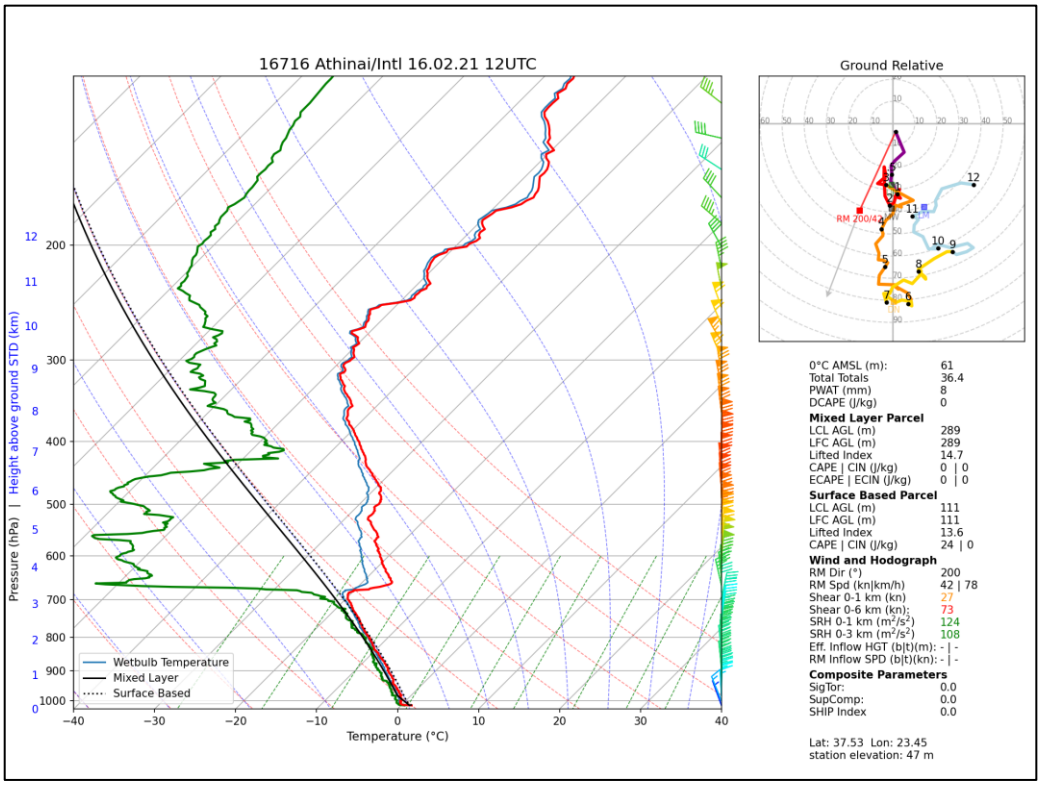


Fig. 5.29: Skew-T diagram from radiosonde data at station 16716 LGAT Athinai (Airport) on February 16, 2021, at 14:00 local time. (*https://meteologix.com/gr*)

5.2. Satellite Data Analysis

In analyzing the Medea snowstorm, we will take a distinctly different approach from that used for Elpida. This is because Medea's impacts were prolonged, lasting several days and affecting a significantly larger part of Greece. Based on GFS reanalysis data, from February 13 to the early hours of February 15, widespread snowfall was recorded across Central and Northern Greece, with rain and sleet affecting regions including Attica, Boeotia, and the Peloponnese. However, starting on the morning of February 15 and continuing through February 16, a lake-effect snow phenomenon developed over the Aegean Sea. This event exclusively impacted Eastern Central Greece and Euboea due to the configuration of atmospheric conditions and the prevailing northeasterly airflow. Given the extensive duration and the dynamic evolution of this event, the analysis will focus on day-by-day satellite data interpretation, highlighting the progression of cloud cover and precipitation patterns. This approach will offer a thorough understanding of Medea's evolution and its impact on the affected areas.

5.2.1. Onset of Snowfall – February 13, 2021

On February 13 at 12:00 UTC, visible satellite imagery (Fig. 5.30) reveals extensive cloud coverage over Greece, with particularly intense white shades observed over Attica, Boeotia, the eastern Peloponnese, and the Cyclades, suggesting thick clouds. These bright white shades indicate significant cloud thickness in these areas. In contrast, slightly less intense white shades are evident over Western, Central, and Northern Greece, suggesting relatively thinner clouds in these regions. In Crete, scattered cloud formations are visible, while clear skies are observed over the Dodecanese.

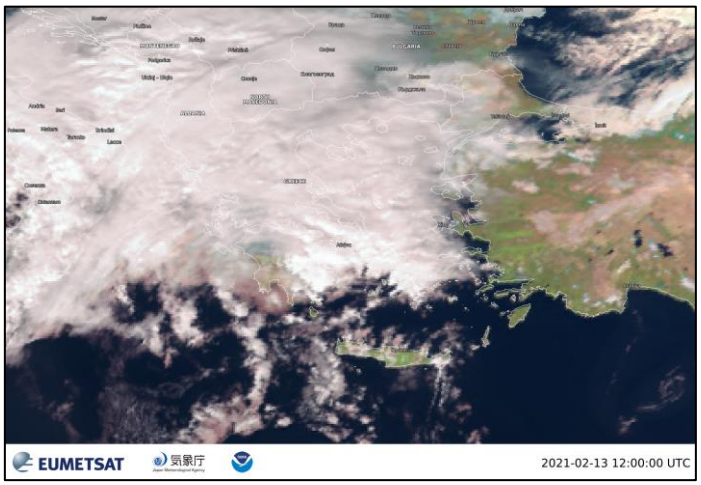


Fig. 5.30: Visible image at 12:00 UTC. (*https://www.eumetsat.int/*)

The infrared imagery (Fig. 5.31) provides further insight into cloud height and structure. Over Attica, Boeotia, and the eastern Peloponnese, gray tones are predominant,

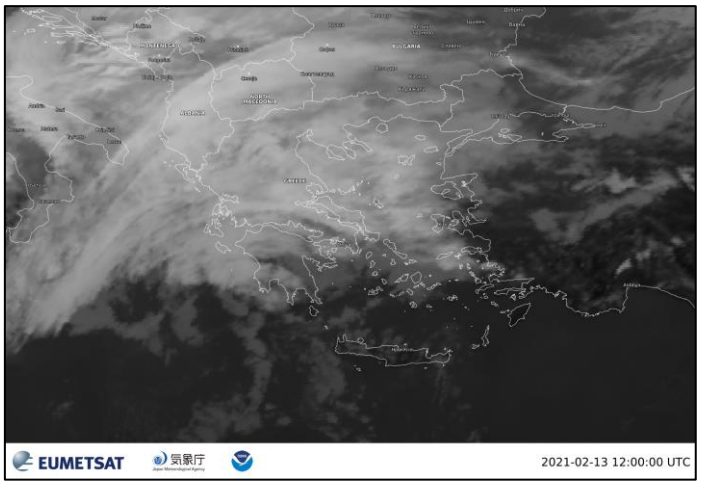


Fig. 5.31: Infrared image at 12:00 UTC. (*https://www.eumetsat.int/*)

indicating that thick clouds identified in the visible spectrum are located at mid-level altitudes. In contrast, the presence of lighter shades over Western, Central, and Northern Greece suggests clouds extending to higher altitudes in these areas. Examining the CTH product (Fig. 5.32), we observe cloud tops reaching approximately 8-9 km over much of Greece, with prevalent green and light green-yellow hues. Notably, over the eastern Peloponnese, cloud tops are lower, around 4 km in altitude. This variation in cloud height aligns with the differing cloud thickness and vertical extent observed in visible and infrared imagery across the region.

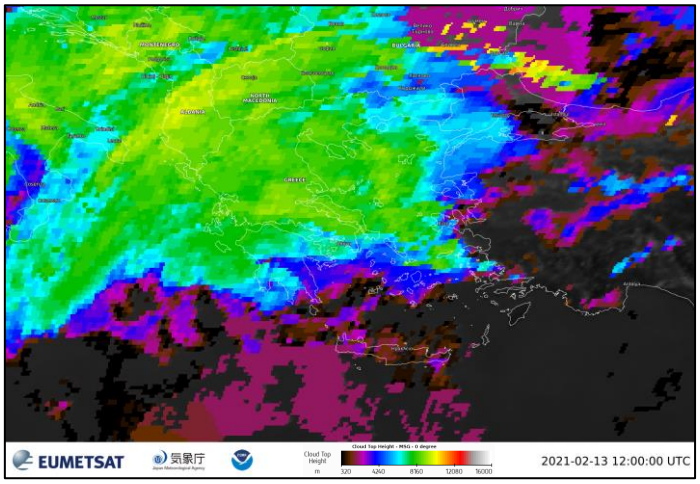


Fig. 5.32: CTH at 12:00 UTC. (*https://www.eumetsat.int/*)

Furthermore, according to Day Microphysics RGB image (Fig. 5.34), over central, western, and northern Greece, the observed mix of orange and red shades (labels 2 and 1, respectively) indicates thick clouds with substantial ice content at higher altitudes. This combination implies the presence of vertically developed clouds, rich in ice content, that are consistent with the development of significant precipitation. Additionally, we can recognize low- to mid-level thick water clouds (label 6) over southeastern Peloponnese.

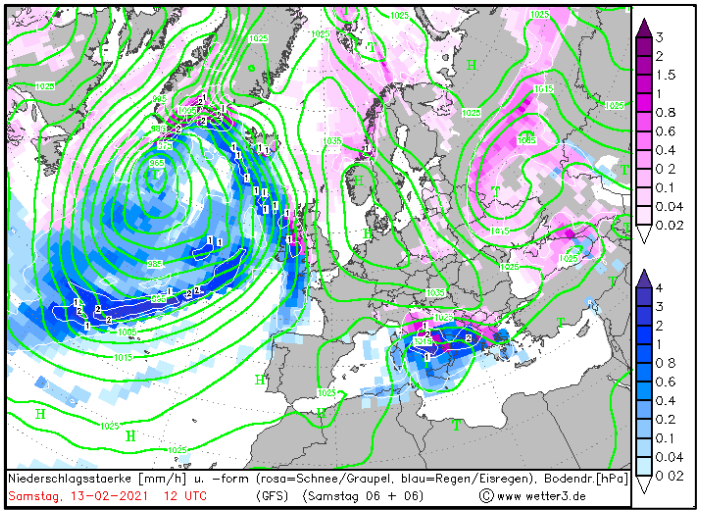


Fig. 5.33: Precipitation (phase/intensity) at 12:00 UTC. (*https://www.wetter3.de/*)

According to Severe Convection RGB (Fig. 5.35), these clouds could be indicated as super-cooled water clouds (label 5). In contrast, over Attica, the Cyclades and the eastern Peloponnese, the cloud structure appears to differ, with a lighter shade of orange with hints of yellow or green. This probably suggests that the clouds over the aforementioned areas have distinct microphysical properties compared to those over southeastern Peloponnese. Thus, this lighter orange-yellow hue may indicate lower, thick cloud tops with a mix of water and ice particles or smaller ice crystals (mix of labels 2 and 6), typical of mid-level clouds, which are consistent with what we observed in both visible and infrared images previously. Moreover, this mixed-phase cloud structure may lead to less intense precipitation over these areas (Fig. 5.33).

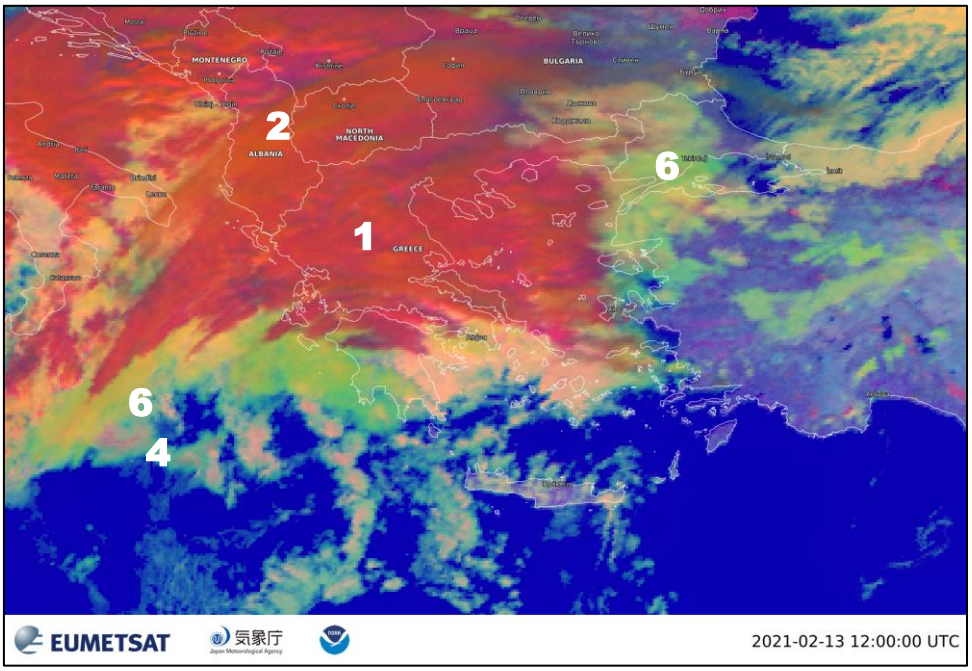


Fig. 5.34: Day Microphysics RGB at 12:00 UTC. (*https://www.eumetsat.int/*)

As for the air mass analysis, according to the Airmass RGB (Fig. 5.36), it reveals a complex interplay of polar, tropical and dry air masses. Northern Greece and the Balkans are influenced by a cold, ozone rich polar air mass (label 1) evident from the blue hues, which brings stability and

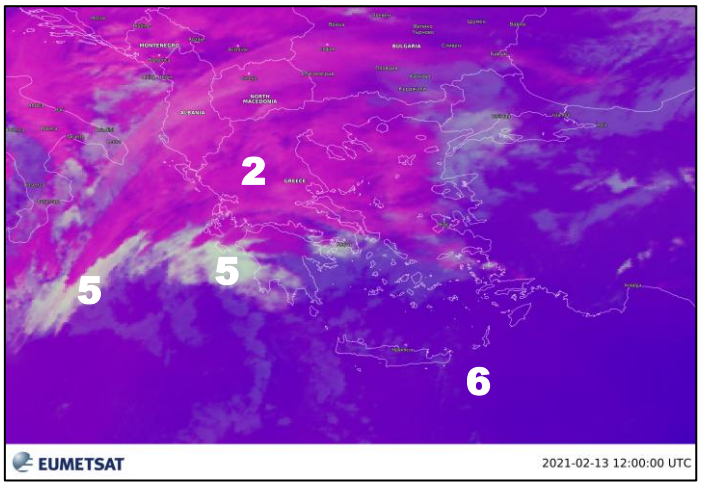


Fig. 5.35: Severe Convection RGB at 12:00 UTC. (*https://www.eumetsat.int/*)

colder temperatures. In contrast, the southern areas, such as Crete and the southern Aegean, show greenish-yellow colors, indicative of a warm, ozone poor tropical air mass (label 2), introducing a more humid and warmer conditions. West of Greece, the presence of reddish hues signals a dry air mass, likely associated with jet stream subsidence, which influences the atmospheric dynamics.

Over Attica, the Cyclades, and eastern Peloponnese, we observe shades corresponding to label "6", indicating mid-level clouds composed of both ice and water particles, which aligns with findings from other EUMETSAT products. Additionally, much of Greece is covered by high-level thick clouds (label 5).

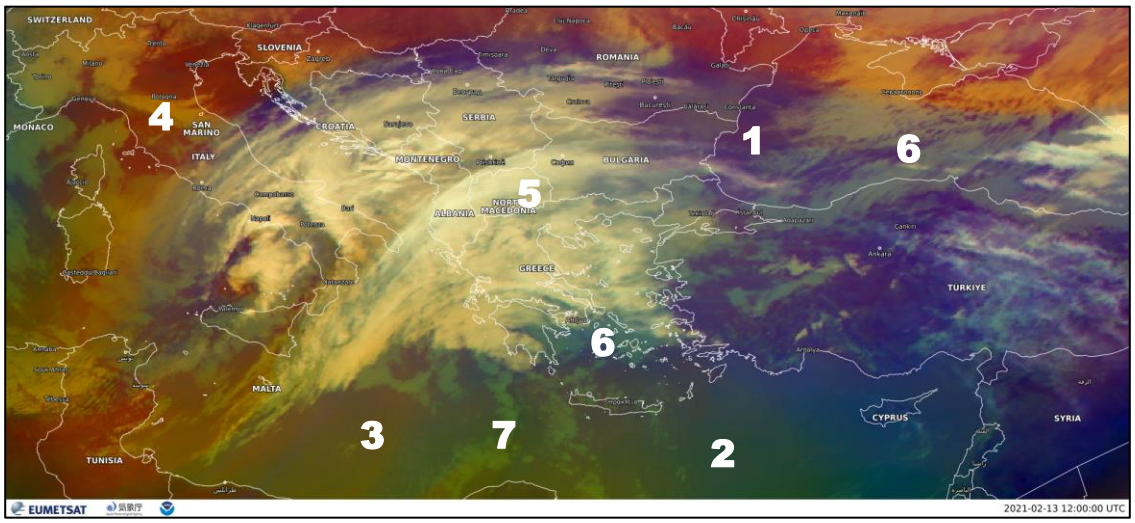


Fig. 5.36: Airmass RGB image at 12:00 UTC. (*https://www.eumetsat.int/*)

5.2.2. Continued Snowfall Expansion – February 14, 2021

On February 14 at 12:00 UTC, visible satellite imagery (Fig. 5.37) reveals that most of Greece, including regions extending down to the Dodecanese Islands, is covered with bright white shades, indicating widespread cloud cover across the country, which suggests the presence of thick cloud structures. However, when examining the infrared imagery (Fig. 5.38), we observe grayish shades, similar to the tones seen the previous day over Attica, the eastern Peloponnese, and the Cyclades, which means that the clouds are characterized by a substantial thickness, but at

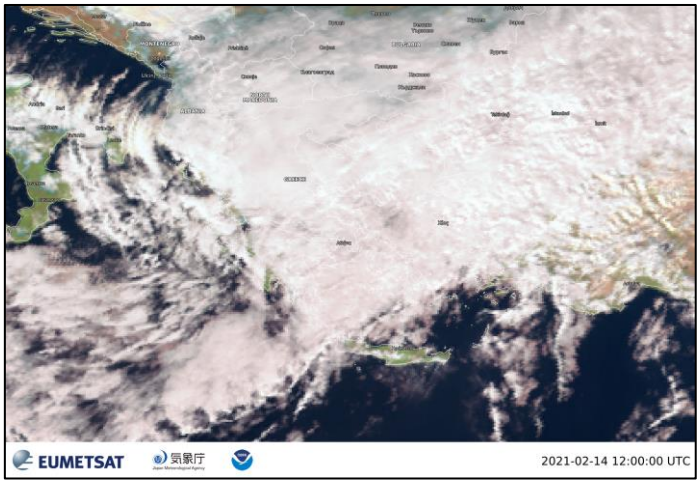


Fig. 5.37: Visible image at 12:00 UTC. (*https://www.eumetsat.int/*)

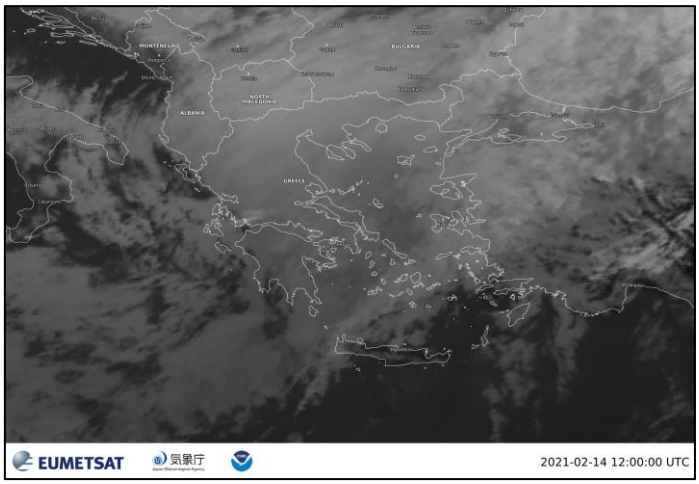


Fig. 5.38: Infrared image at 12:00 UTC. (*https://www.eumetsat.int/*)

lower altitudes. This pattern implies a more stable cloud system, with moderate vertical development, indicative of significant but not extreme atmospheric uplift across the area.

Examining the CTH data (Fig. 5.39), we observe that most of Greece is covered by clouds with altitudes generally ranging up to 4-5 km, indicating a prevalence of low to mid-level clouds across the region. However, there are notable localized areas with higher cloud tops over Aetolia-Acarnania, reaching heights of approximately 8 km, suggesting more substantial vertical development. This observation aligns well with GFS reanalysis data from the same period, which indicates heavy precipitation between 06:00 and 12:00 UTC. The increased cloud height in this area likely reflects stronger convective processes, supporting heavier precipitation events (Fig. 5.40).

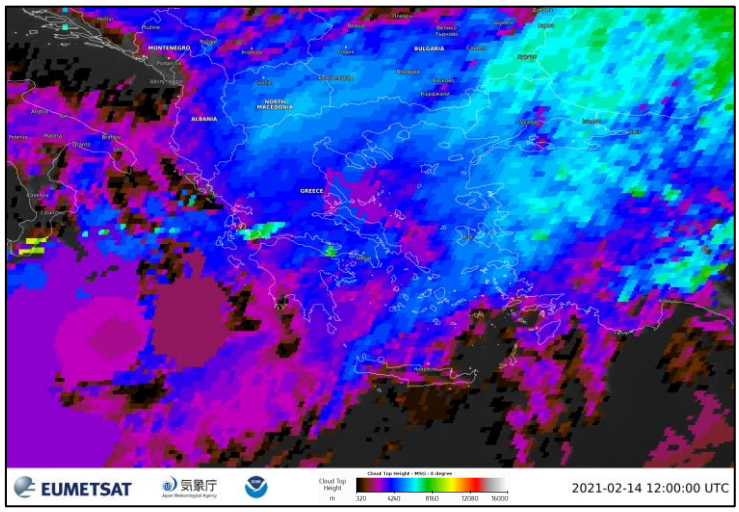


Fig. 5.39: CTH at 12:00 UTC. (*https://www.eumetsat.int/*)

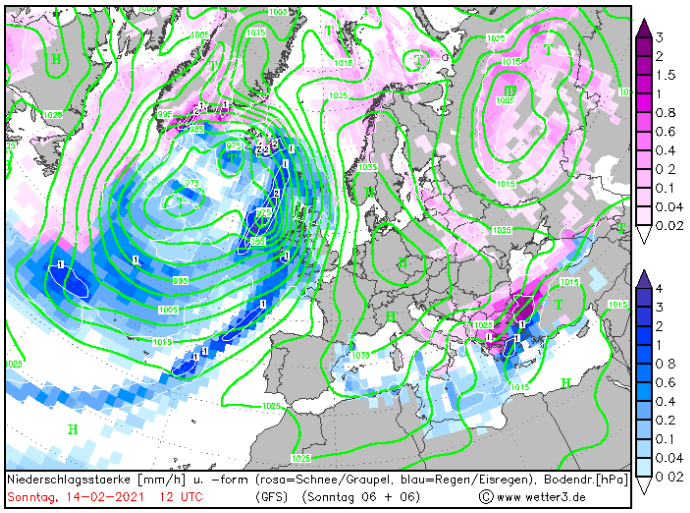


Fig. 5.40: Precipitation (phase/intensity) at 12:00 UTC. (*https://www.wetter3.de/*)

According to the Day Microphysics RGB imagery (Fig. 5.41), much of Greece is covered with hues like those observed over Attica, the eastern Peloponnese, and the Cyclades on the previous day, suggesting thick clouds with

relatively lower tops containing a mixture of water and ice particles or smaller ice crystals, characteristics of mid-level clouds. This observation is consistent with both visible and infrared imagery findings, and the Severe Convection RGB (Fig. 5.42), which show lower cloud tops across the region. A distinct contrast is seen in the coloration over the Black Sea, where orange shades (label 2) signify thick clouds with small ice particles, indicative of stronger convective activity, aligning with the darker hues in the GFS analysis data (Fig. 5.40), which points towards heavy snowfall over this region.

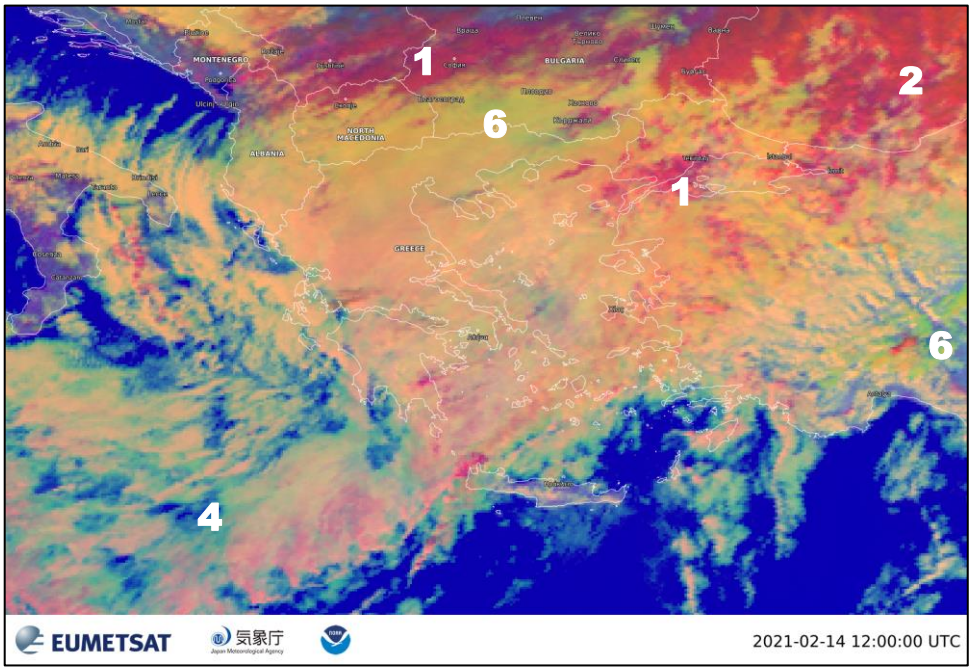


Fig. 5.41: Day Microphysics RGB at 12:00 UTC (*https://www.eumetsat.int/*)

Furthermore, we also observe orange hues over Aetolia-Acarnania, suggesting thick clouds, and aligning with the higher cloud tops detected in the CTH data for the same region. This reinforces the hypothesis of severe convective activity occurring locally in that region, which is also corroborated by the GFS model, since it displays a more intense purple hue over this area, indicating substantial precipitation. Additionally, localized red areas (label 1) appear in Eastern Thrace, the eastern Aegean, and parts of the eastern Peloponnese. These red

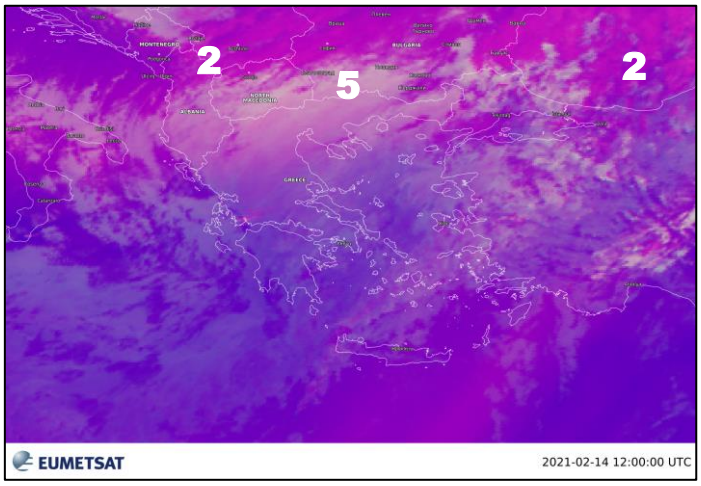


Fig. 5.42: Severe Convection RGB at 12:00 UTC. (*https://www.eumetsat.int/*)

hues indicate thick clouds with large ice particles, signaling zones of more intense convective processes. This assessment is consistent with the slightly darker precipitation shades in the GFS analysis data (Fig. 5.40), suggesting stronger precipitation events compared to the general conditions over the rest of Greece.

As for the Airmass RGB imagery (Fig. 5.43), we can observe cold, ozone-rich polar air masses (label 1) dominating the Black Sea, while warm, ozone-poor tropical air masses (label 2) in southern parts of Greece, drawn northward by synoptic-scale weather systems. A notable contrast is observed between these air masses, with dry, subsiding air (label 4) seen over the Adriatic Sea and the surrounding areas (central Italy and western Balkans). High-level thick clouds (label 5) cover the Black Sea and the northern parts of Greece, while mid-level ice and water clouds (label 6) are seen in the rest of Greece, aligning with the data from the other EUMETSAT products. This interplay of air masses, combined with cloud structures, underscores the potential for the dynamic weather activity observed during that day.

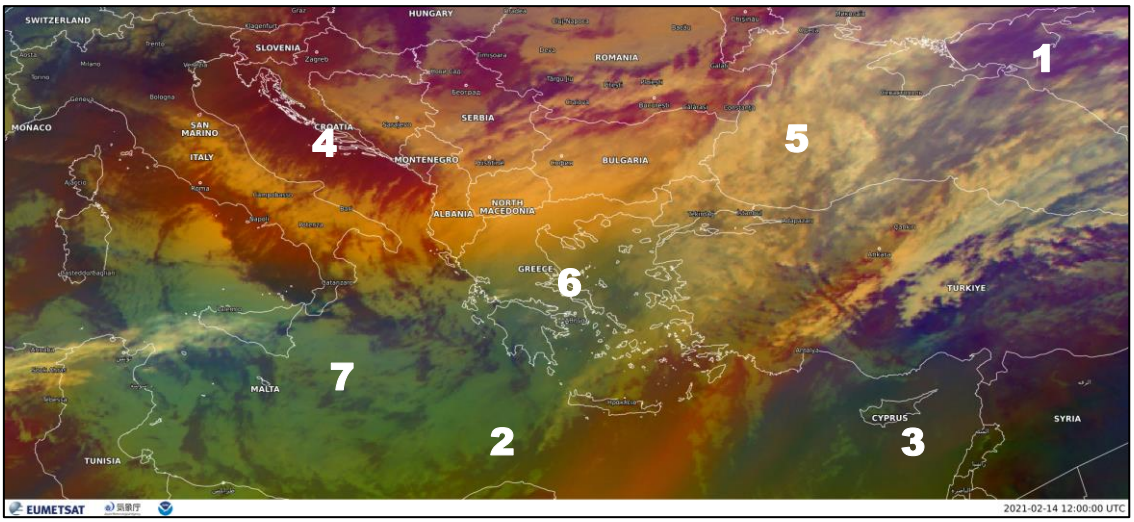


Fig. 5.43: Airmass RGB image at 12:00 UTC. (*https://www.eumetsat.int/*)

5.2.3. Lake-Effect Snow Intensification – February 15, 2021

From this point onward, the focus shifts primarily to the eastern and southern parts of Greece, with a particular emphasis on the region of Attica, because the lake-effect mechanism was activated on the morning of February 15, 2021, leading to the first snowfall events within the Athens basin, especially affecting the western suburbs. In the broader area of Attica, the western and northern parts of the region experienced more snowfall. This is evident in the visible satellite imagery (Fig. 5.44), which reveals thicker cloud cover over western Attica. This fact is also confirmed by the Day Microphysics RGB imagery (Fig. 5.48). Notably, snow accumulation was observed even at sea level

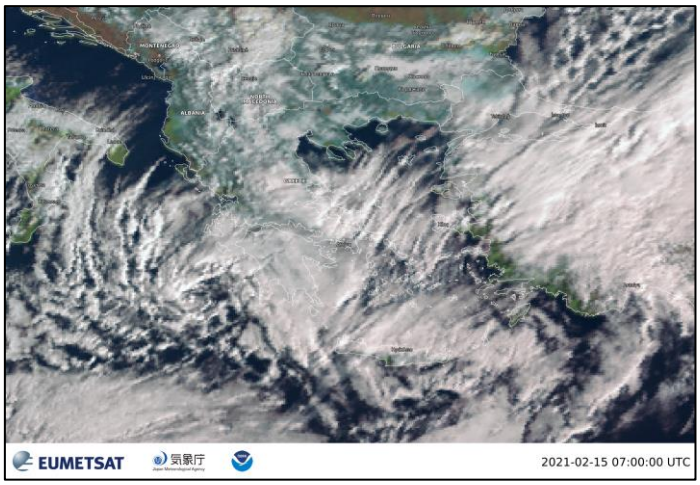


Fig. 5.44: Visible image at 07:00 UTC. (*https://www.eumetsat.int/*)

in the aforementioned areas, primarily covering surfaces during the early morning hours. Although similar conditions persisted throughout the day, the atmospheric temperature distribution around midday and into the afternoon influenced snowfall intensity and accumulation.

Based on the CTH data, higher loud tops are observed over central and southern Greece, with higher altitudes reaching approximately 4-6 km. Additionally, around Crete, a distinct line of clouds is evident, reaching altitudes of 8-10 km. This line of clouds observed represents the initial stage of a cold front that is beginning to develop. Over the following hours and days, it continues to evolve, eventually extending as far as Cyprus. Noteworthy cloud heights are also observed over northern Turkey, where cloud tops range from 6 to 8 km and cover a substantial area. These clouds are also thick, consisting of small ice crystals on top (Fig. 5.46). According to the GFS model (Fig. 5.47), these regions experienced significant snowfall, with rain or sleet occurring in areas further south and closer to coastal areas.

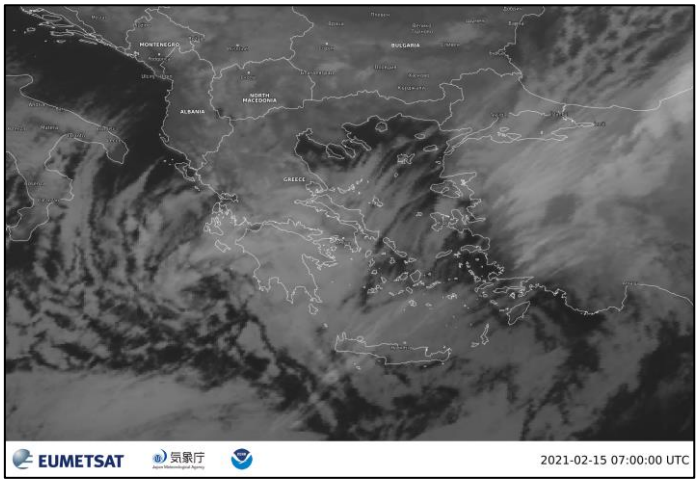


Fig. 5.45: Infrared image at 07:00 UTC. (*https://www.eumetsat.int/*)

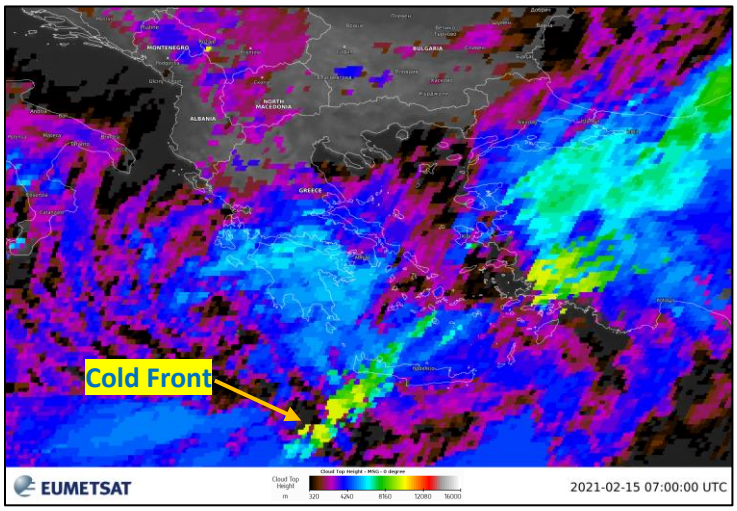


Fig. 5.46: CTH at 07:00 UTC. (*https://www.eumetsat.int/*)

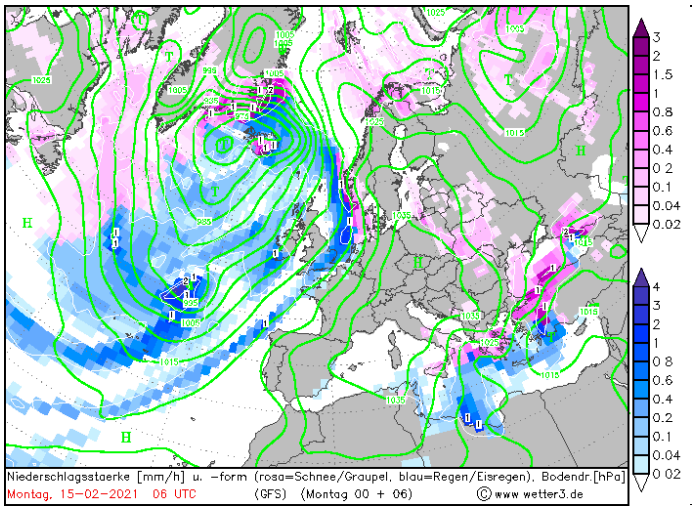


Fig. 5.47: Precipitation (phase/intensity) at 06:00 UTC. (*https://www.wetter3.de/*)

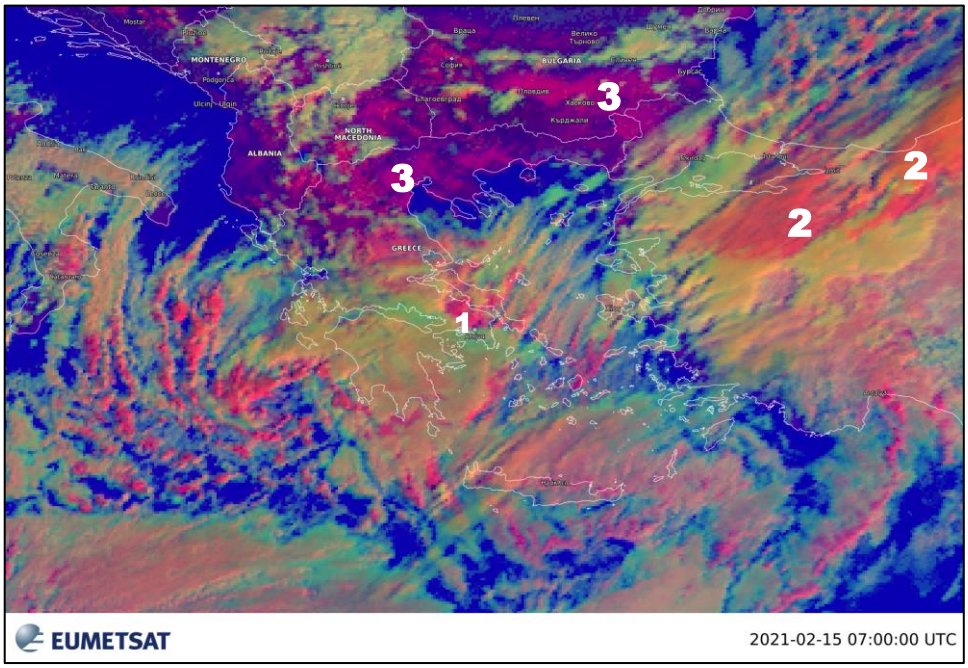


Fig. 5.48: Day Microphysics RGB at 07:00 UTC (*https://www.eumetsat.int/*)

In the Airmass RGB image (Fig. 4.49), we observe cold, ozone-rich polar air masses, (label 1) descent from the north over northern Italy, Slovenia and Croatia, while warm, ozone-poor tropical air masses with high moisture levels (label 2) are observed over the western Mediterranean. In contrast, dry subsiding air with PV anomalies (label 4) appears over northern Greece, Bulgaria, and the Adriatic Sea, enhancing instability in these regions. Also, we can recognize warm air masses with low upper tropospheric humidity (label 3) over Cyprus. The image also shows mid-level clouds with mixed-phase particles over central Greece (6), indicative of moderate precipitation potential. Finally, high-level thick clouds (5) are visible over northern Turkey, indicating heavier precipitation.

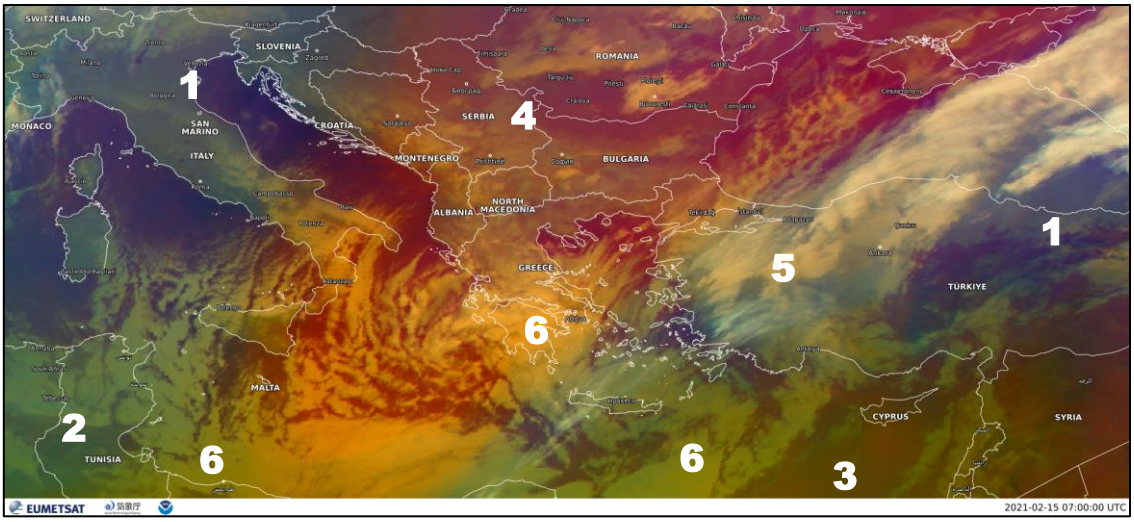


Fig. 5.49: Airmass RGB image at 07:00 UTC. (*https://www.eumetsat.int/*)

5.2.4. Peak Snowfall Impact in Eastern Regions – February 16, 2021

From late night of February 15 through the morning of February 16, the snowstorm in Attica reached its peak intensity. Notably, snow accumulation was observed across the entire Attica basin, including coastal areas. This phenomenon was supported by the vertical atmospheric temperature distribution, as analyzed in the synoptic setup, as well as the lake-effect snow mechanism. Wind directions favored the enhancement of moisture flux into the region, leading to widespread snowfall. This occurred as a result of wind convergence zones forming over the broader area. This condition persisted throughout

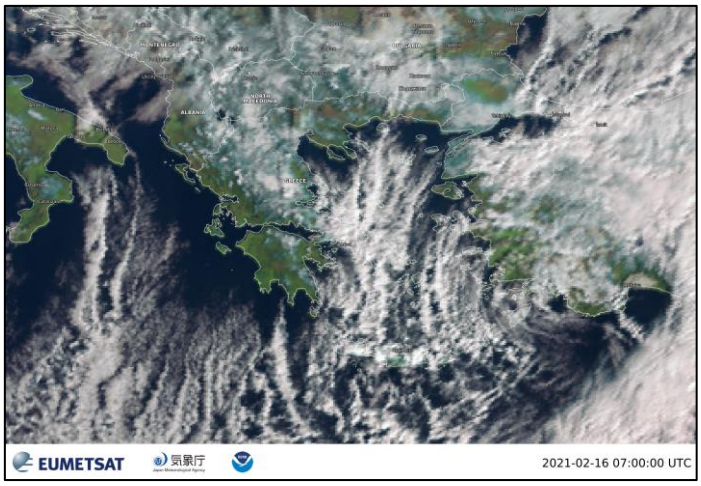


Fig. 5.50: Visible image at 07:00 UTC. (*https://www.eumetsat.int/*)

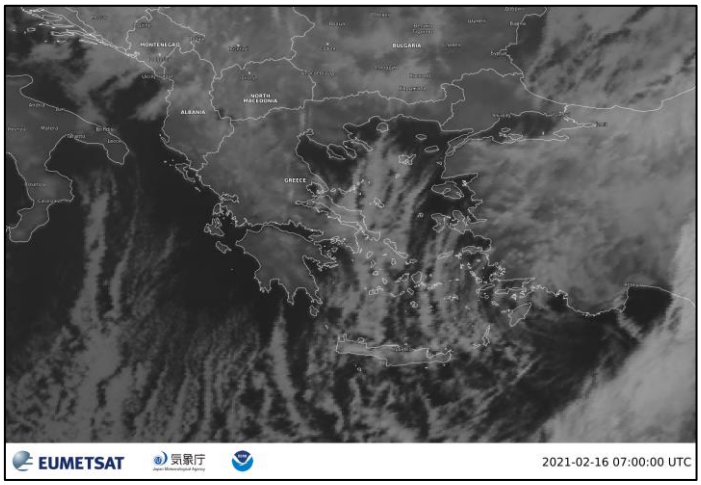


Fig. 5.51: Infrared image at 07:00 UTC. (*https://www.eumetsat.int/*)

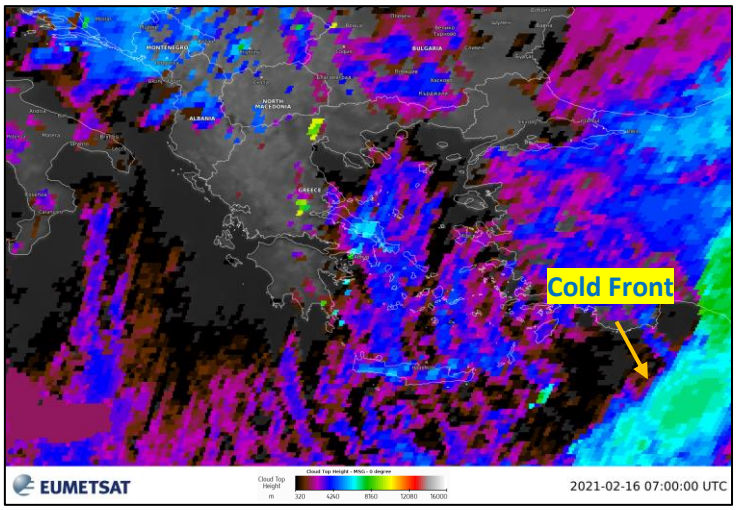


Fig. 5.52: CTH at 07:00 UTC. (*https://www.eumetsat.int/*)

the day, with significant snow bursts observed in various parts of the basin, particularly in the western suburbs.

These observations are corroborated by satellite imagery. Visible satellite images (Fig. 5.50) reveal dense cloud coverage, evident from the intense white shades over areas such as Euboea, Attica, the Cyclades and Crete. Infrared imagery (Fig. 5.51) further confirms the presence of vertically developed mid- to high-level clouds, as suggested by bright white shades. CTH data (Fig. 5.52) supports this conclusion, as cloud heights of approximately 5-6 km (light blue shades) are observed over areas such as the western suburbs of Athens.

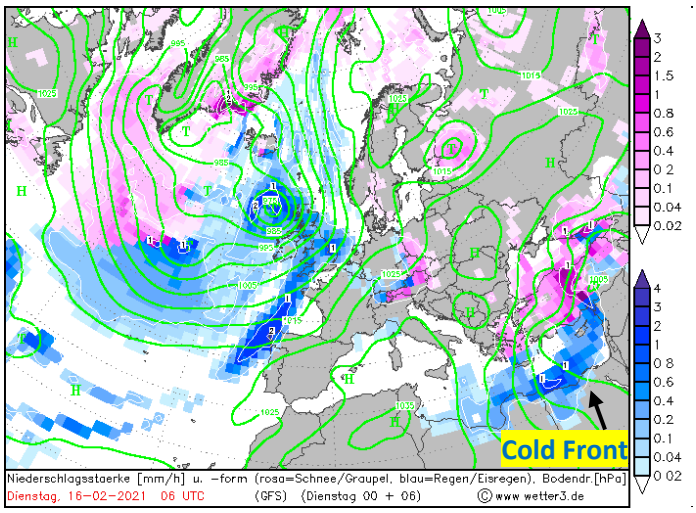


Fig. 5.53: Precipitation (phase/intensity) at 06:00 UTC. (*https://www.wetter3.de/*)

Additionally, we can also observe the significant expansion of the cold front towards the southeast, progressing toward Cyprus and eastern Turkey. This cold front, in combination with an existing warm front located more centrally over Turkey, effectively formed a frontal occlusion (Fig. 5.9).

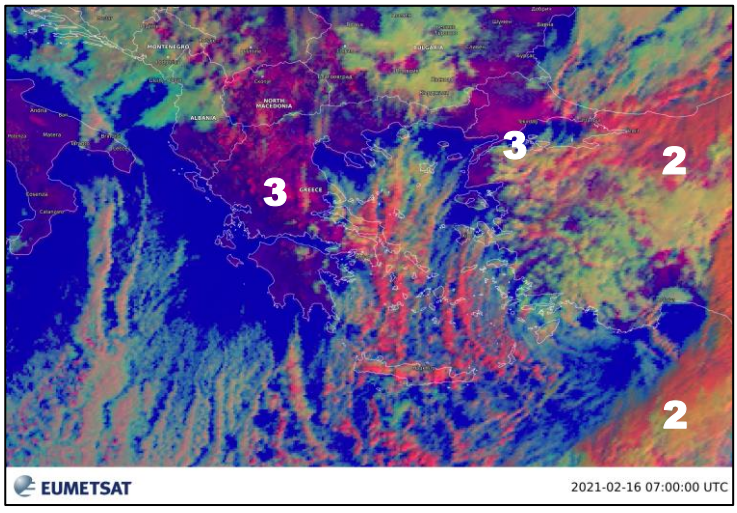


Fig. 5.54: Day Microphysics RGB at 07:00 UTC. (*https://www.eumetsat.int/*)

Moreover, the Day Microphysics RGB imagery (Fig. 5.55) further validates

these findings, with red-orange shades (labels 1 and 2) over Euboea, Attica and the Cyclades, apparent in the morning hours (07:00 UTC), indicative of thick clouds with large ice particles. By 12:00 UTC, these shades became more localized, with lighter orange-yellow hues dominating, suggesting thick clouds with relatively lower tops, for which we talked about in the previous units. This evolution in cloud structure aligns with the ongoing atmospheric dynamics and patterns observed throughout the day. These observations are further supported by the GFS precipitation phase and intensity data (Fig. 5.53), which reveal significant snowfall occurring in Euboea, Attica and the northern islands of Cyclades. Additionally, in the rest of the Cyclades and Crete, notable precipitation events are evident, with rainfall or sleet dominating coastal regions, while heavy snowfall impacts the mountainous and semi-mountainous areas.

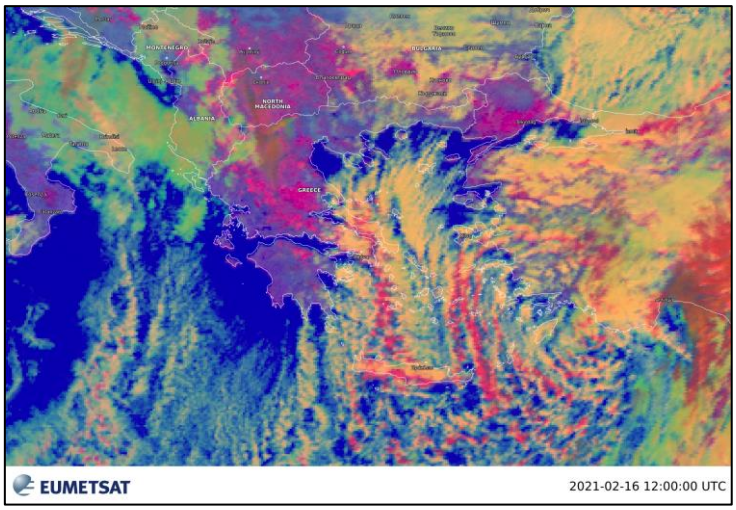


Fig. 5.55: Day Microphysics RGB at 12:00 UTC. (*https://www.eumetsat.int/*)

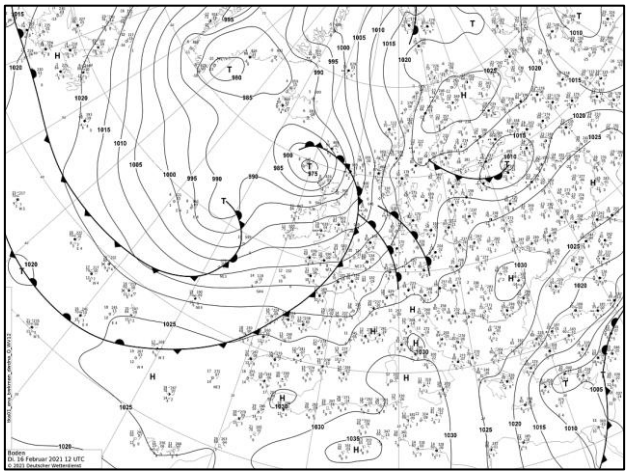


Fig. 5.56: DWD Surface Analysis at 12:00 UTC. (*https://www.wetter3.de/*)

The Airmass RGB image (Fig. 5.57) shows cold, we can indicate ozone-rich polar air masses over central-western Balkans (label 1). In contrast, in the eastern Mediterranean (Black Sea, Aegean Sea, Turkey & Crete), dry, subsiding air masses linked to potential vorticity anomalies (label 4) can be observed. Mid-level ice and water clouds (label 6) extend over the Aegean Sea, indicating cloud structures associated with moderate instability and active weather systems. Additionally, high-level thick clouds (label 5) are present over Turkey and parts of the Mediterranean, representing active frontal systems, as seen also in the DWD surface analysis (Fig. 5.56).

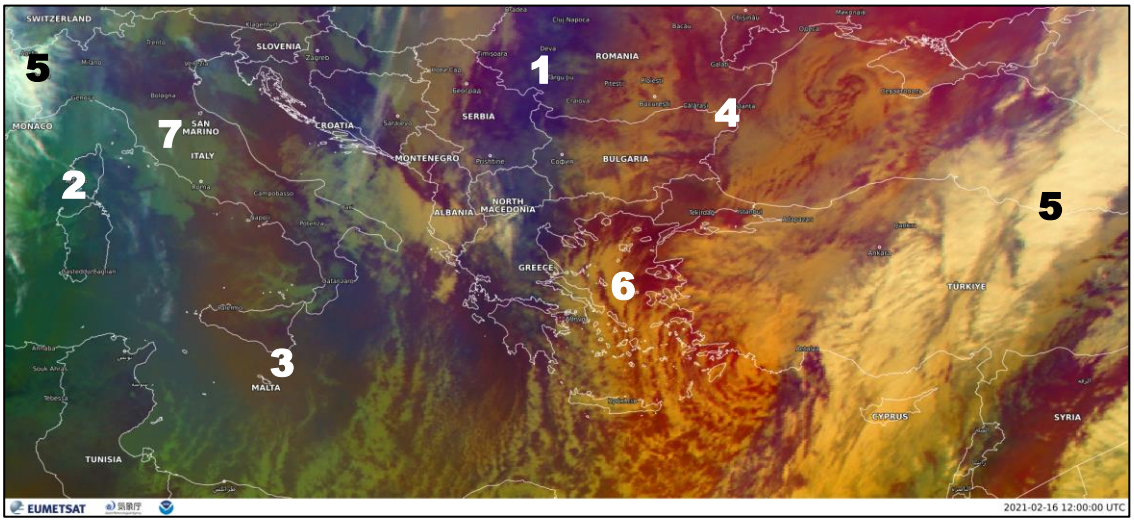


Fig. 5.57: Airmass RGB image at 07:00 UTC. (*https://www.eumetsat.int/*)

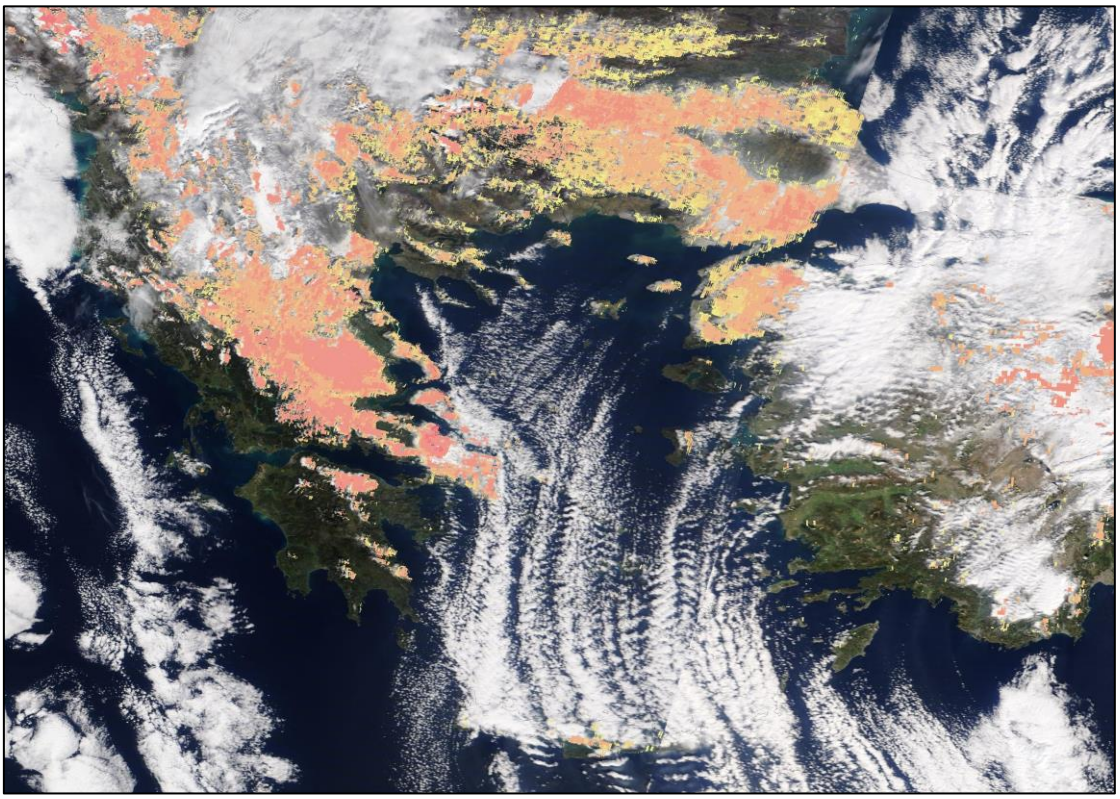


Fig. 5.58: Snow cover on February 17, 2021. Clouds depicted in white, while the intensity of snow cover is presented by color shades – the deeper orange-red hues indicate higher snow depths, whereas lighter yellow tones signify areas with less snow accumulation. (*https://worldview.earthdata.nasa.gov*)

6. COMPARISON BETWEEN THE TWO CASES AND DISCUSSION

6.1. Structure Scientific Comparison: 'Medea' vs. 'Elpida' Snowstorms

While 'Medea' and 'Elpida' shared similar synoptic and thermodynamic structures, their distinct cyclonic organization, convective dynamics, and geographical impacts highlight the diverse characteristics of extreme snowfall events in Greece. The closed cyclonic structure and stronger atmospheric instability of Elpida resulted in a more intense but shorter-duration snowstorm, whereas the broader reach and prolonged effects of Medea underscore its significance as a widespread event. Examining these differences provides crucial insights into the mechanisms driving such phenomena and enhances our ability to forecast similar events in the future.

Table 6.1: *Key Meteorological Parameters of Medea and Elpida Snowstorms.*

	Snowfall Conditions for Athens	**Medea (16/02/2021, 06:00 UTC)**	**Elpida (24/01/2022, 18:00 UTC)**
Thickness (1000–500 hPa)	≤5400 gpm	~5200 gpm	~5160 gpm
Geopotential Height (500 hPa)	5270-5385 gpm (Type A) or 5400-5460 gpm (Type B)	~5380 gpm	~5320 gpm
Geopotential Height (850 hPa)	1330-1485 gpm (Type A) or 1390-1505 gpm (Type B)	~1460 gpm	~1445 gpm
Surface winds	NW (Type A) or NE (Type B)	NNW	NNE
Mid-Level winds (950–750 hPa)	N	N	N
Upper-Level winds	NW	N to NW	NW
T-Td (950–800 hPa)	≤3°C	≤3°C	≤3°C
Temperature (850 hPa)	-11.5°C to -5.5°C (Type A) or -13°C to -7°C (Type B)	-9.1°C	-10°C to -8°C
Temperature (500 hPa)	-35°C to -28.4°C (Type A) or -31.6°C to -23.4°C (Type B)	-29.9°C	-40°C to -38°C
Cloud Development and Convective Characteristics	-	Moderate vertically developed clouds (4-6 km), indicative of sufficient convection	Exceptionally high vertically developed clouds (8-10 km), indicative of strong convection

Table 6.1 provides a comparative analysis of the two significant snowfall events, focusing on key meteorological parameters associated with snowfall conditions in Athens. It includes data such as thickness levels (1000–500 hPa), geopotential heights at 500 hPa and 850 hPa, surface and upper-level winds, temperature differences (T-Td), and cloud development characteristics. This comparison highlights the similarities in their synoptic and thermodynamic structures while emphasizing the differences in cyclonic organization, convective activity, and atmospheric instability. By illustrating these contrasts, the table offers valuable insights into the diverse dynamics and geographical impacts of these two extreme weather events, enhancing our understanding of the mechanisms driving intense snowfall in Greece.

6.1.1. Genesis and Synoptic Setup

Both Medea and Elpida originated under an Omega block configuration that dominated the upper levels over the North Atlantic. This blocking pattern, characterized by a high-pressure ridge flanked by low pressure systems, disrupted atmospheric circulation. In both cases, the ridge gradually developed dynamically unstable characteristics, allowing an upper-level trough to advance southward over the Balkans.

The key difference between the two storms lies in the nature of their cyclonic circulation. In Elpida, a closed cyclonic circulation developed at high altitudes, accompanied by a polar front jet streak along its western flank. This closed structure enhanced the dynamic and thermodynamic processes that supported strong convection and more intense snowfall. In contrast, Medea displayed a non-closed cyclonic circulation at upper levels, which, while still significant, was less organized, resulting in weaker snowfall compared to Elpida. The closed structure of the upper-level system in Elpida was likely the primary reason for its more extreme characteristics.

6.1.2. Duration and Affected Regions

Medea lasted longer (February 13–16, 2021) and affected a broader area compared to Elpida. The snowfall initially affected central and northern Greece, with snowfall occurring even in lowland areas, while in Peloponnese, Euboea, Attica, and the Cyclades, rain prevailed. There were no significant phenomena in Crete or the southeastern Aegean islands. On February 14, the snowfall extended further south, falling at lower altitudes compared to the previous day, while Crete and the southeastern Aegean islands

experienced rain. On February 15, the phenomena concentrated on Attica, Euboea, and Crete, driven by the activation of the Snow Aegean Effect. Athens experienced snow in the morning, transitioning to sleet for the rest of the day. The heaviest snowfall occurred overnight on February 15–16, peaking in Athens on the morning of February 16. This lake-effect snow mechanism persisted until the evening, causing localized heavy snowfalls, particularly in Attica, Euboea, and mountainous Crete.

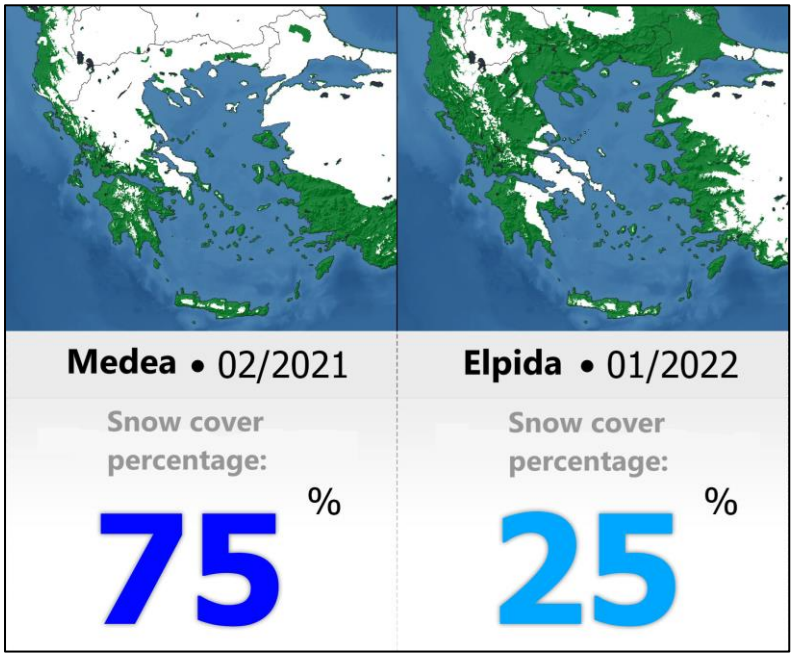


Fig. 6.1: Snow Cover Extent Comparison Between 'Medea' and 'Elpida'. (*https://meteo.gr/*)

In contrast, Elpida (January 23–26, 2022) was a shorter and more geographically limited event (Fig. 6.1). It primarily affected Attica, Euboea, and the Aegean islands, Crete, and areas around Istanbul in Turkey. In Athens, snowfall began on the morning of January 24, accumulating rapidly, peaking in the evening, causing significant disruptions. While its intensity was remarkable, Elpida's reach and duration were more restricted compared to Medea.

6.1.3. Both snowstorms' impact in Athens

In Athens, Medea resulted in uniform snow coverage across all of Attica, including the entirety of the Athens basin. In contrast, Elpida delivered heavier snowfall over a shorter time frame, primarily affecting eastern, northern and southern suburbs of Athens. The rapid snowfall accumulation began in the morning of January 24 and intensified by evening, causing significant disruptions, including paralysis of key roads such as Attiki Odos and widespread issues in the urban transport network. However, the western suburbs and Piraeus experienced less significant snow accumulation.

Notably, during Elpida's peak, thundersnow was observed in parts of Athens, accompanied by lightning and thunder. In certain areas, snowfall transitioned to sleet or

rain after the storm's peak, accelerating melting. Additionally, while areas such as Piraeus saw snow melt by the following day, snow coverage persisted until late January in areas with significant snowfall, such as the eastern and southern suburbs.

6.1.4. Thermodynamic and Dynamic Characteristics

The thermodynamic profiles of both storms were conducive to snowfall, but Elpida exhibited more extreme features. At 500 hPa, temperatures during Elpida were significantly colder, ranging from -40°C to -38°C (Fig. 6.2), compared to -30°C to -28°C in Medea (Fig. 6.3). This marked temperature difference reflects greater atmospheric instability in Elpida, enhancing the potential for convective snowfall. Similarly, the 1000–500 hPa thickness values were slightly lower during Elpida (~5160 gpm) than in Medea (~5200 gpm), reinforcing the presence of a deeper cold air mass.

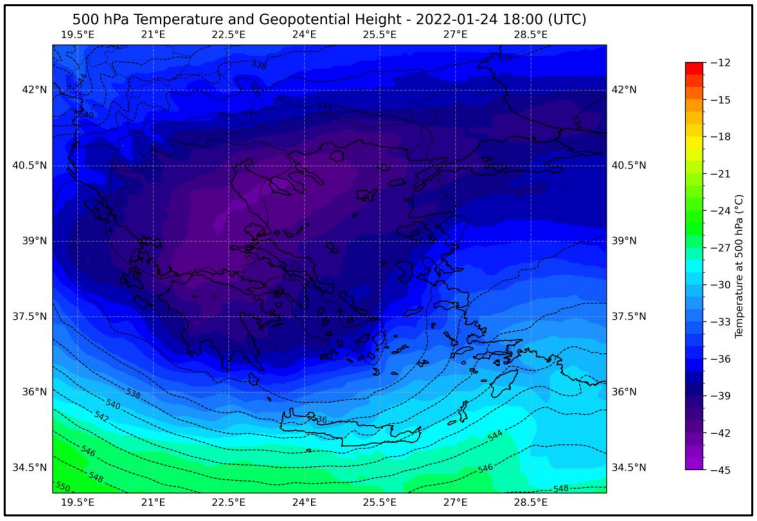


Fig. 6.2: Temperature (°C) at 500 hPa on January 24, 2022, at 20:00 local time. (WRF 9 km)

Both storms exhibited northerly winds in the mid- (950-750 hPa) and upper levels (500–700 hPa), essential for advecting cold air into the region. However, Elpida's surface winds had a more pronounced northeasterly component, increasing moisture transport from the Aegean Sea and intensifying the Snow Aegean Effect (Fig. 6.5), particularly in eastern Attica and Euboea.

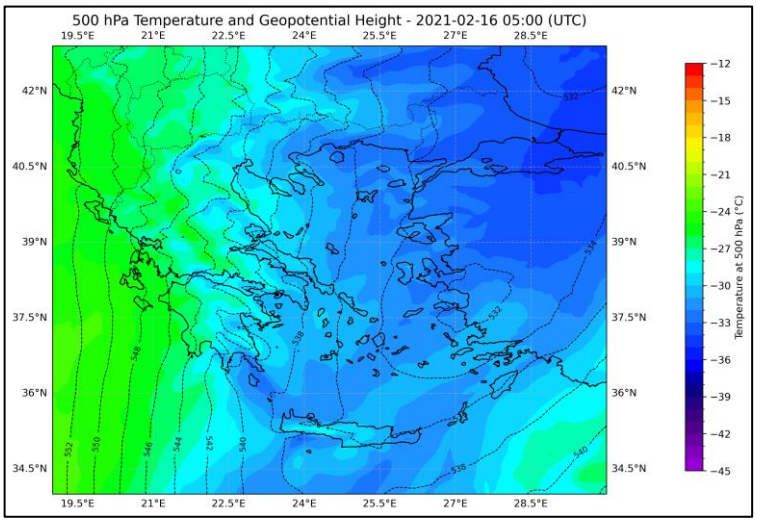


Fig. 6.3: Temperature (°C) at 500 hPa on February 16, 2021, at 07:00 local time. (WRF 9 km)

A key factor contributing to the heavier snowfall in eastern and southern suburbs during Elpida was the interaction

of the northeasterly surface wind with Mount Hymettus (Fig. 6.4). This topographic barrier caused orographic lifting of the moist and relatively warmer air from the Aegean Sea, enhancing convective processes and forming higher-altitude clouds. The warm Aegean waters further intensified this lifting, which produced stronger snowfall rates around Mount Hymettus, particularly in the eastern and southern suburbs of Athens (Fig. 6.19).

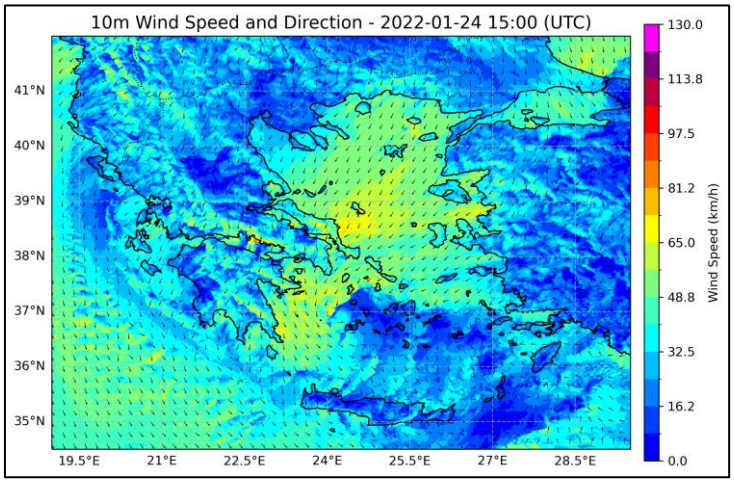


Fig. 6.4: 10m wind speed and direction on January 24, at 17:00 local time. (WRF 1 km)

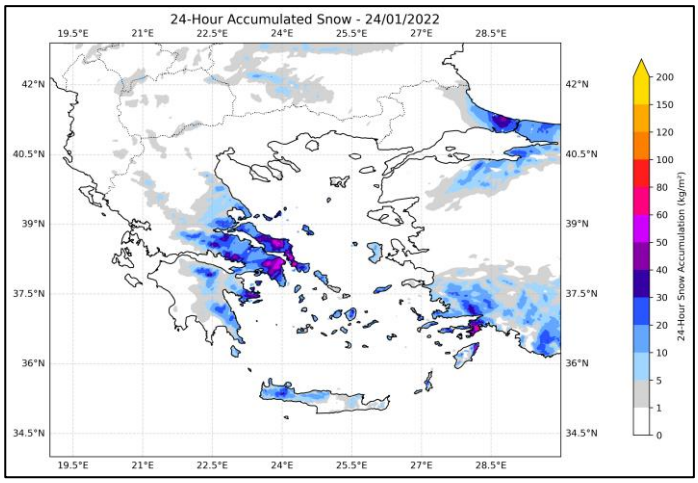


Fig. 6.5: 24-hour Accumulated Snow (kg/m^2) on 24/01/2022. (WRF 1 km)

Due to Mount Hymettus's relatively low elevation –with its highest peak at 1026 meters and other summits ranging from 600-800 meters– orographic lifting was insufficient to produce a significant rain shadow, allowing moist air to continue across the mountain and contribute to snowfall on its western (leeward) side, further amplifying the already intense weather phenomena in the southeastern suburbs. Satellite imagery from EUMETSAT revealed cloud density enhancements around the mountain, confirming the persistence of convective activity across both sides (Fig. 6.7 - Fig. 6.18). As for the western suburbs and Piraeus, the urban heat island effect, combined with the warming influence of the northeasterly

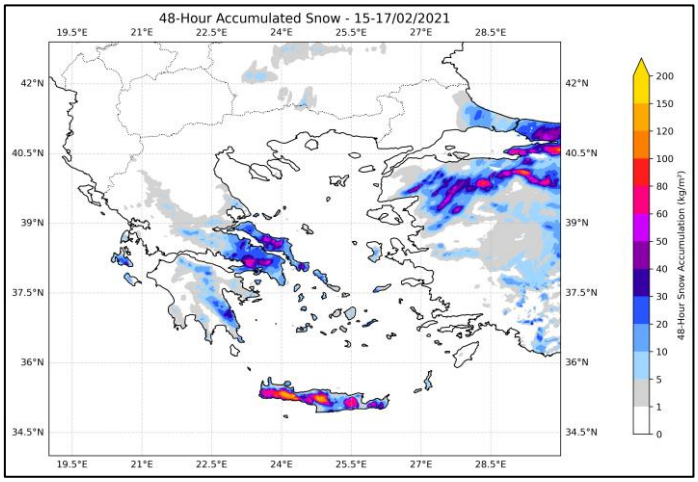


Fig. 6.6: 48-hour Accumulated Snow (kg/m^2) on 15-16/02/2021. (WRF 1 km)

wind as it traversed the Athens basin, resulted in marginal conditions for snowfall accumulation. In contrast, during Medea, convective clouds were less developed with winds predominantly northwesterly, limiting snowfall intensity in these areas (Fig. 6.6).

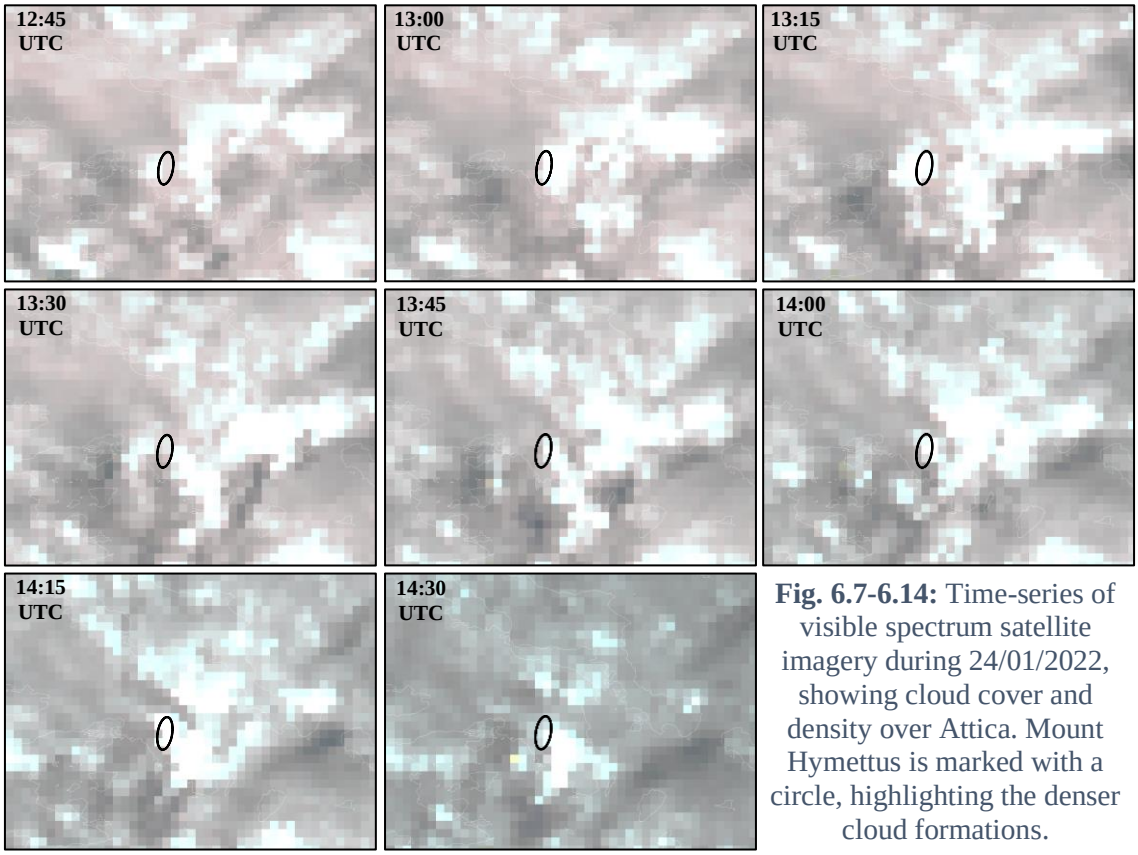


Fig. 6.7-6.14: Time-series of visible spectrum satellite imagery during 24/01/2022, showing cloud cover and density over Attica. Mount Hymettus is marked with a circle, highlighting the denser cloud formations.

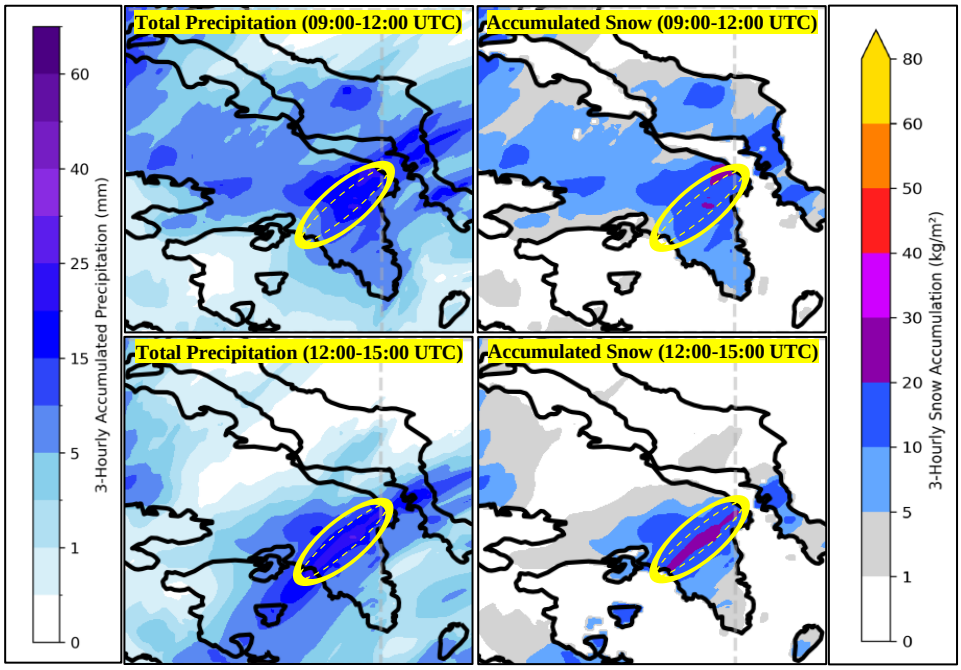


Fig. 6.15-6.18: Maps of total precipitation and accumulated snow during 24/01/2022, showing intensity variations over Attica. Areas around Mount Hymettus, circled to highlight intensity, demonstrate orographic enhancement of snowfall and precipitation, with denser accumulations on the eastern and southern suburbs, reflecting the influence of northeasterly winds and topography. (WRF 1 km)

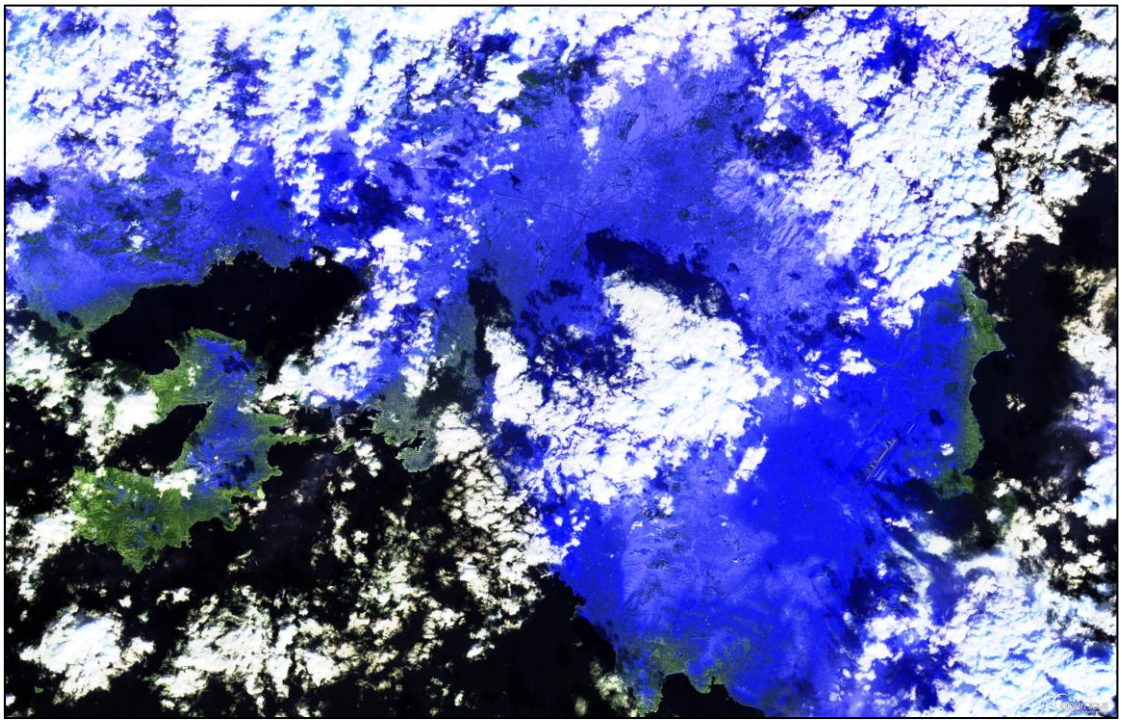


Fig. 6.19: Spatial distribution of snow cover in the Athens basin during Elpida: Sentinel-2 observations highlighting contrasts between western and southern-eastern Suburbs. (*https://browser.dataspace.copernicus.eu/*)

6.1.5. Snow Type and Density analysis

The analysis of radiosonde data during the Elpida (24/01/2022) and Medea (16/02/2021) snowstorms indicates that wet snow occurred in both cases. For both events, the thermal and humidity profiles near the surface were strikingly similar throughout the snowfall. According to the radiosonde data for Elpida at 12:00 UTC, surface temperature was around 0.2°C with relative humidity near 96%, while at 925 hPa temperature was -4.5°C with 95% humidity.



Fig. 6.20: Tree collapses onto a power line and a parked car in Exarchia due to heavy snowfall, on 24/01/2022. (*https://www.avgi.gr/*)

A similar atmospheric profile was also observed during Medea at 06:00 UTC, with slightly lower surface temperatures (-0.5°C) than in Elpida, and similar levels of relative humidity (96%). At 925 hPa, the temperature was -4.7°C with 95% humidity, closely resembling the conditions recorded during Elpida. The relatively higher temperatures observed during both events resulted in greater water content in the snowflakes, which significantly increased their weight per unit area. Additionally, wet snow is less prone to being carried by near-surface winds. It is worth noting that wind intensities during Elpida and Medea were significantly lower compared to snowstorm events in the past, further reducing the likelihood of snow transport.



Fig. 6.21: A fallen tree blocks the road in Nea Smyrni, further disrupting vehicle traffic already strained by heavy snowfall, on 16/02/2021. (*https://www.iefimerida.gr/*)

These comparable conditions during both storms strongly favored the formation of wet, dense snow, which led to impacts such as collapsed tree limbs and power lines (Fig. 6.20 & Fig. 6.21). This highlights the importance of near-surface thermal and moisture conditions during snowfall events, as even small variations can influence snow density and its associated hazards.

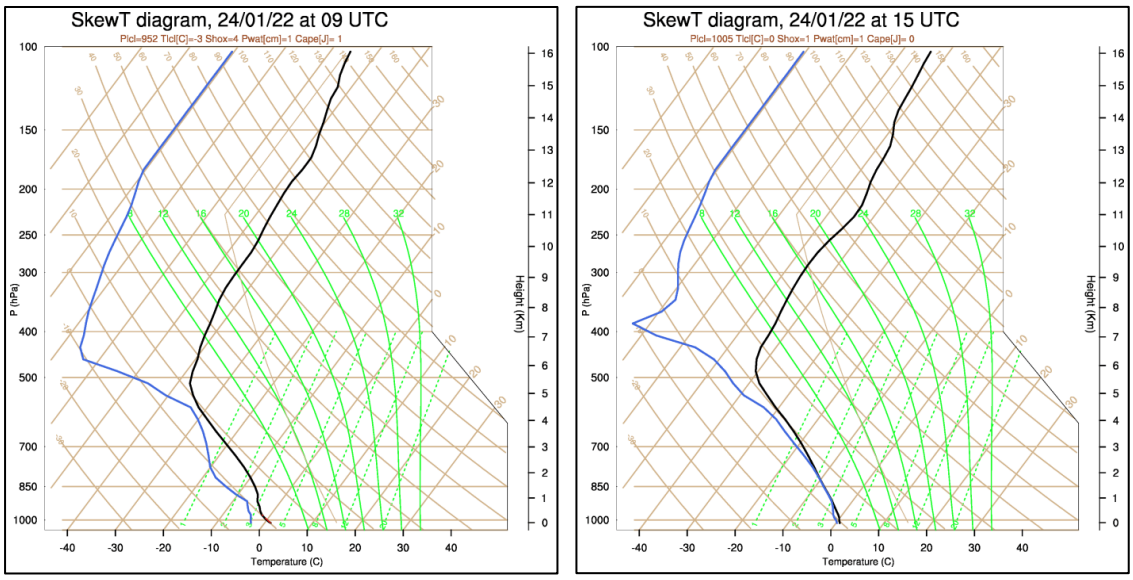


Fig. 6.22 & 6.23: Skew-T diagram at Elliniko on January 24, 2022, at 11:00 and 17:00 local time, respectively, based on WRF reanalysis data.

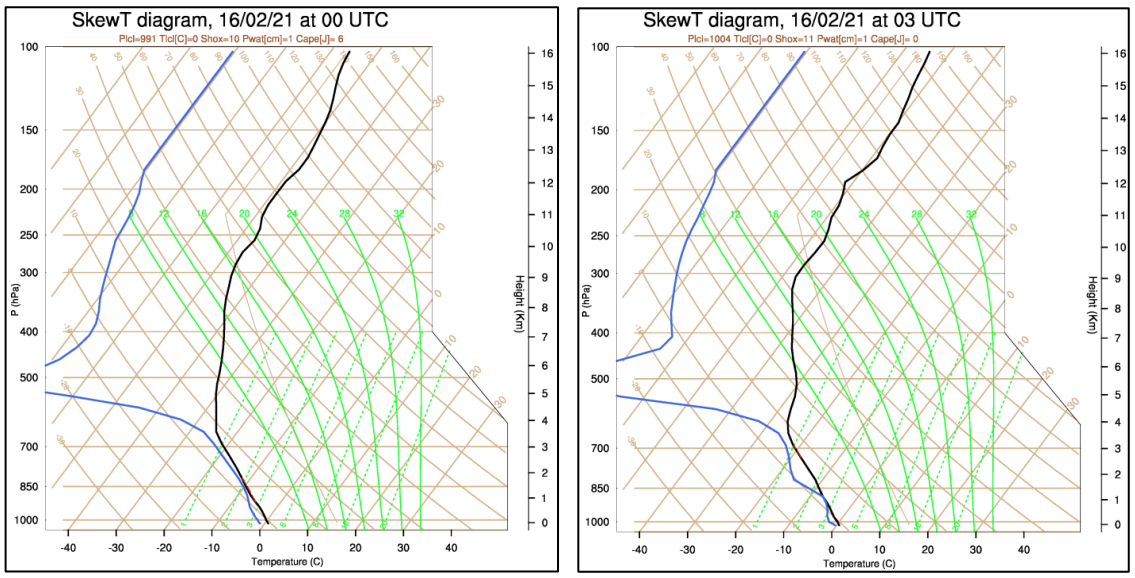


Fig. 6.24 & 6.25: Skew-T diagram at Piraeus on February 16, 2021, at 02:00 and 05:00 local time, respectively, based on WRF reanalysis data.

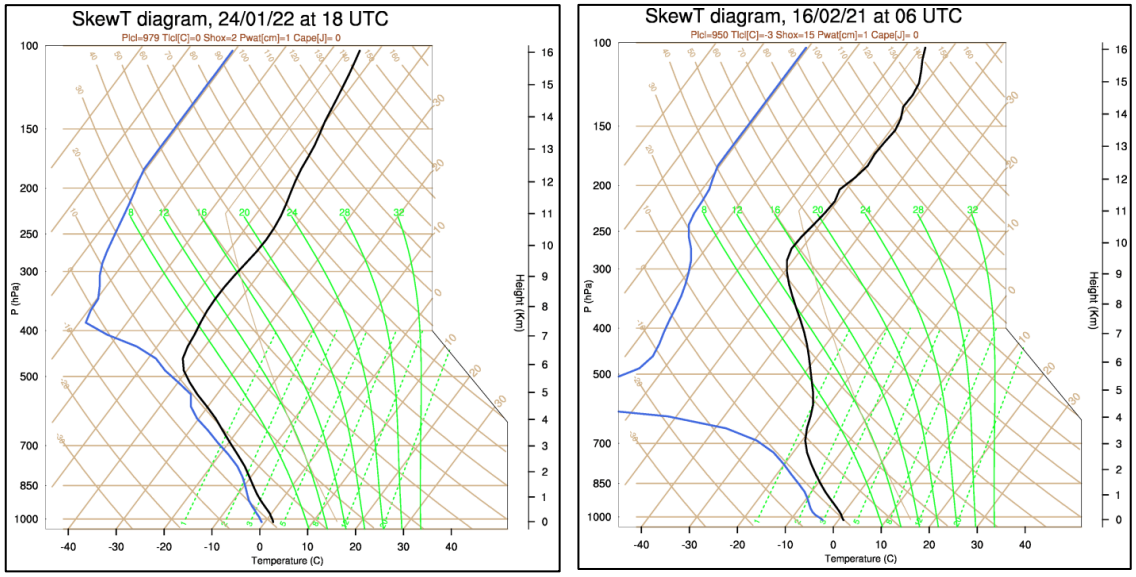


Fig. 6.26 & 6.27: Skew-T diagram at Elliniko on January 24, 2022, vs. Piraeus on February 16, 2022, respectively, during the peak of each snowfall, based on WRF reanalysis data.

6.1.6. Convective Dynamics and Cloud Development

Cloud development during the two storms reflected their respective intensities. Medea produced moderate vertically developed clouds, with tops reaching approximately 6 km. This level of convection was sufficient for widespread snowfall but lacked the intensity observed in Elpida. In contrast, Elpida featured exceptionally high cloud tops, reaching 8-10 km, signaling strong convective processes and more intense snowfall. This was further supported by the presence of a closed upper-level low, which facilitated organized vertical motion and robust snow production. The more vigorous convection in Elpida also contributed to phenomena such as thundersnow, highlighting its dynamic nature compared to Medea.

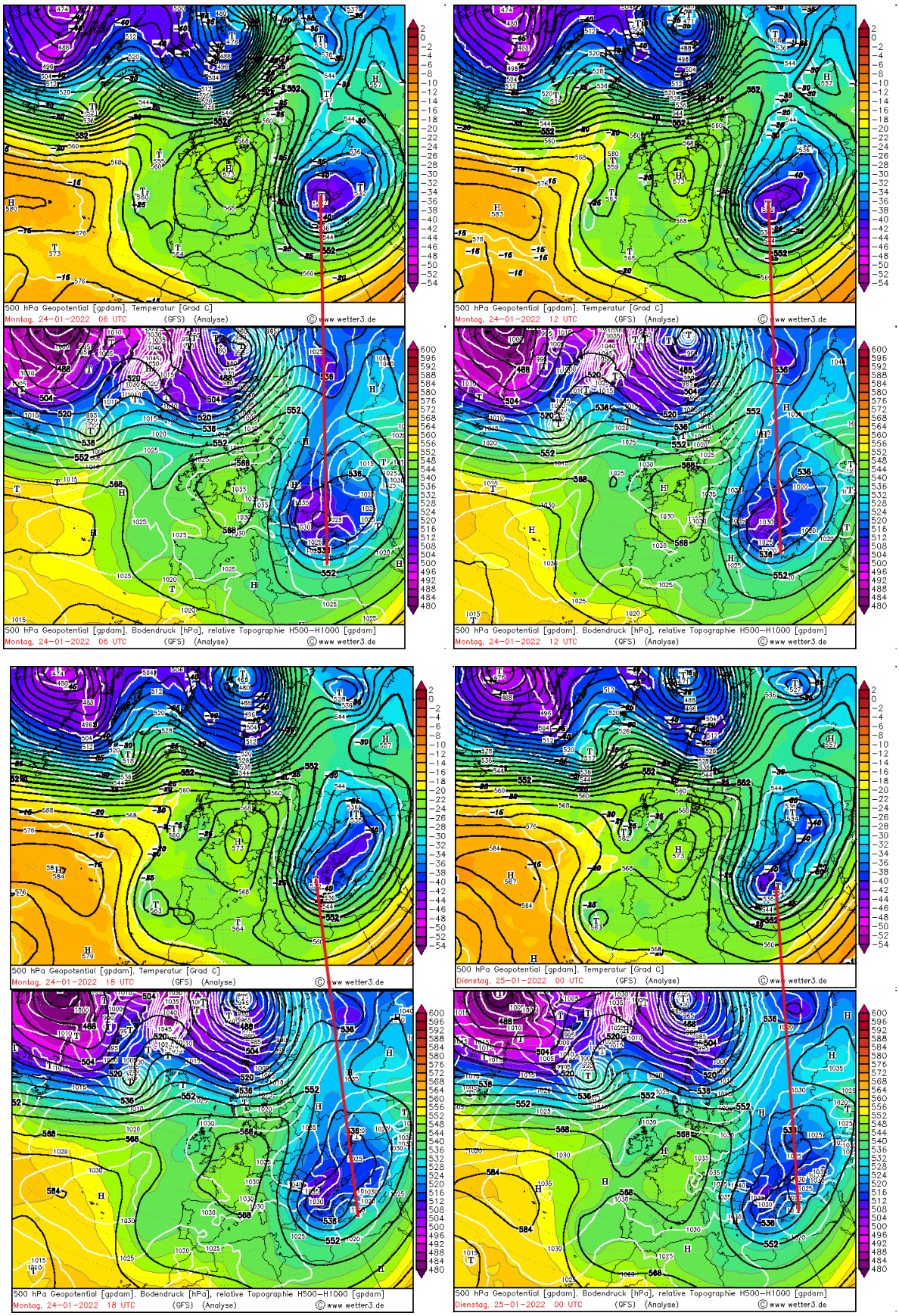


Fig. 6.28-6.35: Evolution of baroclinicity and cyclogenesis during the Elpida Snowstorm. (*https://www.wetter3.de/*)

Focusing further on Elpida's dynamic processes, the sequence of maps above (Fig. 6.28 - Fig. 6.35) illustrates the evolution of baroclinicity during its development and progression on January 24, 2022. At 06:00 UTC, baroclinicity was relatively weak, corresponding to the initial stages of the system, where dynamic support for convection and uplift was limited. By 12:00 UTC, increasing baroclinicity, driven by enhanced thermal gradients between the surface and 500 hPa levels, supported the strengthening of the surface low and the intensification of cyclogenesis. At 18:00 UTC, the system exhibited peak baroclinicity, coinciding with the peak intensity of the phenomena, as stronger thermal gradients drove intense uplift and dynamic processes. Finally, by 00:00 UTC on January 25, baroclinicity decreased, marking the onset of the occlusion process, the weakening of the surface low, and a subsequent reduction in precipitation and wind intensity.

6.2. Snowfall Forecast Indices for Nowcasting Applications

The accurate prediction of snowfall, particularly in the Mediterranean region, requires a combination of advanced satellite imagery, numerical weather prediction models, and in-depth understanding of atmospheric thermodynamics and dynamics. Importantly, these thermodynamic and dynamic characteristics are highly dependent on the specific geographical region, including factors such as latitude, altitude, and vicinity to water bodies. For instance, Athens requires specific atmospheric setups for snowfall due to its low elevation and its interaction with the Aegean Sea, whereas other regions with different geographical and topographical features might exhibit distinct requirements. Two indices, for both day and night, were developed in the study to enhance the nowcasting capabilities of snowfall events. These indices aim to classify snowfall based on intensity and provide real-time tools for monitoring meteorological conditions.

These indices integrate satellite data with atmospheric thermodynamic parameters such as temperature, humidity and wind profiles. The foundation for their development is the recognition of specific atmospheric conditions conducive to snowfall, particularly temperature and dewpoint proximity ($T\text{-}T_d \leq 3°C$) in the 950-800 hPa layer, along with the presence of favorable synoptic patterns as defined by Prezerakos (1984). While the indices share this common framework, they differ in their focus: the General Snowfall

Index identifies conditions for moderate snowfall, while the Severe Snowfall Index targets more extreme and localized phenomena (Table 6.2).

Table 6.2: *Classification of General and Severe Snowfall indices.*

	General Snowfall Index (Day)	**General Snowfall Index (Night)**	**Severe Snowfall Index (Day)**	**Severe Snowfall Index (Night)**
Day Microphysics RGB	Red/orange hues indicate thick clouds with ice crystals at cloud tops; moderate upward motion	-	Orange hues dominate, indicating smaller ice particles formed through rapid upward motion	-
Night Microphysics RGB	-	Reddish-brown hues, limited green speckles	-	Reddish-brown hues with prominent green speckles
Severe Convection RGB	Red/yellow hues indicate moderate convection; conclusive to widespread snowfall	-	Vivid red with yellow tones signal intense convection linked to severe snowfall	-
Cloud Top Height (CTH)	>4 km (moderate cloud development)		>6 km; peaks of 8–10 km for extreme events	
Synoptic Conditions	Stable stratification; Type A and Type B setups with moderate cyclonic activity		Strong cyclonic activity; deep trough at 500 hPa; cyclogenesis	
Wind Patterns	Northern winds (950–750 hPa layer); northwesterly at higher altitudes		Strong northerly winds enhanced by 'Snow Aegean Effect'	
Precipitation Intensity	Moderate and widespread snowfall		Localized, intense snowfall with possible thundersnow	

6.2.1. General Snowfall Index

The General Snowfall Index is designed to capture the synoptic and mesoscale atmospheric features that contribute to widespread, moderate-intensity snowfall. It relies on the meteorological and satellite-based criteria to identify snow-producing conditions during both day and night.

6.2.1.1. Day

Daytime snowfall detection utilizes the Day Microphysics RGB, a key satellite tool for detecting clouds with characteristics indicative of snowfall. Red and orange hues in this imagery signal the presence of thick ice crystal layers at cloud top, typically associated with upward motion and sufficient condensation to produce snow.

Complementary insights are provided by the Severe Convection RGB, where red and yellow hues highlight areas of convection, aiding in identifying regions of enhanced upward motion.

Additionally, the Cloud Top Height (CTH) data verifies the vertical development of clouds, with snow-producing systems typically exhibiting heights greater than 4 km. Atmospheric conditions supportive of snowfall include stable stratification, cold air advection, and favorable wind patterns. In Athens, for instance, northern winds dominate the 950-750 hPa layer, transitioning to northwesterly at higher altitudes, a setup typical during Type A and Type B snowfall events.

6.2.1.2. Night

Nighttime detection within the General Snowfall Index relies on the Night Microphysics RGB, replacing the Day Microphysics and Severe Convection RGBs. This product identifies reddish-brown hues with limited or no green speckles, indicative of thick ice clouds associated with upward motion and sufficient condensation to produce snow.

As with the daytime index, the CTH data is used to verify the vertical extent of clouds, with snow-producing systems typically exhibiting heights greater than 4 km. Combining Night Microphysics with CTH data allows for accurate identification of snow-generating cloud structures during nighttime. The atmospheric conditions supportive of snowfall remain consistent with those during the day.

6.2.2. Severe Snowfall/Thundersnow Index

6.2.2.1. Day

For daytime severe snowfall detection, the Day Microphysics RGB reveals orange hues that indicate small ice particles formed through rapid updrafts, a hallmark of strong convection. Simultaneously, the Severe Convection RGB emphasizes vigorous convection through vivid red and yellow hues, signaling regions of extreme atmospheric instability.

Snow-producing clouds during such events often exceed 6 km in height, with peaks reaching 8 to 10 km in the most extreme cases. These vertical extents, combined with the thermal instability evident in temperature and humidity profiles, underscore the convective intensity driving intense snowfall. The synoptic conditions include a deep

trough at the 500 hPa level, strong cyclonic activity, and low-pressure systems over the southeastern Mediterranean. In Type B events, for example, moisture advection from the Aegean Sea, amplifies snowfall through the “Snow Aegean Effect”, creating localized but intense precipitation patterns. The Elpida storm serves as a benchmark for the Severe Snowfall Index, as it exhibited all the hallmarks of extreme snowfall: cloud top heights exceeding 8 kilometers, robust convective instability, and strong northern winds in the mid-troposphere, resulting in significant localized snowfall.

6.2.1.2. Night

The Severe Snowfall/Thundersnow Index for nighttime applications uses the Night Microphysics RGB alongside the CTH product to identify extreme snowstorms with convective characteristics. Reddish-brown hues interspersed with prominent green speckles in Night Microphysics RGB highlight areas of very cold thick ice clouds formed by rapid updrafts and intense convection.

Cloud top heights exceeding 6 km, with peaks often reaching 8-10 km, indicate convective activity. These markers are further validated by thermal instability in atmospheric profiles, signifying intense snowfall and possible electrical phenomena, such as thundersnow. The atmospheric and synoptic conditions during nighttime severe snowfall remain similar to their daytime counterparts. As demonstrated during the Elpida storm, Night Microphysics RGB effectively identified regions of severe convection and thundersnow, confirming its utility for nowcasting extreme snowfall events during night.

6.2.3. Validation of Snowfall Indices

This section focuses on validating the developed snowfall indices using satellite-derived imagery and precipitation data from ERA-5 reanalysis. To ensure that proposed indices accurately capture snowfall conditions, the analysis compares key satellite products, such as Day and Night Microphysics RGBs and Cloud Top Height (CTH), with reanalysis-based precipitation maps. These comparisons aim to confirm the spatial and temporal consistency of the indices with observed precipitation patterns.

During the daytime case (Fig. 6.13 - Fig. 6.18), regions displaying intense orange hues in Day Microphysics RGB are associated with areas of strong convection, which are characterized by thick ice clouds and enhanced upward motion. This is further supported by CTH data, which indicates significant cloud development, with cloud tops

exceeding 4 km in height. Furthermore, the ERA-5 precipitation map verifies that these regions correspond to areas of higher snowfall intensity. These results underscore the ability of Day Microphysics RGB to effectively identify areas of moderate to intense snowfall driven by convective dynamics.

Similarly, the nighttime case (Fig. 6.36 - Fig. 6.45) utilizes Night Microphysics RGB to detect snowfall regions. Reddish-brown areas with green speckles are indicative of thick ice clouds formed by strong upward motion and active convection. As with the daytime analysis, CTH data confirms vertical cloud development, and the ERA-5 precipitation map validates these findings by highlighting the areas of increased snowfall intensity. This alignment showcases the effectiveness of Night Microphysics RGB in capturing convective snowfall patterns during the night.

By integrating satellite-derived observations with precipitation reanalysis data, this validation highlights the strength of the snowfall indices for both daytime and nighttime scenarios. The consistency between the satellite indicators, cloud dynamics, and precipitation fields underscores their utility in nowcasting applications, providing a comprehensive framework for real-time snowfall monitoring and analysis. Furthermore, integrating higher-resolution satellite imagery and leveraging machine learning techniques could enhance the accuracy of spatiotemporal precision of these indices, enabling improved nowcasting of localized and extreme snowfall events.

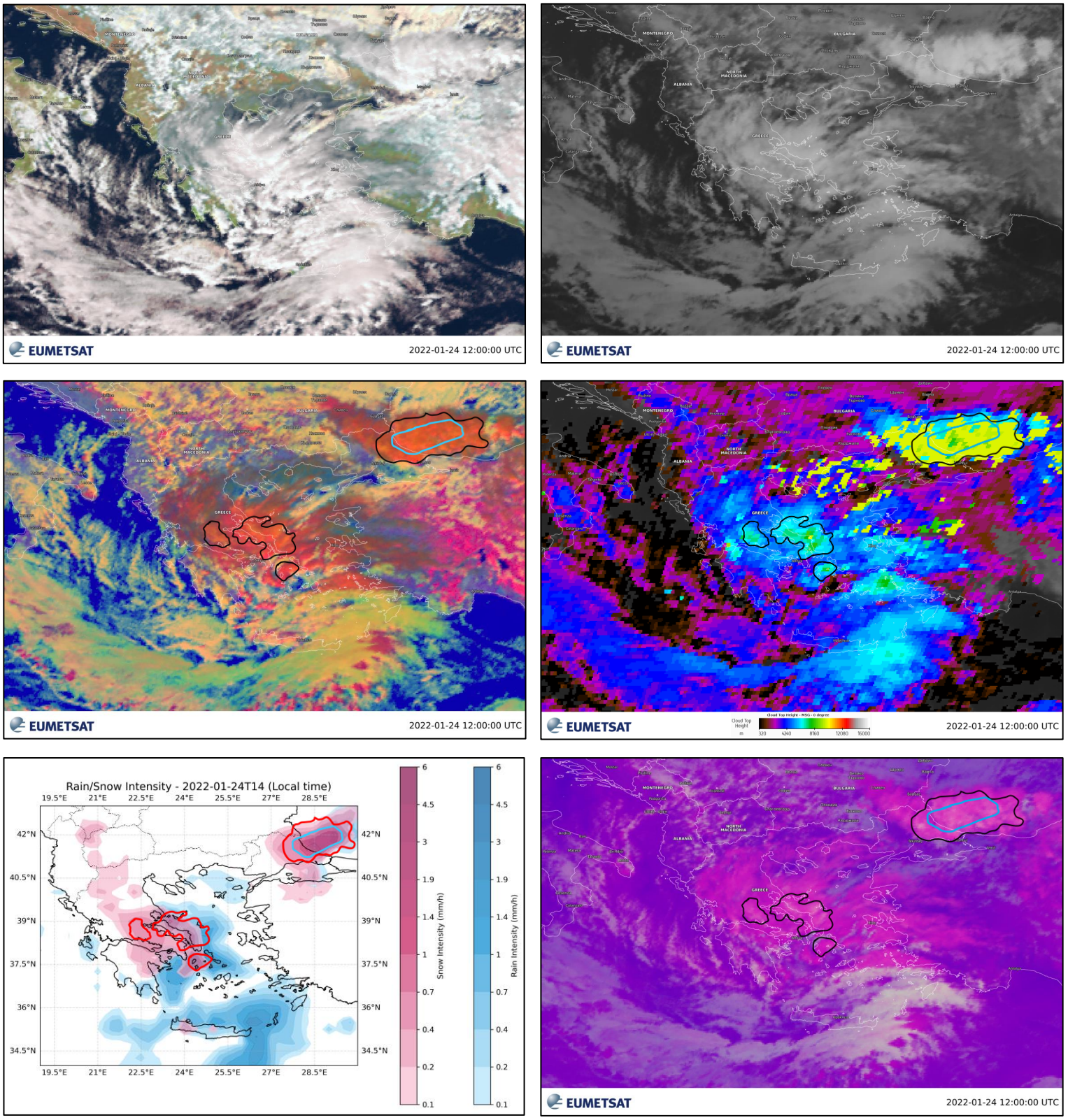


Fig. 6.36-6.41: Daytime Satellite-Derived Indicators and Precipitation Validation for Snowfall Nowcasting, using precipitation intensity maps generated by processing ERA5 reanalysis data in Python, retrieved from the Copernicus Climate Data Store. Areas with significant precipitation have been outlined, indicating either snowfall or rainfall depending on the vertical temperature distribution of the area. (*https://www.eumetsat.int/*)

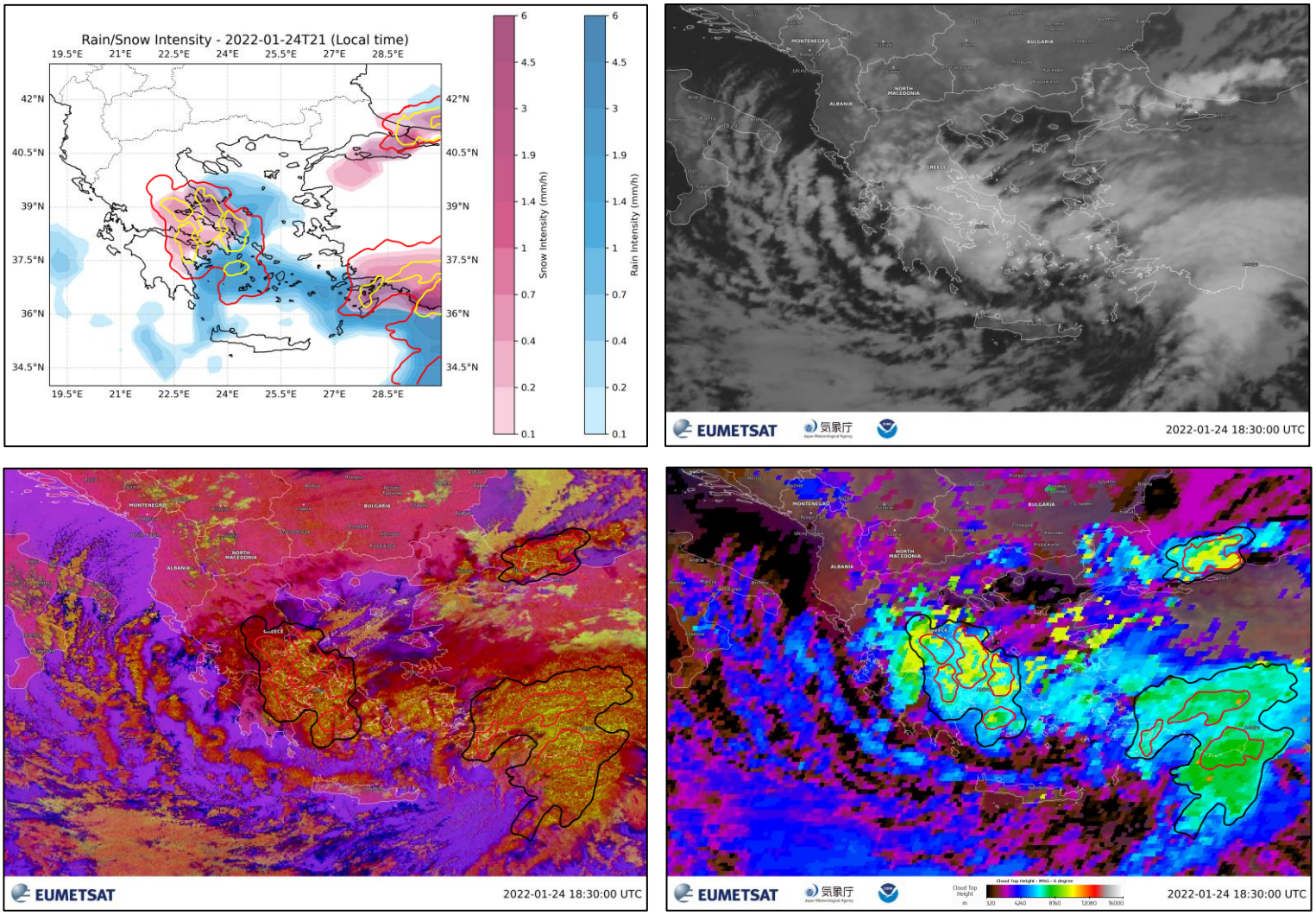


Fig. 6.42-6.45: Nighttime satellite-derived indicators and precipitation validation for snowfall nowcasting, using precipitation intensity maps generated by processing ERA5 reanalysis data in Python, retrieved from the Copernicus Climate Data Store. Areas with significant precipitation have been outlined, indicating either snowfall or rainfall depending on the vertical temperature distribution of the area. (*https://www.eumetsat.int/*)

6.3. Critical Analysis and Comparison of Snowfall Indices: Forecasting vs. Nowcasting

This section provides a critical and comparative analysis of the developed snowfall indices, focusing on their strengths, weaknesses, and limitations. The analysis is divided into two parts: forecasting and nowcasting applications, reflecting the different contexts in which the indices are used.

6.3.1. Forecasting Applications

Forecasting relies on medium- to long-term predictions based on synoptic-scale and mesoscale analyses. The General Snowfall Index (GSI) and Severe Snowfall Index (SSI) are valuable tools for identifying snowfall conditions when used in combination with numerical weather prediction models. The GSI captures widespread snowfall patterns effectively by relying on meteorological parameters such as geopotential heights, wind profiles, and temperature thresholds (e.g. T-Td $\leq$ 3°C in the 950-800 hPa layer). Its emphasis on stable atmospheric stratification ensures reliable identification of moderate snowfall conditions, particularly in areas like Athens, where Type A or Type B synoptic setups are common. On the other hand, SSI excels at pinpointing intense events and localized snowfall events associated with strong convection.

Despite their strengths, the indices have limitations. Both rely heavily on predefined synoptic conditions, such as cyclogenesis or low-pressure systems, which may not fully capture smaller-scale or transient phenomena. This reliance can reduce their accuracy in rapidly evolving weather environments. Additionally, the indices are geographically specific, designed for the Mediterranean region, mainly Attica and Euboea, and may require significant adjustments for application in regions with differing climatic or topographical features.

To enhance their effectiveness, the integration of machine-learning techniques could be explored, using historical data to refine the thresholds and adapt the indices to a broader range of scenarios. Moreover, combining these indices with probabilistic forecasting models, such as ensemble predictions, could address uncertainties in medium- to long-term forecasts and improve their overall reliability.

6.3.2. Nowcasting Applications

Nowcasting focuses on real-time or near-real-time monitoring of weather events over short timescales, ranging from minutes to a few hours. In this context, the use of satellite-derived products is particularly advantageous. The Day and Night Microphysics RGBs and Severe Convection RGB provide continuous observations of atmospheric conditions, offering insights into cloud microphysics, particle sizes and vertical development. The high temporal resolution of satellite data, such as 15-minute updates from Meteosat Second Generation (MSG) satellites, ensures timely detection of rapidly developing weather phenomena like thundersnow.

However, nowcasting also faces limitations. Nighttime detection is less effective compared to daytime, as the Night Microphysics RGB struggles to resolve convective structures with the same precision as its daytime counterpart. Furthermore, the effectiveness of nowcasting indices depends on the availability of high-resolution satellite data, which can be compromised in areas with limited coverage data acquisition interruptions. These limitations highlight the need for complementary observational systems to enhance nowcasting accuracy.

A significant challenge in Greece is the lack of extensive meteorological radar coverage, which poses challenges for real-time monitoring and analysis of localized weather phenomena. Currently, the country is in the process of acquiring and installing a network of meteorological radars to address this gap, with the expected completion of these systems in the coming years. Until these radars become operational, the use of satellite-derived products, such as the snowfall indices developed in this study, serves as a vital tool to bridge the gap. The integration of indices like GSI and SSI with satellite data enables effective nowcasting of snowfall events, particularly in regions where conventional radar coverage is absent or limited.

To address these challenges, the integration of blended satellite products, such as combining SEVIRI/LEO MW precipitation data with RDT products, could significantly enhance the accuracy of nowcasting. Additionally, real-time automated algorithms could streamline the identification of critical thresholds, such as rapid cloud top height growth or Severe Convection RGB signals, improving the speed and precision of nowcasting.

Table 6.3: *Comparative analysis of forecasting and nowcasting applications for snowfall indices, highlighting strengths, limitations, and technological needs.*

	Forecasting	**Nowcasting**
Primary Strength	Long-term identification of synoptic-scale snowfall setups	Real-time detection of convective and localized snowfall
Key Limitation	Sensitivity to synoptic uncertainties	Limited effectiveness under poor satellite coverage or interruptions
Key Product	GSI for widespread snowfall prediction, based on synoptic-scale and mesoscale analyses	SSI for detecting severe, convective snowfall, based on satellite-derived products
Proposed Solution	Probabilistic weather forecasting with machine learning	Use of blended satellite products and automated analysis
Contextual Advantage	Effective for planning and resource allocation	Crucial for rapid response to evolving severe weather events
Technological Need	Improved integration with ensemble prediction systems	Expansion of radar networks and enhanced satellite observations

7. EMERGING SATELLITE-DERIVED PRODUCTS FOR ENHANCING SNOWFALL INDICES

This chapter presents emerging satellite-derived products –such as those from the MTG satellites in 2024– and their potential applications in future studies to enhance the snowfall indices developed in the previous section. These advanced tools offer significant opportunities for improving the accuracy and efficiency of snowfall nowcasting, providing a pathway for continued advancements in meteorological analysis.

7.1. Cloud Phase RGB

The Cloud Phase RGB product represents a breakthrough in cloud microphysics analysis, offering detailed information about cloud phase and particle size. Designed specifically for daytime applications, it uses three satellite channels to distinguish between water and ice clouds and assess the microphysical properties of cloud tops (Table 7.1).

Table 7.1: *Key spectral channels in Cloud Phase RGB and their role in cloud characterization and microphysical analysis. (https://www.eumetsat.int/)*

Color-Channel [µm]	Physically relates to	Smaller contribution to the signal of	Larger contribution to the signal of
Red (NIR1.6)	Cloud Phase (and cloud top particle size)	Thick ice clouds	Thick water clouds
Green (NIR2.25)	Cloud top particle size (and phase)	Thick clouds with large particles	Thick clouds with small particles
Blue (VIS0.67)	Cloud optical thickness	Thin clouds	Thick clouds

One of its most notable advantages is its ability to monitor convection by detecting cloud top glaciation and highlighting areas of small ice particles at the cloud tops. These features often indicate strong updrafts and active convection, which are closely associated with heavy precipitation and intense snowfall. This ability to separate thick ice clouds from thick water clouds and to highlight microphysical variations (Fig. 7.1) makes it a valuable tool for assessing severe weather potential, especially in developing snowstorms.

The product also enhances the reliability of cloud phase detection compared to earlier SEVIRI RGBs, such as the Day Microphysics RGB. While both products can analyze cloud microphysics, the Cloud Phase RGB provides superior differentiation of particle size and phase, enabling identification of convective regions. This improvement makes it particularly advantageous for identifying areas of severe snowfall potential.

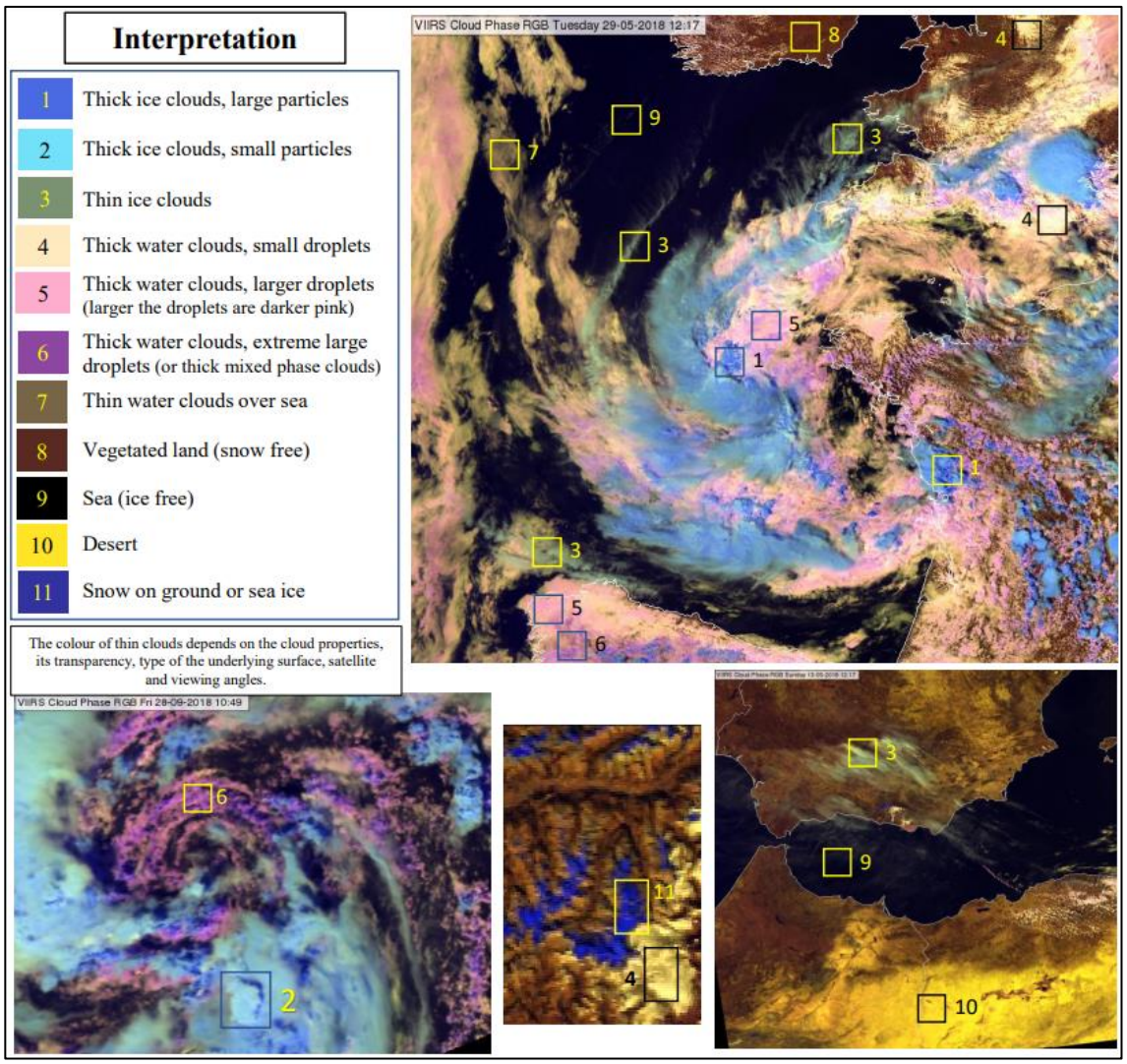


Fig. 7.1: This color interpretation provides visual guidance for distinguishing between various cloud types, phases, and surface features. (*https://www.eumetsat.int/*)

By integrating the Cloud Phase RGB with other satellite data, such as IR10.8 imagery or the CTH product, meteorologists can enhance their ability to track snowstorms and better understand the underlying atmospheric processes driving snowfall intensity. Despite its limitations, the Cloud Phase RGB is a valuable addition to the suite of the satellite products available for snowstorm analysis, offering a deeper insight into cloud structure and dynamics.

7.2. Cloud Type RGB

The Cloud Type RGB product represents a significant advancement in satellite-based atmospheric analysis, offering comprehensive insights into cloud classification and structure. Utilizing the newly advanced channels on the MTG satellites, this product differentiates between various cloud types, including low and mid-level clouds, thin and thick high clouds, and supercooled water clouds. By combining cloud optical thickness, cloud height, and cloud phase into a single product, the Cloud Type RGB enables a higher level of precision in cloud analysis compared to previous SEVIRI RGBs.

Table 7.2: *Key spectral channels in Cloud Phase RGB and their contribution to cloud classification and atmospheric analysis. (https://www.eumetsat.int/)*

Color-Channel [µm]	Physically relates to	Smaller contribution to the signal of	Larger contribution to the signal of
Red (NIR1.38)	Cloud height and optical depth	Low-level clouds	High clouds
Green (VIS0.64)	Cloud optical thickness	Thin clouds	Thick clouds, Snow covered land, Sea ice
Blue (NIR1.61)	Cloud phase	Green vegetation, Water, Snow/ice, Ice clouds	Thick water clouds

One of the key strengths of this product is its ability to detect high and thin clouds with unprecedented clarity (Table 7.2). The addition of a specific water vapor absorption channel significantly enhances the identification of cirrus clouds, even over land and sea. Furthermore, the product excels in distinguishing water from ice clouds and provides strong color contrasts between different cloud types, making it particularly effective at identifying convective activity. This capability allows for a clearer separation between towering convective clouds and thinner anvil layers, which is crucial for tracking severe weather phenomena, including extreme snowfall events.

In the context of snowfall nowcasting, Cloud Type RGB's ability to highlight supercooled water clouds and thick ice clouds provides valuable insights into the microphysical and thermodynamic processes providing snowstorm development (Fig. 7.2). By capturing both cloud height and optical thickness, it helps meteorologists assess the vertical structure of clouds and their precipitation potential, enabling timely and precise predictions of intense snowfall or even thundersnow.

When combined with products like the Severe Convection RGB, the Cloud Type RGB enhances understanding of the convective processes that drive severe snowstorm dynamics. This synergy between products offers a more comprehensive view of snowstorm development, aiding in real-time decision-making and warning systems.

Although Cloud Type RGB is not yet operational, it is expected to become available with the full deployment of the MTG satellites. Once implemented, this product is anticipated to revolutionize the real-time monitoring of severe weather systems, including those involving snowfall. Its utility will be further enhanced when used alongside complementary tools like Cloud Phase RGB, together providing a comprehensive view of cloud microphysics and atmospheric processes.

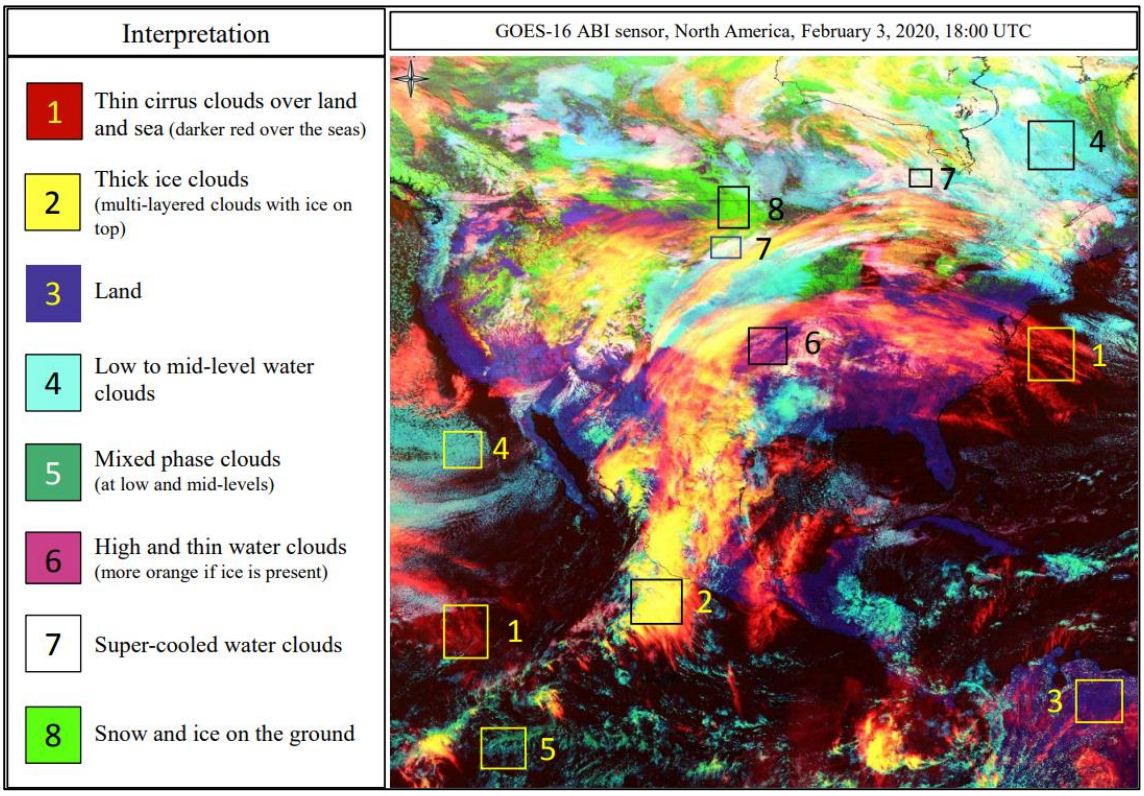


Fig. 7.2: This color interpretation provides visual guidance for differentiating cloud types, highlighting key features such as cloud height, phase, and optical thickness. (*https://www.eumetsat.int/*)

7.3. Combining Blended SEVIRI/LEO MW Precipitation and Rapidly Developing Thunderstorms Products

The integration of the Blended SEVIRI/LEO MW Precipitation and Rapidly Developing Thunderstorms (RDT) products provides a robust framework for nowcasting, including snowfall events. Individually, each product offers valuable insights into precipitation and convective activity, but their combination significantly

enhances the ability to monitor, analyze, and predict high-impact weather phenomena with precision.

The Blended SEVIRI/LEO MW Precipitation product synthesizes data from geostationary (GEO) satellites, such as the Meteosat Second Generation (MSG), and low Earth orbit (LEO) microwave sensors, including those onboard satellites like NOAA, MetOp, and GPM (Global Precipitation Measurement), to generate real-time precipitation maps. It thus combines thermal infrared data from MSG with rain rate measurements from passive MW sensors, delivering reliable estimates of precipitation intensity. The blending algorithm, known as "Rapid Update", calibrates the IR imagery using MW-derived precipitation data, ensuring improved accuracy and timeliness (Turk et al., 2000).

The NEFODINA software further enhances its functionality by refining the detection of convective precipitation, enabling a more precise separation between stratiform and convective precipitation (Melfi et al., n.d.). This differentiation is particularly valuable for identifying intense snowfall compared to broader, moderate precipitation and improves the spatial and temporal precision of precipitation intensity estimates, especially in convective regions.

The RDT product, based on MSG satellite data, specializes in identifying, tracking and analyzing convective systems at various scales. Moreover, it excels in detecting rapidly developing convective cells and monitoring their evolution, providing critical parameters, such as motion vectors, cloud top height, cooling rates, as well as the intensity of convective activity.

Together, these two products create a powerful synergy for snowfall nowcasting. RDT identifies areas of active convection, while Blended SEVIRI/LEO MW Precipitation quantifies precipitation intensity in these areas. The combination is particularly effective in capturing convective snowfall events, such as thundersnow, allowing meteorologists to distinguish it from stratiform snow, improving both spatial and temporal precision of snowfall forecasts.

By leveraging the continuous monitoring capabilities of GEO satellites, these products provide near-real-time updates, which are crucial for tracking rapidly evolving weather systems. The detailed precipitation rate data from Blended SEVIRI / LEO MW complements the spatial and convective insights offered by RDT, enabling a complete understanding of convective snowfall dynamics.

The integration represents a significant step forward in nowcasting capabilities. While particularly effective analyzing snowfall, it is equally valuable for rainfall and mixed-phase precipitation. The availability of these advanced tools post-2022 enhances the ability of meteorologists to issue timely and accurate warnings for high-impact weather events, thereby enhancing preparedness and reducing weather-related risks.

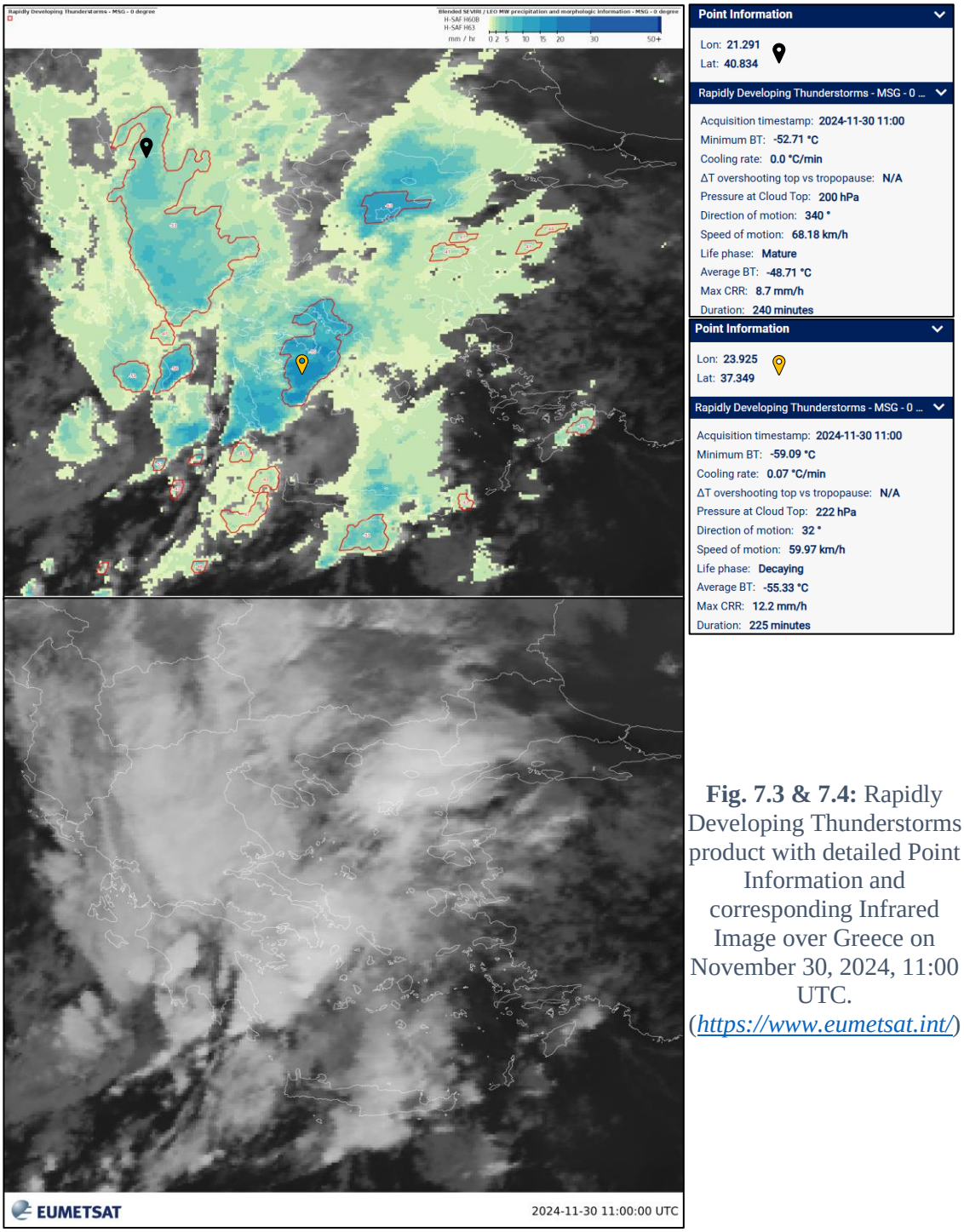


Fig. 7.3 & 7.4: Rapidly Developing Thunderstorms product with detailed Point Information and corresponding Infrared Image over Greece on November 30, 2024, 11:00 UTC. (*https://www.eumetsat.int/*)

8. CONCLUSIONS

The following conclusions highlight key findings, limitations, and future directions of the study on snowfall analysis in Greece, aiming to enhance forecasting and nowcasting in the Mediterranean region.

- **Comparative Analysis of 'Medea' and 'Elpida' Snowstorms:** The study highlighted key differences between 'Medea' (February 2021) and 'Elpida' (January 2022) despite their similar synoptic and thermodynamic structures. Elpida's closed cyclonic circulation and greater instability resulted in a shorter but more intense snowstorm, with higher cloud tops and localized impacts, particularly in eastern and southern Athens. In contrast, Medea's broader, non-closed circulation led to a prolonged, widespread snowfall event with moderate convection and uniform snow coverage across Attica.
- **Role of Atmospheric Conditions:** Both snowstorms formed under favorable thermodynamic conditions for wet, dense snow, as evidenced by near-surface temperatures close to 0°C and high humidity (95–96%). However, Elpida's colder upper atmosphere (-40°C to -38°C at 500 hPa) led to a stronger "Snow Aegean Effect", intensifying snowfall rates, whereas Medea's broader cold air mass ensured sustained precipitation. These findings underscore the critical role of topography and sea-atmosphere interactions in shaping snowfall characteristics in Greece.
- **Development of Snowfall Indices:** Two indices **–General Snowfall Index (GSI)** and **Severe Snowfall Index (SSI)–** were introduced and validated using satellite RGB composites (Day/Night Microphysics, Severe Convection), and Cloud Top Height (CTH), along with ERA-5 precipitation reanalysis data. The **GSI** effectively captured moderate, widespread snowfall, while the **SSI** successfully identified intense, convective snowfall events such as thundersnow, improving nowcasting capabilities for Mediterranean snowstorms.
- **Strengths and Limitations of Indices:** While GSI and SSI enhanced nowcasting precision, their forecasting potential was constrained by their reliance on predefined synoptic patterns and regional specificity (Attica and Euboea). Moreover, nighttime detection using Night Microphysics RGB was less effective

than daytime detection, highlighting the need for enhanced observational tools, particularly in Greece, where meteorological radar coverage remains limited.

- **Emerging Satellite Products for Snowfall Detection:** The advanced MTG satellite products **–Cloud Phase RGB** and **Cloud Type RGB–** offer significant enhancements to the GSI and SSI snowfall indices. Cloud Phase RGB's superior differentiation of cloud phase and particle size, combined with Cloud Type RGB's refined cloud classification, improve the detection of convective snowfall and microphysical processes.
- **Synergy of Blended Satellite Products:** The integration of **Blended SEVIRI/LEO MW Precipitation** and **Rapidly Developing Thunderstorms (RDT)** products demonstrated a powerful approach for snowfall nowcasting. By combining **real-time precipitation intensity estimates** with **convective cell tracking**, these products provided **higher spatial** and **temporal accuracy** in detecting **intense snowfall** and **thundersnow** events, surpassing traditional forecasting methods.
- **Future Directions and Technological Advancements:** The study emphasizes the need for further integration of **machine learning and probabilistic forecasting models** to refine index thresholds and reduce uncertainties. Additionally, blending satellite products with automated detection algorithms can further enhance nowcasting precision. The **ongoing expansion of Greece's meteorological radar network** will play a crucial role in bridging observational gaps, complementing satellite-based tools, and significantly improving real-time snowfall monitoring.

9. REFERENCES

Alcott, T. I., & Steenburgh, W. J. (2013). Orographic Influences on a Great Salt Lake–Effect Snowstorm. *Monthly Weather Review*, *141*(7), 2432–2450. https://doi.org/10.1175/MWR-D-12-00328.1

Barriopedro, D., García-Herrera, R., Lupo, A. R., & Hernández, E. (2006). A Climatology of Northern Hemisphere Blocking. *Journal of Climate*, *19*(6), 1042–1063. https://doi.org/10.1175/JCLI3678.1

Barriopedro, D., García-Herrera, R., & Trigo, R. M. (2010). Application of blocking diagnosis methods to General Circulation Models. Part I: A novel detection scheme. *Climate Dynamics*, *35*(7–8), 1373–1391. https://doi.org/10.1007/s00382-010-0767-5

Bott, A. (2012). *Synoptische Meteorologie: Methoden der Wetteranalyse und -prognose*. Springer Berlin Heidelberg. https://doi.org/10.1007/978-3-642-25122-1

Heymsfield, A. J., Miloshevich, L. M., Schmitt, C., Bansemer, A., Twohy, C., Poellot, M. R., Fridlind, A., & Gerber, H. (2005). Homogeneous Ice Nucleation in Subtropical and Tropical Convection and Its Influence on Cirrus Anvil Microphysics. *Journal of the Atmospheric Sciences*, *62*(1), 41–64. https://doi.org/10.1175/JAS-3360.1

Hobbs, P. V. (2010). *Ice Physics*.

Hong, S.-Y., Noh, Y., & Dudhia, J. (2006). A New Vertical Diffusion Package with an Explicit Treatment of Entrainment Processes. *Monthly Weather Review*, *134*(9), 2318–2341. https://doi.org/10.1175/MWR3199.1

Hoskins, B., & Berrisford, P. (1988). A POTENTIAL VORTICITY PERSPECTIVE OF THE STORM OF 15–16 OCTOBER 1987. *Weather*, *43*(3), 122–129. https://doi.org/10.1002/j.1477-8696.1988.tb03890.x

Houssos, E. E., Lolis, C. J., & Bartzokas, A. (2007). The atmospheric conditions over Europe and the Mediterranean, favoring snow events in Athens, Greece. *Advances in Geosciences*, *12*, 127–135. https://doi.org/10.5194/adgeo-12-127-2007

Iacono, M. J., Delamere, J. S., Mlawer, E. J., Shephard, M. W., Clough, S. A., & Collins, W. D. (2008). Radiative forcing by long-lived greenhouse gases: Calculations with the AER radiative transfer models. *Journal of Geophysical Research: Atmospheres*, *113*(D13), 2008JD009944. https://doi.org/10.1029/2008JD009944

Kain, J. S. (2004). The Kain–Fritsch Convective Parameterization: An Update. *Journal of Applied Meteorology*, *43*(1), 170–181. https://doi.org/10.1175/1520-0450(2004)043<0170:TKCPAU>2.0.CO;2

Kartalis, K., & Feidas, H. (2013). *Αρχές και εφαρμογές δορυφορικής τηλεπισκόπησης*. TZIOLA.

Kotroni, V., Lagouvardos, K., Bezes, A., Dafis, S., Galanaki, E., Giannaros, C., Giannaros, T., Karagiannidis, A., Koletsis, I., Kopania, T., Papagiannaki, K., Papavasileiou, G., Vafeiadis, V., & Vougioulas, E. (2021). Storm Naming in the Eastern Mediterranean: Procedures, Events Review and Impact on the Citizens Risk Perception and Readiness. *Atmosphere*, *12*(11), 1537. https://doi.org/10.3390/atmos12111537

Lagouvardos, K., Kotroni, V., & Dafis, S. (2021). *Εξι ερωτήματα με αφορμή την ψυχρή εισβολή Μήδεια*. https://www.meteo.gr/article_view.cfm?entryID=1643

Louka, P., Boucouvala, D., Gofa, F., Balami, M., & Ziakopoulos, D. (2010). Operational forecasting of a snowfall event over the Greater Athens Area. *Advances in Geosciences*, *23*, 25–30. https://doi.org/10.5194/adgeo-23-25-2010

Mass, C. (2021). *The Weather of the Pacific Northwest* (2nd ed.). University of Washington Press.

Melfi, D., Zauli, F., Biron, D., Sist, M., & Leonibus, L. D. (n.d.). *LATEST DEVELOPMENTS OF NEFODINA SOFTWARE IN THE FRAMEWORK OF HYDROLOGICAL SAF PROJECT*.

Papapetrou, A., & Karatarakis, N. (2021). *ΧΙΟΝΟΠΤΩΣΕΙΣ ΣΤΗΝ ΑΤΤΙΚΗ 15-17 ΦΕΒΡΟΥΑΡΙΟΥ 2021—ΚΛΙΜΑΤΙΚΑ ΣΤΟΙΧΕΙΑ*.

Patlakas, P., Chaniotis, I., Hatzaki, M., Kouroutzoglou, J., & Flocas, H. A. (2024). The eastern Mediterranean extreme snowfall of January 2022: Synoptic analysis and impact of sea-surface temperature. *Weather*, *79*(1), 25–33. https://doi.org/10.1002/wea.4397

Pelly, J. L., & Hoskins, B. J. (2003). A New Perspective on Blocking. *Journal of the Atmospheric Sciences*, *60*(5), 743–755. https://doi.org/10.1175/1520-0469(2003)060<0743:ANPOB>2.0.CO;2

Powers, J. G., Klemp, J. B., Skamarock, W. C., Davis, C. A., Dudhia, J., Gill, D. O., Coen, J. L., Gochis, D. J., Ahmadov, R., Peckham, S. E., Grell, G. A., Michalakes, J., Trahan, S., Benjamin, S. G., Alexander, C. R., Dimego, G. J., Wang, W., Schwartz, C. S., Romine, G. S., … Duda, M. G. (2017). The Weather Research and Forecasting Model: Overview, System Efforts, and Future Directions. *Bulletin of the American Meteorological Society*, *98*(8), 1717–1737. https://doi.org/10.1175/BAMS-D-15-00308.1

Prezerakos, N. G. (1984). *Δομή της ατμόσφαιρας κατά τη διάρκεια των χιονοπτώσεων στην Αθήνα*.

Prezerakos, N. G., & Angouridakis, V. E. (1984). Synoptic consideration of snowfall in Athens. *Journal of Climatology*, *4*(3), 269–285. https://doi.org/10.1002/joc.3370040305

Prezerakos, N. G., & Flocas, H. A. (1996). The formation of a dynamically unstable ridge at 500 hPa as a precursor of surface cyclogenesis in the central Mediterranean. *Meteorological Applications*, *3*(2), 101–111. https://doi.org/10.1002/met.5060030201

Prezerakos, N. G., Flocas, H. A., & Michaelides, S. C. (1999). Upper-tropospheric downstream development leading to surface cyclogenesis in the central Mediterranean. *Meteorological Applications*, *6*(4), 313–322. https://doi.org/10.1017/S1350482799001218

Rex, D. F. (1950). Blocking Action in the Middle Troposphere and its Effect upon Regional Climate. *Tellus*, *2*(4), 275–301. https://doi.org/10.1111/j.2153-3490.1950.tb00339.x

Roe, G. H. (2005). OROGRAPHIC PRECIPITATION. *Annual Review of Earth and Planetary Sciences*, *33*(1), 645–671. https://doi.org/10.1146/annurev.earth.33.092203.122541

Sahsamanoglou, H. S. (1989). Summer snowfalls over the mount Olympus area. *International Journal of Climatology*, *9*(3), 309–319. https://doi.org/10.1002/joc.3370090307

Skamarock, W. C., Klemp, J. B., Dudhia, J., Gill, D. O., Barker, D. M., Duda, M. G., Huang, X.-Y., Wang, W., & Powers, J. G. (2008). *A Description of the Advanced Research WRF Version 3*.

Skamarock, W. C., Klemp, J. B., Dudhia, J., Gill, D. O., Liu, Z., Berner, J., Wang, W., Powers, J. G., Duda, M. G., Barker, D. M., & Huang, X.-Y. (2019). *A Description of the Advanced Research WRF Model Version 4*.

Thompson, G., Rasmussen, R. M., & Manning, K. (2004). Explicit Forecasts of Winter Precipitation Using an Improved Bulk Microphysics Scheme. Part I: Description and Sensitivity Analysis. *Monthly Weather Review*, *132*(2), 519–542. https://doi.org/10.1175/1520-0493(2004)132<0519:EFOWPU>2.0.CO;2

Turk, J. F., Rohaly, G., Hawkins, J., Smith, E. A., Marzano, F. S., Mugnai, A., & Levizzani, V. (2000). Analysis and assimilation of rainfall from blended SSMI, TRMM and geostationary satellite data. *Proceedings of the 10th AMS Conference on Satellite Meteorology and Oceanography*, *9*.

Voudouri, K. A., Ntona, M. M., & Kazakis, N. (2023). Snowfall Variation in Eastern Mediterranean Catchments. *Remote Sensing*, *15*(6), 1596. https://doi.org/10.3390/rs15061596

Williams, E., Mushtak, V., Rosenfeld, D., Goodman, S., & Boccippio, D. (2005). Thermodynamic conditions favorable to superlative thunderstorm updraft, mixed phase microphysics and lightning flash rate. *Atmospheric Research*, *76*(1–4), 288–306. https://doi.org/10.1016/j.atmosres.2004.11.009

Woollings, T., Barriopedro, D., Methven, J., Son, S.-W., Martius, O., Harvey, B., Sillmann, J., Lupo, A. R., & Seneviratne, S. (2018). Blocking and its Response to Climate Change. *Current Climate Change Reports*, *4*(3), 287–300. https://doi.org/10.1007/s40641-018-0108-z

Ziakopoulos, D. (2008). *Καιρός—Ο γιος της Γης και του Ήλιου* (Vol. 1).